Geodätisch-geophysikalische Arbeiten in der Schweiz

(Fortsetzung der Publikationsreihe
«Astronomisch-geodätische Arbeiten in der Schweiz»)

herausgegeben von der

Schweizerischen Geodätischen Kommission
(Organ der Akademie der Naturwissenschaften Schweiz)

Einundachtzigster Band
Volume 81

Global Gravity Field Determination Using the GPS Measurements Made Onboard the Low Earth Orbiting Satellite CHAMP

Lars Prange

2010

Adresse der Schweizerischen Geodätischen Kommission:

Institut für Geodäsie und Photogrammetrie
Eidg. Technische Hochschule Zürich
ETH Zürich
8093 Zürich
Switzerland

Internet: http://www.sgc.ethz.ch

ISBN 978-3-908440-25-3

Redaktion des 81. Bandes:
Dr. L. Prange, J. Müller-Gantenbein, Prof. Dr. A. Geiger
Druck: Print-Atelier ADAG, Zürich

VORWORT

Herr Lars Prange hat aus den Daten des GPS-Empfängers (Global Positioning System) an Bord des Satelliten CHAMP (CHAllenging Minisatellite Payload) im Rahmen seiner Arbeit das bestmögliche Gravitationsfeld bestimmt. Er verwendete dazu den am AIUB entwickelten Celestial Mechanics Approach, der für die spezifische Aufgabe angepasst und weiterentwickelt worden ist.

Der Satellit CHAMP hatte eine fast polare Bahn, umkreiste nach seinem Start im Jahre 2000 die Erde in einer Höhe von 470km und sank bis Ende 2009 auf eine Höhe von etwa 300km ab, ehe er im September 2010 nach seinem Wiedereintritt in die Atmosphäre verglühte. Die Bahn konnte mit GPS rein geometrisch, d.h. ohne Kenntnis des Gravitationsfeldes, mit der Genauigkeit von wenigen Zentimetern rekonstruiert werden. Die so bestimmten GPS-Positionen flossen als Beobachtungen in einen kombinierten Bahn- und Gravitationsfeld-bestimmungsprozess ein.

Das finale Gravitationsfeld AIUB-CHAMP03S basiert auf acht Jahren kontinuierlichen und homogen ausgewerteten GPS-Beobachtungen und stellt zur Zeit das wohl weltweit beste nur auf CHAMP beruhende Gravitationsfeld dar. Das Feld enthält signifikante Anteile bis etwa Grad und Ordnung 100, wobei keine Vorinformationen eingeführt worden sind.

Die in Bern entwickelte Methode zur globalen Gravitationsfeldbestimmung wurde von Herrn Pange auf die konkrete Aufgabenstellung angepasst. Er hat die der Methode inhärenten Möglichkeiten voll ausgelotet, um zahlreiche wichtige Fragen zu beantworten. Es wurde insbesondere klar, dass ausgezeichnete Lösungen auch ohne Verwendung von Akzelerometer Messungen (Messungen der nicht-gravitativen Beschleunigungen im Satelliteninnern) erzielt werden können. Als ein weiterer Höhepunkt sind die mittleren jahreszeitlichen Variationen aus den über mehrere Jahre akkumulierten Monatslösungen zu erwähnen, die man in solcher Schärfe bisher bei rein CHAMP-basierten Gravitationsfeldern noch nicht gesehen hat.

Herr Prange hat das Schlussresultat sehr systematisch erarbeitet: Von der Einjahreslösung AIUB-CHAMP01S über die Sechsjahreslösung AIUB–CHAMP02S zur Achtjahreslösung AIUB–CHAMP03S ist auch eine deutliche Steigerung qualitativer und nicht nur quantitativer Natur festzustellen. Herr Prange hat insbesondere die bei der Lösung AIUB-CHAMP02S aufgetretenen Probleme, die mit Änderungen der Auswertestrategie am CODE Rechenzentrum (Center for Orbit Determination in Europe) zusammenhingen, systematisch untersucht und entsprechende Lösungen aufgezeigt. Diese Einsichten sind über die vorliegende Arbeit und über das Thema Gravitationsfeldbestimmung hinaus von Bedeutung.

Der Schweizerischen Akademie für Naturwissenschaften danken wir für die Übernahme der Druckkosten.

Prof. Dr. Gerhard Beutler
Astronomisches Institut
Universität Bern

Prof. Dr. Alain Geiger
ETH Zürich
Präsident der SGK

PREFACE

Utilisant les données du récepteur GPS (Global Positioning System) à bord du satellite CHAMP (CHAllenging Minisatellite Payload), Dr. Lars Prange a dérivé le meilleur champ global de gravité terrestre possible uniquement basé sur des données CHAMP. Pour ce faire, il a utilisé l'*Approche de la Mécanique Céleste* (*Celestial Mechanics Approach*) développée par l'Institut Astronomique de l'Université de Berne (AIUB), qu'il a adaptée à ses besoins, et dont il a étendu le développement.

CHAMP, mis en orbite quasi polaire en 2000 à une altitude d'environ 470 km, est descendu progressivement pour atteindre une altitude de 300 km en 2009, avant de ré-entrer dans l'atmosphère terrestre en septembre 2010. L'orbite de CHAMP a été reconstruite avec une précision de quelques centimètres en utilisant des techniques GPS de positionnement cinématique, sans utiliser aucune information sur le champ de gravité terrestre. Les positions GPS ont servi d'observations dans un processus combiné de calcul d'orbite et de champ de gravité.

Le champ de gravité final AIUB-CHAMP03S est basé sur huit ans de données GPS continues et homogènes. C'est probablement le meilleur champ de gravité à ce jour uniquement basé sur des données CHAMP. Le champ de gravité possède suffisamment de puissance jusqu'au degré 100, ce qui est remarquable étant donné qu'aucune information *a priori* n'a été utilisée.

Après avoir adapté la méthode à CHAMP, Lars Prange a exploré pleinement les options offertes par l'Approche de la Mécanique Céleste. Les réponses à beaucoup de questions importantes ont ainsi pu être apportées. En particulier, il est montré de manière claire que des représentations du champ de gravité d'excellente qualité peuvent être dérivées sans avoir recours aux données d'un accéléromètre (déterminant les accélérations non-gravitationnelles en mesurant les accélérations d'une masse test à l'intérieur du satellite). La détection de variations saisonnières du champ de gravité sur la base de champs cumulés mensuels sur cette période de huit ans est un autre résultat remarquable, probablement unique.

Lars Prange a travaillé de manière très systématique. La qualité des résultats ainsi que la quantité de données traitées se sont accrues de manière substantielle entre la solution AIUB-CHAMP01S qui portait sur une année de données et la solution AIUB-CHAMP03S, en passant par la solution AIUB-CHAMP02S qui portait sur six années de données. Lars Prange a pu mettre en évidence que les problèmes liés à la solution AIUB-CHAMP02S étaient dus à des modifications de la stratégie d'analyse de CODE (Center for Orbit Determination in Europe), un des Centres d'Analyse (AC) de l'IGS (International GNSS Service). Les avancées faites par Dr. Prange dépassent de loin le cadre de la détermination du champ de gravité terrestre, de surcroît celui uniquement basé sur des données CHAMP.

Nous remercions l'académie Suisse des sciences naturelles pour la prise en charge des frais d'impression.

Prof. Dr. Gerhard Beutler
Institut Astronomique
Université de Berne

Prof. Dr. Alain Geiger
ETH Zürich
Président de la CGS

FOREWORD

Using the data of the GPS (Global Positioning System) receiver onboard the CHAMP (CHAllenging Minisatellite Payload) spacecraft Dr. Lars Prange determined the best possible CHAMP-only global gravity field of the Earth. To that end he used the AIUB's so-called *Celestial Mechanics Approach*, which he adapted to and further developed for the specific task.

CHAMP, with its almost polar orbit, was deployed in the year 2000 at a height of about 470km, sank to a height of about 300km till 2009, and eventually re-entered the Earth's atmosphere in September 2010. The CHAMP orbit was reconstructed, without knowledge of the Earth's gravity field, with an accuracy of a few centimetres using GPS kinematic positioning techniques. The GPS positions served as observations in a combined orbit and gravity field determination process.

The final gravity field AIUB-CHAMP03S is based on eight years of continuous and homeogeneous GPS observations. It probably is currently the best gravity field based uniquely on CHAMP data. The determined field has power up to the limiting degree of 100 – which is remarkable, in particular in view of the fact that no prior information was introduced.

After adapting the method to the CHAMP case, Lars Prange fully explored the options inherent in the Celestial Mechanics Approach. Many important questions could be answered. It became in particular clear that excellent gravity field solutions can also be achieved without making use of accelerometer measurements (determining the non-gravitational accelerations by acceleration measurements of a test mass in the satellite's interior). The determination of mean seasonal variations of the gravity field using the CHAMP-derived accumulated monthly gravity fields of the eight year period is another impressive, probably unique achievement.

Lars Prange worked in a very systematic way. The quality improved substantially and not only quantitatively from the one-year solution AIUB-CHAMP01S to the six-year solution AIUB-CHAMP02S, and eventually to the eight-year solution AIUB-CHAMP03S. He was in particular able to show that the problems associated with the solution AIUB-CHAMP02S, were caused by changes in the analysis strategy of the CODE (Center for Orbit Determination in Europe) analysis center of the IGS (International GNSS Service). The insights gained by Dr. Prange are of value far beyond the CHAMP-only case and beyond gravity field determination.

We are grateful to the Swiss Academy of Sciences for financing the printing costs.

Prof. Dr. Gerhard Beutler
Astronomical Institute
University of Berne

Prof. Dr. Alain Geiger
ETH Zürich
President of SGC

Contents

List of Figures

List of Tables

Frequently Used Acronyms

1/rev.	once per revolution
A/m	area to mass ratio
AC	Analysis Center
AIUB	Astronomical Institute of the University of Bern, Switzerland
BPE	Bernese Processing Engine
BSW	BERNESE GPS Software
CHAMP	CHAllenging Minisatellite Payload
CMA	Celestial Mechanics Approach
CODE	Center for Orbit Determination in Europe, Bern, Switzerland
DOF	Degree Of Freedom
DOY	Day Of Year
ERP	Earth Rotation Parameter
ESA	European Space Agency
GFZ	Helmholtz-Zentrum Potsdam Deutsches GeoForschungsZentrum (GFZ-Potsdam), Potsdam, Germany
GNSS	Global Navigation Satellite System
GOCE	Gravity field and steady-state Ocean Circulation Explorer
GPS	Global Positioning System
GRACE	Gravity Recovery And Climate Experiment
IAPG	Institute for Astronomical and Physical Geodesy, Munich, Germany
IAU	International Astronomical Union
IERS	International Earth Rotation and Reference Systems Service
IGS	International GNSS Service
ILRS	International Laser Ranging Service
L_1	L_1 carrier signal frequency (1575.42 MHz)
L_2	L_2 carrier signal frequency (1227.60 MHz)
L_3	ionosphere-free linear combination
LC	Linear Combination
LEO	Low Earth Orbit(er)
LSA	Least-Squares Adjustment
NASA	National Aeronautics and Space Administration
NEQ	Normal EQuation
PCA	Piecewise Constant Acceleration
PCO	Phase Center Offset
PCV	Phase Center Variation
POD	Precise Orbit Determination

PPP	Precise Point Positioning
RINEX	Receiver-INdependent EXchange format
RMS	Root Mean Square
SH	Spherical Harmonic
SLR	Satellite Laser Ranging
SNR	Signal-to-Noise Ratio
SST	Satellite-to-Satellite Tracking
STAR	Space Triaxial Accelerometer for Research missions
TUM	Technische Universität München, Germany

1 Introduction

This work deals with gravity field determination using satellites, which are equipped with Global Positioning System (GPS) receivers. It is a logical continuation of the work done by Heike Bock (2004) and Adrian Jäggi. Heike Bock's work marks the beginning of the orbit determination of Low Earth Orbiters (LEOs), equipped with on-board GPS receivers at the Astronomical Institute of the University of Bern (AIUB). Her methods make use of the highly accurate GPS ephemerides, Earth rotation parameters (ERPs), and GPS clock corrections provided by the Center for Orbit Determination in Europe (CODE, Dach et al, 2009). CODE is an analysis center of the International GNSS Service (IGS, Dow et al, 2009) and is located at the AIUB. With his research on pseudo-stochastic orbit parameters Adrian Jäggi (2007) further improved the precise orbit determination (POD) of LEO satellites using GPS observations. Furthermore he established independent validation methods for LEO satellite orbits using K-band range measurements and Satellite Laser Ranging (SLR) measurements and provided extensive time series of reduced-dynamic orbits and kinematic positions of the CHAMP (Reigber et al, 1998) and GRACE (Tapley and Reigber, 2001) satellites.

We make use of the Celestial Mechanics Approach (CMA, Beutler, 2005; Beutler et al, 2010b) to solve for gravity field parameters using kinematic LEO positions, generated at the AIUB from GPS measurements. A data screening and a gravity field processing infrastructure had to be established. Extensive experiments concerning the parameterization, the use of CHAMP accelerometer measurements, and processing optimization were performed with the goal to acquire the experience necessary for generating CHAMP-only gravity fields using the CMA. For the resulting first gravity field model generated at the AIUB, the AIUB-CHAMP01S (Prange et al, 2009), one year of kinematic CHAMP positions were used, already made available by Adrian Jäggi. As the resulting model was among the best gravity field models based on the same set of CHAMP GPS data, it demonstrated the capabilities of both — the Celestial Mechanics Approach, and Adrian Jäggi's LEO orbit determination.

The next gravity field model, the AIUB-CHAMP02S, was computed from six years of CHAMP GPS data (Prange et al, 2010). In order to provide the required GPS ephemerides, ERPs, and GPS clock corrections in a consistent way and based on the latest IGS standards, the GPS data of the IGS ground station network for the years 2002 to 2007 was reprocessed. The reprocessing was necessary because several model and processing changes occurred in the original CODE series within this long time interval. The amount of available data asked for a high level of automation. The comparison of AIUB-CHAMP01S and AIUB-CHAMP02S allowed extensive studies on the influence of

model changes in the processing of Global Navigation Satellite System (GNSS) data on the estimation of gravity field models from this kind of data (Prange et al, 2010).

Extensive empirical tests were performed in order to demonstrate the capability for further improvements of the gravity field determination using GPS measurements. The tests included a higher data sampling rate. A part of the CODE processing routine was modified to process the necessary high rate (5 s) GPS clock corrections for the years 2002 to 2006. Other experiments addressed the impact of correlations between the kinematic positions referring to subsequent epochs, the benefits of using phase center variation (PCV) models for the LEO GPS antenna, and the impact of an elevation-dependent weighting of the GPS measurements in the LEO POD. The results of these experiments were considered when the AIUB-CHAMP03S gravity field model was generated from eight years of CHAMP GPS data. AIUB-CHAMP03S is, to our knowledge, currently the best static gravity field model based on CHAMP data only.

Knowledge about the shape of the Earth's gravity field is important for many Earth sciences: The orthometric height systems used in the geodesy refer to the geoid, which is defined as the surface of constant gravity potential at mean sea level, whereas geometric heights derived by GPS refer to a reference ellipsoid. The knowledge of geoid undulations allows the combination of GPS with classical leveling techniques. A precise global geoid model could be used to define a global height reference system, which would make local or continental height systems comparable. In the field of oceanography the sea surface topography can be determined from the difference of the sea surface height (measured by satellite altimetry) and the geoid height (computed from a gravity field model). The sea surface topography is used to model the ocean circulation, which plays an important role in the global heat balance. This information is an important input value for global climate models. Temporal changes of the Earth's gravity field indicate changes in the global mass balance such as the melting of the polar ice caps, mean sea level changes, or seasonal changes in the water balance of large river basins. Gravity field data is therefore useful for improving hydrological and glaciological models and for the monitoring of processes related to global change. As the shape of the gravity field is to a wide extend determined by the mass distribution in the Earth's interior, a better gravity field model can contribute to the improvement of the geophysical and geodynamical models. Such models are useful, e.g., for the research on earthquakes, vulcanism, plate tectonics, and for the exploration of natural resources. Last but not least global gravity field models are necessary for the accurate determination of satellite orbits. In summary we can assert that accurate gravity field information is a useful information for many fields of science and engineering and an important component of an integrated geodetic-geodynamic monitoring system, which helps to improve the understanding of the system Earth (Ilk et al, 2005).

Satellites are the best tools to measure the long wavelengths of the Earth's gravity field, because they provide a global coverage with a homogeneous measurement accuracy and access remote areas including the oceans. With these qualities they are a good complement for the terrestrial gravimetric methods. In the first decades of spaceflight dynamic

satellite orbits determined using Doppler, optical, radar, or SLR tracking, as well as measurements from altimetry satellites contributed to global gravity field models. The launch of the CHAMP satellite in the year 2000 initiated a new era of gravity field recovery using LEOs equipped with geodetic GPS receivers. The huge amount of measurements of the on-board GPS receivers allowed an accurate kinematic positioning with an almost complete spatial and temporal coverage. A variety of new global gravity field models using different innovative approaches emerged (Reigber et al, 2003; Gerlach et al, 2003; Mayer-Gürr et al, 2005; Liu, 2008). After the launch of the two GRACE satellites in the year 2002, the research focus moved to the analysis of the very precise inter-satellite K-band measurements, which allowed a more precise estimation of gravity field models well above degree and order 100. The launch of the GOCE satellite with an on-board gradiometer in the year 2009 will further advance the gravity field research.

When starting this work in 2006, measurements from superior gravity field missions were already available (GRACE) or within view (GOCE). Nevertheless our focus is on gravity field recovery using CHAMP data because:

- Gravity field determination using GPS data is also part of the GRACE, GOCE, and possible follow-on missions. The infrastructure, processing scheme, and experience could be used as a basis for processing data from these missions.
- While the K-band (GRACE) and gradiometer (GOCE) instruments provide "in-situ" measurements for the high degree coefficients of the Earth's gravity field, the GPS-derived satellite trajectories remain a major source of information for the low degree coefficients.
- The performance of the Celestial Mechanics Approach for gravity field determination and the LEO orbit determination from GPS measurements at the AIUB should be compared to other approaches. Different gravity field models derived using the same one-year-set of CHAMP data existed at that time and were well described in corresponding publications (Mayer-Gürr et al, 2005; Badura et al, 2006; Liu, 2008).
- Due to the launch of the space mission GRACE already in 2002 with the focus on K-band inter-satellite measurements, the full potential of the CHAMP GPS data has never been fully explored. It is therefore the main goal of this work to exploit the full potential, but also the limitations of CHAMP for gravity field determination by using GPS measurements from a long time series. Thereby the focus is clearly on the practical aspects of CHAMP-only gravity field determination.
- Superior gravity field models derived from GRACE data were already available and could be used for a reliable validation of GPS-only gravity field models.
- The existing gravity field missions were expected to soon reach the end of their lifetime (the GRACE satellites have exceeded their design life time of five years and GOCE is designed for a two-year mission). There may be no dedicated missions to monitor the temporal changes of the Earth's gravity field for several years. On the

other hand an increasing number of satellite missions not dedicated to gravity field research will be equipped with space-borne GPS receivers and could contribute to the gravity field research. The COSMIC and SWARM missions are examples for this kind of missions.

- Therefore we also wanted to find out whether temporal changes of the gravity field may be extracted from GPS-derived kinematic LEO positions.

We conclude the introduction with an outline of the subsequent chapters: Chapter 2 gives a brief overview of history and methods of geoid and gravity field determination. Chapter 3 introduces the basic theory of the LEO orbit determination, gravity field estimation using the Celestial Mechanics Approach, and least-squares adjustment (LSA). Chapter 4 contains a short introduction to GPS. Chapter 5 presents the practical aspects of gravity field recovery including the data processing. Chapter 6 lists experiments and simulation studies accompanying and supporting the generation of the final gravity field models. Chapter 7 shows the validation results of the gravity field models developed in this work. Chapter 8 summarizes the essential results and conclusions.

2 Measuring the Earth's gravity field

Concepts about the nature of the free fall of bodies to the ground were already mentioned in antiquity by authors in India and Greece. In the 17^{th} century Galileo Galilei performed free fall experiments and recognized the free fall as an accelerated motion. Few decades later Sir Isaac Newton formulated the law of gravitation as a function of the masses of bodies and the distance between them.

In the 18^{th} century leading scientists recognized that the Earth cannot be a sphere but must be flattened due to the Earth's rotation (Hoffmann-Wellenhof and Moritz, 2006). In order to determine the shape of the Earth, the length of meridian arcs measured at different latitudes (one close to the North pole and one close to the Equator) were compared. This was done by a combination of astronomical observations (to define the latitude) and complex triangulation campaigns. The results of these measurements confirmed the flattening of the Earth and the shape of the planet was approximated by a mathematical figure — the rotational ellipsoid. The ellipsoid (with updated parameters) is the basis for the computation of coordinates and map projections in geodesy.

In the 19^{th} century Gauss introduced the geoid as the physical figure of the Earth. The geoid is defined as the equipotential surface of the Earth's gravity field at mean sea level. Orthometric height measurements refer to the geoid. The geoid deviates from well fitting ellipsoids by up to 100 m (Hoffmann-Wellenhof and Moritz, 2006). If measurements based on the geoid should be compared or used together with measurements that rely to an Earth ellipsoid (e.g., GPS measurements), the local difference between both surfaces, the so called geoid-undulation, must be known.

2.1 Terrestrial geodesy

Today the gravity on the Earth's surface is measured by gravimeters, i.e., accelerometers measuring the gravitational acceleration. The unit for gravimeter measurements is Gal ($1\,Gal = 0.01\,m/s^2$). Typically, gravimeters are stationary instruments. Gravity measurements over large-scale, ocean, or remote areas are, however, provided by marine and airborne gravimetry. Due to accelerations and vibrations of the moving platforms the measurement accuracy is reduced for these methods (Verdun et al, 2003). Gravimeter measurements are, among other tasks, used for gravimetric geoid determination, e.g., by Yun (1999). Other terrestrial techniques for geoid determination are the astronomical leveling and the GPS leveling. Both methods are also used for the local validation of gravity field models derived from other observables (see, e.g., Gruber, 2004; Hirt and Flury, 2007).

The strengths of terrestrial measurement techniques are their high accuracy at local level and their ability to resolve the fine structures of the gravity field. These methods are, however, not similarly accurate at global scales. Moreover, it is almost impossible to establish a consistent global gravity field model with terrestrial methods due to economic, political, and practical reasons (e.g., limited access to remote regions, conflict areas).

2.2 Satellite geodesy

Satellites are well suited to establish global gravity fields. If their orbits are chosen accordingly (with high inclinations) they are able to provide a global coverage. A satellite can carry sensors (e.g., altimeter or gradiometer) or may be treated itself as a probe in the gravity field, the orbit of which may be determined precisely. Satellite orbits are disturbed by gravity perturbations caused by the irregular mass distribution inside the Earth. The deflection of the true satellite orbit from an undisturbed Kepler orbit may be used to determine the deviation of the true gravity field from a spherically symmetric gravity field. Every tracking method providing measurements of a satellite orbit with a sufficient accuracy and every satellite with a precisely known orbit may potentially contribute to global gravity field determination. Because satellite orbits are very sensitive to the large-scale structures of the gravity field and — depending on the orbit height — less to the fine structures, they are a good complement to terrestrial gravimetric methods.

The roots of satellite geodesy reach back to the early 19^{th} century, when Laplace used observations of the lunar nodal motion to determine the flattening of the Earth (Seeber, 2003). The breakthrough of satellite geodesy came, however, with the launch of the first artificial satellite Sputnik-1 in 1957. Thanks to early theoretical work (e.g., Sedwick, 1956), first scientific results came out soon after the Sputnik launch. Already in 1958 the value of the Earth's flattening could be improved significantly from observing some of the first artificial satellites. In 1959 the third zonal harmonic could be determined (Seeber, 2003).

2.2.1 Optical observations

An important observation method in the early years of satellite geodesy was the photographic determination of directions (photographic astrometry) with satellite cameras (see, e.g., Fig. 2.1 (b)). Satellite observing stations were established worldwide. The angular distance of the satellite trail relative to background stars with known coordinates in the celestial coordinate system was measured (Seeber, 2003). Such observations were used to compute the first standard Earth model SAO-SE1 up to degree 8 (Lundquist and Veis, 1966).

In principle, every bright satellite illuminated by the sun could be observed at night with such cameras. In the 1960ies a variety of satellites, especially suited for optical observations was launched. Balloon satellites such as Echo-1A (1960), Echo-2 (1964), and PAGEOS (1966, see Fig. 2.1 (a)) had a large reflecting surface. Some of them were passive.

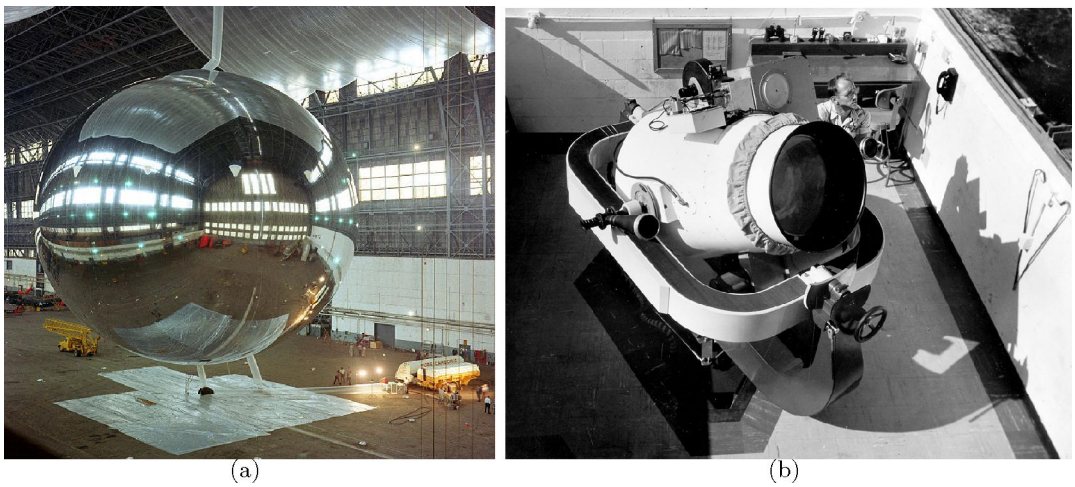

(a) (b)

Figure 2.1: **Left:** PAGEOS geodetic satellite (courtesy by NASA). **Right:** Baker-Nunn satellite camera (courtesy by Smithsonian Institution).

Their high area to mass ratio (A/m-ratio), however, made this kind of satellite susceptible to the influence of non-conservative disturbing forces. Other early type geodetic satellites like ANNA-1B (1962), GEOS-1 (1965), and GEOS-2 (1968) were equipped with optical beacons sending light flashes to the Earth (Seeber, 2003).

Optical tracking suffers from its dependency on weather, daytime (observations are only possible at night), the reflection behavior of the satellites, and the limited accuracy of the photographic astrometry. From the mid 1970ies onwards the method was gradually replaced by better tracking methods (Seeber, 2003). In combination with other techniques optical observations of satellites contributed to gravity field research until the 1980ies. Today, optical measurements with CCD-cameras are, e.g., used for space debris surveillance.

2.2.2 Microwave methods

Since the early days of space age different microwave techniques were used for tracking and orbit determination of satellites and contributed to gravity field estimation. All microwave techniques have the advantage of being independent from weather and day-time.

Doppler measurements belong to the oldest and most widely used satellite tracking methods (Seeber, 2003). The Doppler effect is the frequency shift of a signal that is transmitted by or received on a moving object. If the signal frequency at the transmitter is known, the relative motion between emitter and receiver can be computed from the frequency shift of the received signal. Because already the first satellites continuously transmitted radio signals on stable frequencies, Doppler measurements could be used to estimate their orbital velocity (Seeber, 2003). This is why many satellites not especially manufac-

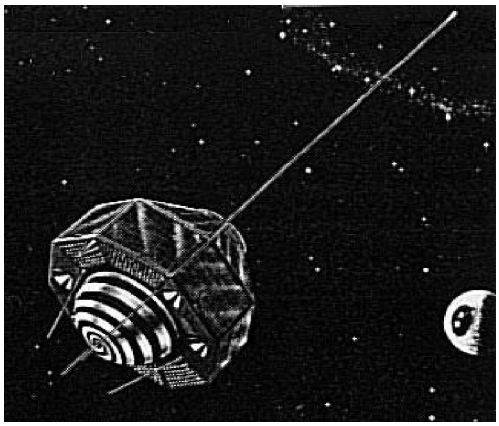

Figure 2.2: GEOS-1 geodetic satellite (courtesy by NASA).

tured for gravity field determination could be used for this purpose anyway. A modern Doppler measurement system is the French DORIS (Doppler Orbitographie et Radiopositionnement Intégrés par Satellite). Radio signals with known and stable frequencies are continuously emitted by ground stations and received by satellites equipped with a DORIS receiver. DORIS is used for LEO POD since 1990 and allows it to reconstruct orbits with an accuracy of a few centimeters (Seeber, 2003). Doppler measurements contributed to the recovery of Earth gravity field models until the 1990ies and are still the major data source for the determination of gravity fields of other celestial bodies within the solar system using space probes.

Radar was adapted to satellite tracking in the late 1950ies (Seeber, 2003). The observables are the range between ground antenna and satellite and the Doppler shift of the radar signal due to the relative velocity between satellite and station. An advantage of the radar is the circumstance that no special equipment on-board the satellite is required. The disadvantages are the requirement of large and expensive ground antennas and the limited accuracy of the range measurements. The ranging accuracy can be increased, if a satellite is equipped with a radar transponder. This was, e.g., the case for the geodetic satellites GEOS-1 (Fig. 2.2), -2, and -3. Today radar is used for satellite tracking with low accuracy demands (Montenbruck and Gill, 2000) and space debris search.

In the early space age different other microwave tracking technologies contributed to the gravity field determination. Examples are the MINITRACK (direction measurements) and the GRARR (range and Doppler shift measurements) systems (Seeber, 2003). Both techniques required special equipment on the satellites and on the ground and were, apart from other tracking devices used on the geodetic satellites GEOS-1 and 2. In the 1990ies the German PRARE system was used for the precise orbit determination of few remote sensing satellites. Its range and Doppler measurements contributed to the GRIM5S1 gravity field model (Biancale et al, 2000).

2.2.3 Satellite Laser Ranging (SLR)

The Satellite Laser Ranging (SLR) technique measures the traveling time of a laser pulse from a ground station (see, e.g., Fig. 2.3 (b)) to a satellite and back. With the measured light traveling time and the known velocity of light the distance between ground station and satellite can be computed. The target satellite needs to carry arrays of retro-reflectors.

The first satellite equipped with retro-reflectors, Beacon Explorer-B, was launched in 1964 (Noll and Pearlman, 2009). More than 100 satellites equipped with retro-reflector arrays were launched since then (ILRS, 2010). In 2007/2008 about 35 satellites were tracked. For all of these satellites precise orbits may be determined and the orbits may, in principle, be used for gravity field determination. Satellite orbits are, however, usually affected by non-conservative forces like atmospheric drag (only LEOs) and radiation pressure. Therefore a special type of massive, passive, spherical, geodetic SLR satellites was developed. These satellites have a core made of very dense material in order to achieve a low A/m-ratio (Seeber, 2003). This reduces the non-gravitational accelerations acting on the satellites. The spherical shape simplifies the modeling of the remaining non-gravitational forces. The surface is covered with retro-reflectors with known offsets to the satellite's center of mass. The first satellite of this type, Starlette, was launched in 1975. Similar satellites

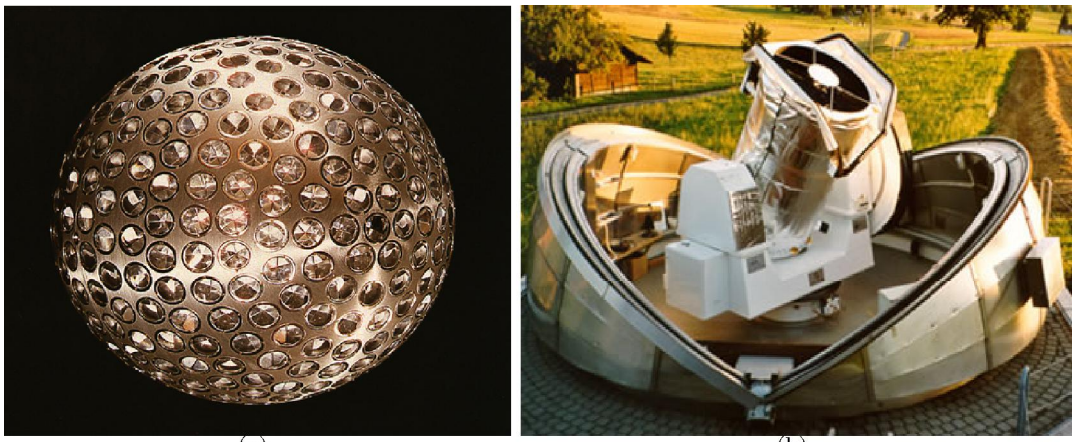

(a) (b)

Figure 2.3: **Left:** LAGEOS-1 geodetic satellite (courtesy by NASA). **Right:** SLR tracking station at Zimmerwald.

with higher orbits like LAGEOS-1+2 (orbital heights of more than 5500 km, Fig. 2.3 (a)) and ETALON-1+2 (orbital heights of more than 19000 km) are not affected by air-drag. As the signal of the fine structures of the gravity field is attenuated with increasing orbital height, the orbits of the LAGEOS and ETALON satellites are not disturbed by the short wavelength terms of the Earth's gravity field. These satellites contributed significantly to the determination of the low-degree parameters of the gravity field and the geocentric gravitational constant GM (Seeber, 2003). In order to also improve the recovery of the

higher degrees of the Earth's gravity field the passive geodetic satellite GFZ-1 was released in 1994 into a LEO orbit of only 400 km height. Due to atmospheric drag its orbit decayed fast and the satellite reentered the atmosphere in 1999 (Seeber, 2003).

Since the first test in the mid 1960ies also the ground tracking network evolved. The ranging accuracy improved from some meters to few millimeters and the number of usable measurements increased (Seeber, 2003). The number of laser ranging observatories contributing to the International Laser Ranging Service (ILRS) has increased to about 40 (ILRS, 2010). Together with other measurement techniques SLR contributed significantly to most global gravity field models published between 1970 and 2000.

The technique has also disadvantages: Like all optical tracking methods SLR is weather-dependent. An SLR station can only track one satellite at the same time. Due to the high costs for building and maintenance, the existing ILRS stations are concentrated in countries, which can afford to run them. The result is a rather sparse and inhomogeneous distribution of measurements. The orbits of SLR satellites are only partly covered by measurements. As a consequence the estimated satellite orbits are dynamical orbits with relatively long arcs (more than one day) and a low number of orbit parameters. They are dependent on dynamical force models with their accuracy limitations. If higher orbits are chosen in order to avoid the influence of atmospheric drag (and reduce the need of setting up many orbit parameters), the orbits are no longer sensitive to the higher degree parameters of the Earth potential. In the more recent combined gravity field models (published after the launch of CHAMP in 2000) SLR measurements, therefore, mainly contributed to the very low degrees, where alternative methods are not as sensitive.

2.2.4 Satellite altimetry

Satellite altimetry measures the vertical distance between a satellite and the Earth's surface. The method is particularly used over the oceans. An altimetry satellite carries a radar-altimeter, which transmits a radar impulse to the ground. The pulse is reflected by the sea surface and received by the radar antenna on-board the satellite. The altitude of the satellite above the ground is computed from the two-way travel time of the radar signal. The orbital height above the reference ellipsoid must be known. Therefore, a precise orbit determination is necessary. The difference between the orbital height above the ellipsoid and the measured altitude is the height of the instantaneous sea surface above the reference ellipsoid (Seeber, 2003). The radar measurements are weather-independent. Altimeter measurements are, however, affected by different error sources such as orbit errors, instrumental errors, and signal propagation errors. The treatment of these errors evolved over the years and significantly improved the accuracy of the method from the meter-level to several centimeters (Seeber, 2003).

The first altimeter satellite, GEOS-3 (Fig. 2.4 (a)), was launched in 1975. A variety of more and more sophisticated satellites followed (e.g., Jason-2, Fig. 2.4 (b)) or are scheduled. Apart from the altimeter the satellites carry payloads supporting a precise orbit determination and attitude control. Altimeter satellites often have nearly circular LEO

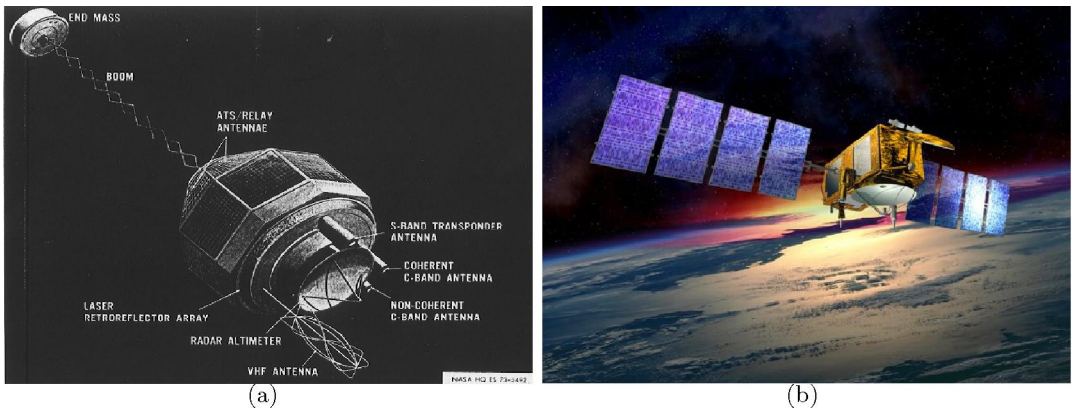

(a) (b)

Figure 2.4: **Left:** GEOS-3 geodetic satellite (courtesy by NASA). **Right:** Jason-2 radar altimetry satellite (courtesy by NASA).

orbits with heights between 800 and 1400 km and medium to high inclinations. With these characteristics they are able to provide globally well distributed measurements of the ocean surface height with a high resolution within a short time interval.

In a first approximation the sea surface height would be equal to the geoid undulation. In fact, however, the instantaneous sea surface differs from the geoid by up to 2 m. The difference is called sea surface topography or dynamic sea surface height (Seeber, 2003). The mean sea surface topography depends on the water salinity and the ocean currents and may be described by hydrographic models. Moreover it is superimposed by a time-dependent component that might be described by different models such as weather models, ocean tide models, and solid Earth tide models (Seeber, 2003). This makes satellite altimetry being a rather complex method, whose accuracy depends on the quality of a variety of models and corrections. Nevertheless, between the late 1970ies and late 1990ies satellite altimetry measurements contributed significantly to many combined global gravity field models such as the JGM-3 (Tapley et al, 1996) or the EGM96 (Lemoine et al, 1998). The large amount of globally well distributed, relatively dense spaced measurements over the oceans were a good complement to other satellite geodetic techniques and ground measurements.

The superposition of geoid undulation, mean sea surface topography, and time-variable sea surface topography raised the question of how to separate the single contributions to the sea surface height. By the late 1990ies the quality of the hydrographic models limited the accuracy of altimetry-derived marine geoid models to a level of a few decimeters (Fu and Chelton, 2001). Beyond this level satellite altimetry could no further contribute to gravity field determination. The problem of separating the geoid undulation and the sea surface topography could either be solved by improvements of the oceanographic models or by finding an independent way for determining the marine geoid at medium to short wavelengths with an accuracy comparable or better than altimetry (Ilk et al, 2005).

2.2.5 High-low SST of CHAMP

The CHAllenging Minisatellite Payload (CHAMP) was designed to study the Earth's gravity and magnetic fields as well as the Earth's atmosphere (Reigber et al, 1998). The mission was initiated and is operated by the GFZ-Potsdam (Helmholtz-Zentrum Potsdam Deutsches GeoForschungsZentrum). CHAMP was launched on July 15, 2000 with a designated life time of five years. Due to orbital maneuvers performed in June and December 2002, in March 2006, in March 2009, and thanks to the low solar activity in the later years of the mission, the satellite was operating until September 2010. The CHAMP mission was a logical next step in gravity field research using satellites: in the 1990ies the improvements in satellite altimetry raised the question how to separate the geoid height and the sea surface topography (see Sect. 2.2.4). This stimulated the development of alternative methods for the estimation of the global geoid. At the same time new precise instruments like space-borne GPS receivers and accelerometers became operational. The GFZ-1 satellite demonstrated the potential of particular low satellite orbits for measuring the terms of higher degrees of the Earth's gravity field (see Sect. 2.2.3).

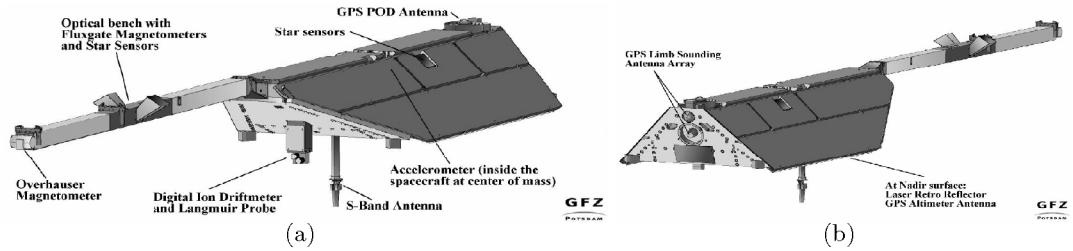

Figure 2.5: CHAMP satellite: Front (left) and rear (right) view (courtesy by GFZ Potsdam).

Figure 2.5 shows the front and rear side of CHAMP. Its dimensions are 8.33 m × 1.62 m × 0.75 m (Reigber, 2000). From the gravity field determination point of view, the satellite may be considered as a probe following the distortions of the Earth's gravity field. The LEO satellite is affected by non-gravitational accelerations due to solar and albedo radiation pressure, and atmospheric drag. In order to measure these accelerations CHAMP carries a STAR (Space Triaxial Accelerometer for Research missions) accelerometer (Touboul et al, 1998). It uses electrostatic forces to keep a proof-mass, which is located inside an electrode cage in the spacecraft's center of mass, in position. The required current is a measure of the total non-gravitational acceleration acting on the proof mass. The accuracies of the measured linear accelerations are $3 \cdot 10^{-9}$ m/s^2 for the along-track and the cross-track axes, and $3 \cdot 10^{-8}$ m/s^2 for the radial axis (Grunwaldt and Meehan, 2003). It turned out that the radial accelerometer component does not work properly (Reigber, 2001). The values in this direction are derived from the measurements in the other directions (Reigber, 2002b). Instead of using the accelerometer measurements the influence of

the non-conservative forces might also be considered in the traditional way by applying dynamical force models. In along-track direction the profile of the satellite has a relatively low A/m-ratio, which reduces the impact of the atmospheric drag forces.

Other ways of mitigating the impact of the non-conservative forces are the estimation of more arc-specific parameters or the choice of short orbital arcs. Both approaches are feasible because CHAMP's GPS receiver provides a large number of measurements with a dense spacing. The space-qualified, geodetic BlackJack GPS receiver (Kuang et al, 2001) has a primary and a redundant board, collects dual-frequency phase and pseudo-range measurements and serves four antennas: one zenith-viewing POD antenna equipped with a choke ring, two limb-viewing atmosphere sounding helix antennas, and one nadir-viewing experimental antenna. The receiver is theoretically able to track up to twelve GPS satellites for POD. The actual number is, however, lower and changed several times due to receiver firmware updates (Grunwaldt and Meehan, 2003). From mid 2006 onwards the behavior of the receiver changed due to clock steering problems, which are related to the extended mission duration (Michalak 2008, private commun.). The receiver was temporarily switched to its redundant board, but stayed operational. After switching back to the main receiver the clock corrections became much larger (up to 10 μs). In late 2008 the receiver was finally switched to its redundant board and tracks with a reduced number of channels since then. The receiver events and the maximum number of trackable GPS satellites are listed in Table 2.1. The mean number of simultaneously tracked GPS satellites is shown in Fig. 2.6. From DOY 250/2009 (2009.09.07) on this value decreased once more. The sampling interval of the publicly available ("Level1") GPS measurements

Table 2.1: Events related to CHAMP's GPS receiver.

Date of change		Number of trackable	General
(YYYY.MM.DD)	(DOY/YYYY)	GPS satellites	information
2000.07.17	199/2000	7	Activation
2001.03.22	081/2001	8	Firmware update
2002.03.05	064/2002	10	Firmware update
2006.07.02	183/2006	7	Switch to redundant board
2006.08.04	216/2006	10	Switch to main board; large clock corrections
2008.10.05	279/2008	7	Switch to redundant board

is 10 s. As the receiver is tracking permanently since the year 2000 this results in a huge amount of data and a very dense global coverage. The tracking of a LEO satellite using measurements from higher flying satellites, such as GPS, is called high-low satellite-to-satellite tracking (hl-SST). CHAMP is also equipped with a retro-reflector array allowing it to support or validate the POD with SLR measurements.

The precise orientation (attitude) of the satellite w.r.t. the stars is measured by ASC

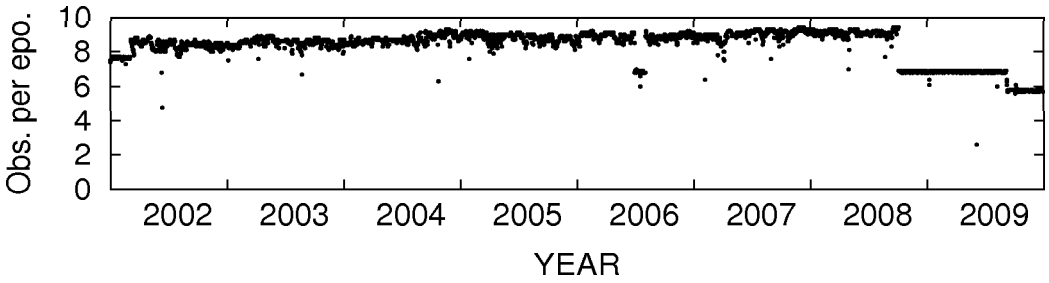

Figure 2.6: Mean number of GPS satellites simultaneously tracked by CHAMP's GPS receiver.

(Advanced Stellar Compass) instruments (Jorgensen, 1999). One ASC is mounted on the boom to support magnetometry and the other one on the spacecraft main body. Each instrument consists of two CCD cameras, whose images are compared with star positions computed from an on-board star catalogue. The ASCs provide attitude data with a precision of about 4 arcsec. This information may be used for the proper modeling of the GPS antenna and SLR retro-reflector offsets. CHAMP's attitude is actively maintained. Attitude maneuvers are performed regularly (between 70 and 200/day) by small thruster pulses of the cold gas propulsion system to keep the orientation of the satellite within a few degrees w.r.t. the nominal orientation. Nominally, the boresight vector of the GPS POD antenna coincides with the radial direction and the magnetometry boom is oriented in flight direction.

CHAMP was launched into an almost circular, near-polar orbit with an initial height of about 455 km and an inclination of 87°. The initial height was a compromise between the requirements of the different mission goals, and guaranteed a multi-year mission duration despite the presence of atmospheric drag, which continuously lowers the satellite's orbital height. Figure 2.7 shows the descending orbit during the mission time. The slope of the descent is correlated with the solar activity, showing big descent rates around the solar maximum in the year 2002. Therefore, two orbital maneuvers have been performed in 2002 to raise the altitude. With the weaker solar activity in the later years of the mission the orbit descent rate decreased, allowing it to extend the mission. Additional orbital maneuvers took place in 2006 and 2009. In late 2009 the descent rate increased again due to the higher density of the atmosphere at the lower altitude that CHAMP has meanwhile reached.

The launch of CHAMP marks the beginning of a new era in global gravity field recovery, because the use of the on-board GPS receiver allowed a kinematic positioning with an, at that time, unprecedented accuracy, spatial, and temporal coverage. This resulted in the determination of a variety of new global gravity field models based on different approaches. An overview of the approaches is provided by Liu (2008). Already the very first CHAMP-only solution, EIGEN-1S (Reigber et al, 2002), which was derived from only 3

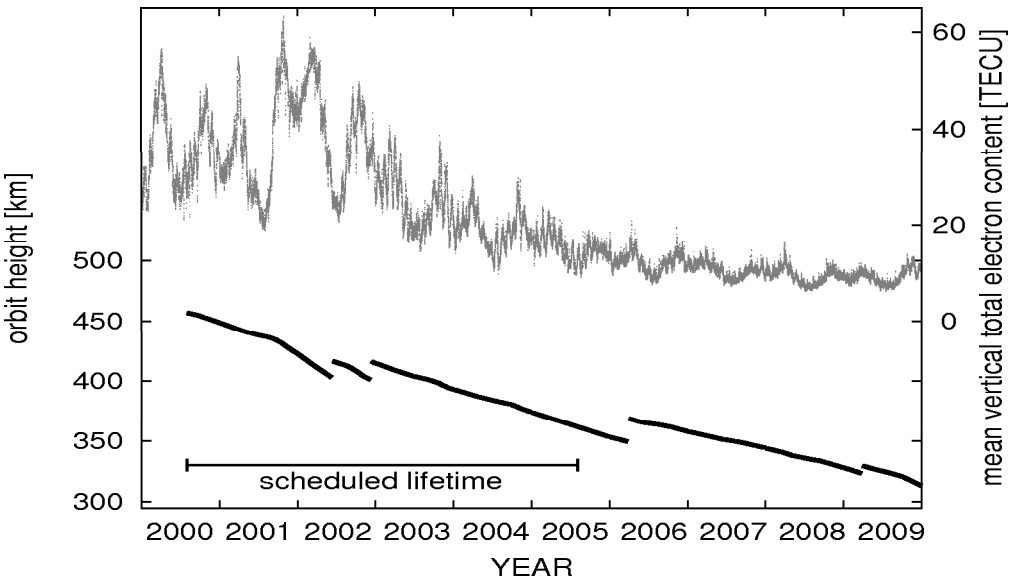

Figure 2.7: CHAMP orbit altitude and solar activity (represented by the total electron content of the Earth's ionosphere).

months of CHAMP data, was twice as accurate as the best pre-CHAMP satellite-only gravity field models, although these models were based on measurements with different techniques to some tens of satellites over a time span of years or even decades. EIGEN-1S was, like the following models of the EIGEN-family, processed using the classical orbit perturbation analysis approach based on the numerical orbit integration using the GPS and accelerometer measurements. The observations were directly introduced into the gravity field determination. Many scientific groups, however, used GPS-derived kinematic positions as pseudo-observations in the gravity field estimation process. Some of these groups used the energy integral approach to estimate gravity field models such as TUM-2S (Wermuth et al, 2004) and TUG-CHAMP04 (Badura et al, 2006). The application of the acceleration approach resulted in the DEOS_CHAMP-02S_70 model (Liu, 2008). The kinematic pseudo-observations may, however, also be introduced into a classical orbit determination based on the numerical integration of the variational equations. The strength of this approach was proven by the so-called short-arc method that was used to generate the ITG-CHAMP01S model (Mayer-Gürr et al, 2005). A similar, more general version of that approach is used in this work.

Due to the launch of the more sophisticated GRACE mission already in 2002, the research focus of the scientific community moved towards that mission rather rapidly. This is why the full potential of the CHAMP GPS data has never been fully exploited and explored. One goal of this work is therefore to sound the limitations of CHAMP for gravity field determination by using long time series of CHAMP GPS data and by applying improve-

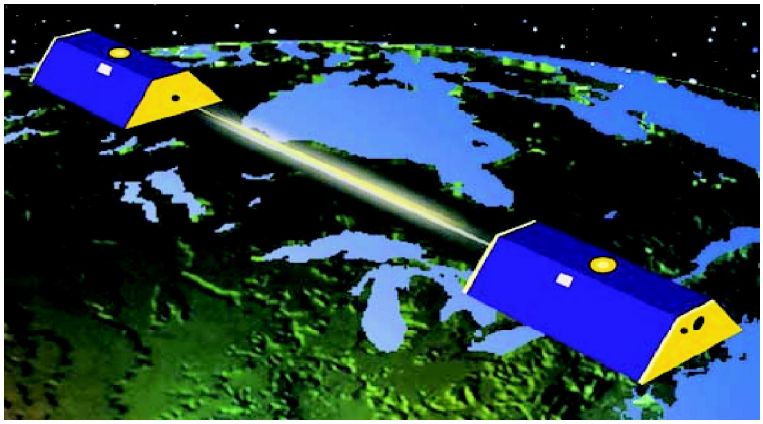

Figure 2.8: GRACE mission configuration (courtesy by NASA).

ments in the GPS data processing. CHAMP can be seen as a technological testbed for the more sophisticated gravity field missions GRACE and GOCE, because they make use of GPS receivers and accelerometers as well. Furthermore the analysis of CHAMP data allows to assess the value of future non-dedicated satellites equipped with GPS receivers (e.g., SWARM) for gravity field research.

2.2.6 Low-low SST with GRACE

The Gravity Recovery And Climate Experiment (GRACE, Tapley and Reigber, 2001) is a joint mission of NASA (National Aeronautics and Space Administration) and DLR (Deutsches Zentrum für Luft- und Raumfahrt). GRACE was launched on March 17, 2002 with a scheduled lifetime of five years. It is still operational in 2010 and the end of the mission is expected not before 2015 (NASA, 2010). The space segment consists of two satellites of identical construction. They follow each other in a nominal distance of 220 km on the same orbital trajectory (see Fig. 2.8). The distance variation between the two satellites is measured by a new instrument, a K/Ka-Band Ranging (KBR) system with a very high precision. This allows the measurement of differential perturbations between the orbits of both spacecraft.

The GRACE satellites are similar in construction to the CHAMP satellite. Like CHAMP, they represent free falling proof-masses in the Earth's gravity field. In order to measure the non-gravitational perturbations forces, each satellite carries a SuperSTAR accelerometer (Touboul et al, 1999), which is an improved version of the STAR instrument used on CHAMP.

Each GRACE satellite carries an improved space-qualified BlackJack GPS receiver (Dunn et al, 2003). It collects dual-frequency phase and pseudo-range measurements and serves three GPS antennas: one zenith-viewing POD antenna equipped with a choke ring, a backup POD antenna, and a helix antenna for atmosphere sounding. The sampling in-

terval of the openly available ("Level1B") GPS measurements is 10 s. The GPS measurements provide the information about the low degrees of the gravity field and the connection to the global reference frame. The GRACE satellites are also equipped with SLR retro-reflectors. A star camera assembly provides the precise orientation (attitude) of each satellite w.r.t. the stars.

The K/Ka-Band Ranging system is the key science instrument of the GRACE mission (Dunn et al, 2003). Each satellite is equipped with a horn antenna for the transmission and reception of the K- and Ka-band microwave signals, an ultra-stable oscillator and a signal processing unit. The phase-shift between received and generated signal is measured with an accuracy of about $0.2\,\mu$m/s for the range-rate and $10\,\mu$m for the range (Dunn et al, 2003). The K-Band measurements are sensitive to small structures in the gravity field and thus provide the main information about the medium and high degrees of the gravity field solution. Measurements between LEO satellites are also called low-low satellite-to-satellite tracking (ll-SST).

The GRACE satellites were launched into an almost circular, near-polar orbit with an initial height of about 500 km and an inclination of 89°. The separation between the two satellites is actively controlled in order to stay within 170 and 270 km. This is accomplished by orbital maneuvers.

The main mission objective is the mapping of changes of the Earth's gravity field with a temporal resolution of about one month (Tapley et al, 2004). This goal can be achieved, because the orbital characteristics, and the amount and precision of the continuous K-band measurements allows it to determine accurate gravity field models even from short time series of data. GRACE data is used in addition to improve the accuracy of the static gravity field models. GRACE data provides the main information for determining the lower and medium degrees (up to about $n = 150$) of all current combined global gravity field models.

2.2.7 Satellite gradiometry with GOCE

The Gravity field and steady-state Ocean Circulation Explorer (GOCE, Fig. 2.9) was launched on March 17, 2009 with a scheduled operation time of 20 months. The satellite is operated by the ESA (European Space Agency). The main mission purpose is the determination of the stationary part of the Earth's gravity field with the highest possible spatial accuracy and resolution: The geoid shall be determined with an accuracy of 1 cm, and gravity anomalies with 1 mGal with a spatial resolution of about 100 km (Drinkwater et al, 2006). In order to achieve these goals the satellite has some new characteristics.

GOCE was launched into an almost circular, sun-synchronous orbit with an inclination of 96.5° and an initial height of only about 280 km. The low orbit altitude minimizes the attenuation of the gravity field signal, which makes the orbit more sensitive to the higher degrees of the gravity potential. On the other hand the atmospheric drag forces are much stronger at low altitudes, which would usually result in a rapid orbit descent.

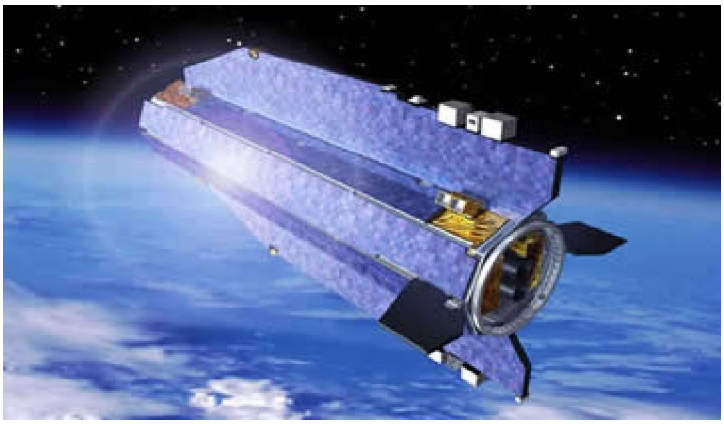

Figure 2.9: GOCE satellite (courtesy by ESA Publications Division).

Therefore the satellite is equipped with an ion engine, compensating the atmospheric drag. The thrust control information is provided by the gradiometer instrument. The three-axis gravity gradiometer is the core instrument of the GOCE mission. It measures the fine structures of the Earth's gravity field. This new kind of instrument consists of three pairs of orthogonally mounted three-axis accelerometers and is located in the spacecraft's center of mass. The difference of the accelerations measured by the two accelerometers forming a pair is (apart from rotational accelerations) the gravity gradient in the direction joining them. The gravity gradient is the basic gradiometer observable. Half of the sum of the measured accelerations is proportional to the externally induced non-gravitational accelerations in the corresponding direction. The along-track value of this measurement is the input value for the thrust control of the ion engine.

The LAGRANGE GPS receiver (Zin et al, 2006) on-board GOCE is a dual-frequency space-qualified receiver. It measures code and phase observations with a sampling interval of 1 s, and serves a GPS helix antenna (Dilssner et al, 2006). A redundant receiver and antenna are available. The GPS data is used for POD, but also for the recovery of the long wavelength part of the gravity field, which is outside of the measurement bandwidth of the gravity gradiometer. The GOCE satellite is also equipped with SLR retro-reflectors. The precise orientation (attitude) of the satellite w.r.t. the stars is measured by three CCD star cameras. Attitude changes are also measured by the gradiometer. The correct attitude is actively maintained by three orthogonally mounted magnetic torquers.

The GOCE orbits and gravity field models ("Level2" products), the gradiometer- and GPS-data ("Level 1b" products), and the GOCE calibration and validation products are provided by the High-level Processing Facility (HPF, Koop et al, 2006), which is operated by the European GOCE Gravity Consortium (EGG-C). The Astronomical Institute of the University of Bern (AIUB) is member of the HPF and is in charge of the generation of the Precise Science Orbit product.

3 Orbit determination and gravity field recovery

In this chapter the theoretical basics of satellite orbit and gravity field determination using the Bernese GPS Software package (BSW, see Sect. 4.7) are described. Gravity field determination as practiced in this work is interpreted as a generalized orbit determination problem with the parameters describing the gravity field being estimated in addition to the orbit parameters. For a more detailed discussion of this so-called Celestial Mechanics Approach (CMA) we refer to Beutler (2005) and Beutler et al (2010b).

3.1 Least squares adjustment

In GPS data processing, orbit determination, and gravity field recovery large numbers of parameters have to be estimated. In order to perform this task, the parameter estimation method least-squares adjustment (LSA) is implemented in the BSW and used in this work. LSA is a mathematical computing scheme making extensive use of the instruments of linear algebra. The method was originally developed by Gauss in the 19^{th} century and is described in many textbooks (e.g., Helmert, 1872; Reissmann, 1980; Koch, 1988; Wolf, 1997; Wolf and Ghilani, 1997; Niemeier, 2008). The notation used in this work leans on the notation used in Jäggi (2007) and Dach et al (2007).

3.1.1 Basic concept

When using the LSA, it is assumed that each observation may be expressed as a function of the parameters of a linearized mathematical model. There have to be at least as much observations as parameters. If the number of observations is larger, the measurement corrections are allocated in a way that minimizes the sum of the squares of the observation corrections. The relation between the observation vector $\boldsymbol{L}$ and the model function $\boldsymbol{F}$ may be described by a system of linearized observation equations:

$$\boldsymbol{L} + \boldsymbol{v} = \boldsymbol{F}(\boldsymbol{X}_0) + \boldsymbol{A}\,\boldsymbol{x} \;, \tag{3.1}$$

with the column arrays of the

$\boldsymbol{v}$ corrections of the original observations,

$\hat{\boldsymbol{v}} = -\boldsymbol{v}$ observation residuals,

$\boldsymbol{X}_0$ a priori values of the model parameters,

$\boldsymbol{x}$ solution vector (corrections of the a priori parameters),

$\boldsymbol{X} = \boldsymbol{X}_0 + \boldsymbol{x}$ adjusted model parameters.

The design matrix $\boldsymbol{A}$ contains the partial derivatives of the model function w.r.t. the parameters:

$$\boldsymbol{A} = \left.\frac{\partial \boldsymbol{F}(\boldsymbol{X})}{\partial \boldsymbol{X}}\right|_{\boldsymbol{X}=\boldsymbol{X}_0} \tag{3.2}$$

The observation corrections may be expressed as

$$\boldsymbol{v} = \boldsymbol{A}\,\boldsymbol{x} - \boldsymbol{l}\ , \tag{3.3}$$

where $\boldsymbol{l} = \boldsymbol{L} - \boldsymbol{F}(\boldsymbol{X}_0)$ is the "observed-minus-computed" (O–C) array.

If observations of different accuracy are used together they may be weighted:

$$\boldsymbol{P} = \sigma_0^2\ \boldsymbol{C}_{ll}^{-1} = \boldsymbol{Q}_{ll}^{-1}\ , \tag{3.4}$$

with the

$\boldsymbol{P}$ weight matrix of the observations,

σ_0 a priori standard deviation of unit weight,

$\boldsymbol{C}_{ll}$ covariance matrix of the observations, and

$\boldsymbol{Q}_{ll}$ cofactor matrix of the observations.

The weight matrix $\boldsymbol{P}$ is a diagonal matrix, if the observations are uncorrelated and a unit matrix, if the observations shall be equally weighted.

The goal of the least-squares adjustment is the minimization of the quadratic sum of the observation corrections ("least squares"), which is expressed by the term $\boldsymbol{v}^T\,\boldsymbol{P}\,\boldsymbol{v}$. Therefore the normal equation (NEQ) system has to be established:

$$\boldsymbol{N}\,\boldsymbol{x} = \boldsymbol{b}\ , \tag{3.5}$$

with the

$\boldsymbol{N} = \boldsymbol{A}^T\,\boldsymbol{P}\,\boldsymbol{A}$ normal equation (NEQ) matrix and

$\boldsymbol{b} = \boldsymbol{A}^T\,\boldsymbol{P}\,\boldsymbol{l}$ right-hand side of the NEQ system.

$\boldsymbol{N}$ is a quadratic and symmetric matrix. The dimension corresponds to the number of adjusted model parameters. If it is regular, the NEQ system may be solved by inversion of the NEQ matrix:

$$\boldsymbol{x} = \boldsymbol{N}^{-1}\,\boldsymbol{b}\ . \tag{3.6}$$

The estimated (a posteriori) standard deviation of unit weight (also called root mean square (RMS) error) is computed as:

$$m_0 = RMS = \sqrt{\frac{\boldsymbol{v}^T \boldsymbol{P}\, \boldsymbol{v}}{f}}\,, \; f > 0\,, \tag{3.7}$$

with the

$f = n - u$ degree of freedom (DOF),

n number of observations, and

u number of adjusted model parameters.

The covariance matrix $\boldsymbol{C_{xx}}$ of the adjusted model parameters is defined as

$$\boldsymbol{C_{xx}} = m_0^2\, \boldsymbol{N}^{-1} = m_0^2\, \boldsymbol{Q_{xx}}\,. \tag{3.8}$$

The (a posteriori) standard deviations of the adjusted model parameters are given by

$$m_x = \sqrt{C_{xx}}\,, \tag{3.9}$$

where C_{xx} is the x^{th} diagonal element of the covariance matrix.

3.1.2 LSA techniques

LSA offers many techniques for special parameter handling. A subset of techniques that are important for this work is introduced here. For more information we refer to Dach et al (2007).

Parameter pre-elimination:

If large numbers of model parameters need to be handled efficiently, it can be helpful to pre-eliminate parameters, which are a part of the model, but whose explicit solution is not required. In the context of gravity field determination the arc-specific orbit parameters are, e.g., pre-eliminated because only the gravity field parameters are of interest. The dimension of the NEQ system can be reduced significantly, resulting in a more rapid inversion of the final NEQ matrix when computing the solution vector. The NEQ system (3.5) may be subdivided into two parts (Dach et al, 2007):

$$\begin{pmatrix} \boldsymbol{N}_{11} & \boldsymbol{N}_{12} \\ \boldsymbol{N}_{21} & \boldsymbol{N}_{22} \end{pmatrix} \cdot \begin{pmatrix} \boldsymbol{x}_1 \\ \boldsymbol{x}_2 \end{pmatrix} = \begin{pmatrix} \boldsymbol{b}_1 \\ \boldsymbol{b}_2 \end{pmatrix}\,. \tag{3.10}$$

The solution sub-vector $\boldsymbol{x}_1$ contains the parameters we are interested in, while sub-vector $\boldsymbol{x}_2$ contains the parameters to be pre-eliminated. The subdivided NEQ system may be re-arranged to

$$\boldsymbol{N}_{11}^{*}\, \boldsymbol{x}_1 = \boldsymbol{b}_1^{*}\,, \tag{3.11}$$

with the

$\boldsymbol{N}_{11}^{*} = \boldsymbol{N}_{11} - \boldsymbol{N}_{12}\,\boldsymbol{N}_{22}^{-1}\,\boldsymbol{N}_{21}$ NEQ matrix of the model parameters $\boldsymbol{x}_1$ and

$\boldsymbol{b}_1^{*} = \boldsymbol{b}_1 - \boldsymbol{N}_{12}\,\boldsymbol{N}_{22}^{-1}\,\boldsymbol{b}_2$ corresponding right-hand side of the NEQ system.

$\boldsymbol{N}_{11}^{*}$ and $\boldsymbol{b}_1^{*}$ contain the effect of the pre-eliminated parameters on the remaining parameters of the NEQ system. Thus the pre-eliminated model parameters $\boldsymbol{x}_2$ are correctly taken into account in the modified NEQ system, although their estimates are not explicitly available (but may be obtained by back-substitution, see Dach et al, 2007). The results for the remaining parameters $\boldsymbol{x}_1$ are the same as without pre-elimination.

Parameter constraining:

Additional information may be introduced into NEQ systems in form of constraints. This might, e.g., be useful if a NEQ system becomes singular (and therefore not solvable), if the observations are not sensitive to all parameters in the mathematical model, or if parameters are correlated. The constraints suppress too large excursions of weakly determined model parameters from their a priori values (absolute constraining) or from other parameter values (relative constraining). A parameter may be constrained to its a priori value by introducing an artificial observation equation constraining the parameter improvement to zero (Dach et al, 2007):

$$0 = x_i \ . \tag{3.12}$$

The artificial observation has the weight

$$P_i = \frac{\sigma_0^2}{\sigma_i^2} \ , \tag{3.13}$$

where σ_i is the standard deviation of the artificial observation. The DOF counter is incremented by 1 for each artificial observation.

Normal equation stacking:

When computing long time series of data the processing time interval is usually subdivided into sessions of predefined length (e.g., one day) for practical reasons (e.g., file handling, memory consumption, separate solutions for short time intervals). For each session an individual NEQ system is set up and stored separately. The session-wise NEQ systems may contain parameters, which are identical in the entire processing interval (e.g., parameters describing the static part of the gravity field). Moreover parameters might be determined using different observation types that should be used for a combined solution (e.g., a combined gravity field solution using GPS, K-band, and SLR observations). To solve for these parameters, it is necessary to stack the individual NEQ systems into one NEQ system and combine the common parameters. This may be done by performing a linear transformation according to Brockmann (1997). The principle shall be illustrated with an example: Two NEQ systems containing common parameters, may be subdivided in the following way:

$$\begin{pmatrix} \boldsymbol{N}_{11} & \boldsymbol{N}_{1g} \\ \boldsymbol{N}_{1g}^{T} & \boldsymbol{N}_{gg} \end{pmatrix} \cdot \begin{pmatrix} \boldsymbol{x}_1 \\ \boldsymbol{x}_g \end{pmatrix} = \begin{pmatrix} \boldsymbol{b}_1 \\ \boldsymbol{b}_g \end{pmatrix} \ , \tag{3.14}$$

$$\begin{pmatrix} \boldsymbol{N}_{22} & \boldsymbol{N}_{2g} \\ \boldsymbol{N}_{2g}^T & \boldsymbol{N}_{gg} \end{pmatrix} \cdot \begin{pmatrix} \boldsymbol{x}_2 \\ \boldsymbol{x}_g \end{pmatrix} = \begin{pmatrix} \boldsymbol{b}_2 \\ \boldsymbol{b}_g \end{pmatrix} , \tag{3.15}$$

with the

$\boldsymbol{x}_1$, $\boldsymbol{x}_2$ solution sub-vectors containing the parameters that should not be stacked (e.g., arc-specific parameters),

$\boldsymbol{x}_g$ solution sub-vectors containing the parameters that are common in both NEQ systems and shall be stacked (e.g., gravity field parameters).

The combined NEQ system may then be written

$$\boldsymbol{N}' \cdot \boldsymbol{x}' = \boldsymbol{b}' \text{ or block-wise } \begin{pmatrix} \boldsymbol{N}_{11} & \boldsymbol{N}_{1g} & \boldsymbol{0} & \boldsymbol{0} \\ \boldsymbol{N}_{1g}^T & \boldsymbol{N}_{gg} & \boldsymbol{0} & \boldsymbol{0} \\ \boldsymbol{0} & \boldsymbol{0} & \boldsymbol{N}_{22} & \boldsymbol{N}_{2g} \\ \boldsymbol{0} & \boldsymbol{0} & \boldsymbol{N}_{2g}^T & \boldsymbol{N}_{gg} \end{pmatrix} \cdot \begin{pmatrix} \boldsymbol{x}_1 \\ \boldsymbol{x}_g \\ \boldsymbol{x}_2 \\ \boldsymbol{x}_g \end{pmatrix} = \begin{pmatrix} \boldsymbol{b}_1 \\ \boldsymbol{b}_g \\ \boldsymbol{b}_2 \\ \boldsymbol{b}_g \end{pmatrix} . \tag{3.16}$$

The stacked NEQ system

$$\tilde{\boldsymbol{N}}\,\tilde{\boldsymbol{x}} = \tilde{\boldsymbol{b}} \text{ or rather } \begin{pmatrix} \boldsymbol{N}_{11} & \boldsymbol{0} & \boldsymbol{N}_{1g} \\ \boldsymbol{0} & \boldsymbol{N}_{22} & \boldsymbol{N}_{2g} \\ \boldsymbol{N}_{1g}^T & \boldsymbol{N}_{2g}^T & \boldsymbol{N}_{gg} + \boldsymbol{N}_{gg} \end{pmatrix} \cdot \begin{pmatrix} \boldsymbol{x}_1 \\ \boldsymbol{x}_2 \\ \boldsymbol{x}_g \end{pmatrix} = \begin{pmatrix} \boldsymbol{b}_1 \\ \boldsymbol{b}_2 \\ \boldsymbol{b}_g + \boldsymbol{b}_g \end{pmatrix} , \tag{3.17}$$

consisting of the

$\tilde{\boldsymbol{N}} = \boldsymbol{C}^T\,\boldsymbol{N}'\,\boldsymbol{C}$ stacked NEQ matrix,

$\tilde{\boldsymbol{b}} = \boldsymbol{C}^T\,\boldsymbol{b}'$ right-hand side of the stacked NEQ system, and

$\tilde{\boldsymbol{x}}$ solution array of the stacked NEQ system,

is obtained from Eq. (3.16) by applying the transformation matrix

$$\boldsymbol{C} = \begin{pmatrix} \boldsymbol{1}_{[u1,u1]} & \boldsymbol{0}_{[u1,u2]} & \boldsymbol{0}_{[u1,ug]} \\ \boldsymbol{0}_{[ug,u1]} & \boldsymbol{0}_{[ug,u2]} & \boldsymbol{1}_{[ug,ug]} \\ \boldsymbol{0}_{[u2,u1]} & \boldsymbol{1}_{[u2,u2]} & \boldsymbol{0}_{[u2,ug]} \\ \boldsymbol{0}_{[ug,u1]} & \boldsymbol{0}_{[ug,u2]} & \boldsymbol{1}_{[ug,ug]} \end{pmatrix} , \tag{3.18}$$

consisting of

$\boldsymbol{1}$ unit matrices, and

$\boldsymbol{0}$ zero matrices, with

$u1, u2, ug$ the dimensions of the sub-matrices defined by the number of unknown parameters in the arrays $\boldsymbol{x}_1$, $\boldsymbol{x}_2$, and $\boldsymbol{x}_g$.

The stacked NEQ system Eq. (3.17) may then be solved in analogy to Eq. (3.6). For more detailed information we refer to Brockmann (1997).

3.2 Coordinate systems

3.2.1 Geocentric quasi-inertial system

The motion of Earth-orbiting satellites is usually described in a geocentric quasi-inertial coordinate system, also called Geocentric Celestial Reference System (GCRS, Hoffmann-Wellenhof et al, 2008). The quasi-inertial system has its origin in the Earth's center of mass, but its axes are parallel to the axes of the inertial system, i.e., they are not rotating with the Earth. The r_{I1}-axis points to the vernal equinox (on the intersection line of equatorial and ecliptic plane) at the reference epoch January 1, 2000, 0^h, 0^{min}, 0^s (J2000.0). The r_{I3}-axis points to the Celestial Ephemeris Pole (CEP) at J2000.0. The r_{I2}-axis complements the other axes to a right-handed equatorial system. Because the system is not a true inertial system, relativistic effects must be taken into account (Hoffmann-Wellenhof et al, 2008).

3.2.2 Earth-fixed coordinate system

The description of locations on or within the Earth is best done in an Earth-fixed coordinate system such as the International Terrestrial Reference System (ITRS, McCarthy and Petit, 2004). Its origin is located in the Earth's center of mass. The r_{E3}-axis is pointing to the mean rotational pole of the Earth at a defined epoch (IERS Reference Pole, IRP). The r_{E1}-axis points to the intersection of the IERS Reference Meridian (IRM, close to the Greenwich meridian) with the equatorial plane. The r_{E2}-axis lies in the equatorial plane 90° to the east and complements the r_{E1}- and r_{E3}-axis to a right-hand-system. The transformation from the quasi-inertial to the Earth-fixed coordinate system and back may be described as follows (Hoffmann-Wellenhof et al, 2008):

$$\begin{aligned} \boldsymbol{r}_E &= \boldsymbol{R}_M \boldsymbol{R}_S \boldsymbol{R}_N \boldsymbol{R}_P \, \boldsymbol{r}_I \ , \\ \boldsymbol{r}_I &= \boldsymbol{R}_P^T \boldsymbol{R}_N^T \boldsymbol{R}_S^T \boldsymbol{R}_M^T \, \boldsymbol{r}_E = \boldsymbol{T} \, \boldsymbol{r}_E \ , \end{aligned} \tag{3.19}$$

with the

$\boldsymbol{r}_I$ coordinate vector in the quasi-inertial system,

$\boldsymbol{r}_E$ coordinate vector in the Earth-fixed system,

$\boldsymbol{R}_M$ rotation matrix for polar motion,

$\boldsymbol{R}_S$ rotation matrix for Greenwich sidereal time,

$\boldsymbol{R}_N$ rotation matrix for nutation,

$\boldsymbol{R}_P$ rotation matrix for precession,

$\boldsymbol{T}$ full transformation matrix.

The computation of the nutation and precession matrices (for the rotation of the CEP from epoch J2000.0 to the true epoch), and of the Greenwich sidereal time (for taking into account the Earth rotation) is defined by the conventions of the International Astronomical Union (IAU, 2000), see also Seidelmann (1992) and Hoffmann-Wellenhof et al (2008). Celestial pole offsets w.r.t. the values given by the IAU models, the excess of the length of day, and the pole coordinates (to take into account the deflection of the IRP from the CEP at the true epoch due to polar motion) are provided by the International Earth Rotation and Reference Systems Service (IERS, McCarthy and Petit, 2004). In this work the IGS realizations (IGS00, IGS00b, IGS05) of the ITRS are used.

3.2.3 Satellite-fixed coordinate system

Some entities such as residuals, non-gravitational perturbation accelerations, and sensor offsets are best described in a satellite- or body-fixed coordinate system with its origin in the satellite's center of mass. One realization of such a system is the so-called RSW-system (Beutler, 2005). R denotes the axis pointing in radial direction away from the central body (i.e., parallel to the position vector). S denotes the axis, which lies normal to the R-axis in the orbital plane and coincides with the velocity vector for a circular orbit. Therefore it is approximately the "along-track" direction. The W-axis is normal to the orbital plane and is therefore called "out-of-plane" or "cross-track" direction. The unit vectors $\boldsymbol{e}_r$, $\boldsymbol{e}_s$, and $\boldsymbol{e}_w$ in the radial, along-track, and cross-track directions at epoch t are computed from the satellite's position vector $\boldsymbol{r}$ and velocity vector $\dot{\boldsymbol{r}}$ in the quasi-inertial system:

$$\begin{aligned} \boldsymbol{e}_r(t) &= \frac{\boldsymbol{r}(t)}{|\boldsymbol{r}(t)|} , \\ \boldsymbol{e}_w(t) &= \frac{\boldsymbol{r}(t) \times \dot{\boldsymbol{r}}(t)}{|\boldsymbol{r}(t) \times \dot{\boldsymbol{r}}(t)|} , \\ \boldsymbol{e}_s(t) &= \boldsymbol{e}_w(t) \times \boldsymbol{e}_r(t) . \end{aligned} \tag{3.20}$$

3.3 Satellite orbits

An Earth satellite is a celestial body that orbits the Earth and obeys Newton's law of gravity. In a first approximation a satellite orbit is an elliptic curve that can be described by Kepler's laws of planetary motion. In fact, however, satellite orbits are disturbed. Gravitational perturbations are caused by the masses of third celestial bodies (other planets, Sun, and Moon) and by the irregular shape, mass distribution, and tidal deformation of the Earth. Non-gravitational perturbations are caused by the Earth's upper atmosphere (only LEOs), by the Sun's direct radiation pressure, and by albedo pressure due to radiation re-emitted from the Earth's surface. Satellites are extended objects with a sometimes complex shape. This has to be considered when modeling the non-gravitational forces acting on the satellite.

The equation of motion describes the motion of the satellite's center of mass around the Earth in the quasi-inertial coordinate system, while the measurements refer to the reference point of the measurement device (in this work the GPS antenna or the SLR reflector). Therefore the offset vector of the device, w.r.t. the satellite's center of mass has to be known. Some measurements are provided in a satellite-fixed coordinate system (e.g., accelerometer measurements). The orientation of the offset vectors and the instruments in the inertial space is determined by the satellite's attitude. On active satellites the attitude is maintained and/or measured.

3.3.1 Dynamic orbits

A dynamic satellite orbit is described by a set of initial values or of boundary values and by a force model, which allows a continuous computation of satellite positions (Beutler, 2005). The initial values define particular solutions of the satellite's equation of motion and refer to the satellite's center of mass in the quasi-inertial system. They may be defined by the position ($\boldsymbol{r}_0$) and velocity vector ($\dot{\boldsymbol{r}}_0$) of the satellite at the initial epoch t_0 (together called initial state vector). Starting from the initial state vector the satellite's position vector $\boldsymbol{r}(t)$ and velocity vector $\dot{\boldsymbol{r}}(t)$ (together called state vector) at every subsequent epoch t might be computed by numerical integration of the equation of motion.

A dynamic orbit might also be described by a set of six Kepler elements at t_0. Both representations are equivalent and can be transformed into each other (see, e.g., Montenbruck and Gill, 2000; Beutler, 2005). The relation between the state vector representation and the orbit representation by the six Kepler elements a, e, i, Ω, ω, and u_0 at time t_0 is illustrated in Fig. 3.1. The semi-major axis a and the numerical eccentricity e describe the size and shape of the orbit, the inclination i and the right ascension Ω of the ascending node the orientation of the orbital plane w.r.t. the Earth's equator, the argument ω of the perigee Π describes the orientation of the orbit in the orbital plane, and the argument of latitude u_0 describes the satellite's position in its orbit relative to the ascending node Ω at time t_0 (Beutler, 2005). The initial Kepler elements (subsequently called initial conditions) are estimated in a dynamic orbit determination from original measurements (e.g., GPS, SLR, or Doppler measurements) or from pseudo-observations (e.g., kinematic positions). For an undisturbed Kepler orbit (two-body problem) the six Kepler elements would be constant in time.

In reality, however, satellite orbits are disturbed and the Kepler elements are changing in time. The elements (at epoch t) resulting from $\boldsymbol{r}(t)$ and $\dot{\boldsymbol{r}}(t)$ according to the formulas of the two body problem are called osculating elements. Precise orbit determination asks for the use of realistic dynamic models for the perturbation forces acting on the satellite: The Earth cannot be considered to be a point mass. Its mass distribution must be taken into account by using a sophisticated gravity field model. This is especially important for LEO satellites. The required maximum degree of the gravity field model depends on the orbit characteristics of the satellite. The lower the satellite orbit, the stronger the influence of the high degree terms of the gravity field. The solid Earth tides, the ocean

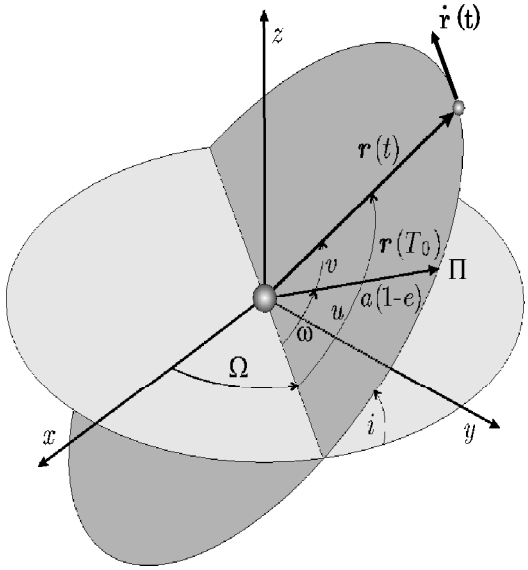

Figure 3.1: Osculating elements a, e, i, Ω, ω, u and state vector $\boldsymbol{r}(t)$, $\dot{\boldsymbol{r}}(t)$.

tides, and the gravitational attractions of third bodies (other planets, Sun, Moon) must also be considered. The third bodies are far away and may usually be treated as point masses (Beutler, 2005). The non-gravitational forces acting on the satellite can be taken into account by dynamical force models. The most important non-gravitational perturbations are air-drag, direct solar radiation pressure, and Earth albedo pressure. For a more complete list we refer to Beutler (2005). Every model is of limited accuracy. Especially the aerodynamic forces acting on LEO satellites are difficult to model due to the large uncertainties of the upper atmosphere density models (Bruinsma et al, 2004). The effect of model uncertainties may be reduced by estimating model parameters (e.g., scaling factors, offsets) in addition to the initial conditions. On the other hand the estimated model parameters themselves may be of interest. This is exactly the case, when satellite orbits are used for gravity field recovery, where the differences of the gravity field parameters as "sensed" by the actual orbit to the parameters of an a priori gravity field model are of interest.

Non-gravitational perturbing forces may alternatively be measured on-board the satellite, e.g., by the on-board accelerometers of the CHAMP and GRACE satellites. These measurements are, however, also affected by errors, noise, offsets, scales, and instrument drifts. Instrument parameters such as scale and offset values may be estimated in addition to the initial conditions.

Perturbations that are not or not sufficiently covered by force models or measurements may be described approximately by constant, polynomial, or trigonometric functions in the force model. The coefficients of these functions might be estimated in the orbit deter-

mination. For more details consult Beutler et al (1994) and Bock (2004). Subsequently the coefficients of force functions, model parameters, and scaling/offset parameters of accelerometer measurements are called dynamical parameters.

For LEO satellites unmodeled or insufficiently modeled perturbations can accumulate to a noticeable size after short time intervals. Therefore the orbit is sub-divided into so-called orbit arcs of pre-defined length. For every arc a new set of initial conditions is estimated. An extreme example is the so-called short-arc approach with arc lengths of, e.g., only 5–30 minutes. However, such an orbit representation shows discontinuities at the arc boundaries.

3.3.2 Reduced-dynamic orbits

Insufficiently modeled perturbations may instead be absorbed by pseudo-stochastic (also called empirical) orbit parameters (Beutler et al, 1994). In contrast to the short-arc method the continuity of the orbit is preserved. Two types of empirical parameters implemented into the BSW are used in this work: Pseudo-stochastic pulses are instantaneous velocity changes at pre-defined epochs in pre-determined directions (Beutler et al, 1994; Beutler, 2005). Piecewise constant accelerations are empirical accelerations in pre-determined directions, constant for a certain time-interval (Jäggi, 2007). If pseudo-stochastic orbit parameters are estimated in addition to the six initial conditions, we speak of a reduced-dynamic orbit. If the time interval between the pseudo-stochastic parameters approaches the spacing of the observations we speak of a highly reduced-dynamic orbit (Jäggi et al, 2006). The number of empirical parameters and the size of their constraints determine, whether a reduced-dynamic orbit is purely deterministic, purely kinematic, or something in between. Therefore the empirical parameters are a very flexible but delicate instrument for modeling satellite orbits with different characteristics. The influence of certain perturbing forces depends, e.g., on the orbit characteristics of the satellite. Gravitational perturbations, which are very important for LEO satellites become less important with increasing orbital height (due to signal attenuation). The same is true for atmospheric drag. Therefore reduced-dynamic orbits of satellites at high altitudes (e.g., GPS satellites) are usually modeled in a "less reduced and more dynamic" mode than LEO orbits. A comparison of the perturbing accelerations acting on LEO and GPS satellites is given by Beutler (2005). The properties and the efficient handling of different types of pseudo-stochastic parameters in the orbit determination using LSA is described by Jäggi (2007).

3.3.3 Kinematic orbits

The kinematic orbit representation is a list or table of discrete satellite positions at certain epochs. The position time series may contain data gaps. Today kinematic positions of LEO satellites may be determined with GNSS (Švehla and Rothacher, 2002). Depending on the noise level and observation geometry of the coordinate estimation the kinematic positions may scatter more or less around the true trajectory. Kinematic LEO coordinates

may be given in the Earth-fixed reference system or in the quasi-inertial system. They may refer to any part of an object (e.g., the GPS antenna). For a satellite, however, it makes sense, when they describe the trajectory of the spacecraft's center of mass. Kinematic positions are purely geometric information. They are well suited as pseudo-observations in a gravity field determination, because they are not affected by a priori force model information of the LEO satellite. One should, however, keep in mind that kinematic positioning is influenced by the force models used for the dynamic determination of the GNSS orbits.

3.4 The equation of motion

A satellite in the quasi-inertial system obeys the equation of motion, which is written in a generic way (tidal accelerations neglected) by Beutler (2005):

$$\ddot{\boldsymbol{r}} = -G \int_{V_E} \rho(\boldsymbol{r}_p) \frac{\boldsymbol{r} - \boldsymbol{r}_p}{|\boldsymbol{r} - \boldsymbol{r}_p|^3} \, dV_E - G \sum_{j=1}^{n} m_j \left(\frac{\boldsymbol{r} - \boldsymbol{r}_j}{|\boldsymbol{r} - \boldsymbol{r}_j|^3} + \frac{\boldsymbol{r}_j}{{r_j}^3} \right) + \sum \boldsymbol{a}_{ng} \ , \tag{3.21}$$

with the

$\ddot{\boldsymbol{r}}$ total acceleration vector of the satellite,

$\boldsymbol{r}$ geocentric position vector of the satellite,

$\boldsymbol{r}_p$ geocentric position vector of the Earth's mass element p,

$\boldsymbol{r}_j$ geocentric position vector of the celestial body j,

m_j mass of the attracting celestial body j,

$\rho(\boldsymbol{r}_p)$ density of the Earth at position $\boldsymbol{r}_p$,

dV_E volume element of the Earth,

G gravity constant, and

$\boldsymbol{a}_{ng}$ non-gravitational acceleration.

The first term on the right-hand side of Eq. (3.21) describes the gravitational acceleration of the Earth acting on the satellite. The mass M_E of the Earth is given as integral of the density function $\rho(\boldsymbol{r}_p)$ over all volume elements dV_E forming the planet:

$$M_E = \int_{V_E} \rho(\boldsymbol{r}_p) \, dV_E \ . \tag{3.22}$$

The second term on the right-hand side of Eq. (3.21) describes the gravitational attraction of the satellite by other celestial bodies. The third term represents the sum of the non-gravitational accelerations. The gravitational acceleration of the Earth (first term in

Eq. (3.21)) could also be written as the gradient of the gravitational potential $V(\boldsymbol{r})$:

$$\ddot{\boldsymbol{r}} = \boldsymbol{\nabla} V(\boldsymbol{r}) \ . \tag{3.23}$$

The gravitational potential of the Earth is then:

$$V(\boldsymbol{r}) = G \int_{V_E} \frac{\rho(\boldsymbol{r}_p)}{|\boldsymbol{r} - \boldsymbol{r}_p|} \, dV_E \ . \tag{3.24}$$

Because the density function refers to the Earth, which is rotating with respect to the quasi-inertial system, the Earth's gravitational potential is described in the Earth-fixed coordinate system and rotated into the quasi-inertial system using the transformation matrix $\boldsymbol{T}$ that is defined in Eq. (3.19). The equation of motion may finally be expressed as:

$$\ddot{\boldsymbol{r}} = \boldsymbol{T} \boldsymbol{\nabla} V(\boldsymbol{r}) - G \sum_{j=1}^{n} m_j \left(\frac{\boldsymbol{r} - \boldsymbol{r}_j}{|\boldsymbol{r} - \boldsymbol{r}_j|^3} + \frac{\boldsymbol{r}_j}{{r_j}^3} \right) + \sum \boldsymbol{a}_{ng} \ . \tag{3.25}$$

Subsequently we focus on the Earth's gravity potential $V(\boldsymbol{r})$ in the first term on the right-hand side of Eq. (3.25).

3.5 Spherical harmonic representation of the gravitational potential

The Earth's gravity potential (Eq. (3.24)) may be expressed for every point outside the Earth (described by its spherical coordinates) by a spherical harmonic (SH) expansion (Heiskanen and Moritz, 1967):

$$V(r, \lambda, \phi) = \frac{GM}{r} \sum_{n=0}^{\infty} \left(\frac{a_E}{r} \right)^n \sum_{m=0}^{n} P_n^m(\sin\phi) \left(C_{nm} \cos m\lambda + S_{nm} \sin m\lambda \right) \ , \tag{3.26}$$

with the

a_E equatorial radius of the Earth,

n degree of the SH expansion,

m order of the SH expansion,

P_n^m associated Legendre functions of degree n and order m,

C_{nm}, S_{nm} SH coefficients of degree n and order m, and

r, ϕ, λ spherical geocentric coordinates of the satellite (radius, latitude, longitude).

The Legendre functions are defined as:

$$\begin{aligned} P_n^0(x) &= P_n(x) = \tfrac{1}{2^n n!}\tfrac{d^n}{dx^n}\left((x^2-1)^n\right) \\ P_n^m(x) &= (1-x^2)^{\frac{m}{2}}\tfrac{d^m}{dx^m}\left(P_n(x)\right)\ ,\ m = 0,1,\ldots,n\ , \end{aligned} \tag{3.27}$$

where $P_n(x)$ are the Legendre polynomials. In the gravity field determination the dimensionless coefficients C_{nm} and S_{nm} of the SH functions are the unknown parameters. Often (and also in this work) the fully normalized form $\bar{C}_{nm}$ and $\bar{S}_{nm}$ of the SH coefficients is used. The fully normalized SH coefficients and Legendre functions are defined by Heiskanen and Moritz (1967):

$$\begin{aligned} \bar{C}_{n0} &= \tfrac{1}{\sqrt{2n+1}}\ C_{n0} \\ \bar{C}_{nm} &= \sqrt{\tfrac{(n+m)!}{2(2n+1)(n-m)!}}\ C_{nm}\ ,\ m>0 \\ \bar{S}_{nm} &= \sqrt{\tfrac{(n+m)!}{2(2n+1)(n-m)!}}\ S_{nm}\ ,\ m>0 \\ \bar{P}_n^0(sin\phi) &= \sqrt{2n+1}\ P_n^0(sin\phi) \\ \bar{P}_n^m(sin\phi) &= \sqrt{\tfrac{2(2n+1)(n-m)!}{(n+m)!}}\ P_n^m(sin\phi)\ ,\ m>0\ . \end{aligned} \tag{3.28}$$

In Eq. (3.26) the terms with $m = 0$ are called zonal coefficients. They do not depend on the longitude and describe a rotationally symmetric body with $n+1$ latitude zones. Terms with $n = m$ are not latitude-dependent. These sectorial coefficients define $2n$ sectors. The tesseral terms with $m \neq 0$ and $m \neq n$ depend on latitude and longitude. The C_{00} term is equal to one. If the coefficients refer to a coordinate system with its origin in the Earth's center of mass (this is the case in this work), the values of the C_{10}, C_{11}, and S_{11} coefficients are zero. If the axes of the coordinate system coincide with the Earth's principal axes of inertia (this is not the case in this work), the coefficients C_{21}, S_{21}, and S_{22} are zero, too (Beutler, 2005). The C_{20}-term is the largest perturbation term. It characterizes the flattening of the Earth. The S_{n0} coefficients are zero by definition. The term $\left(\frac{a_E}{r}\right)^n$ in Eq. (3.26) reflects the stronger attenuation of the gravity field signal of the higher SH degrees with increasing distance from the Earth's surface.

The half wavelength resolution of the SH expansion

$$res \approx \frac{40000\,\mathrm{km}}{2n_{max}}\ , \tag{3.29}$$

depends on the maximum degree n_{max}. The number of SH coefficients is given by

$$u_{SH} = (n_{max}+1)^2\ . \tag{3.30}$$

The power of the gravity potential signal at degree n of the SH expansion may be expressed by the signal degree amplitude SDA_n (Ilk et al, 2005):

$$SDA_n = \sqrt{\sum_{m=0}^{n} \left(\bar{C}_{nm}^2 + \bar{S}_{nm}^2\right)} \; . \tag{3.31}$$

Different gravity field models a and b may be compared degree-wise by computing the difference degree amplitude $DDA_{ab,n}$ (Ilk et al, 2005):

$$DDA_{ab,n} = \sqrt{\sum_{m=0}^{n} \left(\Delta\bar{C}_{nm}^2 + \Delta\bar{S}_{nm}^2\right)} \; , \tag{3.32}$$

with $\Delta\bar{C}_{nm} = \bar{C}_{a,nm} - \bar{C}_{b,nm}$ and $\Delta\bar{S}_{nm} = \bar{S}_{a,nm} - \bar{S}_{b,nm}$. The error degree amplitude EDA_n represents the formal error (covariances neglected) of a gravity field model at degree n and may be described as a function of the formal errors of the SH coefficients (Ilk et al, 2005):

$$EDA_n = \sqrt{\sum_{m=0}^{n} \left(\sigma_{\bar{C}_{nm}}^2 + \sigma_{\bar{S}_{nm}}^2\right)} \; . \tag{3.33}$$

The SH coefficients may be used to compute functionals of the disturbing gravitational potential. The disturbing potential is obtained by subtracting an ellipsoidal normal potential from the gravity potential. The normal potential is expressed by the low even zonal SH coefficients ($\bar{C}_{00}^{ell}$,$\bar{C}_{20}^{ell}$,...) of a selected reference ellipsoid. The geoid undulation (or geoid height) is the deviation of the geoid from the reference ellipsoid. It is expressed by Ilk et al (2005) as:

$$N(a_E, \lambda, \phi) = a_E \left(\sum_{n=0}^{n_{max}} \sum_{m=0}^{n} \bar{P}_n^m(\sin\phi) \left(\bar{C}'_{nm} \cos m\lambda + \bar{S}_{nm} \sin m\lambda \right) \right) \; , \tag{3.34}$$

with $\bar{C}'_{nm} = \bar{C}_{nm} - \bar{C}_{nm}^{ell}$. The gravity anomaly (or free-air anomaly) is the difference between the gravity at a point on the geoid and the (normal) gravity at the corresponding point on the normal potential surface (the reference ellipsoid) (Hoffmann-Wellenhof and Moritz, 2006). In Ilk et al (2005) it is expressed as:

$$\begin{aligned} \Delta g(a_E, \lambda, \phi) \;\; = \;\; & \frac{GM}{a_E^2} \left(-\bar{C}'_{00} + \sum_{n=2}^{n_{max}} (n-1) \sum_{m=0}^{n} \bar{P}_n^m(\sin\phi) \right. \\ & \left. \left(\bar{C}'_{nm} \cos m\lambda + \bar{S}_{nm} \sin m\lambda \right) \right) \; . \end{aligned} \tag{3.35}$$

3.6 Orbit and gravity field determination

Orbit determination estimates the parameters describing a particular arc of a dynamic or a reduced-dynamic orbit (orbit parameters or arc-specific parameters, see Sect. 3.3). In the case of gravity field determination the coefficients $\bar{C}_{nm}$ and $\bar{S}_{nm}$ of the SH expansion (see Eqs. (3.26, 3.28)) are determined in addition as general, non arc-specific dynamical parameters. The parameter array $\boldsymbol{P}$ may then be written as:

$$\boldsymbol{P} \in \{O_1, \ldots, O_6, D_1, \ldots, D_d, S_1, \ldots, S_s\} \ , \tag{3.36}$$

with the

$O_1, \ldots, O_6$ six osculating elements $(a, e, i, \Omega, \omega, u_0)$ at the initial epoch t_0,

$D_1, \ldots, D_d$ d dynamical parameters (orbit and gravity field parameters), and

$S_1, \ldots, S_s$ s pseudo-stochastic orbit parameters.

In this work the parameters are estimated in a LSA using kinematic positions as pseudo-observations. In order to compute the observed-minus-computed term in the LSA we need to compute the satellite positions from the orbit model, which is described by the satellite's equation of motion Eq. (3.21), for every observation epoch. This is done by performing a numerical integration of the so-called initial value problem of the primary equations, which is defined by the equation of motion and the satellite's state vector (Sect. 3.3.1) at the initial epoch (Beutler, 2005):

$$\begin{aligned} \ddot{\boldsymbol{r}} &= \boldsymbol{f}(t, \boldsymbol{r}, \dot{\boldsymbol{r}}, \boldsymbol{P}) \ , \\ \boldsymbol{r}_0 &= \boldsymbol{r}(t_0; a, e, i, \Omega, \omega, u_0) \ , \\ \dot{\boldsymbol{r}}_0 &= \dot{\boldsymbol{r}}(t_0; a, e, i, \Omega, \omega, u_0) \ , \end{aligned} \tag{3.37}$$

with the

$\boldsymbol{f}$ satellite's equation of motion Eq. (3.21), and

$\boldsymbol{r}_0$, $\dot{\boldsymbol{r}}_0$ state vector at the initial epoch t_0.

In addition we need to define the design matrix of the LSA in Eq. (3.2), containing the partial derivatives of the orbit w.r.t. the estimated parameters $\boldsymbol{P}$ as a function of time. This is done by performing a numerical integration of the so-called variational equations. The system of variational equations belonging to parameter P_j is defined by Beutler (2005) as:

$$\begin{aligned} \ddot{\boldsymbol{z}}_{P_j} &= \boldsymbol{A}_0 \cdot \boldsymbol{z}_{P_j} + \boldsymbol{A}_1 \cdot \dot{\boldsymbol{z}}_{P_j} + \boldsymbol{f}_{P_j} \ , \\ \boldsymbol{z}_{0,P_j} &= \boldsymbol{z}_{P_j}(t_0; a, e, i, \Omega, \omega, u_0) \ , \\ \dot{\boldsymbol{z}}_{0,P_j} &= \dot{\boldsymbol{z}}_{P_j}(t_0; a, e, i, \Omega, \omega, u_0) \ , \end{aligned} \tag{3.38}$$

where $\boldsymbol{A}_0$ and $\boldsymbol{A}_1$ are 3×3 matrices that are defined as:

$$\begin{aligned} A_{0,ik} &= \frac{\partial f_i}{\partial r_k} , \\ A_{1,ik} &= \frac{\partial f_i}{\partial \dot{r}_k} , \end{aligned} \tag{3.39}$$

i.e., they contain the partial derivatives of the components of $\boldsymbol{f}$ w.r.t. the components of the state vector. The column arrays $\boldsymbol{z}_{P_j}$ and $\dot{\boldsymbol{z}}_{P_j}$ are defined as:

$$\begin{aligned} \boldsymbol{z}_{P_j} &= \frac{\partial \boldsymbol{r}}{\partial P_j} , \\ \dot{\boldsymbol{z}}_{P_j} &= \frac{\partial \dot{\boldsymbol{r}}}{\partial P_j} , \end{aligned} \tag{3.40}$$

i.e., they contain the partial derivatives of the position and velocity vectors w.r.t. the parameter P_j. $\boldsymbol{f}_{P_j}$ is a column array containing the explicit derivatives of the components of $\boldsymbol{f}$ w.r.t. the parameter P_j:

$$\boldsymbol{f}_{P_j} = \frac{\partial \boldsymbol{f}}{\partial P_j} . \tag{3.41}$$

$\boldsymbol{f}_{P_j}$ is zero for the initial osculating elements. The initial values $\boldsymbol{z}_{0,P_j}$ and $\dot{\boldsymbol{z}}_{0,P_j}$ are zero for the dynamical parameters. For each unknown parameter P_j a separate initial value problem of the type Eq. (3.38) has to be set up.

3.6.1 Numerical integration of the primary equations

The initial value problem Eq. (3.37) is solved by numerical integration. In a numerical integration the integration interval (e.g., one orbit arc) is subdivided into subintervals of a certain length. Within each subinterval an initial value problem is set up and is numerically approximated by a polynomial. In the first subinterval the initial conditions belonging to the initial epoch t_0 are used. In the subsequent subintervals the initial values are the computed solutions at the end of the previous subinterval. The basic numerical integration method (Euler method) uses a second order polynomial to approximate the initial value problem Eq. (3.37):

$$\begin{aligned} \boldsymbol{r}(t) &= \boldsymbol{r}_0 + (t - t_0) \cdot \dot{\boldsymbol{r}}_0 + \tfrac{1}{2}(t - t_0)^2 \cdot \boldsymbol{f}(t_0, \boldsymbol{r}_0, \dot{\boldsymbol{r}}_0, \boldsymbol{P}) , \\ \dot{\boldsymbol{r}}(t) &= \dot{\boldsymbol{r}}_0 + (t - t_0) \cdot \boldsymbol{f}(t_0, \boldsymbol{r}_0, \dot{\boldsymbol{r}}_0, \boldsymbol{P}) . \end{aligned} \tag{3.42}$$

In the CMA the collocation method is used for orbit integration. It is implemented into the BSW. The collocation method uses approximation functions with a higher polynomial degree of q. They are described by Beutler (2005) as:

$$\boldsymbol{r}(t) = \sum_{i=0}^{q} \frac{1}{i!}(t - t_0)^i \boldsymbol{r}_0^{(i)} \quad , q \geq 2 , \tag{3.43}$$

where the $\boldsymbol{r}_0^{(i)}$ are the coefficients. The coefficients are determined by setting up $q-1$ condition equations that are solved iteratively. For a detailed discussion we refer to Beutler (2005).

3.6.2 Numerical integration of the variational equations

In the variational equations Eq. (3.38) belonging to the six initial osculating elements the values of $\boldsymbol{f}_{P_j}$ are zero. For this parameter type the system of variational equations consists only of the so-called homogeneous part. The homogeneous variational equations are, like the primary equation, solved by numerical integration.

In the variational equations belonging to the dynamical parameters (including the gravity field parameters) $\boldsymbol{f}_{P_j}$ is different from zero. On the other hand the initial conditions $\boldsymbol{z}_{0,P_j}$ and $\dot{\boldsymbol{z}}_{0,P_j}$ are zero. The variational equations belonging to these parameters are inhomogeneous. Use is made of the fact that each solution of the inhomogeneous variational equations may be written as a linear combination of six independent solutions of the homogeneous variational equations (Beutler, 2005). The coefficients of these linear combinations are expressed by definite integrals that are solved in an efficient way using the technique of numerical quadrature (Beutler, 2005).

The variational equations belonging to the pseudo-stochastic parameters are inhomogeneous, as well. Their very efficient computation from a linear combination of the partial derivatives of the a priori orbit w.r.t. the six initial osculating elements at t_0 is described by Jäggi (2007).

4 Global Positioning System - GPS

This chapter provides a short and general overview of the GPS, GPS signal processing, the IGS, and the GPS processing software used in this work. The information is based on Leick (1995), Teunissen and Kleusberg (1998), Dach et al (2007), Jäggi (2007), and Hoffmann-Wellenhof et al (2008). More detailed information may be found in these references.

4.1 History

The Navigation Satellite System for Timing and Ranging - Global Positioning System, short NAVSTAR-GPS (GPS), is a Global Navigation Satellite System (GNSS). Its development by the U.S. Department of Defence (DoD) started in the 1970ies. A first series of ten experimental GPS Block-I satellites was launched between 1978 and 1985 for concept validation. From 1989 onwards the first operational satellites of the Block-II type were launched. The first Block-IIA satellite followed in 1990. In late 1993 GPS achieved its initial operational capability and was declared fully operational in spring 1995, meaning that the full constellation of 24 operational satellites was in orbit for the first time. In the following years the constellation was modernized by replacing old vehicles reaching the end of their lifetime by new, more enhanced satellites. The first Block-IIR satellite was launched in 1997, the first Block-IIR-M satellite in 2005 and the first Block-IIF satellite in 2010. GPS is a military system, but it is open for civilian use. From spring 2000 on the "Selective Availability" deteriorating the satellite clock frequency information for civilian users, was turned off. Although GPS was intended as a navigational system (i.e., for kinematic positioning) it is also used stationary and for other purposes than positioning.

4.2 Basic measurement principle

The GPS measurement principle is based on the arc section of range measurements from different GPS satellites to the receiver. The orbital elements of the satellites are known. They are emitted by the satellites as part of the so-called navigation message. With this information a receiver may compute the satellite positions at their signal emission times. With the known velocity of light the distance between a GPS satellite and the receiver is determined by measuring the one-way traveling time of the microwave signal emitted by the satellite. Therefore, the emission time at the satellite is modulated as a time-code on the carrier signal and compared with the reception time at the receiver. Transmitting and reception time must refer to a common time reference — the GPS system time. The GPS system time has a constant offset of 19 seconds w.r.t. the TAI, the

international atomic time (Hoffmann-Wellenhof et al, 2008). Each GPS satellite carries redundant highly accurate and stable atomic clocks. The receivers usually use a less stable quartz-oscillator to generate the time signal. For kinematic positioning at least four measurements are required at every observation epoch, because the receiver clock correction has to be estimated (synchronized to GPS system time) in addition to the three coordinates defining the receiver position. For non-kinematic applications less than four measurements per epoch are required, because the measurements of several observation epochs can contribute to a solution.

4.3 GPS orbit constellation and satellites

The constellation of the operational GPS satellites is established in a way that provides a global coverage with at least four simultaneous observable satellites over 15 ° elevation (Hoffmann-Wellenhof et al, 2008). This is accomplished by at least 24 satellites, which are distributed in six orbital planes that are equally separated by 60 ° on the equator. The GPS orbits are almost circular, have a semi major axis of about 26560 km, and an inclination of 55 ° w.r.t. the equatorial plane. The orbital period is 11 hours and 58 minutes (half of a sidereal day).

The GPS satellites consist mainly of the satellite body, containing the navigational equipment, and two large solar panels. The antenna array is located on the front side of the satellite body, which is permanently pointing towards the Earth. The orientation of the spacecraft is measured by Earth- and Sun-sensors and is actively maintained by reaction wheels. In eclipsing phases the sun sensors are not usable and the satellite's attitude might not be nominal (Bar-Sever, 1994, 1996). Their large surface makes GPS satellites susceptible for radiation pressure forces, which must be taken into account in a precise orbit determination. Atmospheric drag may be neglected at this altitude. Due to the high orbit and the signal attenuation, the influence of high degree terms of the Earth's gravitational and tidal potential is small and only the low degrees need to be considered. GPS satellite orbits are described as dynamic orbits or reduced-dynamic orbits with a very low number of empirical orbit parameters. For a comparison of LEO and GPS satellite orbits regarding their sensitivity to different orbit perturbations we refer to Beutler (2005).

4.4 GPS signals

The notation used in this section and in Sect. 4.5 is based on the notation used by Jäggi (2007) and Dach et al (2007). The GPS satellites send their information on two carrier signals (L_1 and L_2) in the L-band. Starting with the Block-IIF satellites (first launch on 17 April 2010) GPS supports a third carrier signal (L_5). The carrier frequencies are derived from a fundamental frequency, which is generated by the satellite oscillator (atomic clock). The time-code and the navigation message are modulated on the carrier signals. The code consists of so-called pseudo-random noise (PRN) sequences, which are

unique for each satellite (Dach et al, 2007). The currently available GPS carrier signals and the accompanying code sequences are listed in Table 4.1. The so-called coarse/acquisition

Table 4.1: GPS signal types (Hoffmann-Wellenhof et al, 2008).

Carrier	Frequency [MHz]	Wavelength [cm]	PRN code	GPS satellite type
L_1	$f_1 = 1575.42$	$\lambda_1 = 19.0$	C/A	All
			P(Y)	All
			M	Block-IIR-M and later
L_2	$f_2 = 1227.60$	$\lambda_2 = 24.4$	P(Y)	All
			L2C	Block-IIR-M and later
			M	Block-IIR-M and later
L_5	$f_5 = 1176.45$	$\lambda_5 = 25.5$	L5C	Block-IIF and later

(C/A)-code and the new $L2C$ and $L5C$ codes are intended for civilian use. The more precise P-code is intended for military use. It is usually encrypted by a procedure called "Anti-Spoofing" (AS), converting it into the Y-code. The M-code is a new military code. For more information about present and future GPS signals we refer to Hoffmann-Wellenhof et al (2008).

The navigation message contains information concerning the satellite clock (e.g., clock correction, time since beginning of current GPS-week), the satellite orbit (e.g., orbital elements, initial epoch, correction terms), and the satellite health status. Using the orbital elements from the navigation message (the so-called broadcast ephemerides) the positions of the GPS satellites may be computed with an accuracy of several meters in real-time (Dach et al, 2007).

GPS receivers provide code measurements with a noise level of some decimeters (Dach et al, 2007). The code observation P_i^k is the measured distance between satellite k and receiver i and may be expressed as:

$$P_i^k = c\,(T_i - T^k)\ , \tag{4.1}$$

with the

P_i^k code observation (in meters),

c velocity of light,

T_i arrival time of the signal, measured by the clock of receiver i, and

T^k transmission time of the signal, measured by the clock of satellite k.

Geodetic GNSS receivers are also able to correlate the received and the reference carriers and measure the phase-shift between both carriers with an accuracy of a few millimeters (Dach et al, 2007). The distance between satellite and receiver is measured in units of

signal cycles. A full signal cycle complies with the signal's wavelength. The number of full signal cycles at the beginning of the tracking is unknown. The so-called initial phase ambiguity n_i^k must therefore be estimated in the parameter estimation. Its value is constant as long as the corresponding satellite is tracked without interruption. A phase measurement between satellite k and receiver i may be expressed as:

$$L_i^k = \lambda \left(\phi_i - \phi^k + n_i^k \right) , \tag{4.2}$$

with the

L_i^k phase observation (in meters),

λ wavelength of the carrier signal,

ϕ_i carrier phase of the reference signal generated by the receiver i at measured arrival time T_i,

ϕ^k carrier phase of the transmitted signal at measured transmission time T^k, and

n_i^k initial carrier phase ambiguity (in integer cycles of λ).

The usual ensemble of measurements provided by a geodetic GPS receiver consists of the C/A- and/or P_1- (both modulated on the L_1-carrier), $L2C$ and/or P_2-code (modulated on the L_2-carrier) measurements, and the L_1- and L_2-carrier phase measurements. Some GPS receivers do not strictly stick to this scheme: The BlackJack GPS receiver, which is used on the CHAMP and GRACE satellites, provides C/A-, P_1-, and P_2-code, and LA-, L_1-, and L_2-phase measurements (Köhler, 2001). The L_1-phase is reconstructed using either the C/A-code (LA-observable) or the P_1-code (L_1-observable). The LA-observable has a lower noise level than the L_1-observable (Dunn et al, 2003; Montenbruck and Kroes, 2003). Therefore the LA-phase observation is used instead of the L_1-observation for CHAMP POD in this work.

4.5 Modeling GPS observables

This section briefly reviews the GPS observation equations, the forming of observation differences, and the most important linear combinations. The most important error sources are considered. For a more detailed discussion we refer to the literature, e.g., Rothacher (1992), Mervart (1995), Teunissen and Kleusberg (1998), and Schaer (1999).

4.5.1 Observation equations

The code and phase measurements are influenced by satellite and receiver clock offsets w.r.t. the GPS system time, which are related to to the measured transmission (T^k) and arrival (T_i) times in the following way:

$$\begin{aligned} T^k &= t^k + \delta t^k , \\ T_i &= t_i + \delta t_i , \end{aligned} \tag{4.3}$$

with the

t^k signal transmission time at satellite k in the GPS time system,

t_i signal reception time at receiver i in the GPS time system,

δt^k clock offset of satellite k,

δt_i clock offset of receiver i.

The receiver clock offset δt_i is usually estimated for each observation epoch. Predictions of the satellite clock offsets δt^k are transmitted to the receiver by the navigation message. For some applications (e.g., zero-difference positioning with high accuracy demands) the predicted clock offsets may not be accurate enough. More accurate, epoch-wise estimated GPS satellite clock corrections are, e.g., provided by the IGS.

Furthermore, GPS measurements are affected by the Earth's atmosphere, which delays the signal. For microwave signals such as GPS signals, two parts of the atmosphere are of interest: the troposphere and the ionosphere. They influence GPS signals in different ways and are thus specified separately in the observation equation of a code measurement (Dach et al, 2007):

$$P_i^k = s_i^k + c \cdot \delta t_i - c \cdot \delta t^k + \delta s_{i,trop}^k + \delta s_{i,ion}^k \ , \tag{4.4}$$

with the

s_i^k slant range,

$\delta s_{i,trop}^k$ signal delay due to the troposphere (in meters), and

$\delta s_{i,ion}^k$ signal delay due to the ionosphere (in meters).

The corresponding carrier phase observation equation may be formulated as (Dach et al, 2007):

$$L_i^k = s_i^k + c \cdot \delta t_i - c \cdot \delta t^k + \delta s_{i,trop}^k - \delta s_{i,ion}^k + \lambda \cdot n_i^k \ . \tag{4.5}$$

The tropospheric refraction $\delta s_{i,trop}^k$ is the effect of the neutral, non-ionized part of the Earth's atmosphere on the signal propagation. It does not depend on the frequency and is the same for code and phase observations. The tropospheric refraction may be modeled to a large extent. Tropospheric zenith path delays and tropospheric gradients may as well be estimated. At LEO altitudes the tropospheric delay is negligible.

The ionosphere is the ionized part of the Earth's higher atmosphere. It is dispersive for microwave signals. The ionospheric refraction $\delta s_{i,ion}^k$ is at first order proportional to $1/f^2$ (Dach et al, 2007). It delays the code measurements and advances the carrier phases. The absolute value is the same for both measurement types. Dual frequency data processing makes use of the dispersive nature of the ionosphere to eliminate the effect by forming an ionosphere-free linear combination (to be explained later). For single frequency data processing ionospheric measurements, such as the ionosphere maps provided by the IGS,

may be used to model the effect.

The slant range s_i^k in Eqs. (4.4) and (4.5) is the geometric distance between receiver i and satellite k and might be expressed by:

$$s_i^k = c\,(t_i - t^k) = |\boldsymbol{r}_i - \boldsymbol{r}^k| \;, \tag{4.6}$$

with the

$\boldsymbol{r}^k$ position vector of the transmission antenna of satellite k at signal transmission time t^k and

$\boldsymbol{r}_i$ position vector of receiver antenna i at signal reception time t_i.

The slant range establishes the geometric relation between the usually known satellite position at transmission time and the usually unknown receiver position at signal reception time. Predicted satellite orbits (the so-called broadcast ephemerides) are known from the navigation message (see Sect. 4.4). For precise post-processing applications more accurate estimated GPS orbits are provided, e.g., by the IGS.

The geometric distance s_i^k in fact refers to the phase centers of the transmitting and receiving GPS antennas. The antenna phase center varies for different directions of outgoing/incoming GPS signals (phase center variations (PCV)) and might be corrected by a phase center model (Dach et al, 2007):

$$\Delta\Phi(\alpha, z) = \Delta\Phi'(\alpha, z) + \boldsymbol{\Delta r} \;, \tag{4.7}$$

with the

$\Delta\Phi(\alpha, z)$ total phase center correction,

α, z the azimuth and the zenith (receiving antenna) / nadir (transmitting antenna),

$\boldsymbol{\Delta r}$ mean phase center offset (PCO) vector w.r.t. the antenna reference point (receiving antenna) / satellite's center of mass (transmitting antenna), and

$\Delta\Phi'(\alpha, z)$ direction-dependent phase center variation (PCV).

In the case of the relative PCV-model used by the IGS until November 2006 the receiver antennas are calibrated relative to a certain antenna type that is assumed to be "perfect" by definition (i.e., only the phase center differences to the reference antenna are modeled). For the transmitting antennas of the GPS satellites only the phase center offset is considered when using this IGS standard. For more information about PCV-modeling in the BSW and within the IGS we refer to Dach et al (2007). The calibration of LEO POD antennas is, e.g., described by Montenbruck et al (2009) and Jäggi et al (2009b).

In summary, the observation equations for one set of P-code and carrier phase observations typically provided by a geodetic dual-frequency GPS receiver at one measurement

epoch are (Dach et al, 2007):

$$\begin{aligned} P_{i,1}^k &= s_i^k + c \cdot \delta t_i - c \cdot \delta t^k + \delta s_{i,trop}^k + \delta s_{i,ion}^k \\ P_{i,2}^k &= s_i^k + c \cdot \delta t_i - c \cdot \delta t^k + \delta s_{i,trop}^k + \frac{f_1^2}{f_2^2} \delta s_{i,ion}^k \\ L_{i,1}^k &= s_i^k + c \cdot \delta t_i - c \cdot \delta t^k + \delta s_{i,trop}^k - \delta s_{i,ion}^k + \lambda_1 \cdot n_{i,1}^k \\ L_{i,2}^k &= s_i^k + c \cdot \delta t_i - c \cdot \delta t^k + \delta s_{i,trop}^k - \frac{f_1^2}{f_2^2} \delta s_{i,ion}^k + \lambda_2 \cdot n_{i,2}^k \ . \end{aligned} \tag{4.8}$$

4.5.2 Observation differences

Some of the aforementioned biases may be eliminated or reduced by forming differences (Dach et al, 2007). The **single difference** code (P_{ij}^k) or phase (L_{ij}^k) observation is the difference of two code or phase (zero difference) observations measured simultaneously by two GPS receivers i and j:

$$L_{ij}^k = L_i^k - L_j^k \ . \tag{4.9}$$

In single difference observations the satellite clock offset is eliminated. In order to ensure simultaneity the receiver clock synchronization must be performed prior to forming the differences. For taking the motion of the GPS satellites properly into account when computing the slant range using Eq. (4.6), the receiver clock offsets must be known and applied with an accuracy of about one microsecond (Dach et al, 2007).

The difference of two simultaneous code or phase single difference observations of the satellites k and l is called **double difference**:

$$L_{ij}^{kl} = L_{ij}^k - L_{ij}^l = (L_i^k - L_j^k) - (L_i^l - L_j^l) \ . \tag{4.10}$$

In double difference observations also the receiver clock offsets are eliminated. Therefore, double difference observations are widely used in geodetic applications. The dual-frequency double difference code and phase observation equations belonging to one epoch might be written as (Dach et al, 2007):

$$\begin{aligned} P_{ij,1}^{kl} &= s_{ij}^{kl} + \delta s_{ij,trop}^{kl} + \delta s_{ij,ion}^{kl} \\ P_{ij,2}^{kl} &= s_{ij}^{kl} + \delta s_{ij,trop}^{kl} + \frac{f_1^2}{f_2^2} \delta s_{ij,ion}^{kl} \\ L_{ij,1}^{kl} &= s_{ij}^{kl} + \delta s_{ij,trop}^{kl} - \delta s_{ij,ion}^{kl} + \lambda_1 \cdot n_{ij,1}^{kl} \\ L_{ij,2}^{kl} &= s_{ij}^{kl} + \delta s_{ij,trop}^{kl} - \frac{f_1^2}{f_2^2} \delta s_{ij,ion}^{kl} + \lambda_2 \cdot n_{ij,2}^{kl} \ . \end{aligned} \tag{4.11}$$

Error sources, which are constant or changing slowly in time might be eliminated or reduced significantly by forming time differences. This is the case for tropospheric refraction and also for the phase ambiguity (as long as no cycle slip occurs). In the BSW time differences are used in the pre-processing of phase observations (Dach et al, 2007).

4.5.3 Linear combinations

If dual-frequency receivers are used, linear combinations (LCs) of carrier phase and/or code observations may be formed for each level of differentiation. The linear combination of two double difference phase observations $L_{ij,1}^{kl}$ and $L_{ij,2}^{kl}$ belonging to the frequencies f_1 and f_2 is, e.g., defined as:

$$L_{ij,n}^{kl} = \kappa_{1,n} \cdot L_{ij,1}^{kl} + \kappa_{2,n} \cdot L_{ij,2}^{kl} \ , \tag{4.12}$$

where $\kappa_{1,n}$ and $\kappa_{2,n}$ are the coefficients of the linear combination n (Hoffmann-Wellenhof et al, 2008). The linear combination of the code observations is defined in an analogue way. When forming the L_3 LC with the coefficients

$$\kappa_{1,3} = \frac{f_1^2}{f_1^2 - f_2^2} \qquad \text{and} \qquad \kappa_{2,3} = \frac{-f_2^2}{f_1^2 - f_2^2} \tag{4.13}$$

use is made of the fact that the ionospheric refraction is proportional to $1/f^2$. The L_3 LC eliminates most of the ionospheric refraction and is therefore called **ionosphere-free linear combination** (Dach et al, 2007):

$$\begin{aligned} P_{ij,3}^{kl} &= s_{ij}^{kl} + \delta s_{ij,trop}^{kl} \\ L_{ij,3}^{kl} &= s_{ij}^{kl} + \delta s_{ij,trop}^{kl} + \lambda_3 \cdot B_{ij,3}^{kl} \ , \end{aligned} \tag{4.14}$$

with the

λ_3 so-called narrow-lane wavelength $\lambda_3 = \kappa_{1,3} \cdot \lambda_1 + \kappa_{2,3} \cdot \lambda_2 \approx 10.7$ cm,

$B_{ij,3}^{kl}$ ionosphere-free bias parameter.

The tropospheric refraction may be modeled. In the case of a receiver onboard a LEO satellite it may be neglected, further simplifying Eq. (4.14). The real-valued bias parameter $B_{ij,3}^{kl}$ has to be estimated or may be computed from the integer ambiguities $n_{ij,1}^{kl}$ and $n_{ij,2}^{kl}$, if they are known. The ionosphere-free or L_3 LC is widely used in the GPS data analysis — also within this work (e.g., in the orbit and clock reprocessing, in the LEO orbit determination). The noise level of L_3 observations is increased by a factor of three compared to the corresponding L_1 and L_2 observations (Dach et al, 2007). For more information about linear combinations and for information about ambiguity resolution we refer to Mervart (1995), Schaer (1999), and Dach et al (2007).

4.6 The International GNSS Service (IGS)

After a successful test campaign in 1992 the International GPS Service for Geodynamics (IGS) was founded in 1994 as an official, non-commercial service of the International Association of Geodesy (IAG, 2010). Since 2005 the service is named International GNSS Service to emphasize the increasing importance of GLONASS. Meanwhile more than 200

organizations in over 80 countries contribute to the service and share their resources in order to define international standards related to the precise positioning using GNSS, run a global tracking network, and generate highly accurate, redundant, and reliable products (Dow et al, 2009).

Today (2010) more than 350 active IGS stations, distributed worldwide, are permanently tracking GNSS satellites (IGS, 2010). About 130 stations with a sampling rate of 1 Hz contribute to the IGS high-rate network (Bock et al, 2009; IGS, 2010). The tracking data and the IGS analysis products are collected, archived, and made available online by regional and global data centers. Analysis centers (ACs) generate the analysis products using the tracking data provided by the data centers. The contributions of the ACs are combined into the official IGS products by the analysis center coordinator (ACC). The Central Bureau and the Governing Board coordinate the IGS activities. The IGS core products are (IGS, 2010):

- GPS satellite ephemerides and orbit predictions,
- GPS satellite clock corrections,
- Earth orientation parameters (polar motion, polar motion rate, and length of day) with a time resolution of one day,
- coordinates and velocities of the IGS tracking stations,
- tracking data of the IGS stations.

They are distributed in different product lines:

- final products: weekly data basis, 12–18 days delay,
- rapid products: daily data basis, 1–2 days delay,
- ultra-rapid products: sub-daily data basis, few hours delay.

Additional products, e.g., GLONASS orbit products, tropospheric zenith delays at the tracking stations, and ionosphere maps are generated by a subset of ACs (IGS, 2010).

The Center for Orbit Determination in Europe (CODE) is one of the IGS ACs. It is a joint venture of the following institutions:

- the Astronomical Institute of the University of Bern (AIUB), Bern, Switzerland,
- the Swiss Federal Office of Topography (swisstopo), Wabern, Switzerland,
- the Federal Office of Cartography and Geodesy (BKG), Frankfurt a.M., Germany, and
- the Institute for Astronomical and Physical Geodesy (IAPG) of the Technische Universität München (TUM), Germany.

CODE is located at the AIUB. Since 21 June, 1992, the start of the IGS test campaign, CODE has significantly contributed to the IGS with a wide range of products, which were always generated with the latest version of the Bernese GPS Software (BSW). At present the development version 5.1 is used (Dach et al, 2009). The CODE products are used for this work wherever possible. For more information about the CODE products and the applied processing strategies we refer to Dach et al (2009) and CODE (2010).

4.7 Bernese GPS Software (BSW)

The BSW is a software package that was developed at the AIUB since 1984 for the highly accurate post-processing of GNSS data. The programs are controlled and launched via a menu system. The programs, the degree of automation, and the diversity of possible applications evolved over the years. The versatility of the BSW is mirrored in the various IGS products, which are produced with CODE's contribution. Additional applications comprise the LEO orbit determination (e.g., GOCE orbit determination in the framework of the High-level Processing Facility (HPF, Koop et al, 2006)), kinematic positioning, SLR data processing, and the computation of GPS clock corrections with short data intervals (< 30 s). The processing is done session-wise, i.e., the data interval is sub-divided into time intervals of pre-defined length (e.g., one day). The normal equation (NEQ) systems belonging to different sessions may be stacked by the NEQ stacking program of the BSW. This program is also able to pre-eliminate or constrain parameters. For automated data processing the BSW offers the Bernese Processing Engine (BPE). The BPE allows to run programs sequentially or in parallel mode for many sessions at the same time. Computing jobs may be performed on the local machine or sent to an external computing cluster. In the latter case the BPE establishes data connections to the remote hosts.

Gravity field determination in this work is performed with the program GRAVDET. GRAVDET uses kinematic positions as pseudo-observations for orbit and gravity field determination. Observation equations are set up according to Eq. (3.1) at the epochs of the pseudo-observations in order to improve the a priori arc-specific and gravity field parameters. The observation equations may be written in the linearized form as:

$$\boldsymbol{r}_K(t) + \boldsymbol{v}_K(t) = \boldsymbol{r}_0(t, \boldsymbol{P}_0) + \sum_{j=1}^{n_{par}} \frac{\partial \boldsymbol{r}_0(t, \boldsymbol{P}_0)}{\partial P_j}\, dP_j \ , \tag{4.15}$$

with the

$\boldsymbol{r}_K(t)$ satellite position at epoch t,

$\boldsymbol{v}_K(t)$ correction of the satellite position at epoch t,

$\boldsymbol{r}_0(t, \boldsymbol{P}_0)$ position of the satellite (a priori orbit) at epoch t obtained by numerical integration of the initial value problem of the primary equations Eq. (3.37),

$\frac{\partial \boldsymbol{r}_0(t,\boldsymbol{P}_0)}{\partial P_j}$ partial derivative of the a priori orbit at epoch t w.r.t. parameter P_j obtained by numerical integration of the initial value problem of the variational equations Eq. (3.38),

$\boldsymbol{P}$ array of n_{par} parameters (Eq. (3.36)) with $\boldsymbol{P} = \boldsymbol{P}_0 + \boldsymbol{dP}$,

$\boldsymbol{P}_0$ array containing the a priori values of the parameters, and

$\boldsymbol{dP}$ array containing the parameter improvements.

The numerical integration necessary for setting up the observation equations uses a high-order collocation algorithm with automatic step size control (see Beutler, 2005, Vol. 1, Chapter 7). The resulting NEQ system is solved in a least-squares adjustment or written into a file to be used as input for BSW's NEQ stacking program.

The pseudo-observations may be weighted with/without taking the correlations between

Table 4.2: Force models in GRAVDET.

Model	Kind of force	Note
Earth gravity field	Gravitational	
Gravitation of other celestial bodies	Gravitational	Using DE405 JPL Development ephemerides (Standish, 1990)
Solid Earth tides	Gravitational	IERS-conform
Ocean tides	Gravitational	
Atmospheric and ocean de-aliasing	Gravitational	
Relativistic PPN corrections	Gravitational	IERS-conform
Atmospheric drag	Non-gravitational	See Beutler (2005)
Direct solar radiation pressure	Non-gravitational	See Beutler (2005)
Earth albedo radiation pressure	Non-gravitational	See Beutler (2005)

the epochs into account. The variance-covariance matrix of the pseudo-observations may therefore be introduced. The pseudo-observations may be given in the quasi-inertial system or in the Earth-fixed coordinate system. In the latter case they are transformed into the quasi-inertial system for orbit integration. Epoch-to-epoch differences of kinematic positions may be used as alternative pseudo-observations.

The gravitational and non-gravitational force field is described by different background models that are listed in Table 4.2. The use of the non-gravitational force models is optional. The air-drag model uses the MSISe-90 (Hedin, 1991) air density model of the higher atmosphere and requires the A_a/m-ratio (A_a: cross-section area of the satellite normal to the velocity vector of the satellite), the time variable solar flux index F(10.7 cm), and the planetary magnetic index A_p as input information. The direct and albedo radiation pressure models require the A_r/m-ratio (A_r: cross-section area of the satellite normal to the vector between radiation source and satellite) and a coefficient describing

the reflective properties of the satellite surface as input values. The latter models assume a constant A_r/m-ratio. The models are described in detail by Beutler (2005). The non-gravitational forces may instead be taken into account by accelerometer measurements or by arc-specific parameters.

GRAVDET allows the determination of different kinds of parameters that are listed in Table 4.3. The set up of the six initial conditions is mandatory. All other parameters

Table 4.3: Parameter types in GRAVDET.

Parameter	Type	Arc-specific?
Initial osculating elements	Initial conditions	Yes
Empirical force function parameters (constant accelerations, coefficients of periodic acc. functions of the argument of latitude u, coefficients of polynomial acc.)	Dynamical	Yes
Scaling factors of dynamical force models	Dynamical	Yes
Scale and offset of accelerometer data	Dynamical	Yes
Pseudo-stochastic pulses	Pseudo-stochastic	Yes
Piecewise-constant accelerations	Pseudo-stochastic	Yes
Gravity field parameters (SH coefficients)	Dynamical	No

may be set up optionally. Gravity field determination is treated as a generalized orbit determination problem: The improvements of the SH coefficients of the a priori gravity field model are estimated as general dynamical parameters in addition to the arc-specific parameters. The quality of the a priori gravity field model must be good enough to permit a proper determination of the satellite orbit with the arc-specific parameters alone.

GRAVDET may also be used as a simulation tool. The user may define the six osculating elements at an initial epoch. The program computes satellite positions by performing a numerical integration of the initial value problem of the primary equations Eq. (3.37) over a user-defined time interval. The simulated orbits may be degraded by artificial noise and by perturbations taken from dynamical force models or from external accelerometer data.

5 Data processing

The gravity field recovery described subsequently is based on the Celestial Mechanics Approach (CMA, Beutler, 2005; Beutler et al, 2010b). The theoretical basics of this approach are outlined in Chapter 3. Here we focus on the practical aspects of the CMA and on data processing.

The gravity field recovery from a LEO orbit following the CMA is a two step procedure: In the first step a kinematic trajectory of a LEO satellite is computed using the GPS measurements of the on-board receiver. The orbits and the clock corrections of the GPS satellites as well as the Earth rotation parameters (ERPs) are introduced as known in this step. In the second step the kinematic positions are introduced as pseudo-observations into a generalized orbit determination problem. Optionally, also accelerometer data (considered as error-free) may be used in the orbit determination process. The covariance information from the kinematic positioning may be introduced for weighting the pseudo-observations. Kinematic positions are suitable pseudo-observations, because they contain only geometric information and are not affected by physical force models of the LEO satellite, such as an priori gravity field model. Together with the arc-specific parameters (initial osculating elements, dynamical parameters, pseudo-stochastic parameters, accelerometer or model calibration parameters) of the satellite the SH coefficients of the Earth's gravity field are set up as parameters in the orbit determination step. For each daily arc a normal equation (NEQ) system is written. After the pre-elimination of the arc-specific parameters, the daily NEQs are combined into weekly, monthly, annual, and multi-annual NEQs. The NEQ systems may be modified (e.g., by pre-elimination, deletion, or constraining of parameters) without a new time-consuming set up. The combined NEQ systems are inverted in order to solve for the remaining gravity field parameters. This basic concept is underlying the processing of all AIUB-CHAMP gravity field models generated in the context of this work.

This chapter describes in particular the generation of the three gravity field models AIUB-CHAMP01S (Prange et al, 2009), AIUB-CHAMP02S (Prange et al, 2010), and AIUB-CHAMP03S, which are publicly available. These models are solely based on GPS measurements of CHAMP's on-board GPS receiver and on the attitude measurements of the star sensors. No regularization or constraints were applied. Dynamical models for the non-gravitational perturbations or accelerometer data were not used (see Experiments in Sect. 6.1.2 and 6.1.3). The non-gravitational perturbations were absorbed by a large number of estimated pseudo-stochastic parameters, which were left unconstrained. The arc-length was one day in all cases.

All GPS-related computations (orbit and clock reprocessing, high-rate clock processing,

LEO orbit determination) were performed using the Bernese GPS software (BSW, see Sect. 4.7). The program GRAVDET was used in the screening procedure of the kinematic pseudo-observations and for establishing the NEQs in the gravity field recovery process. A modified version of BSW's NEQ stacking program was used for parameter pre-elimination and combination of the NEQs in the gravity field determination. All computations took place on the LINUX cluster of the University of Bern. The automation possibilities of the BSW (BPE, see Sect. 4.7) were extensively used.

5.1 Generation of the AIUB-CHAMP01S gravity field model

AIUB-CHAMP01S was the first CHAMP gravity field model derived at the AIUB. It was based on one year of CHAMP GPS and attitude data of the time interval DOY 70/2002 (March 11, 2002) to DOY 70/2003 (March 11, 2003). The time interval has been chosen, because several other CHAMP-only gravity field models were based on exactly the same data set. The choice of the same data basis allowed a fair comparison of the AIUB-

Table 5.1: Background models and GNSS processing standards underlying AIUB-CHAMP01S.

Model type	Applied model or convention
Geodetic datum:	IGS00 (Kouba et al, 1998)
Nutation model:	IAU80 (Seidelmann, 1982)
Subdaily pole model:	IERS1996 (McCarthy, 1996)
Solid Earth tide model:	IERS1996 (McCarthy, 1996)
Meanpole convention:	IERS1996 (McCarthy, 1996)
Ocean tide model:	CSR3.0(Eanes and Bettadpur, 1996), nmax=20
Gravity field model (GPS):	JGM3 (Tapley et al, 1996), nmax=12
A priori gravity field model (GRAVDET):	EIGEN-2 (Reigber et al, 2003), nmax=90
Antenna phase center (PCV) model (GPS):	Relative
Antenna phase center (PCV) model (CHAMP):	none
Antenna offset (CHAMP):	See Schwintzer et al (2002)
Tropospheric mapping function (GPS):	NIELL mapping function (Niell, 1996)
Radiation pressure model (GPS):	Rock (Fliegel et al, 1992)
Radiation pressure model (CHAMP):	None
Phase-windup effect:	Not considered

CHAMP01S with these models. This was important because one aim for the generation of this model was the validation of the CMA for gravity field determination w.r.t. other approaches. Further goals were the proof of the CMA concept, the assembly of the processing infrastructure, and the gain of a basic understanding of the practical aspects (e.g., parameterization, outlier screening, influence of background models) of the gravity field determination from GPS measurements and the problems related to it.

The kinematic CHAMP positions used for the generation of the AIUB-CHAMP01S were

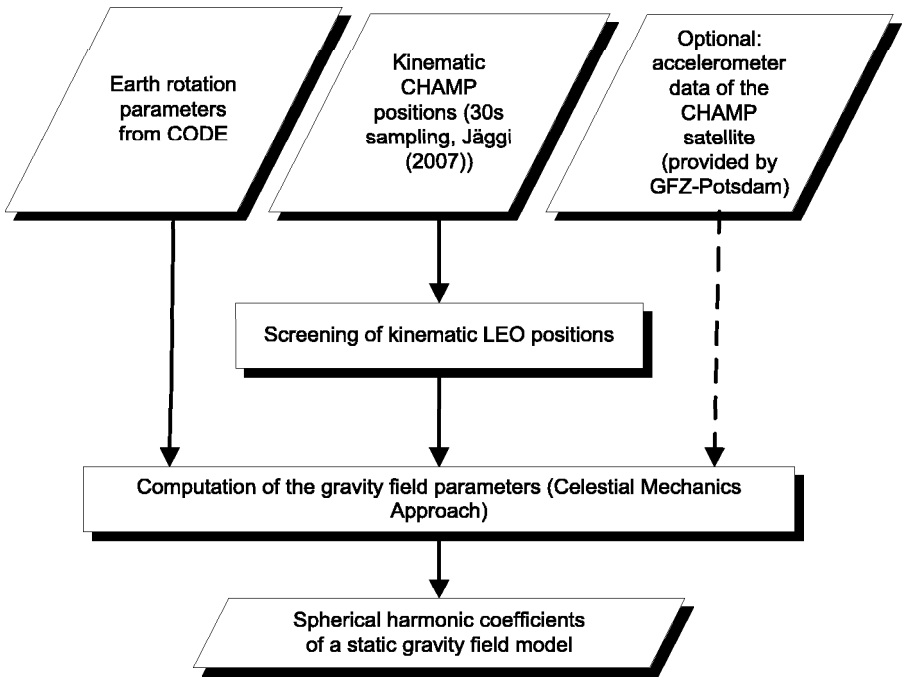

Figure 5.1: Data and processing steps for the generation of AIUB-CHAMP01S.

computed by Jäggi (2007) using the precise point positioning approach (PPP, Zumberge et al, 1997). This approach requires known ERPs, GPS satellite orbits, and clock corrections. The ERPs and GPS satellite orbits were taken from the CODE solution for the IGS final product line (see Sect. 4.6). The 30 s satellite clock corrections were taken from an internal data set generated at the AIUB. The IGS standards underlying these data were also applied to the LEO orbit determination. Only kinematic epochs based on at least five GPS observations were considered in the gravity field determination in order to only use reliable kinematic positions. The use of the BSW in the kinematic processing ensured a high level of consistency, because the same software is used for the generation of the aforementioned GPS products at CODE, as well. The background models and processing standards underlying the CODE processing and the LEO orbit determination were also used in the gravity field recovery (see Table 5.1). A processing flowchart of the AIUB-CHAMP01S is presented in Fig. 5.1.

5.1.1 Data Screening

GPS-derived kinematic LEO positions may contain outliers, jumps, or data gaps. These may, e.g., be caused by tracking problems of the GPS receiver, by multipath effects, by receiver clock problems, or by the setting up of new phase ambiguities due to a changing GPS observation geometry. Because of the low degree of freedom, kinematic positioning is susceptible to such data problems. Outliers and data jumps do not represent the

true satellite trajectory (which is smooth) and may affect gravity field determination (see Sect. 6.1.7). It is therefore necessary to screen the kinematic pseudo-observations for outliers before using them for gravity field recovery.

The kinematic positions are screened iteratively. In the first step a dynamic orbit is determined using the original kinematic positions as observations. The orbit parameterization consists of the six osculating elements and twelve dynamical orbit parameters (a constant acceleration in radial, along-track, and cross-track direction, the coefficients of a polynomial of degree three in along-track direction, the coefficients of once-per-rev functions of the argument of latitude u in radial, along-track, and cross-track direction). The residuals of the orbit determination typically have a size of a few decimeters and are screened for outliers on the meter-level. Furthermore, days with serious problems, i.e., when no reasonable dynamic orbit can be estimated from the pseudo-observations, are recognized and skipped. Such problems are, e.g., caused by a too small number of usable pseudo-observations, by large data gaps, or by orbital maneuvers of the LEO satellite.

The experiments performed in Sect. 6.1.7 showed, that a rough screening usually is not sufficient to get optimal results from CHAMP data. Therefore, the rough screening is complemented by additional screening steps, in which the kinematic trajectory is represented by a reduced-dynamic orbit. In addition to the orbit parameters set up in the first step, pseudo-stochastic pulses in radial, along-track, and cross-track direction are set up every 30 min. The much reduced residual level allows to recognize outliers down to the decimeter-level. The epochs with residuals exceeding the outlier thresholds are flagged in the kinematic data files. Short data pieces in the kinematic coordinate files are also marked as outliers. At the end of each iteration step some statistics are computed and plotted. A detailed discussion about the importance of the data screening and the influence of its settings on the gravity field solution is done in Sect. 6.1.7.

5.1.2 Gravity field recovery

The screened kinematic positions are introduced as pseudo-observations in the final orbit and gravity field determination process. The orbit parameters are the six initial osculating elements, twelve dynamical orbit parameters (a constant acceleration in radial, along-track, and cross-track direction, the coefficients of a polynomial of degree three in along-track direction, the coefficients of once-per-rev terms), and pseudo-stochastic pulses in radial, along-track, and cross-track (RSW, see Sect. 3.2.3) direction every five minutes. The SH coefficients of the Earth's gravity field are estimated up to degree and order 90 (except for the coefficients of degrees 0 and 1, see Sect. 3.5). For each daily arc the NEQ system is written into a separate file.

Each daily NEQ contains 8277 gravity field parameters, 6 initial osculating elements, 12 dynamical orbit parameters, and up to 861 pseudo-stochastic orbit parameters (879 orbit parameters and 9156 parameters in total) and in the best case (when no outliers were detected in the screening process and no data gaps occur) 8640 pseudo-observations (2880 epochs separated by 30 s, 3 pseudo-observations per epoch). The number of unknowns

Table 5.2: Summary of the AIUB-CHAMP01S gravity field recovery.

Processed days:	363 (DOY 70/2002–DOY 70/2003)
Number of kinematic coordinates (before screening):	2881743
Number of kinematic coordinates (used in the LSA):	2829705, i.e., 1.8% outliers
Maximum degree:	90
Number of SH coefficients:	8277
Orbit parameters (pre-eliminated) per arc:	6 osculating elements, 12 dynamical parameters (constant acc. and coefficients of periodic (1/rev.) acc. in RSW, coefficients of a polynomial acc. of degree three along-track), pulses every 5 min (version 1) or every 15 min (version 2) in RSW
Disk space requirement:	About 170 GB for the NEQ systems

(9156) therefore exceeds the number of observations (8640) and the daily NEQ matrices are singular. Assuming that 365 daily NEQs are stacked to an annual NEQ system, the annual NEQ contains 8277 gravity field parameters and 320835 orbit parameters. The number of observations per year is in the best case about 3.15 millions (365 days with 8640 observations per day). The degree of freedom (number of observations minus number of parameters) is big (larger than 2.8 millions) in this case and the annual NEQ matrix is regular. The number of elements in the normal equation matrix is the number of parameters squared. With 8 bytes per matrix element a triangular NEQ matrix containing all parameters would have a size of more than 400 GB. A matrix with so many elements would be difficult to invert. Fortunately, the majority of the parameters are arc-specific parameters, which are not of interest in a gravity field determination. Therefore, the arc-specific parameters are pre-eliminated prior to the NEQ stacking. These parameters still contribute to the solution, but their estimates are not explicitly available (see Sect. 3.1).

In the case of AIUB-CHAMP01S seven consecutive daily NEQs were combined into one weekly NEQ. Four weekly NEQs were combined to one monthly NEQ, respectively. Finally, all monthly NEQs were combined to an annual NEQ. The monthly and annual NEQs were solved by inversion without applying any regularization and the fully normalized SH coefficients of the gravity field were estimated.

Experiments (see Sect. 6.1.1) showed that setting up more pulses strengthens the gravity field solution in the high SH degrees, but weakens the solution for the low SH degrees. This is why two different versions (with pulse intervals of 5 and 15 min, respectively) of gravity field solutions were produced. In the first version all orbit parameters were pre-eliminated. The reduced weekly, monthly, and annual NEQs then contain the information of all orbit parameters. The spacing of the pseudo-stochastic pulses is 5 min. In the second version only every third pseudo-stochastic pulse was pre-eliminated and the other two

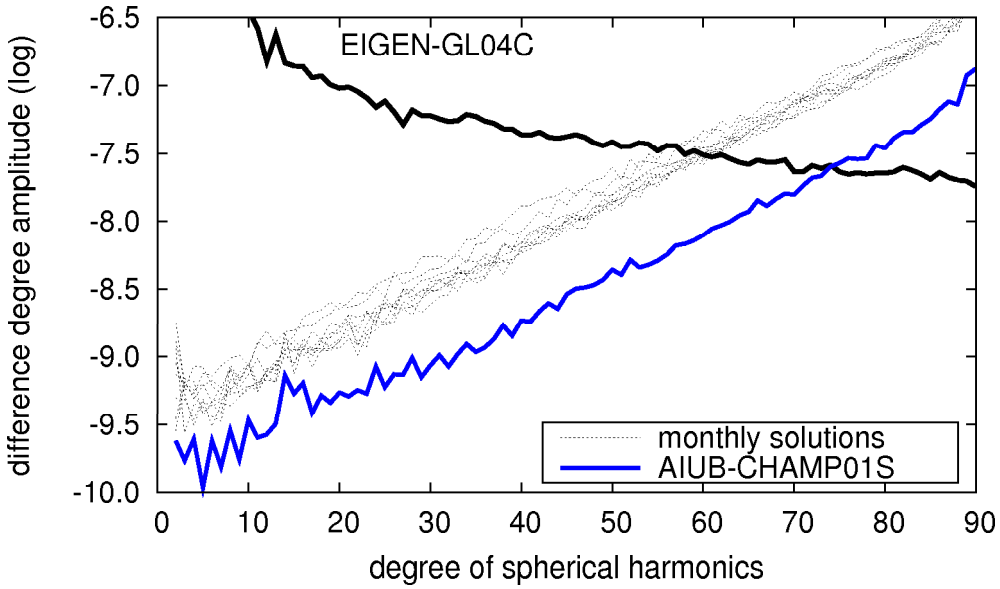

Figure 5.2: Difference degree amplitudes of AIUB-CHAMP01S and monthly gravity field solutions w.r.t. EIGEN-GL04C.

were deleted. The remaining orbit parameters were pre-eliminated like in the first case. The resulting NEQs of version two contain the implicit information of pseudo-stochastic pulses set up with a spacing of 15 min. By combining the annual NEQs belonging to both versions and solving the stacked NEQ system we obtained a gravity field solution that shows optimal results in the whole SH spectrum — the AIUB-CHAMP01S. For more information about this combination we refer to Sect. 6.1.1/**Test6a**. Table 5.2 summarizes the AIUB-CHAMP01S processing.

5.1.3 The AIUB-CHAMP01S gravity field model

The difference degree amplitudes (Eq. (3.32)) of AIUB-CHAMP01S and the contributing monthly solutions w.r.t. EIGEN-GL04C (Förste et al, 2008) are shown in Fig. 5.2. EIGEN-GL04C was chosen as reference model, because it is based on the combination of GRACE data, SLR measurements, and terrestrial gravimetry data and therefore is considered to be superior to CHAMP-based gravity field models. In this kind of plot the "true" gravity field signal is represented by the signal degree amplitudes (Eq. (3.31)) of the SH coefficients of the reference model. A low difference degree amplitude indicates a small deflection of the examined gravity field model from the "truth". If the difference degree amplitude exceeds the signal curve, the error of the examined gravity field model is larger than the signal itself, indicating that the gravity field determination was not sensitive enough to contribute to all SH coefficients of the corresponding degree in a reliable way. Fig. 5.2 shows that for AIUB-CHAMP01S this is the case from degree 74 on. The

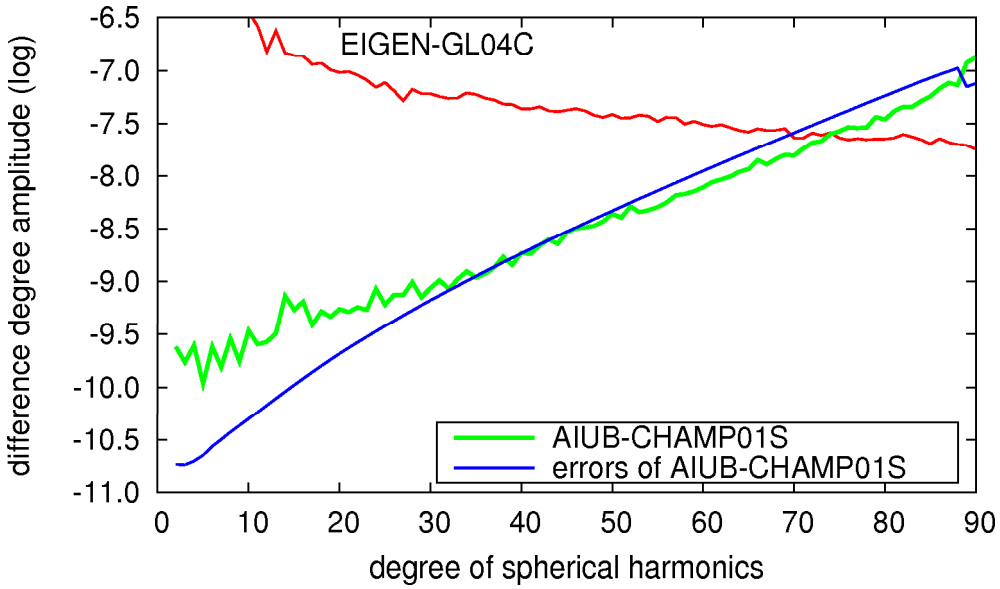

Figure 5.3: Difference degree amplitude and error degree amplitude of AIUB-CHAMP01S.

comparison to other CHAMP-only gravity field models (see Sect. 7.2) shows, that this is a good result — proving the CMA's suitability for gravity field recovery. The comparison of the monthly solutions with the annual solution in Fig. 5.2 also indicates that the gravity field solution profits significantly from a larger amount of processed data. Figure 5.3 shows that below degree 30 the error degree amplitude (Eq. (3.33)) of AIUB-CHAMP01S is significantly lower than the corresponding difference degree amplitude. The formal errors of these SH coefficients, are thus too optimistic. This could indicate systematic errors that are not absorbed by the pseudo-stochastic pulses.

From the SH coefficients functionals of the disturbing gravity potential may be computed (Ilk et al, 2005). They are interesting for different geo-sciences, e.g., oceanography, geophysics, geodesy. The geoid undulations (geoid heights above a reference ellipsoid, Eq. (3.34)) and the gravity anomalies (gravity difference between geoid and reference ellipsoid, Eq. (3.35)) of AIUB-CHAMP01S are presented in Fig. 5.4 and Fig. 5.5. They were computed w.r.t. the GRS80 ellipsoid up to degree and order 70, corresponding to a half wavelength resolution (Eq. (3.29)) of 285 km. The SH coefficients of the normal potential up to degree eight and the ellipsoid parameters were taken from Hoffmann-Wellenhof and Moritz (2006).

Experiments related to AIUB-CHAMP01S are discussed in Sect. 6.1. The model is validated and compared to external models in Sect. 7.2. A condensed presentation of AIUB-CHAMP01S is provided in Prange et al (2009). The coefficients of AIUB-CHAMP01S are available at *http://www.aiub.unibe.ch/content/research /gnss/gnss___research*

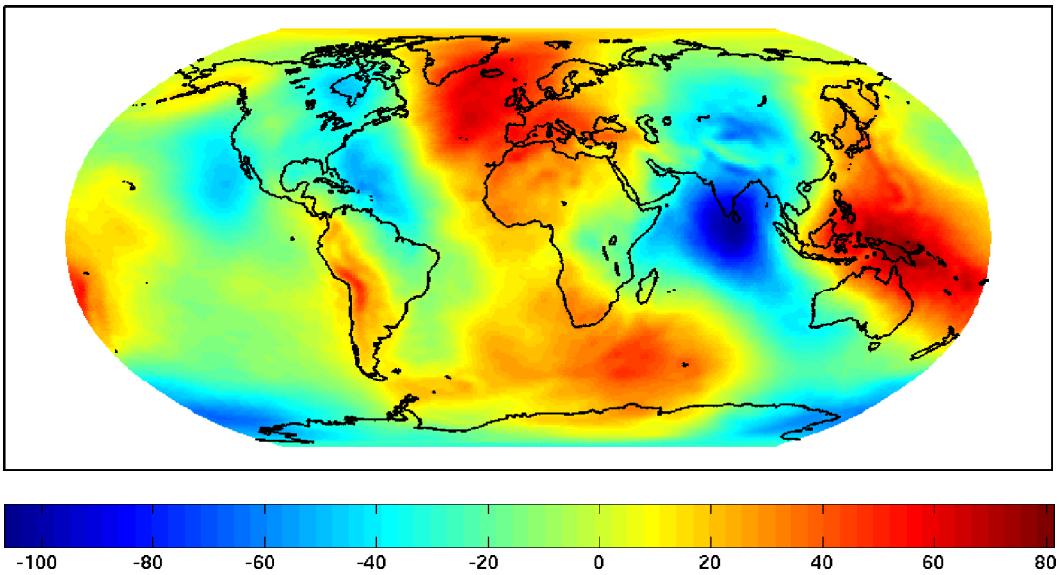

Figure 5.4: Geoid undulations [m] of AIUB-CHAMP01S up to degree 70.

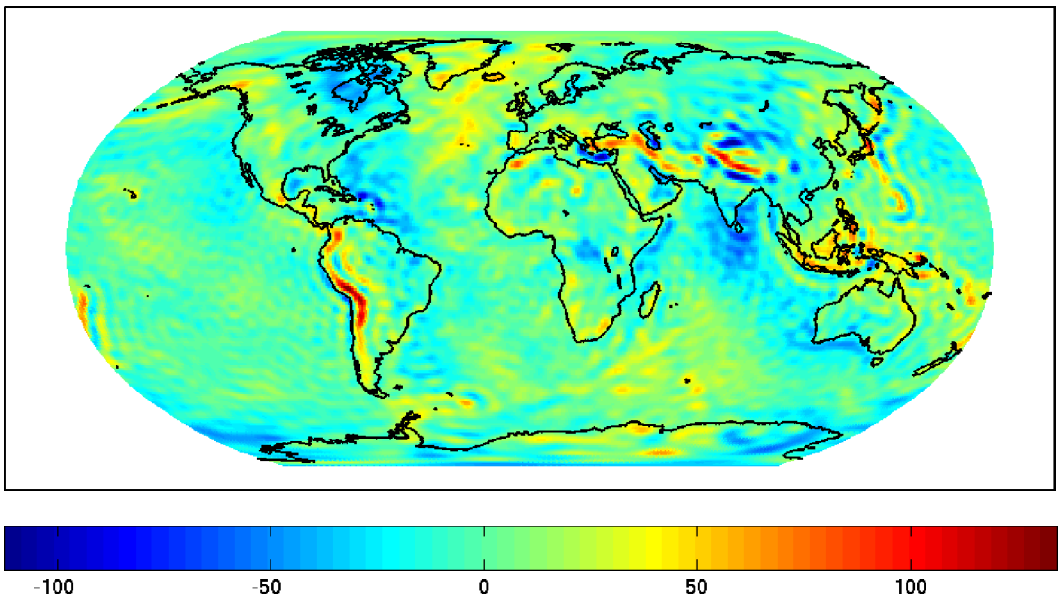

Figure 5.5: Gravity anomalies [mGal] of AIUB-CHAMP01S up to degree 70.

/global_gravity_field_determination/index_eng.html and at
http://icgem.gfz-potsdam.de/ICGEM/ICGEM.html.

5.2 Generation of the AIUB-CHAMP02S gravity field model

It is one of the declared goals of this work to generate the best possible static gravity field using only CHAMP GPS data. This goal can only be achieved if more available data are used to generate a multi-annual solution. As a first step the analyzed series of CHAMP GPS data was extended to six years (2002–2007) for AIUB-CHAMP02S. As in the case of AIUB-CHAMP01S the kinematic CHAMP positions were generated with a spacing of 30 s using the PPP-approach. This approach requires known GPS satellite orbits, ERPs, and high-rate (30 s) GPS satellite clock corrections. Such GPS products are provided by the CODE IGS routine (see Sect. 4.6). Several model changes took place in the routine processing at CODE in the time interval 2002–2007. Moreover, the operational generation of 30 s GPS clock corrections at CODE started in April 2004 (Hugentobler, 2004). Only test data sets of clock corrections with a 30 s spacing were available at the AIUB before that time. These test data sets did not cover the entire time interval from January 2002 to April 2004.

In order to ensure a high consistency of the data and a homogeneous quality of the gravity field solutions over the entire time-span, a reprocessing of the GPS orbit and clock products using the latest processing standards and models of the IGS was performed incorporating the GPS data of the IGS station network. Only GPS was considered, because CHAMP is equipped with a GPS-only receiver. A flowchart of the reprocessing and gravity field determination performed for AIUB-CHAMP02S is provided in Fig. 5.6. Subsequently we describe the GNSS model changes and the individual processing steps of the reprocessing and the recovery of AIUB-CHAMP02S.

5.2.1 GNSS model changes

Between 2002 and 2007 the processing standards of the IGS and the GPS data processing at the CODE analysis center changed substantially. The most important changes and improvements are listed in Table 5.3.

For more detail we refer to the corresponding IGS mails and technical reports (see, e.g., Springer et al, 1998; Hugentobler, 2004; Hugentobler et al, 2006; Schaer, 2006). The GNSS processing standards used after October 2006 are called "new" standards in this work. The new standards were used in the reprocessing. They are based on the IERS2003 conventions (McCarthy and Petit, 2004). The "old" standards are the processing standards valid at the time the data were gathered. They were applied in the original CODE processing. From GPS-week 1400 onwards (November 2006) the "old" and "new" standards were the same. The year 2007 was included into the reprocessing procedure for validating the reprocessing environment.

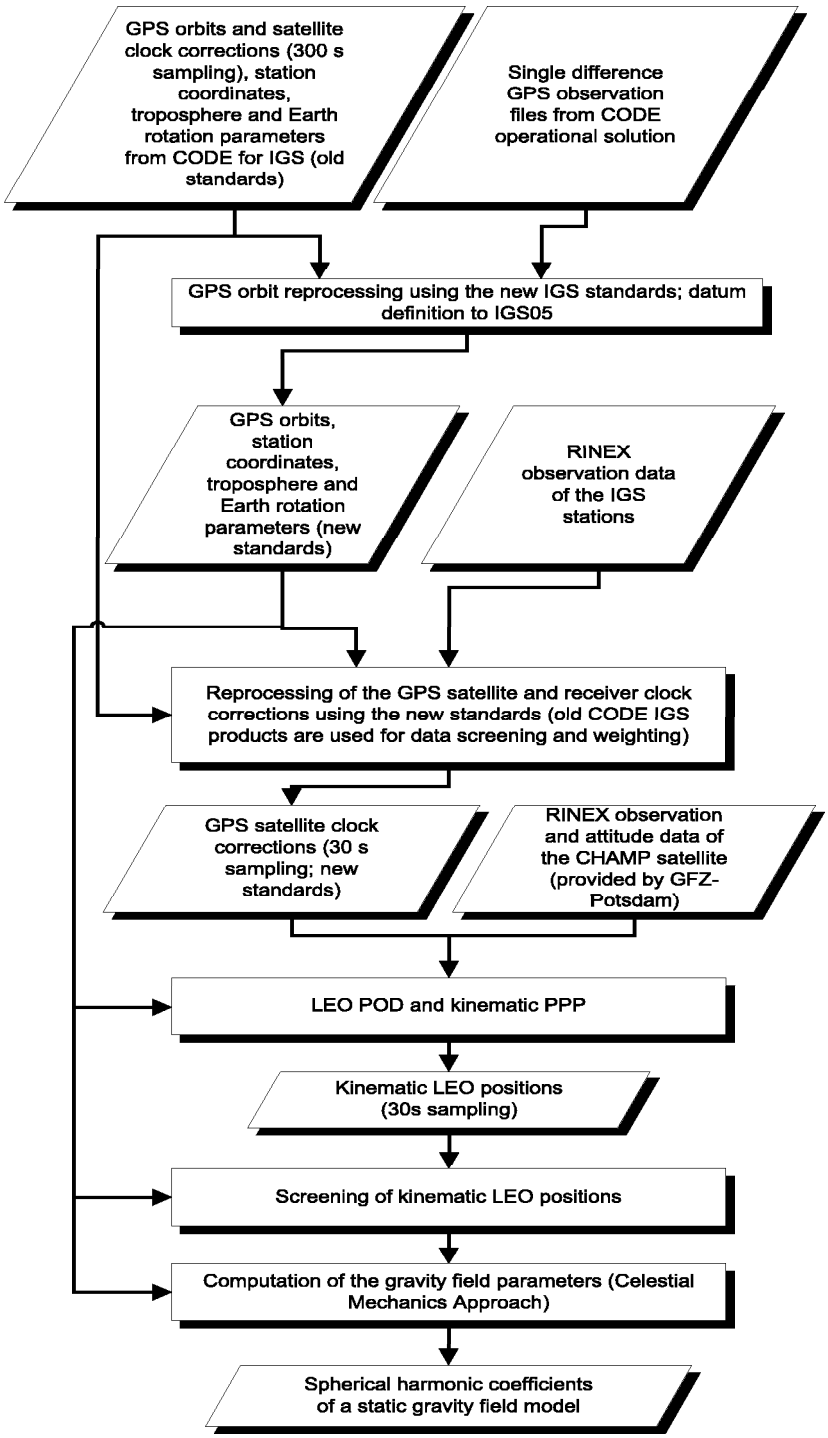

Figure 5.6: Processing chain for the generation of the AIUB-CHAMP02S gravity field model.

Table 5.3: GNSS model changes and processing improvements at the CODE IGS analysis center between early 2002 and late 2006.

Time	Improvement
March 2002	-improvements in the ambiguity resolution (Schaer, 2002)
	-Earth gravity field considered up to degree 12 instead of 8
June 2003	-introduction of GLONASS into the GNSS analysis (Schaer, 2003)
	-improvements in the troposphere modeling (piece-wise linear modeling introduced)
September 2003	-modeling of the geometrical part of the phase-windup effect
October 2003	-subdaily pole model changed from IERS1996 to IERS2000 (McCarthy and Petit, 2000)
April 2004	-start of the generation of 30 s GPS satellite clock corrections
December 2004	-change from DE200 to DE405 JPL planetary ephemerides
June 2005	-change of the geodetic datum from IGS00 to IGS00b (Ferland, 2003)
November 2005	-change of the radiation pressure (RPR) model from Rock to CODE (Springer, 1998)
	-change of the nutation model from IAU80 to IAU2000
November 2006	-change of the geodetic datum from IGS00b to IGS05 (Ferland, 2006)
	-change of the antenna phase center (PCV) model from relative to absolute
	-change from the NIELL mapping function to the global mapping function (GMF, Boehm et al, 2006) in the troposphere modeling
	-introduction of the center of mass correction (CMC) for ocean tidal loading and application of the hardisp interpolation according to IERS2003 conventions (McCarthy and Petit, 2004)
	-modeling of the full phase-windup effect
	-change of the meanpole convention from IERS1996 to IERS2003
	-improvements in the CODE RPR model

5.2.2 GPS orbit reprocessing

The GPS orbit reprocessing was realized through an automated processing chain, which is a modified excerpt of the CODE daily operational analysis, resulting in the contribution to the IGS final products (Dach et al, 2009). The reprocessing procedure started with single difference phase observation files taken from the archive and originating from the CODE final processing (including the results of the pre-processing and ambiguity resolution). The GPS orbits, IGS station coordinates, and ERPs resulting from the operational CODE final processing (based on the old standards) were used as a priori information.

The reprocessing procedure is divided into two parts. A parameter estimation is performed in the first step using the ionosphere-free (L_3) linear combination of the double-difference phase observations. The resulting daily NEQs are saved.

In a second step three consecutive daily NEQs are combined to create three-day arcs. For the middle day of the combined NEQs, the orbit parameters of the GPS-satellites are estimated according to Beutler et al (1996). A new set of coordinates and troposphere parameters of the IGS stations and the ERPs are estimated together with the orbit parameters. Six initial osculating elements, nine dynamical parameters of the radiation pressure model, and pseudo-stochastic pulses every twelve hours are set up for each GPS satellite. At the end of the routine the original and the reprocessed GPS orbits are compared. The comparison results of the reprocessing procedure are discussed in Sect. 6.2.1. The orbit reprocessing is summarized in Table 5.4.

Table 5.4: Statistical information related to the GPS orbit reprocessing.

Processed days:	2180 (Jan. 2002–Dec. 2007)
Single difference observation files:	414360
Single difference observations (L3 LC of phase obs.):	About 3.5×10^9
Number of stations:	120 (early 2002) to 180 (late 2007)
Number of orbit parameters:	1936752
Number of coordinates:	1037652
Number of troposphere parameters:	7641431
Number of Earth rotation parameters:	26160

5.2.3 GPS satellite clock reprocessing

The 30 s GPS satellite clock corrections are based on zero-difference code and phase observations of the global IGS network. The processing procedure is a modified version of the processing scheme used to generate the final clock product at CODE (see Bock et al, 2009). The GPS orbits, coordinates, and troposphere parameters of the IGS stations, and the ERPs generated in the orbit reprocessing (Sect. 5.2.2) were introduced as known and kept fixed.

The clock reprocessing starts with the original RINEX (Gurtner, 1994) observation files of the IGS permanent stations. These files are the same as those used in the CODE operational solution. The processing scheme may be sub-divided into the following main steps:

- Pre-processing on RINEX level: outlier screening of the code and phase observations; cycle slip detection; smoothing of the code observations (according to Springer, 2000).
- Receiver clock synchronization using the code observations.
- Station-wise pre-processing: parameter estimation using code observations; residuals are used for station weighting and detection of misbehaving stations.
- Phase pre-processing: 2^{nd} outlier screening of phase observations; clock jump detection; deletion of short data sequences; set up of phase ambiguities.
- Residual screening: parameter estimation using code and phase observations with station weights being applied; residual screening; detection of misbehaving stations.
- 300 s clock solution: forming of three global clusters containing a maximum of 40 stations each; parameter estimation using the ionosphere-free (L_3) LCs of the smoothed and weighted code and phase observations; estimation of satellite and receiver clock corrections, and phase ambiguities; combination of satellite and receiver clock corrections of the three clusters; selection of a reference clock.

- 30 s clock densification: interpolation of the low-rate (300 s) satellite and receiver clock corrections to 30 s using the phase observations (EHRI-approach, Bock et al, 2009).
- Validation: PPP solutions for a subset of IGS stations (one solution based on the CODE final products and old IGS standards, one solution based on the reprocessed orbit and clock products and the new standards); comparison of kinematic and static coordinates for both solutions.

The results of the reprocessing procedure are discussed in Sect. 6.2.1. Table 5.5 summarizes the GPS clock reprocessing.

Table 5.5: Statistical information related to the GPS satellite clock reprocessing.

Processed days:	2177 (Jan. 2002–Dec. 2007)
RINEX observation files:	About 540000
Number of available observations:	About 48×10^9 code and phase measurements
Number of available stations:	About 265 (early 2002) to 345 (late 2007)
Stations selected for global network solution:	About 102 (early 2002) to 120 (late 2007)
No. of low-rate (5 min) sat. clock corrections:	About 19×10^6
No. of high-rate (30 s) sat. clock corrections:	About 190×10^6

5.2.4 CHAMP orbit determination

As a result of the orbit and clock reprocessing procedures the orbits of the GPS satellites, the ERPs, and the high-rate (30 s) GPS satellite clock corrections, based on the latest IGS standards, are available for the entire time interval 2002–2007 with a high level of consistency. The reprocessed orbit and clock products were introduced as known and kept fixed in the CHAMP orbit determination. The LEO processing routine is based on the routine used to generate the kinematic CHAMP positions (Jäggi et al, 2006) for the recovery of the AIUB-CHAMP01S gravity field. The spacing of the observations was kept at 30 s. The same new processing standards as for the orbit and clock reprocessing (see Sect. 5.2.1) were applied. The absolute phase center variations (PCV) of CHAMP's GPS antenna were given by a nominal PCV model. This model is the result of a robot ground calibration of an antenna of the same type (Montenbruck et al, 2009).

The LEO processing routine may be sub-divided into the following steps:

- Receiver clock synchronization using the code observations.
- Generation of a coarse a priori orbit: kinematic positioning using the code observations; dynamic orbit determination.
- Iterative phase pre-processing: outlier screening; clock jump and cycle slip detection; deletion of short data sequences; set up of phase ambiguities; improvement of the a priori orbit.

- New receiver clock synchronization using the code observations and introducing the improved a priori orbit.
- Final reduced-dynamic LEO orbit determination: using the ionosphere-free (L3) LC of the screened, undifferenced phase observations; orbit parameterization: six initial osculating elements, three constant accelerations in RSW directions, and piecewise constant accelerations every six minutes in RSW directions (constrained to $5\times10^{-9}m/s^2$, for a detailed discussion about the constraining of pseudo-stochastic orbit parameters in the CHAMP orbit determination we refer to Jäggi (2007)).
- Kinematic LEO positioning: using the ionosphere-free (L3) LC of the screened, undifferenced phase observations; estimation of kinematic positions, receiver clock corrections, and phase ambiguity parameters in a PPP solution; epochs with less than five observed GPS satellites are excluded; a priori positions are taken from the reduced-dynamic LEO orbit; epoch-specific covariance information for the three coordinates is saved.
- LEO orbit validation: epoch-wise comparison of reduced-dynamic orbit and kinematic positions; SLR validation of reduced-dynamic orbit and kinematic positions.

The daily 3D-RMS of difference between the kinematic and the reduced-dynamic positions of CHAMP is provided in Fig. 5.7. Both orbit types are moreover validated by SLR-measurements. For validating the kinematic trajectory, the difference between reduced-dynamic orbit and kinematic position is computed for the kinematic epochs before and after the epoch of a SLR normal point. The difference vector is then interpolated to the normal point epoch and added to the reduced-dynamic orbit position at this epoch. This way an interpolated kinematic position at the SLR normal point epoch is obtained. The daily RMS of the SLR validation of the kinematic CHAMP positions is provided in Fig. 5.8. The mean RMS in the whole time interval is 3.7 cm.

Within the time interval considered the characteristics of CHAMP's GPS receiver changed

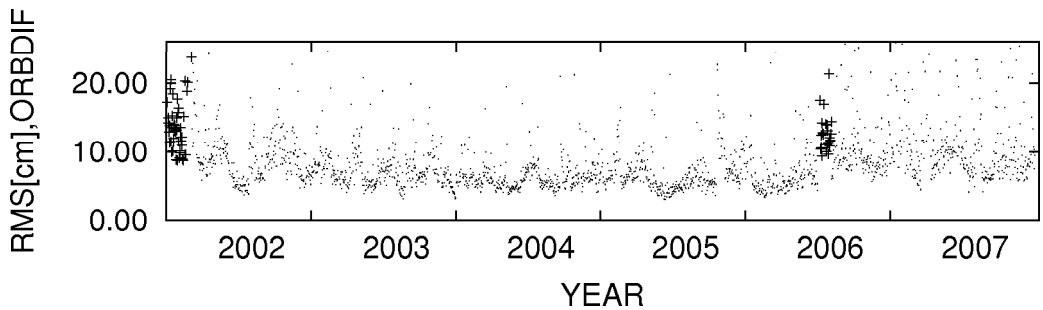

Figure 5.7: Daily 3D-RMS of the difference between kinematic and reduced-dynamic CHAMP orbits. Fine: Up to 10 GPS satellites tracked. **Bold**: Up to 8 (early 2002) or 7 (mid 2006) GPS satellites tracked.

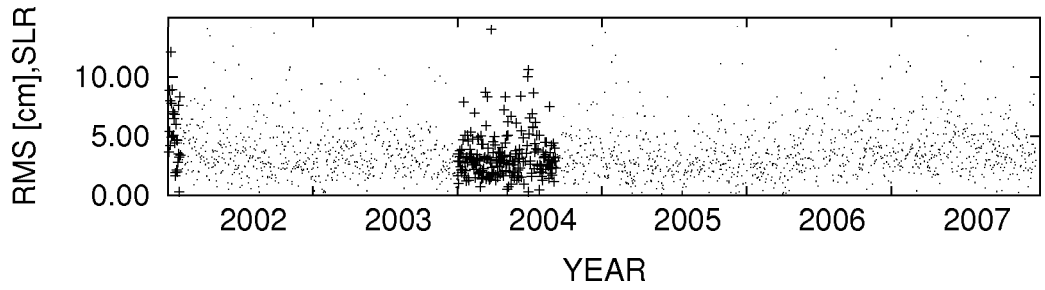

Figure 5.8: RMS of the SLR validation of the kinematic CHAMP orbit. **Bold**: No attitude information available.

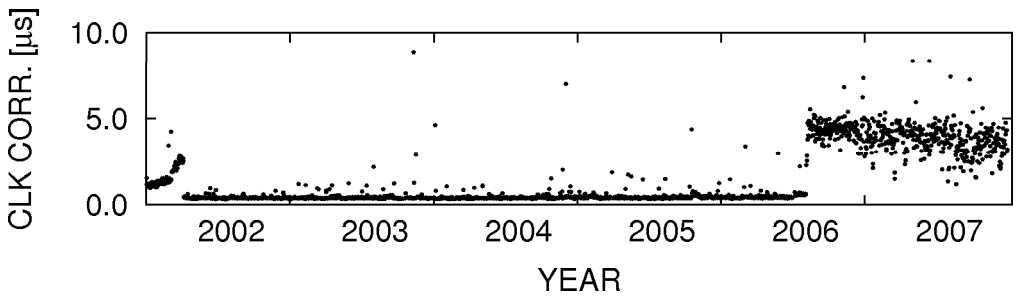

Figure 5.9: Daily mean of the absolute values of the clock corrections of CHAMP's GPS receiver.

several times (see Sect. 2.2.5, Table 2.1). On DOY 64/2002 (March 5, 2002) the number of trackable GPS satellites increased from 8 to 10 due to a receiver software update. From mid 2006 onwards the receiver behavior was affected by clock steering problems, related to the extended mission duration (Michalak 2008, private communication). Between DOY 183 (July 2) and DOY 216 (August 4) in 2006 the receiver was switched to its redundant board. Only up to 7 GPS satellites were tracked simultaneously in that time interval. From DOY 216 on the receiver was switched back to its main board and tracked again up to 10 GPS satellites. The changed receiver behavior is also reflected in the variations of the mean number of simultaneously tracked GPS satellites (see Sect. 2.2.5, Fig. 2.6). The time periods with a reduced number of available tracking channels are marked (**bold**) in Fig. 5.7. The difference between both orbit representations is larger in these time intervals, because the kinematic positioning (with its low degree of freedom) suffers more from the reduced number of GPS observations than the reduced-dynamic orbit determination. After DOY 216/2006 the receiver clock corrections became much larger (up to $10\,\mu$s instead of typical values below $1\,\mu$s, see Fig. 5.9). Due to very large clock corrections an increased number of ambiguities had to be set up. By adapting the phase observation pre-processing settings (clock jump detection) the number of ambigu-

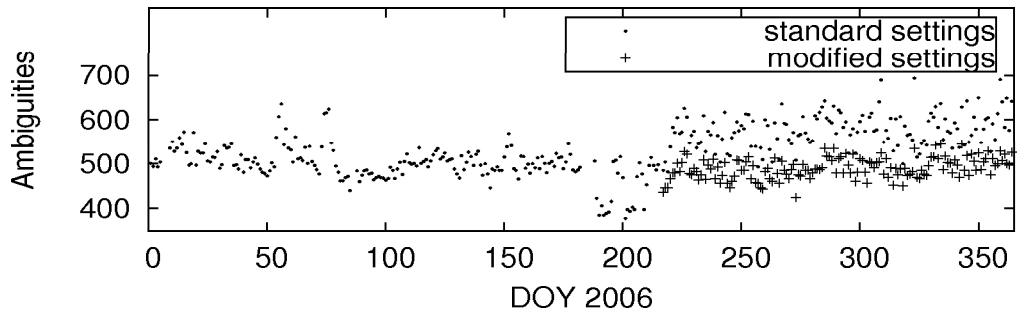

Figure 5.10: Number of estimated phase ambiguities on every processed day during the year 2006 when using standard or adapted settings in the phase preprocessing.

ity parameters could be reduced to a nearly "normal" level (see Fig. 5.10). The adapted settings were used from DOY 216/2006 onwards.

The spacecraft's attitude is required when analyzing LEO data in order to refer the positions to the satellite's center of mass (and not to the GPS antenna phase center). The attitude information is derived from CHAMP's star tracker observations (see Sect. 2.2.5). This information is, together with the CHAMP GPS observation data, usually obtained through the ISDC (Information Systems and Data Center) of the GFZ-Potsdam (Helmholtz-Zentrum Potsdam Deutsches GeoForschungsZentrum). In January 2002 and in the first 243 days of the year 2004 no attitude data was available for CHAMP. According to Jäggi (2007) the deviations between the nominal orbit frame and CHAMP's actual orientation are usually well below 3°. Therefore, CHAMP was assumed to be aligned nominally during the mentioned time intervals. Although an attitude error of 3° implies an error of about 8 cm in the position of the GPS antenna (distance to the spacecrafts center of mass: about 1.5 m) and about 1.3 cm in the position of the retroreflector (distance to the center of mass: about 0.25 m), no significant degradation of the kinematic positions within the mentioned time intervals could be observed in the SLR validation (see Fig. 5.8). Table 5.6 summarizes the main characteristics of the CHAMP orbit determination.

Table 5.6: Summary of the CHAMP orbit determination.

Processed days:	2156 (Jan. 2002–Dec. 2007)
Attitude files:	1919
Number of observations (L3 LC of phase obs.):	About 48×10^6
Number of kinematic coordinates:	About 18×10^6

5.2.5 AIUB-CHAMP02S gravity field recovery

The reprocessed kinematic CHAMP positions were screened according to the procedure described in Sect. 5.1.1. The gravity field recovery procedure changed slightly compared to the one used for AIUB-CHAMP01S. The new IGS standards were used. They are summarized in Table 5.7. The gravity field parameters were set up up to degree and order 120 instead of 90 in order to reduce the influence of omission errors. The gravity field recovery was performed separately for the six years from 2002 to 2007. The combination of the annual NEQs to a multi-annual NEQ was added as the final processing step.

The statistical properties of the AIUB-CHAMP02S are summarized in Table 5.8. Note, that the disk space requirements for gravity field recovery dramatically increased compared to those of AIUB-CHAMP01S. On the one hand this is due to the longer time series, increasing the number of NEQ files by a factor of six. On the other hand we know from Eq. (3.30) that the number of SH coefficients increases with the square of the maximum degree. The number of elements in the normal equation matrix increases in turn with the square of the number of estimated parameters. The change of the maximum SH degree from 90 to 120 therefore is responsible for the growth of the file size by about a factor of three for the combined NEQs. The growth-factor for the un-combined daily NEQs is lower, because the number of arc-specific parameters did not increase. The processing routine was improved in order to reduce the work load when writing, reading, and copying the large NEQ files.

Table 5.7: Background models and GNSS processing standards underlying AIUB-CHAMP02S.

Model type	Applied model or convention
Geodetic datum:	IGS05
Nutation model:	IAU2000
Subdaily pole model:	IERS2000 (McCarthy and Petit, 2000)
Solid Earth tide model:	IERS2000 (McCarthy and Petit, 2000)
Meanpole convention:	IERS2003
Ocean tide model :	CSR 3.0
Gravity field model (GPS):	JGM3, nmax=12
A priori gravity field (LEO and GRAVDET):	EIGEN-2, nmax=120
Antenna phase center (PCV) model (GPS):	Absolute
Antenna phase center (PCV) model (CHAMP):	Absolute ground calibrated
Tropospheric mapping function:	GMF
Radiation pressure model (GPS):	Improved CODE RPR model
Radiation pressure model (CHAMP):	None
Phase-windup effect:	Considered
CMC for ocean tidal loading:	Applied

Table 5.8: Summary of the AIUB-CHAMP02S gravity field recovery.

Processed days:	2156 (Jan. 2002–Dec. 2007)
Kinematic coordinates (before screening):	18106878
Kinematic coordinates (used in the LSA):	17567712, i.e., 3% outliers
Maximum degree:	120
Number of SH coefficients:	14637
Orbit parameters (pre-eliminated) per arc:	6 osculating elements, 12 dynamical parameters (constant acc. and coefficients of periodic (1/rev.) acc. in RSW, coefficients of a polynomial acc. of degree three along-track), pulses every 5 min (version 1) or every 15 min (version 2) in RSW
Disk space requirement:	About 2670 GB

5.2.6 The AIUB-CHAMP02S gravity field model

Figure 5.11 (a) shows the difference degree amplitudes of AIUB-CHAMP01S and AIUB-CHAMP02S w.r.t. EIGEN-GL04C. AIUB-CHAMP02S has much improved compared to its predecessor. The difference degree amplitude starts to exceed the gravity field signal from SH degree 90 on. The comparison to other CHAMP-only gravity field models (see Sect. 7.3) shows that, at the time of its generation, AIUB-CHAMP02S was one of the best gravity field models based only on CHAMP data.

Figure 5.11 (b) shows the degree-wise improvement of the difference degree amplitudes presented in Fig. 5.11. The improvement is lower than expected for SH coefficients with degrees below 30, suggesting that these coefficients are still affected by unmodeled systematic errors. On the other hand the improvement factor is larger than expected in the degrees above 30. This is because the annual gravity field solutions become better in the later years. The difference degree amplitudes of the annual gravity field solutions and AIUB-CHAMP02S w.r.t. EIGEN-GL04C are shown in Fig. 5.12. The better quality of the later annual gravity field solutions is mainly caused by the satellite's decreasing orbital height (see Fig. 2.7 in Sect. 2.2.5). From Sect. 3.5 we know that the gravity field signal of the higher SH degrees is attenuated at higher orbits. Fig. 5.12 shows that the difference degree amplitude of the annual solution of the year 2002 is comparable in quality to AIUB-CHAMP01S (295 out of 365 data days are common). This suggests that the GNSS model changes did not contribute much to the better performance of AIUB-CHAMP02S. The improvement is mainly due to the larger amount of data.

All annual solutions in Fig. 5.12 show noticeable peaks at some of the lower SH degrees. The peaks are even better visible in the difference degree amplitude of the multi-annual solution. This inconsistency is caused by the change from the relative to the absolute PCV model in the GPS data processing. This issue and the impact of other GNSS model

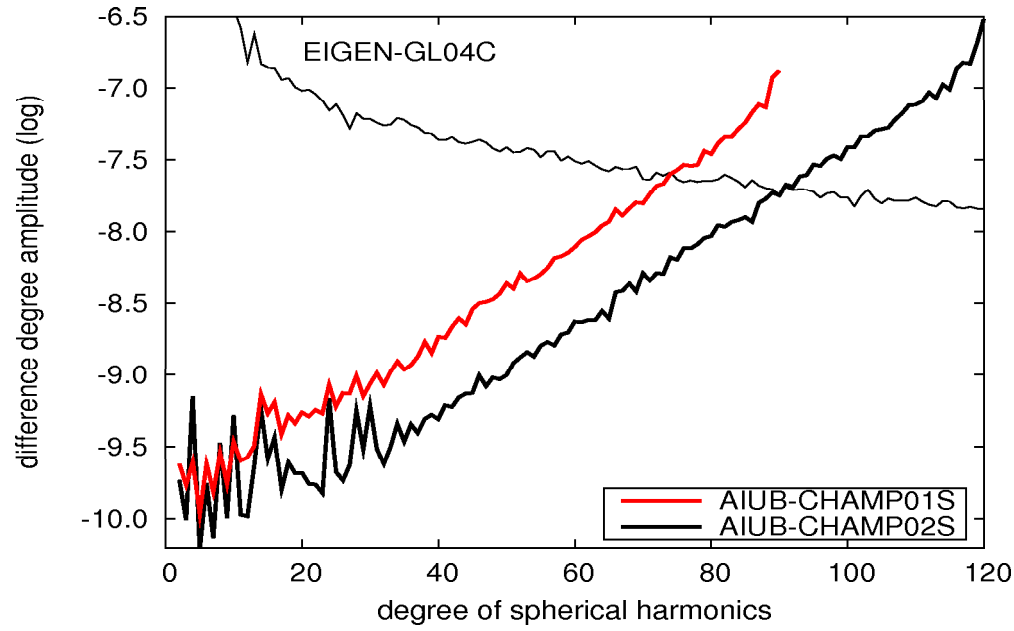

(a)

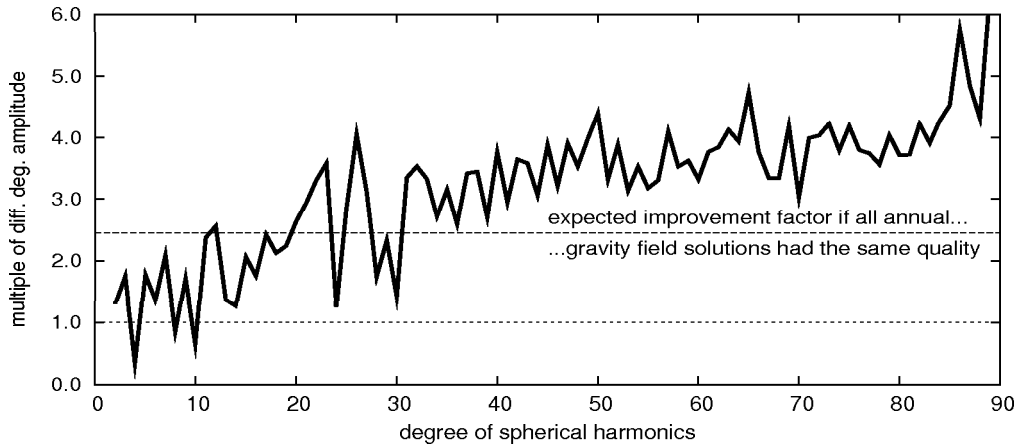

(b)

Figure 5.11: **Top:** Difference degree amplitudes of AIUB-CHAMP01S and AIUB-CHAMP02S w.r.t. EIGEN-GL04C. **Bottom:** Improvement factor between the difference degree amplitudes of AIUB-CHAMP01S and AIUB-CHAMP02S w.r.t. EIGEN-GL04C.

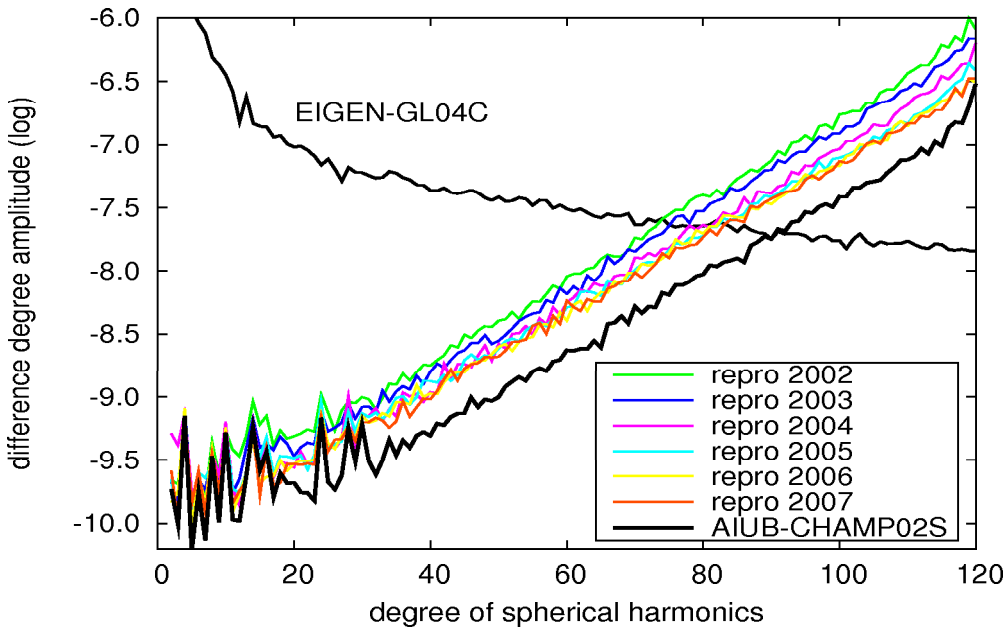

Figure 5.12: Difference degree amplitudes of the annual CHAMP gravity field solutions and the combined AIUB-CHAMP02S w.r.t. EIGEN-GL04C.

changes on the AIUB-CHAMP02S gravity field model are discussed in detail in Sect. 6.2 and in Prange et al (2010). AIUB-CHAMP02S is validated in Sect. 7.3. The coefficients of AIUB-CHAMP02S are available at *http://www.aiub.unibe.ch/content/research/gnss/gnss___research/global_gravity_field_determination/index_eng.html*.

5.3 Generation of the AIUB-CHAMP03S gravity field model

AIUB-CHAMP03S is our best CHAMP-only gravity field model and the major result of this work. Compared to its predecessor it is improved quantitatively and qualitatively. The quantitative improvements include an extended time series of processed CHAMP GPS data (2002–2009) and the utilization of the full data sampling rate of CHAMP's GPS receiver. In order to make use of the high sampling rate GPS satellite clock corrections with at least the same sampling rate were required. Tests showed that the interpolation of the 30 s satellite clock corrections is not sufficient (see Sect. 6.3.3). GPS satellite clock corrections with a sampling interval of 5 s are part of the final product line at CODE since May 2008 (Schaer and Dach, 2008). In the context of the HPF activities (see Sect. 2.2.7) a set of 5 s clock corrections was available starting January 1, 2007 (Bock et al, 2009). The available 5 s clock corrections and the CODE orbit products were used for the determination of a new set of CHAMP orbits for the years 2007–2009. For the years 2002–2006, however, the high-rate GPS clock corrections (with a 5 s spacing) had

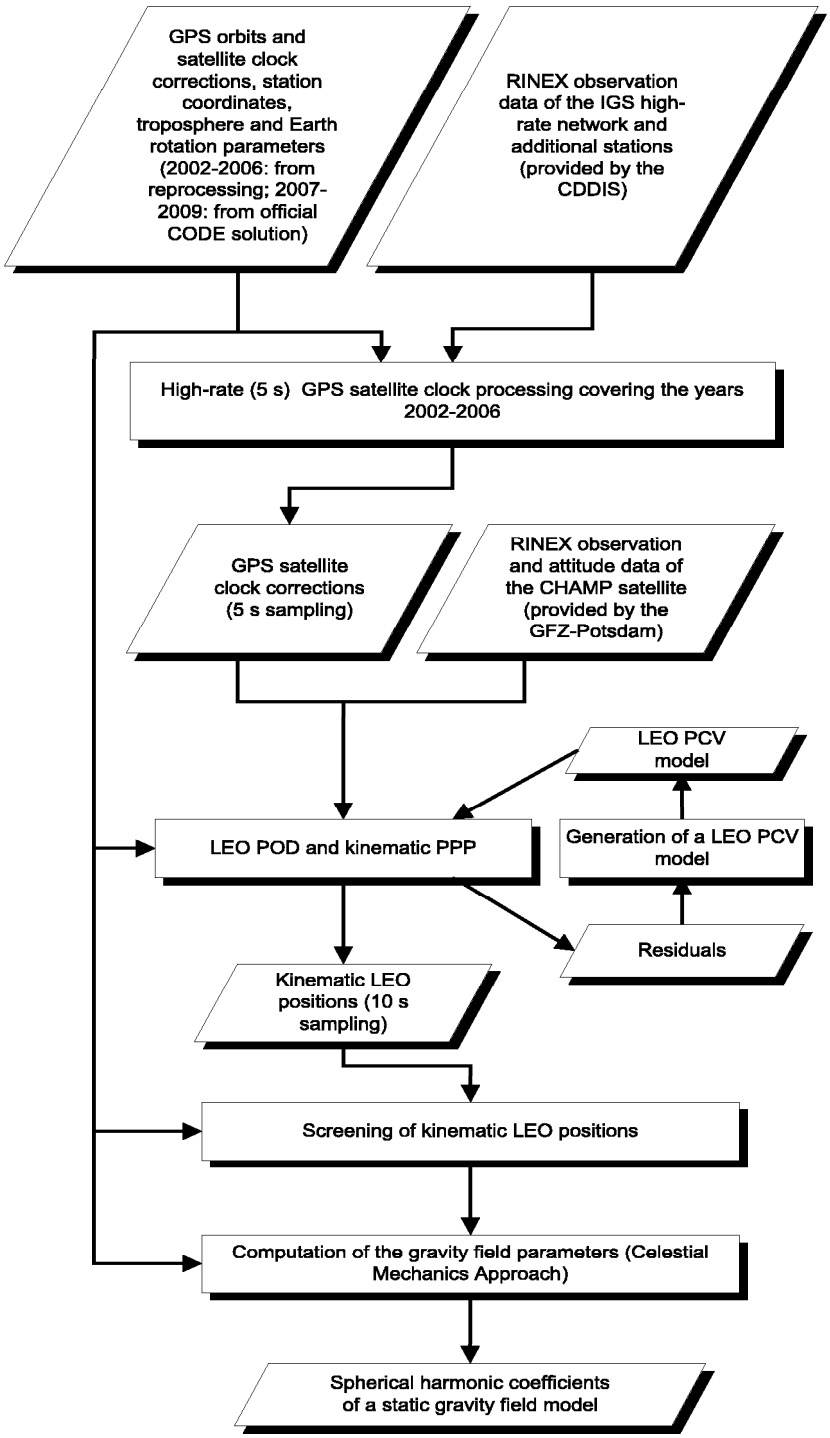

Figure 5.13: Processing chain for the generation of AIUB-CHAMP03S.

to be computed, first. The reference frame for these new clock corrections was defined by the reprocessed products (see Sect. 5.2.2), which were introduced as known and kept fixed.

The major qualitative improvements are the use of an estimated PCV model (see Sect. 6.3.1) for the CHAMP GPS antenna and the elevation-dependent weighting of the GPS observations in the LEO orbit determination. Furthermore, the correlations between the kinematic positions of subsequent epochs have been taken into account in the gravity field determination. The GNSS processing standards and models were the same as those used for AIUB-CHAMP02S. Model changes took solely place in the gravity field recovery procedure itself. In order to increase the processing efficiency (reduction of system load and disk space usage) the super-BPE of the BSW (see Sect. 4.7) was modified and used in the processing routines leading to AIUB-CHAMP03S. The processing chain of the AIUB-CHAMP03S is illustrated in Fig. 5.13.

5.3.1 Estimation of high-rate GPS satellite clock corrections

The high-rate GPS satellite clock processing (with a 5 s spacing) is based on the procedure used to generate the corresponding final product at CODE (Bock et al, 2009) and was modified for this work. Most of the data used for the generation of the 5 s clock corrections comes from the IGS high-rate network (1 Hz sampling, IGS (2010)). The quality of the clock corrections depends on the number and the global distribution of the tracking stations (Bock et al, 2009). In the early years (2002, 2003) the number of high-rate IGS stations was quite small. Therefore, non-IGS stations were included in the processing, as well. The adherence to the IGS standards (e.g., the documentation of equipment changes in the station logs) is not always given for these stations. Furthermore, the (in)completeness of data is an issue for many high-rate stations. The 1 Hz RINEX files were downloaded from the CDDIS (Crustal Dynamics Data Information Service) IGS data center and were down-sampled to 5 s. For several time periods high-rate RINEX data were already available in the AIUB-archives. When available the re-archived data was used to reduce the download time. The archived RINEX files were usually stored with a 5 s spacing. Within the time period DOY 240/2003 to DOY 97/2004 the observation spacing of the archived files was only 10 s. The high-rate satellite clock processing was therefore also limited to 10 s in this case.

Table 5.9: Summary of the high-rate (5 s spacing) GPS satellite clock processing.

Processed days:	1816 (Jan. 2002–Dec. 2006)
Number of used RINEX observation files:	92555
Number of available observations:	About 50×10^9 code and phase measurements
Number of available stations:	About 30 (early 2002) to 90 (late 2006)
Stations selected for global network solution:	About 30 (early 2002) to 80 (late 2006)
No. of high-rate (5 s) sat. clock corrections:	About 810×10^6

The processing procedure consists of the following parts:

- Pre-processing on RINEX level for non-IGS stations: outlier screening of the code and phase observations; cycle slip detection; smoothing of the code observations; receiver clock synchronization using the code observations.
- Station-wise pre-processing for non-IGS stations: parameter estimation using code and phase observations in a PPP approach; iterative residual screening; removal of stations with too few observations after screening; detection of misbehaving stations; estimation of station coordinates and troposphere parameters.
- 5 s clock densification: interpolation of the 30 s satellite clock corrections to 5 s using the phase observations (EHRI-approach); reference clock selection.

The number of stations contributing to the high-rate clock processing increased from about 30 early in 2002 to about 80 in late 2006 (see Table 5.9 and Fig. 5.14). From mid 2003 onwards the number of stations analyzed regularly exceeded 45. The comparison of the station distribution at the beginning and the end of the considered time interval indicates a substantial improvement (see Fig. 5.15). The suitability of the high-rate satellite clock corrections for CHAMP orbit and gravity field determination is examined in Sect. 6.3.3.

Note that a sampling interval of 10 s would have been sufficient for the CHAMP orbit determination. The 5 s spacing was chosen, because the clock corrections were supposed to supplement the high-rate clock corrections available at the AIUB from 2007 onwards.

5.3.2 CHAMP orbit determination

The LEO orbit determination was improved — compared to the processing scheme used to generate AIUB-CHAMP02S. The observation spacing was reduced to 10 s for the processing of data from 2003–2009. The settings in the phase observation pre-processing were adapted to the new observation spacing. The GPS orbit products based on the

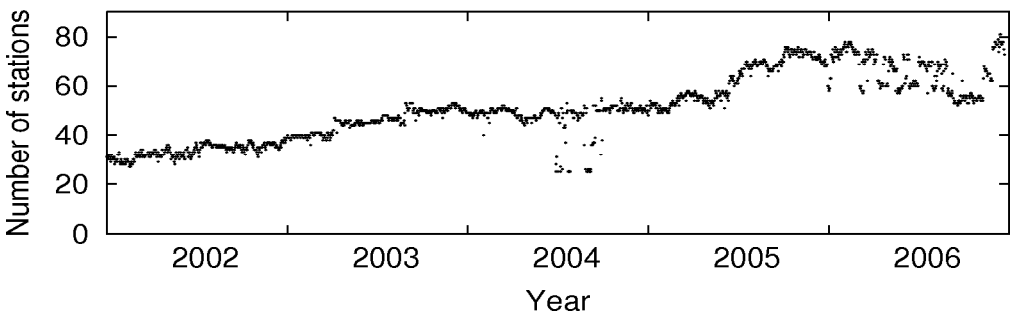

Figure 5.14: Number of GPS tracking stations contributing to the high-rate GPS clock corrections.

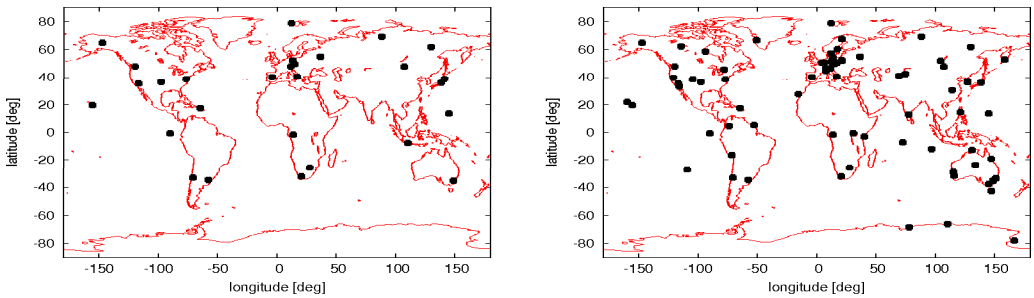

(a) Beginning of the processing: January 2002. (b) End of the processing: December 2006.

Figure 5.15: Distribution of GPS tracking stations contributing to the high-rate GPS clock corrections.

new standards and the high-rate (5 s) GPS satellite clock corrections were introduced as known and kept fixed. For 2002 the sampling interval of 30 s was retained, because tests with a reduced spacing did not lead to acceptable results (see Sect. 6.3.3).

The examination of the impact of GNSS model changes on the gravity field determination (see Sect. 6.2) revealed the importance of a correct antenna phase center modeling. Therefore, an estimated CHAMP PCV model (see Sect. 6.3.1) was introduced for LEO processing. Experiments with elevation-dependent weighting of GPS observations showed very positive results. Eventually, the GPS observations were weighted using an empirically derived weighting function (see Sect. 6.3.2). The observations of Block II and Block IIA GPS satellites in eclipse were excluded from the orbit determination, because the phase center of the antenna array is not located in the radial axis on these spacecraft. In the eclipsing phase the sun sensors are not usable and the satellite's attitude is not nominal (see Sect. 4.3). Tests (see Sect. 6.3.6) showed that gravity field solutions based on data from GPS satellites in eclipse might suffer in quality.

Figure 5.16 shows the number of used GPS observations and estimated kinematic CHAMP coordinates over the entire processing time interval 2002 to 2009. The small number of observations and coordinates in 2002 is due to the 30 s spacing of the observations chosen for that year. On DOY 279/2008 (October 5, 2008) CHAMP's GPS receiver was finally switched to its redundant board and tracks only up to 7 GPS satellites simultaneously, since. This significantly reduced the number of observations (Fig. 5.16) and hence the degree of freedom in the kinematic positioning. As only epochs with at least five GPS observations are accepted, screening became a challenge. The problem was aggravated by data gaps in the high-rate GPS clock corrections (e.g., due to incomplete 1 Hz RINEX observation files). It was therefore allowed to interpolate the satellite clock corrections in gaps since DOY 279/2008 in order not to loose too many observations. Despite all these measures there are more gaps in the series of kinematic positions since DOY 279/2008 (Fig. 5.17). As already seen for AIUB-CHAMP02S the kinematic positions are more af-

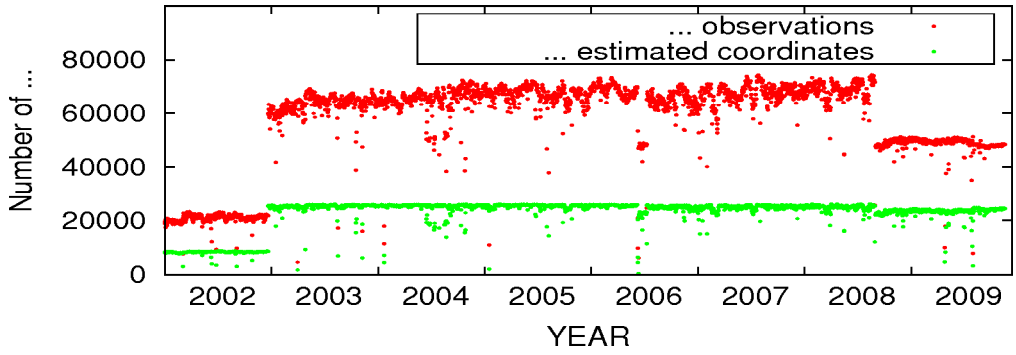

Figure 5.16: Number of used GPS observations and estimated kinematic CHAMP coordinates between 2002 and 2009.

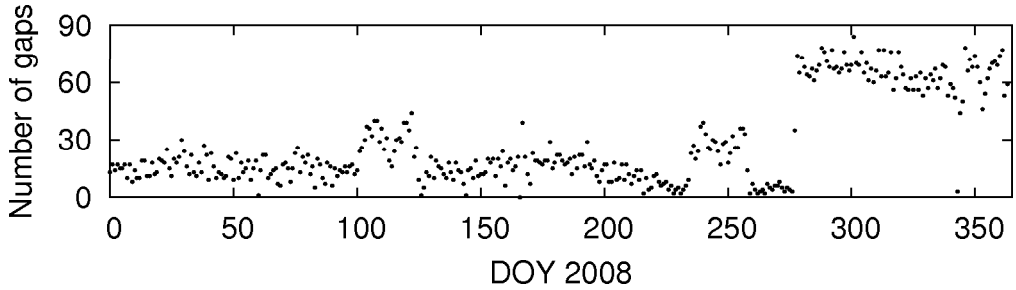

Figure 5.17: Number of gaps per day in the kinematic positions in 2008.

fected by a reduced number of observed GPS satellites than the reduced-dynamic orbits. This leads to larger differences between the kinematic positions and the positions of the reduced-dynamic orbit (Fig. 5.18). The largest differences can be observed in late 2009. From Fig. 2.6 in Sect. 2.2.5 we know that the daily mean of simultaneously tracked GPS satellites decreased below six from DOY 250/2009 on. The LEO POD is summarized in Table 5.10.

Table 5.10: Statistical information related to the CHAMP orbit determination.

Processed days:	2877 (Jan. 2002–Dec. 2009)
Attitude files:	2642
Number of observations (L3 LC of phase obs.):	About 165×10^6
Number of kinematic coordinates:	About 65×10^6

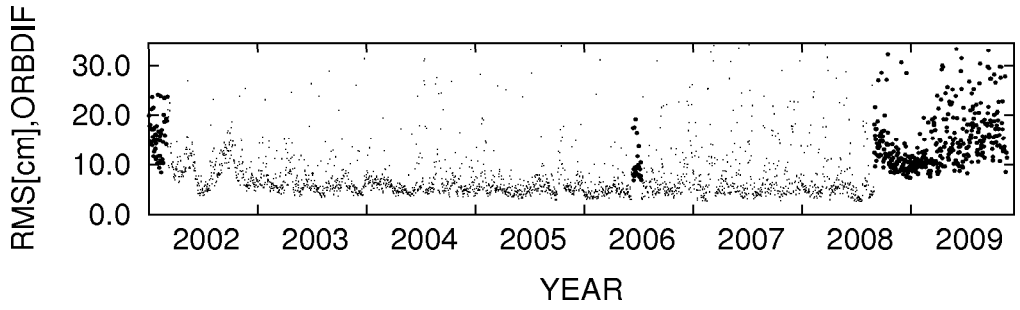

Figure 5.18: Daily 3D-RMS of the difference between the kinematic and reduced-dynamic CHAMP orbits (2002–2009). Fine: Up to 10 GPS satellites tracked. **Bold**: Up to 8 (early 2002) or 7 (mid 2006 and since late 2008) GPS satellites tracked.

5.3.3 Data screening and gravity field recovery

The screening of the kinematic pseudo-observations was performed in the same way as done for the generation of AIUB-CHAMP01S and AIUB-CHAMP02S (see Sect. 5.1.1). The most important improvement in the gravity field processing of AIUB-CHAMP03S concerns the weighting of the kinematic pseudo-observations. As opposed to the determination of AIUB-CHAMP01S and AIUB-CHAMP02S the correlations between the kinematic epochs were taken into account when forming the weight matrix (see Eq. (3.4)). The corresponding covariance matrix was taken from the estimation of the kinematic LEO trajectory. The correlations over 50 epochs (1500 s) were considered for kinematic positions with a spacing of 30 s (data of the year 2002) and 140 epochs (1400 s) in the case of a 10 s spacing of the kinematic epochs (data of the years 2003–2009). The epoch overarching covariance matrices are written into files, which may become rather large. The selected correlation intervals have to be understood as a trade-off between statistical correctness and manageable file size: The kinematic epochs are correlated by the phase ambiguities. The time intervals of uninterrupted visibility of particular GPS satellites (as viewed from the CHAMP receiver) have typical lengths of 20 (1200 s) to 35 min (2100 s). Therefore, the correlation interval of about 1500 s and 1400 s, respectively, seems appropriate.

The background models were selected in such a way that the AIUB-CHAMP03S is compatible to the GRACE-based gravity field models under development at the AIUB (see, e.g., Jäggi, 2010). This includes the use of the EOT08a (Savcenko and Bosch, 2008) ocean tide model and of the atmospheric and ocean de-aliasing products provided by the GFZ-Potsdam (AOD1B-products, Flechtner, 2007). The a priori gravity field model was EGM96 (Lemoine et al, 1998). A summary of the used models and the GNSS processing standards behind AIUB-CHAMP03S may be found in Table 5.11.

The kinematic data of the year 2009 was treated in a special way. As mentioned in Sect. 5.3.2 CHAMP's GPS receiver could only track up to 7 GPS satellites simultane-

Table 5.11: Background models and GNSS processing standards underlying AIUB-CHAMP03S.

Model type	Applied model or convention
Geodetic datum:	IGS05
Nutation model:	IAU2000
Subdaily pole model:	IERS2000
Solid Earth tide model:	IERS2000
Meanpole convention:	IERS2003
Ocean tide model (GPS):	CSR3.0
Ocean tide model (GRAVDET):	EOT08a
Gravity field model (GPS):	JGM3, nmax=12
A priori gravity field model (GRAVDET):	EGM96, nmax=120
Antenna phase center (PCV) model (GPS):	Absolute model
Antenna phase center (PCV) model (CHAMP):	Estimated absolute model
Tropospheric mapping function:	Global mapping function (GMF)
Radiation pressure model (GPS):	Improved CODE RPR model
Radiation pressure model (CHAMP):	None
Phase-windup effect:	Applied
CMC for ocean tidal loading:	Applied
Atmospheric and ocean dealiazing:	AOD1B product applied

ously in 2009. The quality of the kinematic trajectory therefore was not as good as in the preceding years. Many pseudo-observations (about 19%) were lost in the outlier screening, affecting the quality of the gravity field solution for 2009. Experiments (see Sect. 6.3.5) showed that a gravity field solution based on position differences as observables is less sensitive to outliers and comparable in quality. Therefore a third version gravity field solution was computed for the year 2009 using the differences of the unscreened kinematic positions as pseudo-observations. The position-differences were screened using a threshold of 2.5 cm. This way the percentage of screened pseudo-observations was reduced to 10.5. The spacing of the set up pseudo-stochastic pulses was changed to 30 min. The epoch-wise covariance information was used to weight the position-differences, i.e., the correlations between the epochs were not taken into account. For degrees $n > 15$ the resulting gravity field model agrees better with the reference model than the solutions based on the kinematic positions. (On the other hand, the new solution has problems with the degrees $n = 2$ and $n = 3$. The use of position-differences instead of positions as pseudo-observations in the gravity field recovery is discussed in more detail in Sect. 6.3.5.

The solution based on the screened kinematic positions with pulses set up every 5 min (version 1) was combined with the solution based on the position-differences (version 3) on the NEQ-level. Figure 5.19 shows that both input solutions complement each other very well. The combined gravity field solution was therefore selected as the 2009 contribution to AIUB-CHAMP03S. The annual gravity field solutions of the years 2002–2009 were combined to the multi-annual AIUB-CHAMP03S.

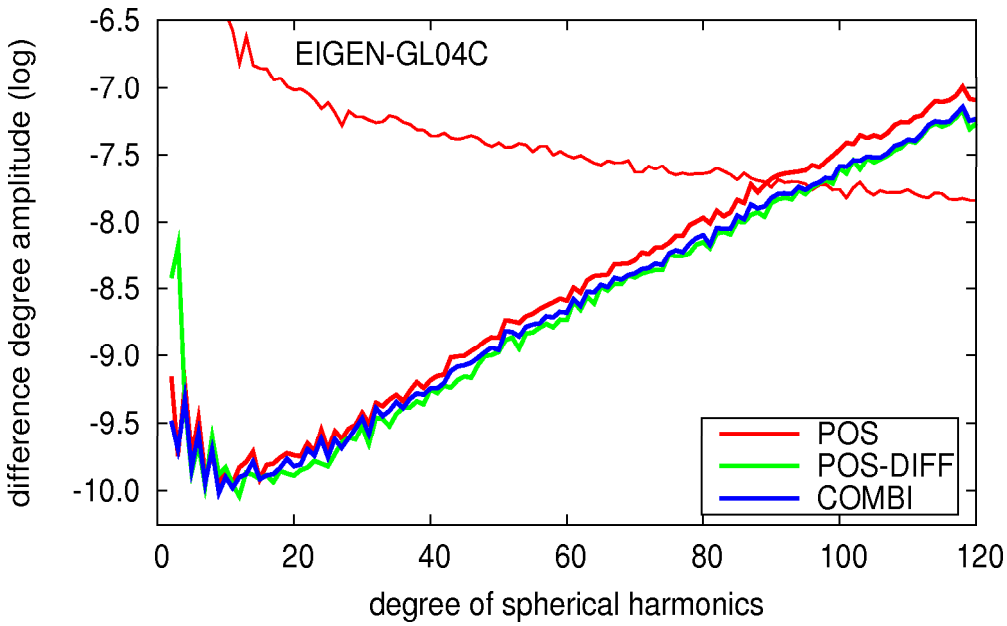

Figure 5.19: Difference degree amplitudes of annual CHAMP gravity field solutions of 2009 based on kinematic positions (POS), position-differences (POS-DIFF), and their combination (COMBI) on the NEQ-level.

A statistical summary of the generation of AIUB-CHAMP03S is provided in Table 5.12. The discrepancy between the theoretical and the practical disk occupancy in Table 5.12 is due to changes in the organizational scheme of the gravity field processing. The daily NEQ files are no longer written to the local machine and combined there. All daily NEQs belonging to the same week are now set up sequentially on one remote machine and then combined there to weekly NEQs. Only the weekly NEQs are saved on the local machine. This approach significantly reduces the disk occupancy and the work load on the local machine. The improvement was enabled by an improved version of the super-BPE of the BSW.

5.3.4 The AIUB-CHAMP03S gravity field model

Figure 5.20 shows the difference degree amplitudes and the error degree amplitudes of AIUB-CHAMP01S, AIUB-CHAMP02S and AIUB-CHAMP03S w.r.t. EIGEN-GL04C. The figure documents the evolution of gravity field recovery from GPS measurements of LEO positions at the AIUB within the recent years. The SH degree at which the difference to the superior reference gravity field exceeds the signal power increased from 74 for AIUB-CHAMP01S, via 90 for AIUB-CHAMP02S to 106 for AIUB-CHAMP03S. This development is confirmed by the formal errors (represented by the error degree amplitude). The formal errors are, however, still too optimistic in the SH degrees below 40 —

Table 5.12: Summary of the AIUB-CHAMP03S gravity field recovery.

Processed days:	2877 (Jan. 2002–Dec. 2009)
Kinematic coordinates (before screening):	64782309
Kinematic coordinates (used in the LSA):	62567250, i.e., 3.4% outliers
Maximum degree:	120
Number of SH coefficients:	14637
Orbit parameters (pre-eliminated) per arc:	6 initial osculating elements, 12 dynamical parameters (constant acc. and coefficients of periodic (1/rev.) acc. in RSW, coefficients of a polynomial acc. of degree three along-track), pulses every 5 min (version 1) or every 15 min (version 2) in RSW
Theoretical disk space requirement:	About 3560 GB
Practical disk space requirement:	About 1010 GB

despite the consideration of the covariances of the pseudo-observations and despite the applied model improvements. The improvement of AIUB-CHAMP03S over its predecessor is also demonstrated by the factor between the difference degree amplitudes of AIUB-CHAMP02S and AIUB-CHAMP03S w.r.t. EIGEN-GL04C, which is shown in Fig. 5.21. The largest improvements were achieved in some of the lower (up to degree 40) even SH degrees. The reason is that an estimated PCV model for CHAMP's GPS antenna was used in the LEO POD for AIUB-CHAMP03S. Therefore the typical inconsistency peaks that are known from AIUB-CHAMP02S disappeared.

The elevation-dependent weighting of the GPS observables in the LEO POD contributed significantly to the improvement of the gravity field solution, too. Additionally, the new solution benefits from the consideration of the correlations between the epochs of the kinematic positions. Furthermore, the change of the spacing between the observation epochs from 30 s to 10 s in the years 2003–2009 has its share on the improvement. Especially the higher SH degrees profit from the densified observation spacing. The impact of the higher sampling rate increases in the later years of the processing time interval, because the high-rate satellite clock corrections perform better in the later years (due to more and better distributed high-rate IGS tracking sites). The impact of the particular processing changes and improvements on the gravity field recovery is discussed in detail in Sect. 6.3.

AIUB-CHAMP03S benefits also from the increased amount of processed data: The years 2008 and 2009 were newly included into the processing. Figure 5.22 shows AIUB-CHAMP03S and the contributing annual solutions. The later years of the mission are especially interesting: Because of CHAMP's orbit decay the gravity field signal in the high SH degrees is less attenuated in the late years. Therefore the slope of the difference-degree curves is less steep for the later years. The difference-degree curve of 2009 is in addition

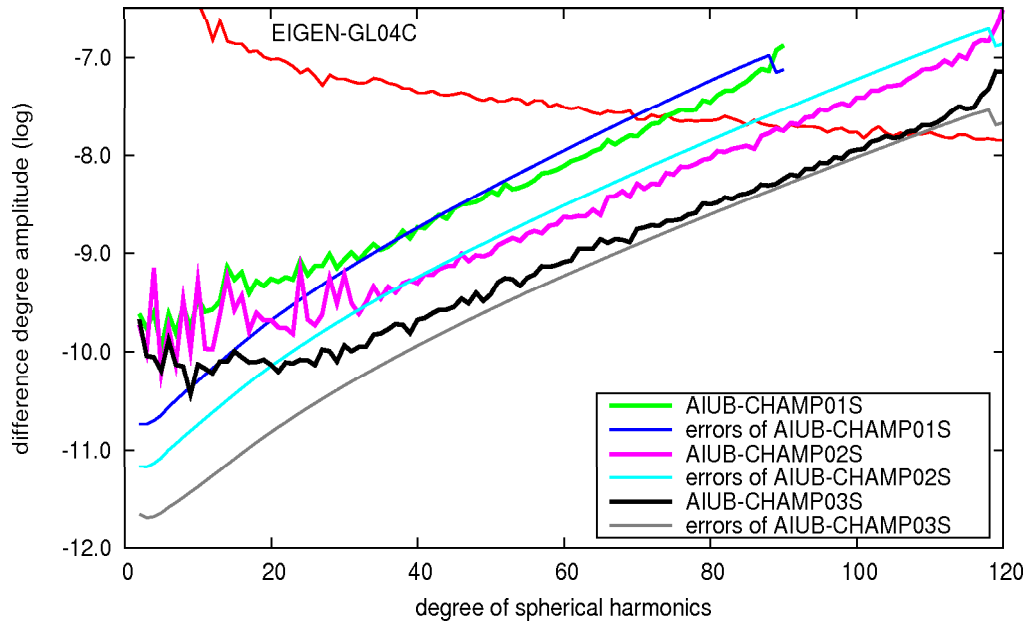

Figure 5.20: Evolution of CHAMP-only gravity field models generated at the AIUB.

influenced by the use of position-differences, further decreasing the slope (see Fig. 5.19). We recognize that the solutions of the years 2007 and 2008 are the best annual solutions. The solution from 2009 suffers from the receiver problems mentioned in Sect. 5.3.2 and Sect. 5.3.3, but still contributes to the determination of the SH coefficients of the higher degrees.

From the SH coefficients of AIUB-CHAMP03S the geoid undulations and the gravity anomalies were computed in the same way as done for AIUB-CHAMP01S in Sect. 5.1.3. The values are shown in Fig. 5.23 and Fig. 5.24. Due to the lower error level of AIUB-CHAMP03S the maximum degree considered in the computation of the functionals could be increased from 70 to 100, improving the half wavelength resolution from 285 to 200 km. Therefore finer details can be resolved — especially in the illustration of the gravity anomalies (compare Fig. 5.5 and Fig. 5.24). This indicates the gain in quality achieved since the generation of AIUB-CHAMP01S.

The comparison to other CHAMP-only gravity field models (see Sect. 7.4) suggests that AIUB-CHAMP03S is, to our knowledge, currently the best gravity field model based only on CHAMP data. Experiments related to AIUB-CHAMP03S are discussed in Sect. 6.3. The coefficients of AIUB-CHAMP03S are available at *http://www.aiub.unibe.ch/content/research/gnss/gnss___research/global_gravity_field_determination/index_eng.html* and at *http://icgem.gfz-potsdam.de/ICGEM/ICGEM.html*.

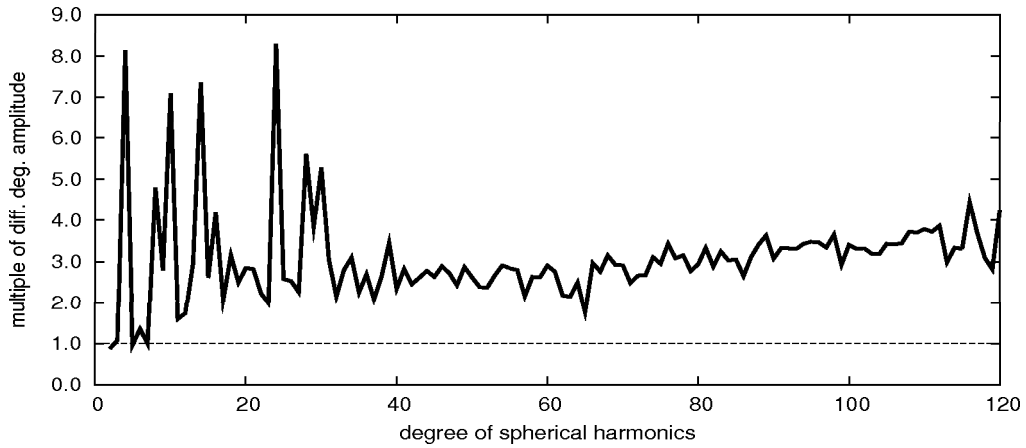

Figure 5.21: Improvement factor between the difference degree amplitudes of AIUB-CHAMP02S and AIUB-CHAMP03S w.r.t. EIGEN-GL04C.

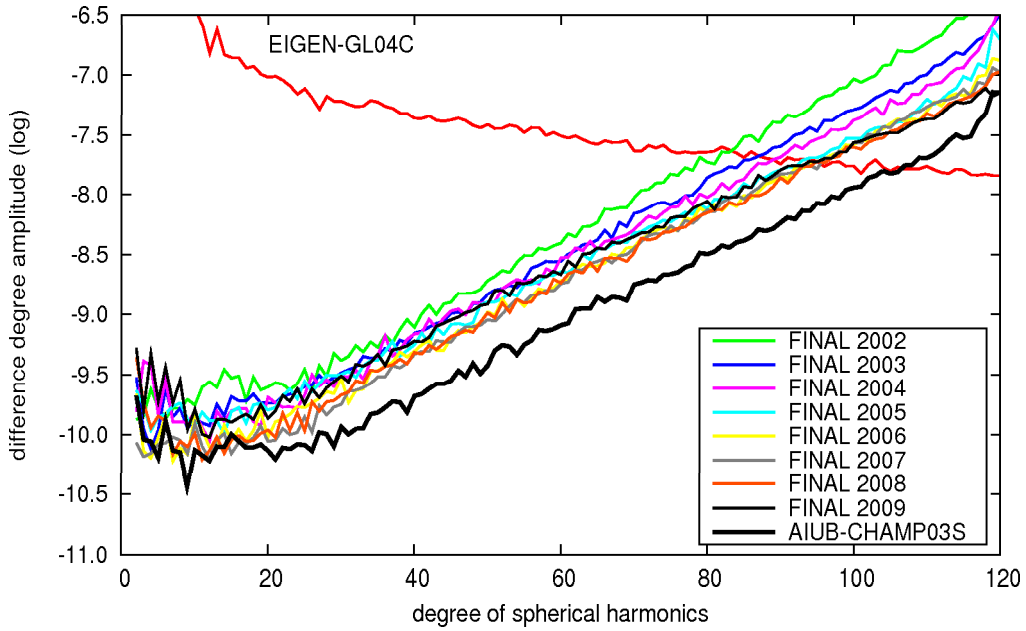

Figure 5.22: Difference degree amplitudes of annual CHAMP gravity field solutions and AIUB-CHAMP03S w.r.t. EIGEN-GL04C.

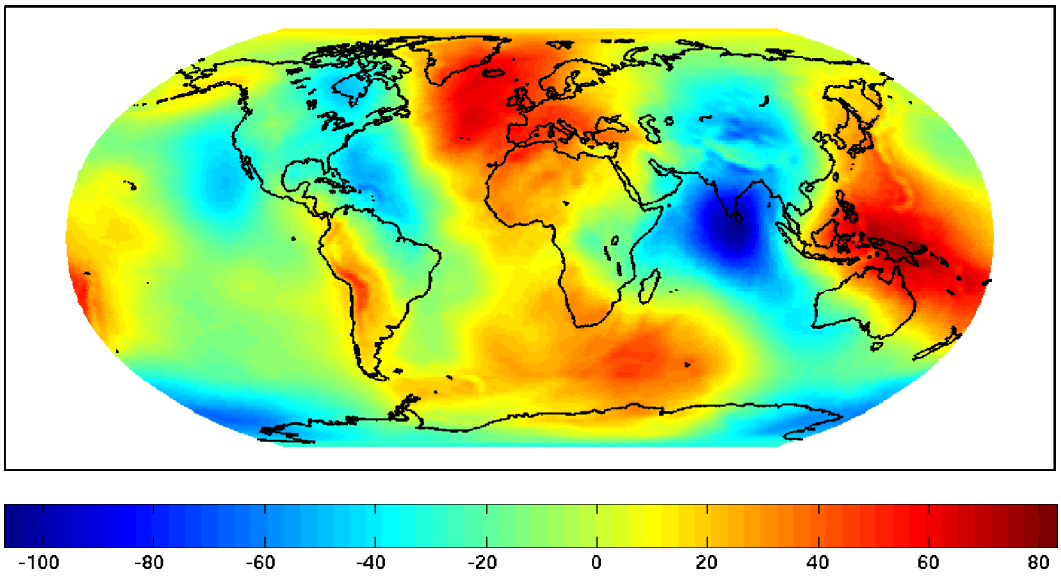

Figure 5.23: Geoid undulations [m] of AIUB-CHAMP03S up to degree 100.

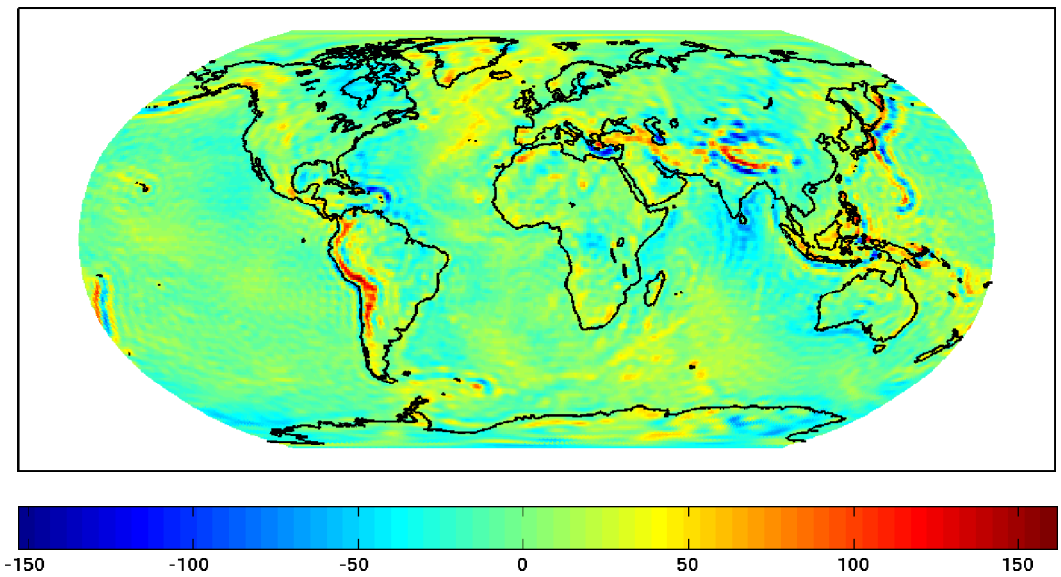

Figure 5.24: Gravity anomalies [mGal] of AIUB-CHAMP03S up to degree 100.

6 Studies and experiments

This chapter describes the most important studies related to the gravity field models AIUB-CHAMP01S, AIUB-CHAMP02S, and AIUB-CHAMP03S. Most experiments are performed in preparation or for optimization of the mentioned models. Some experiments are performed in order to better understand the features of a particular model.

6.1 Studies related to AIUB-CHAMP01S

AIUB-CHAMP01S is the first gravity field model derived at AIUB from real CHAMP data. When the work on this model started, practical experience concerning CHAMP-only gravity field determination using the Celestial Mechanics Approach (CMA) was not available. The most important questions concerned:

- Orbit modeling: arc-specific parameterization; modeling of non-gravitational perturbations with arc-specific parameters, accelerometer data, and dynamical force models; parameter constraining; over-parameterization.
- Impact of different orbit perturbations and modeling deficiencies on orbit and gravity field determination.
- Weighting of the pseudo-observations (Sect. 6.1.5).
- Impact of the a priori gravity field on the solution (i.e., need of an iterative gravity field determination, Sect. 6.1.6).
- Screening of the kinematic positions (Sect. 6.1.7).

The experience necessary for generating AIUB-CHAMP01S was acquired in a series of experiments, the most important of which are presented in this section. At the beginning and the end of each experiment the goals and the results of the experiment are summarized.

A satellite orbit arc is determined by the six initial osculating elements, provided the force field is known. From Sect. 3.3.1 we know that LEO orbits are disturbed by gravitational and non-gravitational perturbations. The gravitational perturbation forces are described by models (e.g., gravity field model, ocean tide model). Non-gravitational perturbations (air drag, direct solar radiation pressure, Earth albedo radiation pressure) may be modeled by appropriate dynamical force models, may be absorbed by dynamical orbit parameters, or may be described by accelerometer measurements in a dynamic orbit determination. For high accuracy demands a purely dynamic LEO orbit determination is

usually not accurate enough due to model errors, measurement errors of the accelerometer data, or omission errors of the gravitational force models. Pseudo-stochastic parameters therefore have to be set up in addition. The compensation of orbit perturbations and the parameterization are of crucial importance for gravity field recovery. Orbit modeling studies are therefore the core topic of this section. Thereby Sect. 6.1.1 focuses on arc-specific parameters, Sect. 6.1.2 on the use of models for the non-gravitational orbit perturbations, and Sect. 6.1.3 on the use of accelerometer data. These studies with real data are supported by a simulation study (Sect. 6.1.4), where different error sources can be separated from each other. The simulation study shall help to better understand the findings of the real data experiments.

The screening and processing environments had to be established. The scripts and the processing scheme used for the generation of AIUB-CHAMP01S (see Sect. 5.1) were developed parallel to or as a result of the experiments described here. The programs were already available. Some programs (in particular GRAVDET, see Sect. 4.7) required adaptations to the new processing environment (e.g., due to compiler changes) and modifications (e.g., file format modifications, mean pole definition, implementation of the CMC).

Using the results of the gravity field processing, the quality changes with time of CHAMP gravity field solutions are studied on the example of the monthly contributions to AIUB-CHAMP01S (Sect. 6.1.8). This aspect is, e.g., important when analyzing temporal variations of the gravity field as done later in this chapter (Sect. 6.3.7).

6.1.1 Orbit modeling with arc-specific parameters

In this section CHAMP's orbit is described without using models for the non-gravitational perturbations and without using accelerometer data (i.e., the non-gravitational perturbations are compensated by arc-specific parameters alone). An appropriate dynamic parameterization shall be defined as the basis for setting up pseudo-stochastic orbit parameters (**Test1**). Different reduced-dynamic parameterizations are then analyzed in orbit determination and gravity field recovery experiments. The compensation of selected orbit perturbations by the arc-specific parameters will be tested in order to find out, whether an orbit modeling based on pseudo-stochastic parameters is suitable for LEO POD and gravity field recovery (**Test2–5**).

The optimal spacing between the pseudo-stochastic parameters is of interest **Test6**. The large number of pseudo-observations (8640 per day with a spacing of 30 s) allows it to set up many pseudo-stochastic parameters with a still large degree of freedom. If the number of parameters becomes too large, however, the problem will be over-parameterized. In this case the parameters also absorb information about the static gravity field, which could pose a problem in a gravity field determination. The over-parameterization limit and possible ways of avoiding over-parameterization effects shall be studied (**Test6a, 7**).

Furthermore, it is important to know, whether CHAMP is sensitive to the higher SH degrees above, let's say, degree 70 and to find appropriate ways to reduce omission errors caused by a limited cut-off degree (n_{max}) of the gravitational force models or in a

CHAMP-only gravity field determination (the maximum SH degree of the true gravity field is infinite, **Test2–3**). An optimum parameterization for CHAMP-only gravity field recovery using the CMA will be defined.

Test1: Dynamic and reduced-dynamic orbit determination using arc-specific parameters

Goals:

- Definition of an appropriate dynamic orbit parameterization for CHAMP.
- Definition of suitable reduced-dynamic orbit parameterizations for CHAMP.

Dynamic orbits with arc-lengths of one day are estimated for 30 days (DOY 171–200/2002) using unscreened kinematic CHAMP positions as pseudo-observations. The kinematic positions referring to different epochs and the coordinates within each epoch are assumed to be independent pseudo-observations with the same accuracy. The gravity field is EIGEN-2 (Reigber et al, 2003) up to degree and order 120. The ocean tide model is CSR3.0 (Eanes and Bettadpur, 1996) up to degree and order 20. Apart from that the background models and standards are the same as those used for the generation of AIUB-CHAMP01S (see Table 5.1 in Sect. 5.1). The orbit determination is repeated with different dynamic and reduced-dynamic orbit parameterizations. The parameterizations, their abbreviations, the corresponding number of arc-specific parameters (n_{par}), and the mean RMS errors of orbit determination are summarized in Table 6.1. The residuals in radial, along-track, and cross-track direction are shown for the example of DOY 196/2002 in Fig. 6.1.

As expected, the six initial osculating elements (OSCELE parameter setting, see Table 6.1 (a) and Fig. 6.1 (a)) are insufficient to describe a disturbed LEO orbit. The along-track residuals reach magnitudes up to 400 m on DOY 196/2002. The mean RMS error is larger than 100 m. The dominating along-track error is mainly caused by the unmodeled

Table 6.1: Mean RMS errors (column 4) of 30 days CHAMP orbit determination in 2002 with different arc-specific parameterizations (column 1, abbreviations (ABB) in column 2, number of parameters (n_{par}) in column 3).

Parameterization	ABB	n_{par}	RMS error
a.) Init. osculating elements	OSCELE	6	137.750 m
b.) like a.) + acceleration in R,S,W	D3	9	3.750 m
c.) like b.) + 1/rev. acceleration in R,S,W	D9	15	1.280 m
d.) like c.) + polynomial acc. of degree 3 in S	DYNPAR	18	0.195 m
e.) like d.) + pulses in R,S,W every 90 min.	DP90	63	0.041 m
f.) like d.) + pulses in R,S,W every 30 min.	DP30	159	0.016 m
g.) like d.) + pulses in R,S,W every 15 min.	DP15	303	0.011 m
h.) like d.) + pulses in R,S,W every 5 min.	DP05	879	0.006 m

air drag, which induces an along-track acceleration against the satellite's flight direction. The drag also causes a cross-track acceleration of much smaller size, because the atmosphere is rotating with the Earth and "hits" CHAMP on its nearly polar orbit from the side (see also Beutler, 2005). The absolute value of the air-drag varies for elliptical orbits with a period of one orbit revolution due to the varying density of the upper atmosphere at different heights. The drag is maximal in the perigee and minimal in the apogee of the LEO orbit.

If constant accelerations in radial (R), along-track (S), and cross-track (W) direction are estimated in addition (D3 parameter setting, see Table 6.1 (b) and Fig. 6.1 (b)), the mean RMS error decreases below a level of four meters and the largest along-track residuals have a size of about 10 m on DOY 196/2002, because the mean part of the perturbing accelerations is absorbed.

The periodic fraction is absorbed by setting up the coefficients of once per revolution (1/rev.) periodic acceleration functions of the argument of latitude u in R, S, and W direction (D9 parameter setting, see Table 6.1 (c) and Fig. 6.1 (c)). This reduces the mean RMS error further to a level of about 1.3 m and the maximum along-track residuals on DOY 196/2002 to about 1.5 m.

The along-track signal still dominates, but can be further reduced by setting up coefficients of a polynomial acceleration function of degree 3 in along-track direction (DYNPAR parameter setting, see Table 6.1 (d) and Fig. 6.1 (d)). With only 18 arc-specific parameters the mean RMS error of the dynamical orbit determination is reduced below 20 cm and the large residuals on DOY 196/2002 are reduced to the decimeter-level. The residuals contain, however, still a strong signal that cannot be absorbed by the applied dynamical orbit parameters. Such a dynamic orbit is suited for orbit determination with limited accuracy demands, e.g., for producing the residuals for a rough outlier screening. For highest accuracy demands (such as gravity field determination) a better orbit representation is necessary.

In addition to the dynamic orbit parameters pseudo-stochastic pulses with different spacings (DP90, DP30, DP15, and DP05 parameter settings, see Table 6.1 (e–h) and Fig. 6.1 (e–h)) are set up in R, S, and W direction. Pulses with 90 min spacing (DP90 setting) already absorb much of the along-track signal (Fig. 6.1 (e)) that is still dominant in the residuals of the best described dynamic orbit. The mean RMS error is reduced to about 4 cm, but the residuals still show a systematic behavior.

When setting up more and more pulses, most of the remaining perturbation signal can be absorbed and the mean RMS error comes down to about 6.5 mm in case of the DP05 setting. The price to pay for the excellent orbit fit is a large number of orbit parameters and therefore a reduced degree of freedom. When many pseudo-stochastic parameters are set up, the residuals are largest in radial direction (corresponding to the UP component of a ground station), which is expected from the GPS error behavior (see, e.g., Hoffmann-Wellenhof et al, 2008).

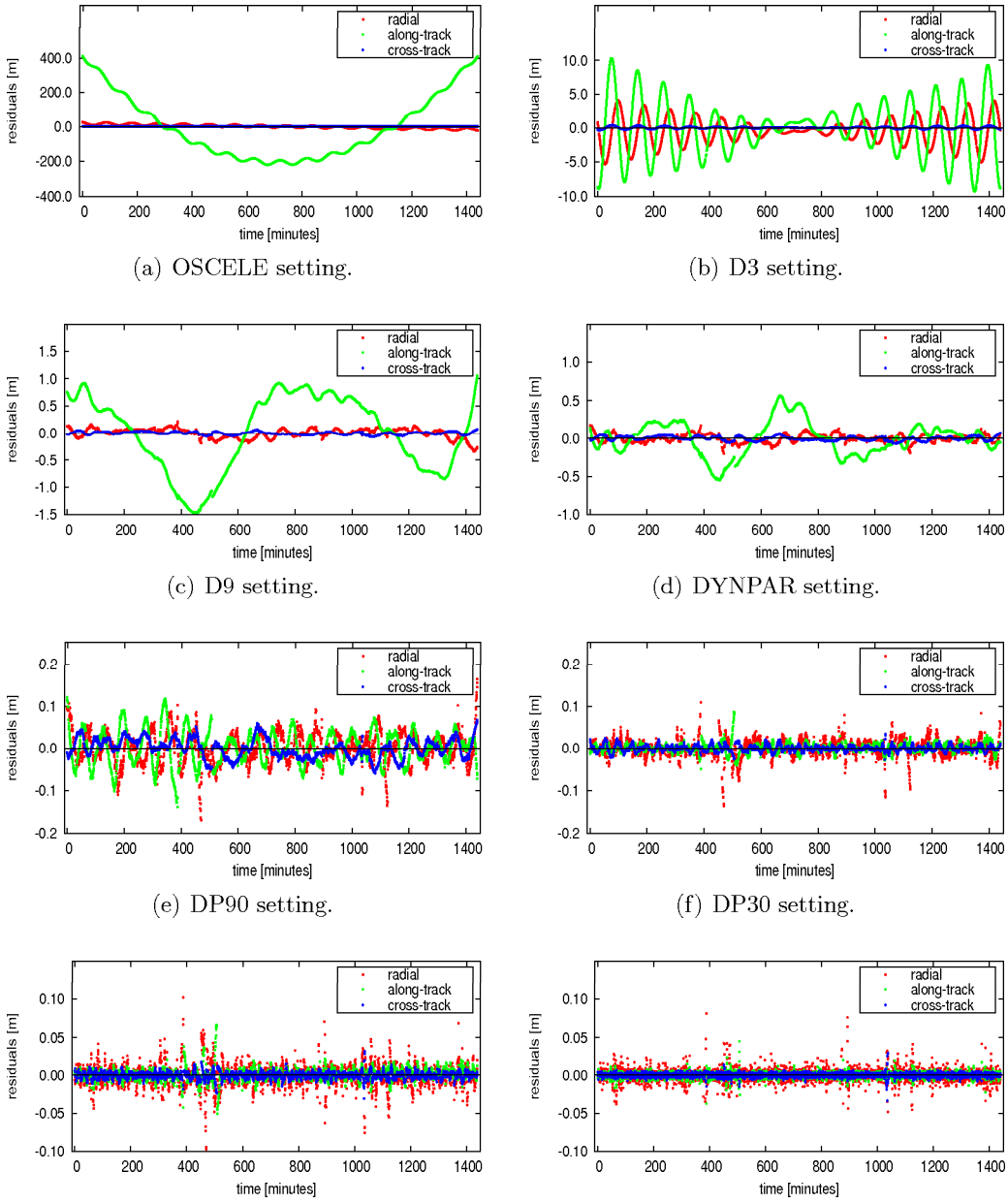

(a) OSCELE setting.

(b) D3 setting.

(c) D9 setting.

(d) DYNPAR setting.

(e) DP90 setting.

(f) DP30 setting.

(g) DP15 setting.

(h) DP05 setting.

Figure 6.1: Residuals of the CHAMP orbit determination on DOY 196/2002 when different arc-specific parameterizations are used. The abbreviations of the parameter settings are defined in Table 6.1. Note the different scales.

Results:

- The DYNPAR setting allows a coarse CHAMP orbit determination with a mean RMS error of approximately 20 cm within the test time interval. The residuals still contain a large signal, indicating that orbit perturbations are only partly compensated.
- The reduced-dynamic orbit parameterizations DP15 and DP05 reduce the mean RMS errors of orbit determination to about 1 cm and 0.6 cm and remove most of the residual signal (i.e., they are able to absorb most of the orbit perturbations).

Test2: Impact of omission errors on CHAMP orbit determination

Questions:

- Is CHAMP's orbit sensitive to SH degrees above 70?
- Which orbit parameterizations found in **Test1** are able to absorb omission errors in an orbit determination?

The test is a repetition of the previous orbit determination (**Test1**) with the cut-off degree (n_{max}) of the EIGEN-2 gravity field model being reduced from 120 to 70. Table 6.2 informs about the tested orbit parameterizations, their abbreviations, the corresponding number of arc-specific parameters (n_{par}), and the mean RMS errors of orbit determination for both cut-off degrees. Figure 6.2 compares the residuals on DOY 196/2002 in radial, along-track, and cross-track direction for both cut-off degrees.

Initially only dynamical orbit parameters are set up (DYNPAR parameter setting, see

Table 6.2: Mean RMS errors (columns 4 and 5) of 30 days CHAMP orbit determination in 2002 with different arc-specific parameterizations (column 1, abbreviations in column 2, number of parameters (n_{par}) in column 3) and cut-off degrees n_{max} of the gravity field model.

Parameterization	Abbreviation	Number of parameters	Mean RMS error with $n_{max} = 70$	Mean RMS error with $n_{max} = 120$
a.) Osc. ele. + dynamical param.	DYNPAR	18	0.304 m	0.195 m
b.) like a.) + pulses every 30 min.	DP30	159	0.022 m	0.016 m
c.) like a.) + pulses every 15 min.	DP15	303	0.012 m	0.011 m
d.) like a.) + pulses every 5 min.	DP05	879	0.006 m	0.006 m

Table 6.2 (a) and Fig. 6.2 (a–b)). The mean RMS error and the residuals are significantly larger if the gravity field is taken into account up to SH degree 70 instead of 120. This shows that CHAMP's orbit is sensitive to the SH coefficients above degree 70. The dynamic orbit parameters are not able to compensate for the resulting omission errors.

If pseudo-stochastic pulses are set up in addition (DP30, DP15, DP05 parameter settings, see Table 6.2 (b–d) and Fig. 6.2 (c–h)), the perturbation signal in the residuals and the mean RMS errors are greatly reduced. The more pulses are set up, the more the solutions with $n_{max} = 70$ and $n_{max} = 120$ become similar. With a pulse spacing of 5 min the residuals and mean RMS errors are almost the same, because the shorter spaced pulses can better absorb the high frequency perturbations caused by ignoring the fine structures of the gravity field in the orbit determination.

Results:

- CHAMP is sensitive to the SH coefficients above degree 70 of the Earth's gravity field.
- The DYNPAR parameterization compensates for omission errors only insufficiently. The DP05 parameterization is able to absorb much of the omission errors in the orbit determination.

Test3: Impact of omission errors on gravity field determination

Questions:

- What is the impact of omission errors on a CHAMP-only gravity field determination when setting up many pseudo-stochastic parameters?
- How can remaining omission errors be reduced in a CHAMP-only gravity field determination?

Two annual gravity field solutions are estimated in the same way as AIUB-CHAMP01S with pulses set up every 5 min (see Sect. 5.1). The SH coefficients are set up up to maximum degrees of 70 and 90, respectively. Any coefficients of higher degrees are ignored, i.e., they are not modeled and not estimated. Both gravity field solutions are compared in Fig. 6.3.

The solution with a cut-off degree of 70 is affected by large omission errors from degree 60 on — despite the set up of pulses every 5 min. The solution with a cut-off degree of 90 is less affected. Only small omission errors close to degree 90 can be recognized. Other than expected from the orbit determination experiment **Test2** even the DP05 parameterization is not able to completely absorb the omission errors in the gravity field determination: A significant part of the omission errors is absorbed by the estimated SH coefficients of high degrees.

From a certain degree on the error of the estimated SH coefficients is larger than their signal. In the case of AIUB-CHAMP01S this limit (let us call it "detectability limit") is reached at degree 74 — at least for the zonal coefficients. The experiment shows, however, that CHAMP is sensitive to SH coefficients of degrees above the "detectability limit" — although these coefficients cannot be determined precisely. It makes therefore sense to select a higher cut-off degree. The higher degree coefficients then absorb a fraction of

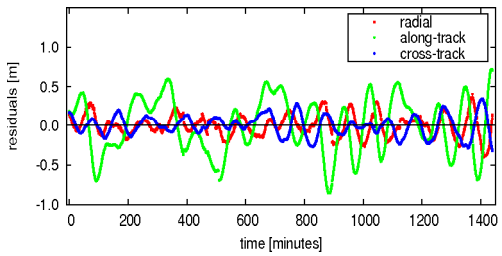

(a) DYNPAR setting, $n_{max} = 70$.

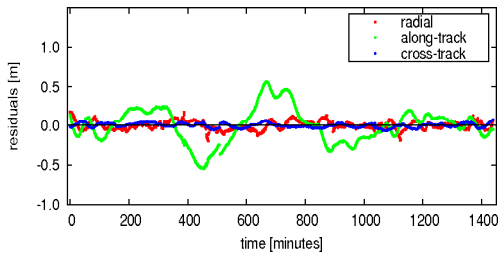

(b) DYNPAR setting, $n_{max} = 120$.

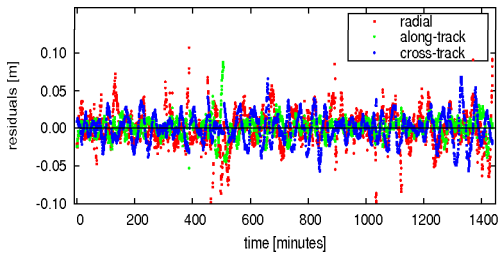

(c) DP30 setting, $n_{max} = 70$.

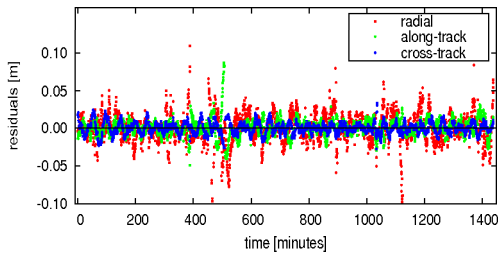

(d) DP30 setting, $n_{max} = 120$.

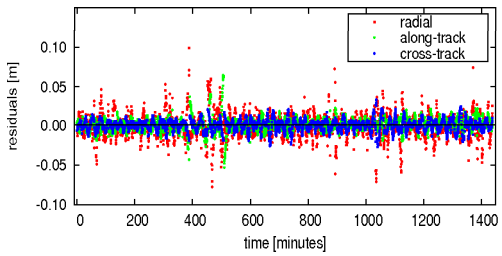

(e) DP15 setting, $n_{max} = 70$.

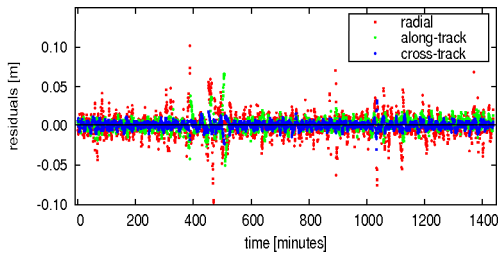

(f) DP15 setting, $n_{max} = 120$.

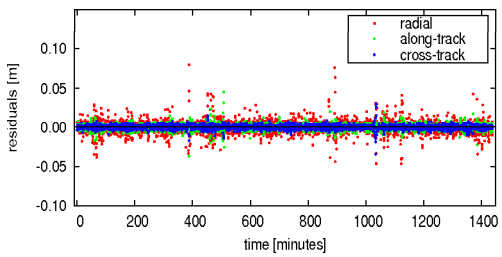

(g) DP05 setting, $n_{max} = 70$.

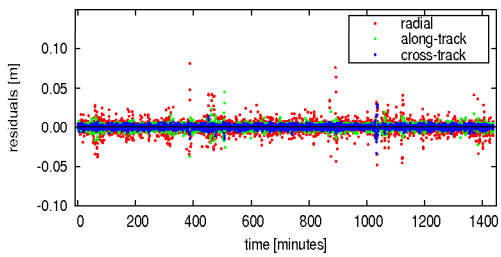

(h) DP05 setting, $n_{max} = 120$.

Figure 6.2: Residuals of the CHAMP orbit determination on DOY 196/2002 when different arc-specific parameterizations are used and the static gravity field is considered up to the maximum SH degree n_{max}. **Left:** $n_{max} = 70$. **Right:** $n_{max} = 120$. The abbreviations of the parameter settings are defined in Table 6.2.

the remaining omission errors that would otherwise affect the SH coefficients (below the "detectability limit") we are interested in. Alternatively the cut-off degree could be chosen close to or even below the "detectability limit" and the information of the higher degree harmonics could be introduced from a good a priori gravity field model (e.g., a GRACE-model). Here we will, however, focus on CHAMP-only gravity field determination. On the basis of this experiment, it was decided to set up the SH coefficients up to degree and order 90 in the case of AIUB-CHAMP01S.

Results:

- Even the DP05 parameterization is not able to completely compensate for the omission errors in the gravity field determination.
- The remaining omission errors affect the SH coefficients of higher degrees more than coefficients of lower degrees. They can be reduced by choosing a high cut-off degree (n_{max}): Although the SH coefficients above the "detectability limit" cannot be estimated accurately they are able to absorb remaining omission errors.

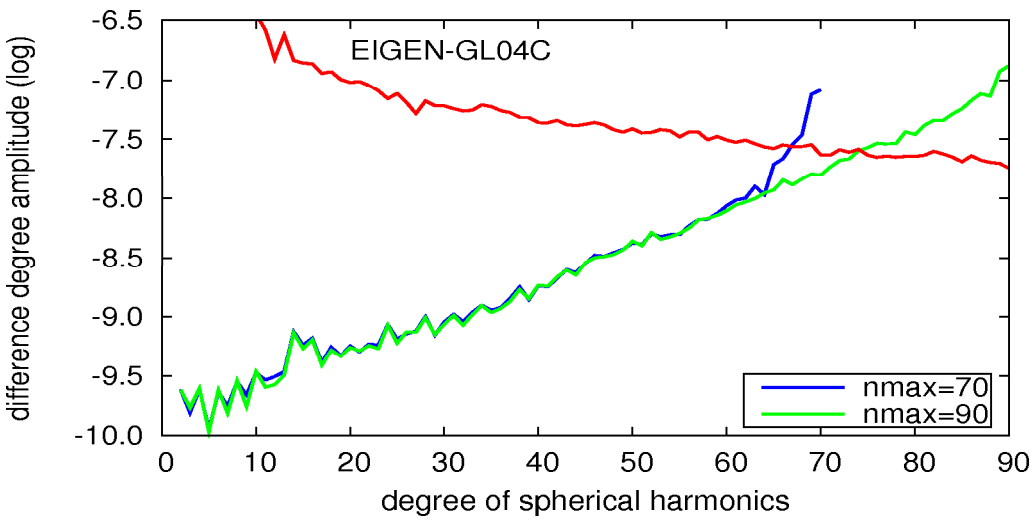

Figure 6.3: Difference degree amplitudes w.r.t. EIGEN-GL04C (Förste et al, 2008) of annual gravity field solutions with the same arc-specific parameterization but different cut-off degrees (n_{max}) of the SH series.

Test4: Compensation of insufficiently modeled ocean tides

Goal:

- Illustration of the absorption of model deficiencies by pseudo-stochastic parameters on the example of the ocean tides.

Not only the static gravity field and the non-gravitational forces might be modeled insufficiently. The models for the time-variable part of the gravitational force field, such as the

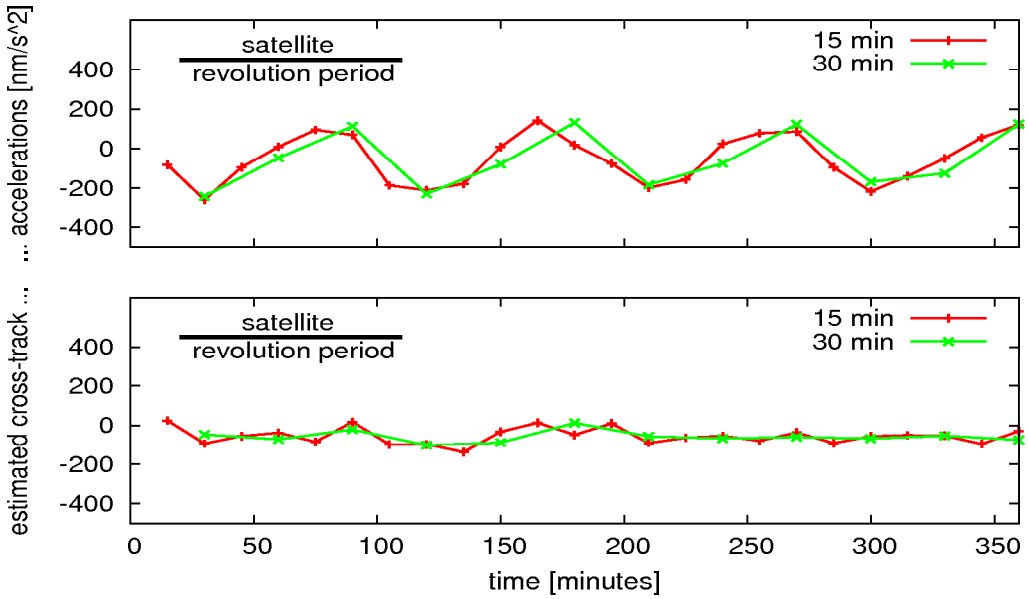

Figure 6.4: Estimated piecewise constant accelerations with spacings of 15 and 30 min in cross-track direction on DOY 196/2002. The ocean tides are modeled up to degree 4 (top) and degree 20 (bottom), respectively.

ocean tides, may have deficiencies, as well. The capability of pseudo-stochastic parameters to absorb such deficiencies is demonstrated in the following orbit determination experiment: CHAMP's orbit on DOY 196/2002 is determined using different reduced-dynamic orbit parameterizations. In addition to the six initial osculating elements, piecewise constant accelerations (PCAs) are set up with different spacings of 15 and 30 minutes, respectively. The ocean tides are those of the ocean tide model CSR3.0. In a first solution series the ocean tides are only considered up to degree 4 (insufficient for a LEO satellite), in a second solution series up to degree 20.

The insufficiently modeled ocean tide signal in the first series is absorbed to a large extent by the estimated PCAs (Fig. 6.4, top). In the case of the properly modeled ocean tides the signal in the PCAs is gone (Fig. 6.4, bottom).

Result:

- Insufficiently modeled ocean tides can be absorbed by pseudo-stochastic parameters to a large extent.

Test5: Gravity field determination with insufficiently modeled ocean tides

Goal:

- Illustration of the compensation of model deficiencies by pseudo-stochastic parameters in the gravity field determination on the example of the ocean tides.

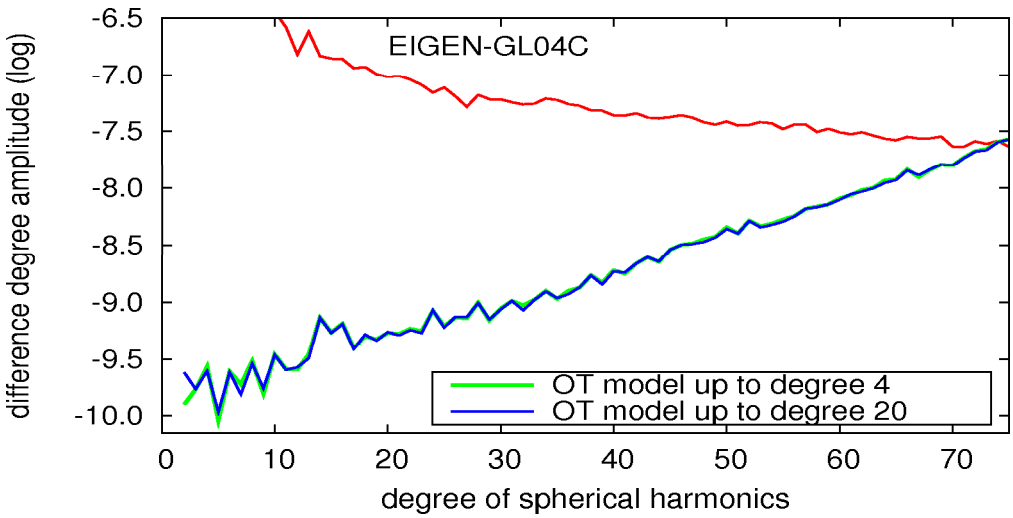

Figure 6.5: Difference degree amplitudes w.r.t. EIGEN-GL04C of annual gravity field solutions with the same parameterization, but different upper limits (4, 20) of the ocean tide model CSR3.0.

The results of **Test4** are propagated from orbit determination to gravity field recovery: Two annual gravity field models are estimated using the options and models underlying AIUB-CHAMP01S (see Sect. 5.1). Pulses are set up every 5 min. The two solutions only differ in the maximum degree (4 vs. 20) of the ocean tide model CSR3.0.

The difference degree amplitudes of both solutions w.r.t. EIGEN-GL04C are very similar (Fig. 6.5), indicating that the effect of the unmodeled ocean tides of SH degrees 5–20 is nearly completely absorbed by the arc-specific parameters (see **Test4**) and does not harm the gravity field solution.

Result:

- Insufficiently modeled ocean tides can be absorbed by pseudo-stochastic parameters and do not harm the gravity field solution.

Test6: Gravity field determination with different pulse spacings

Questions:

- Which reduced-dynamic orbit parameterization from **Test1** is best suited for CHAMP-only gravity field recovery?
- At which pulse spacing the over-parameterization limit is reached?

Test1 shows that large numbers of pseudo-stochastic parameters absorb much of the residual signal in the orbit determination and reduce the RMS error (the error of the LSA generally decreases with an increased number of parameters). This does not automatically

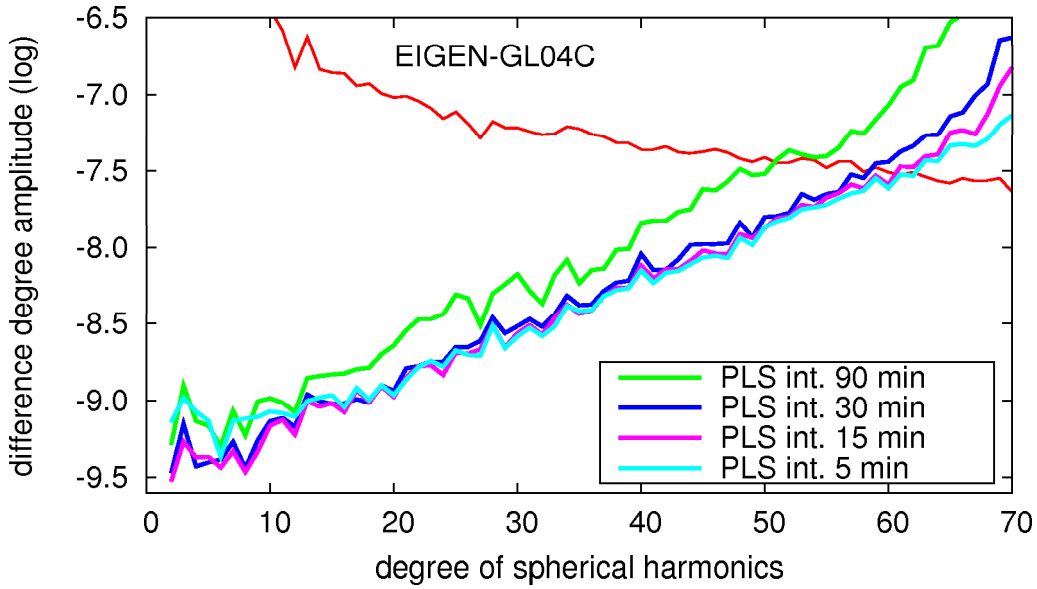

Figure 6.6: Difference degree amplitudes w.r.t. EIGEN-GL04C of gravity field solutions from two months of CHAMP data. The solutions are based on different reduced-dynamic orbit parameterizations (DP90, DP30, DP15, DP05 in Table 6.1).

imply a quality gain for the gravity field determination. The impact of the pulse spacing on gravity field determination is verified by estimating different gravity field models using two months of kinematic CHAMP positions. Different orbit parameterizations (DP90, DP30, DP15, DP05, see Table 6.1) are set up in addition to the SH coefficients of the Earth's gravity field up to degree and order 70.

The difference degree amplitudes of the resulting solutions w.r.t. EIGEN-GL04C are shown in Fig. 6.6. They are generally smaller for the solutions with more pulses. Similar to the orbit determination the gravity field solutions are better with more pulses set up, because the pulses successfully absorb model deficiencies of different kinds (gravitational and non-gravitational). Shorter spaced pulses are able to compensate for perturbation signal with higher frequency. Therefore the high SH degrees benefit a bit more from a shorter pulse spacing.

The results indicate that the separation of the static gravity field signal (to be absorbed by the estimated gravity field parameters) and the perturbation signal (to be absorbed by the arc-specific parameters) generally works fine for CMA when being left to "mathematics" (Beutler et al, 2010b). The solution based on a pulse spacing of only 5 min (DP05) has, however, deficiencies in the low (< 15) SH degrees, indicating that the parameter estimation problem is over-parameterized in this part of the SH spectrum. The un-constrained pulses obviously absorb gravity field signal of long wavelengths. With

Eq. (3.29) the half wavelength resolution corresponding to SH degrees 3 and 10 is about 6650 km and 2000 km, respectively. When assuming an orbital velocity of 7.6 km/s at an altitude of 450 km, CHAMP covers a distance of about 6840 km and 2280 km in 15 and 5 min, respectively. A pulse spacing of 15 min thus roughly corresponds to the half wavelength resolution at SH degree 3. For shorter spacings between the pulses the low degree SH coefficients and the un-constrained pulses cannot be completely separated. On the other hand the SH coefficients of high degrees benefit from pulse spacings shorter than 15 min.

Results:

- A shorter spacing of the pseudo-stochastic parameters generally improves the gravity field recovery — especially for the coefficients of high SH degrees (the DP05 solution shows the best performance for the high SH degrees).
- The over-parameterization limit for the recovery of the low degree harmonics is reached with a pulse spacing of about 15 min (the DP15 solution shows the best performance in the low SH degrees).

Test6a: Combination of gravity field solutions on NEQ-level

Questions:

- Is it possible to combine the advantages of different gravity field solutions in order to avoid over-parameterization effects?

Test6 is repeated using one year of kinematic CHAMP positions. Different gravity field models are generated in the same way as AIUB-CHAMP01S (see Sect. 5.1). Only the orbit parameterization differs between the solution versions: Apart from the SH coefficients up to degree and order 90 the orbit parameterizations DP30, DP15, or DP05 (see Table 6.1) are set up, respectively.

Figure 6.7 (a) confirms the results of the 2-month test. It would be interesting to see whether the strengths of different solution versions (good determination of medium and high degree SH coefficients with 5 min pulse spacing, good determination of low degree SH coefficients with 15 min pulse spacing) could be combined. Therefore two different solutions (with 5 min and 15 min pulse sampling: DP05 and DP15) are combined on the NEQ level with equal weight. The combined NEQ system is solved. Figure 6.7 (a) shows that the difference degree amplitude of the combined solution (CDP0515) matches the DP15 solution in the low SH degrees and is very close to the DP05 solution in the medium and high SH degrees. It therefore combines the strengths of both input solutions and shows one way to avoid over-parameterization effects.

The combination of two solutions using the same pseudo-observations but different parameterizations is questionable from the statistical point of view. Figure 6.7 (b) shows, however, that the formal errors behave very similar to the difference degree amplitudes as they are generally smaller for solutions with more pulses set up. Only in the low (< 10)

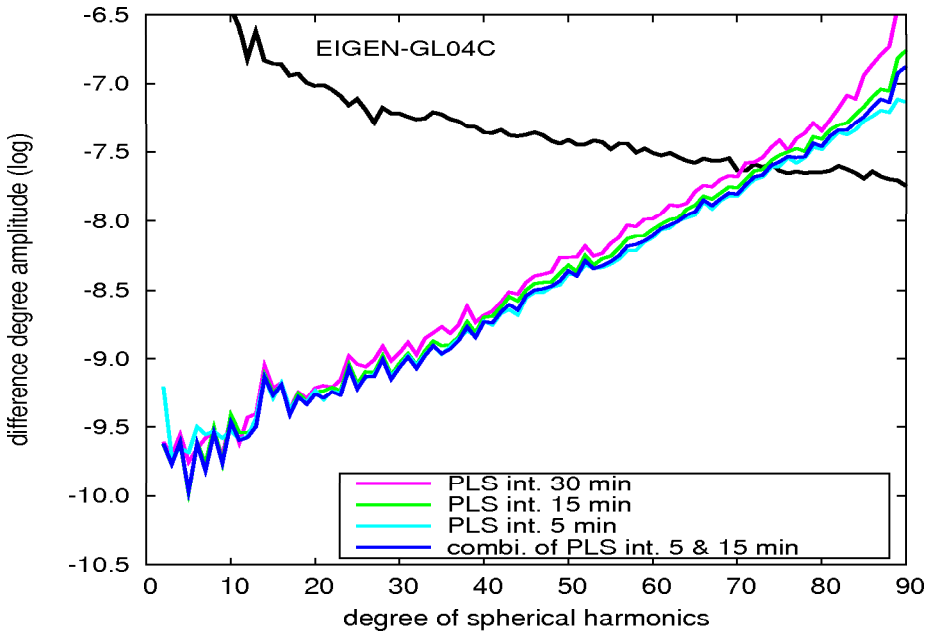

(a)

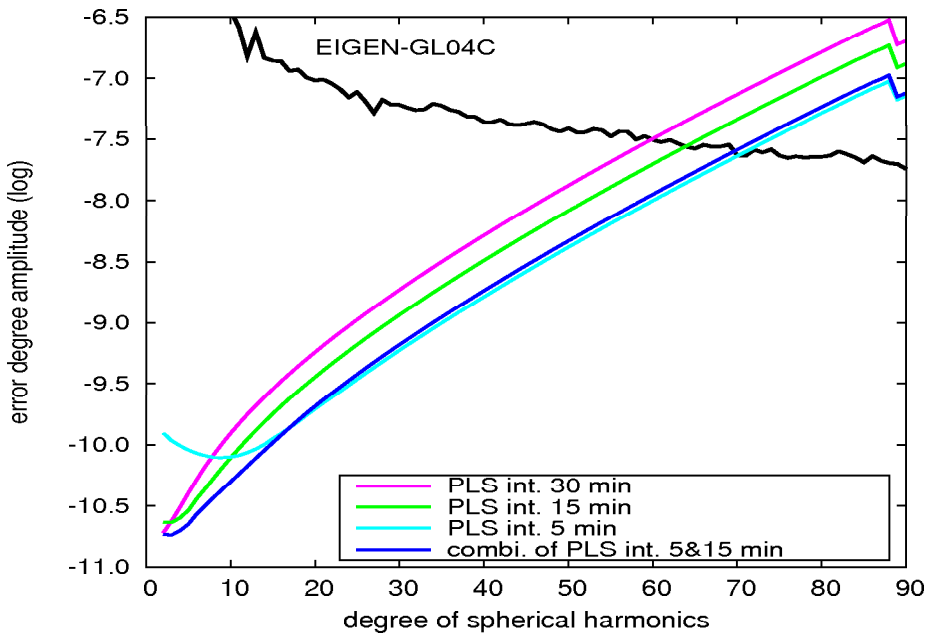

(b)

Figure 6.7: Difference (**top**) and error (**bottom**) degree amplitudes of annual CHAMP gravity field solutions w.r.t. EIGEN-GL04C. The solutions are based on different reduced-dynamic orbit parameterizations (DP30, DP15, DP05 in Table 6.1). The combined solution is the AIUB-CHAMP01S gravity field model.

SH degrees the DP05 solution has larger errors than the other solution versions — indicating the over-parameterization of this solution for the low SH degrees. The formal errors of the combined solution (CDP0515) are close to the errors of DP05 in the medium and high SH degrees and close to the errors of DP15 in the low SH degrees. The errors are, therefore, not more optimistic than those of the uncombined solutions (the formal errors in the lower part of the SH spectrum appear too optimistic for all solutions, when being compared to the corresponding difference degree amplitudes).

Experiment results:

- The advantages of two gravity field solutions may be combined by stacking the NEQs belonging to both solutions. The combined solution shows a good quality for the high degree coefficients and avoids over-parameterization effects in the low SH degrees.
- The formal errors of the combined solution are not more optimistic than the formal errors of the individual solutions.

Test7: Constraining of the pseudo-stochastic parameters

The separability of gravity field and pseudo-stochastic parameters may be improved by constraining the latter parameters. In the case of piecewise constant accelerations (PCAs) constraining also avoids the singularity of the NEQ matrix. For a detailed discussion we refer to Beutler et al (2010b,a).

Questions:

- May over-parameterization effects be avoided by constraining the pseudo-stochastic parameters?
- Are the obtained solutions comparable in quality to solutions using the CDP0515 parameterization (see **Test6a**)?
- Are PCAs better suited for gravity field recovery than pseudo-stochastic pulses?

To the first order a pulse Δv at time t_i in a given direction is equivalent to a constant acceleration Δa over the time interval Δt (spacing between subsequent pulses or interval length for PCAs):

$$\Delta v = \Delta t \cdot \Delta a \ . \tag{6.1}$$

Constraining a pulse is equivalent to introducing an observation equation of type

$$\Delta v = 0 \ , \tag{6.2}$$

with a weight

$$p_v = \frac{\sigma_0^2}{\sigma_v^2} \ . \tag{6.3}$$

In view of Eq. (6.1) one has to apply a weight

$$p_a = \frac{\sigma_0^2}{(\frac{\sigma_v}{\Delta t})^2} \ , \tag{6.4}$$

in order to constrain a solution based on PCAs in an equivalent way as the corresponding solution based on pulses. When estimating PCAs in addition to constant accelerations (constant for the length of one orbit arc) and/or coefficients of periodical accelerations, it is essential that the PCAs are constrained to the values of the constant accelerations, because both parameter types are correlated. Without constraining the PCAs, the NEQ-matrix would therefore be singular. The constant acceleration then absorbs the mean acceleration and the PCAs absorb the fluctuations around the constant acceleration. Pulses, in contrast, may be set up with or without constraints. The interval length Δt is an important property of any reduced-dynamic solution: When Δt is as short as the observation spacing, the (highly) reduced-dynamic orbit is equivalent to a kinematic orbit (Jäggi et al, 2006). For constrained solutions one may put higher weight on the solutions with decreasing Δt (Beutler et al, 2010b).

In this sub-section we present gravity field solutions, whose properties are provided in Table 6.3. The solutions are based on two months of kinematic CHAMP positions from 2002. The SH coefficients are set up up to degree and order 90. The background models are the same as for AIUB-CHAMP01S. Unconstrained/constrained pulses and PCAs with different parameter intervals Δt are used as part of the orbit parameterization (see Table 6.3). The CDP0515 solution is the combination of the DP05 and DP15 solutions on the NEQ-level (see Sect. 6.1.1/**Test6a**). The constraints for the DP05c and DP15c solutions are obtained by numerical experiments. Thereby, solutions with too loose constraints are similar to unconstrained solutions and solutions with too tight constraints are worse in quality than the corresponding unconstrained solutions, because the pseudo-stochastic parameters cannot absorb all perturbations. The constraints of the solutions using PCA (DA05c, DA15c) are derived from the constraints of the DP05c and DP15c solutions using Eq. (6.4). The difference degree amplitudes of all solutions w.r.t. EIGEN-GL04C are computed and compared in order to study the impact of over-parameterization and constraining on solutions with different parameter intervals Δt. The solution based on the CDP0515 parameterization is included as a reference, because it is the best parameterization introduced so far in this work.

Figure 6.8 (a) compares the solutions based on unconstrained pulses. It shows that the DP05 solution is the best solution in the upper part of the SH spectrum (> degree 30) but is over-parameterized for the low degree harmonics (< degree 15). This corresponds with the results of **Test6** in Sect. 6.1.1. Figure 6.8 (b) shows the solutions based on constrained pulses. Due to the constraints the DP05c solution is not over-parameterized for the low SH degrees.

Figure 6.8 (c) shows the solutions based on constrained PCAs. The DA05c and the DA15c solutions are good in the low SH degrees and are not over-parameterized or singular. The solutions are slightly inferior to their DP05c and DP15c counterparts in the high SH de-

Table 6.3: Properties of constraining-test solutions: Name of parameter setting, kind of pseudo-stochastic parameters (PLS=pulses; PCA=piecewise constant accelerations), parameter interval length, constraints.

Test solution	PLS/PCA	Δt	σ
DP15	PLS	15 min = 900 s	—
DP15c	PLS	15 min = 900 s	$900 \cdot 10^{-7} \frac{m}{s}$
DP05	PLS	5 min = 300 s	—
DP05c	PLS	5 min = 300 s	$300 \cdot 10^{-7} \frac{m}{s}$
DA15c	PCA	15 min = 900 s	$1 \cdot 10^{-7} \frac{m}{s^2}$
DA05c	PCA	5 min = 300 s	$1 \cdot 10^{-7} \frac{m}{s^2}$
CDP0515	PLS	combi. 5min/15 min	—

grees. This could possibly be corrected by slightly relaxed constraints. It is, however, assumed that pulses are better suited for gravity field recovery than PCAs, because they do not affect the satellite orbit in-between the pulse epochs (Jäggi et al, 2010a). They do, therefore, absorb less of the gravity field signal. For both types of pseudo-stochastic parameters we notice, however, that the gain in the low SH degrees (due to avoiding over-parameterization) has to be paid with a reduced quality in the high SH degrees, because the constrained pseudo-stochastic parameters are not "free" enough to compensate for all orbit perturbations. The comparison with the CDP0515 solution shows, therefore, that neither uncombined solution, whether constrained or unconstrained, can compete with the combined CDP0515 solution in the whole SH spectrum.

Results:

- Constraining the pseudo-stochastic parameters avoids over-parameterization effects in the low SH degrees of the gravity field solution.
- The gain achieved in the low SH degrees is accompanied by a degradation in the remaining part of the SH spectrum. Therefore no other parameterization shown in this experiment can compete with the CDP0515 parameterization (see **Test6a**) in the whole SH spectrum.
- For the PCAs, as applied in this work, constraining is essential in order to prevent a singularity of the NEQ system. For pulses a constraining is not essential. Furthermore the pulses show a slightly better performance in the gravity field recovery. Pulses are therefore the preferred pseudo-stochastic parameters used in this work.
- An equivalent test series was performed including accelerometer data. The inclusion of accelerometer data did not change the outcome of this experiment (i.e., the effective size of the constraints could not be reduced). Therefore, a separate detailed display of the results is abandoned. One could have expected that the constraints of the pseudo-stochastic parameters might be tightened when using accelerometer

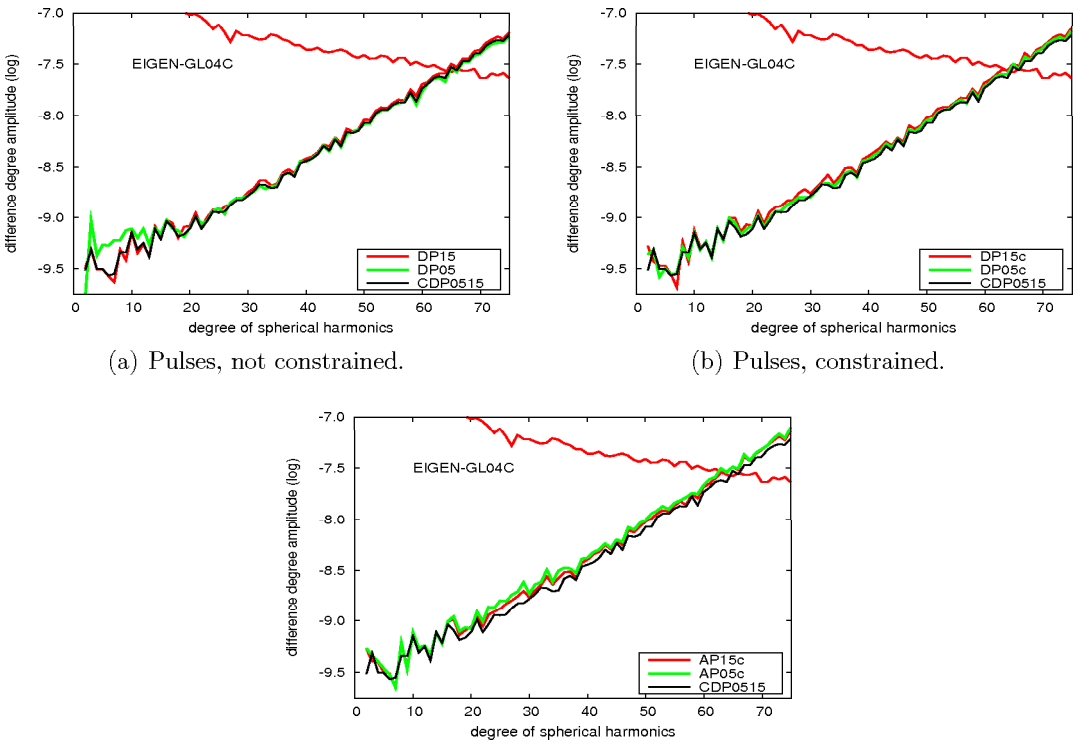

(a) Pulses, not constrained.

(b) Pulses, constrained.

(c) PCAs, constrained.

Figure 6.8: Impact of constraining on gravity field solutions based on pseudo-stochastic pulses or piecewise constant accelerations (PCAs).

data. In Sect. 6.1.1 we show, however, that the CHAMP-only gravity field determination as performed in this work is affected by omission errors. At this point we refer to Sect. 6.1.4 were the interaction of non-gravitational perturbations and omission errors is investigated.

The conclusions of this sub-section are:

- CHAMP's orbit may be modeled with the given background models in a purely dynamic way with a medium accuracy (residuals and RMS errors on the decimeter-level) with only few arc-specific parameters (< 20), without using accelerometer data or force models for the non-gravitational perturbations (**Test1**). This accuracy is sufficient for detecting large outliers in a screening process or for providing a crude a priori orbit. For high accuracy applications (e.g., for gravity field recovery) this orbit representation is not accurate enough.
- For high accuracy applications pseudo-stochastic parameters have to be set up in

addition to the dynamical arc-specific parameters, when using a fixed arc-length of one day (**Test1**).

- Pseudo-stochastic parameters absorb a significant part of unmodeled or insufficiently modeled non-gravitational and gravitational perturbations including omission errors (**Test2–3**) and insufficiently modeled ocean tides (**Test4–5**).
- The shorter the spacing between the set up pseudo-stochastic parameters, the better the orbit perturbations may be absorbed. For CHAMP the over-parameterization limit of unconstrained pseudo-stochastic pulses is reached with a pulse spacing of 15 min. If pulses are set up with shorter spacings, they absorb gravity field signal of the low SH degrees (**Test6**).
- Over-parameterization effects may be avoided by constraining the pseudo-stochastic parameters. The gain achieved in the low SH degrees is accompanied by a degradation in the remaining part of the SH spectrum (**Test7**). The combination of different gravity field solutions based on different orbit parameterizations on the NEQ level (CDP0515 parameter setting) allows to avoid over-parameterization effects without a degradation in the higher part of the SH spectrum (**Test6a**). The formal errors of the combined solution are not more optimistic than the formal errors of the individual solutions.
- CHAMP's orbit is sensitive to SH coefficients above degree 70 of the Earth's gravity field already in 2002 (**Test2–3**). The sensitivity increases in later years due to CHAMPS orbit decay. The higher SH degrees must therefore be considered in an orbit or gravity field determination with high accuracy demands in order to reduce the effect of omission errors.
- The formal errors of the AIUB-CHAMP solutions are too optimistic in the lower part (< 30) of the SH spectrum (**Test6a**), indicating the presence of systematic errors that cannot be compensated by the arc-specific parameters (e.g., GPS antenna phase center variations).

6.1.2 Modeling of non-gravitational perturbations with dynamic force models

Goals:

- Determination of an appropriate dynamic CHAMP orbit using dynamic force models for the non-gravitational perturbations.
- Determination of reduced-dynamic orbits based on this dynamic orbit.
- Comparison of these orbits with the dynamic and reduced-dynamic orbits based solely on arc-specific parameters (Sect. 6.1.1/**Test1**).

Models for non-gravitational perturbations (air drag, direct solar radiation pressure, Earth albedo radiation pressure) are available in GRAVDET (see Sect. 4.7). The capabilities

of these models shall be assessed roughly and be compared to those of the dynamic orbit modeling with dynamical parameters (DYNPAR parameterization) in Sect. 6.1.1. The A_a/m-ratio of CHAMP normal to the velocity vector of the satellite is set to $0.00138\,m^2/\mathrm{kg}$ (Reigber, 2000), the solar flux and magnetic index, scaling the air-drag model (Beutler, 2005), are assumed to be constant with values of 150 SFU and 4 within the considered time interval. These values agree roughly with the predictions for mid 2002 provided by Montenbruck and Gill (2000). The radiation pressure model applied in GRAVDET assumes a constant A_r/m-ratio. This assumption actually only holds for spherical satellites. For CHAMP the A_r/m-ratio normal to the direction radiation source to satellite changes with time. Therefore a mean A_r/m-ratio of $0.013\,m^2/\mathrm{kg}$ is assumed for these models.

Table 6.4: Mean RMS errors (column 4) of 30 days CHAMP orbit determination in 2002 with different arc-specific parameterizations (column 1, abbreviations (ABB) in column 2, number of parameters (n_{par}) in column 3). Dynamical force models for the non-gravitational orbit perturbations are used.

Parameterization	ABB	n_{par}	RMS error
a.) Osc. ele. + dyn. force models for n.g. perturbations	DM	6	53.871 m
b.) like a.) + estimated model scales.	D3M	9	0.668 m
c.) like b.) + pulses every 30 min.	DMP30	150	0.017 m
d.) like b.) + pulses every 15 min.	DMP15	294	0.011 m
e.) like b.) + pulses every 5 min.	DMP05	870	0.006 m

The scenario is similar to Sect. 6.1.1/**Test1**: Dynamic CHAMP orbits are estimated for the same 30 day interval using kinematic positions as pseudo-observations. As opposed to Sect. 6.1.1/**Test1** the non-gravitational perturbations are modeled using the mentioned dynamical force models. Table 6.4 informs about the tested orbit parameterizations, their abbreviations, the corresponding number of arc-specific parameters (n_{par}), and the mean RMS errors of orbit determination. Figure 6.9 shows the residuals on DOY 196/2002 in radial, along-track, and cross-track direction.

If only the six initial osculating elements are estimated, the inclusion of the force models reduces the mean RMS error of orbit estimation (compare Table 6.4 (a) to Table 6.1 (a)), but the along-track residuals are still very large (Fig. 6.9 (a)), indicating that the simplifying assumptions made for the air-drag and radiation pressure model are not optimal. If the model scales are estimated as additional dynamical parameters, the residuals on DOY 196/2002 are greatly reduced to few meters in along-track direction (Fig. 6.9 (b)) and the mean RMS error is about 65 cm (Table 6.4 (b)). The estimated model scales partly compensate for the non-optimal assumptions made regarding the solar flux, magnetic index (scaling the air-drag model), and A_r/m-ratio (scaling the radiation pressure models). We are thus able to determine a rough CHAMP orbit with only 9 arc-specific parameters (D3M setting). This orbit is, however, not as good as the final dynamical

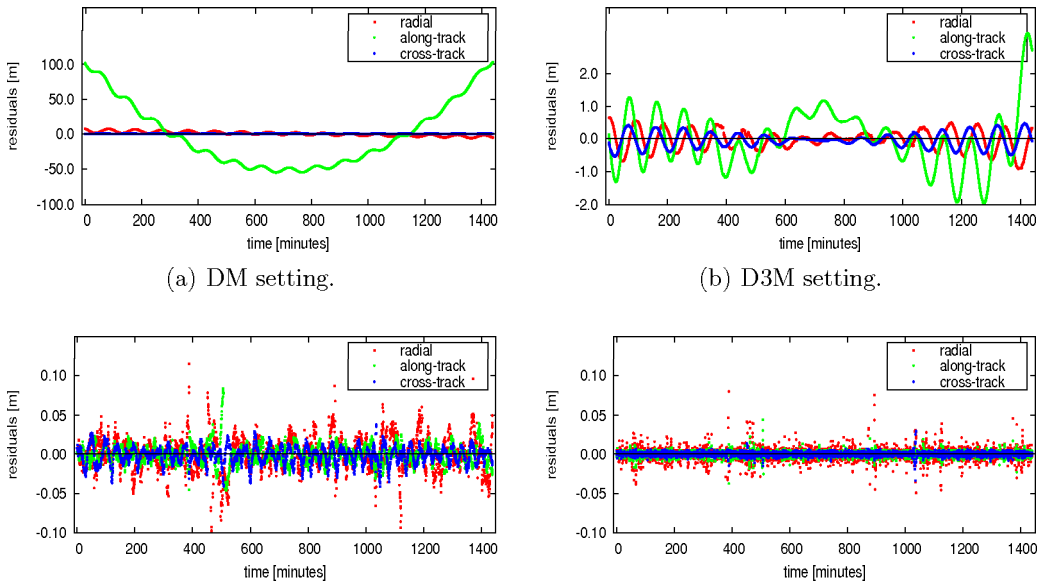

(a) DM setting.

(b) D3M setting.

(c) DMP30 setting.

(d) DMP05 setting.

Figure 6.9: Residuals of the CHAMP orbit determination on DOY 196/2002 with different arc-specific parameterizations. Dynamical force models for the non-gravitational orbit perturbations are used. The abbreviations of the parameter settings are defined in Table 6.4.

orbit generated in Sect. 6.1.1/**Test1** (d). It should be mentioned that there is some potential for improvements: The performance of the air-drag model may be improved by using measured or modeled values for the time variable solar flux and magnetic index or by using a more recent atmospheric density model. The radiation pressure modeling for a CHAMP-like satellite could be improved by taking the varying area and alignment of the spacecraft's particular surfaces due to the varying attitude w.r.t. the radiation source into account (e.g., by using a box-wing model as suggested by Montenbruck and Gill, 2000; Flohrer, 2008).

Different reduced-dynamic orbits are estimated by setting up pulses in R, S, and W direction with different spacings (30, 15, and 5 min, respectively) in addition to the models and dynamical parameters of the D3M-setting. The reduced-dynamic orbits (Table 6.4 (c–e)) are comparable in quality to the corresponding orbits of Sect. 6.1.1/**Test1** (see Table 6.1 (f–h)), because the pseudo-stochastic parameters absorb the remaining orbit perturbation signal (including the insufficiently modeled non-gravitational perturbations). In both test scenarios the accuracy of the reduced-dynamic orbit is given by the number of set up pulses, i.e., by the pseudo-stochastic part of the orbit model.

Results:

- The dynamic force models for the non-gravitational perturbations implemented in GRAVDET are suited to determine a coarse dynamic LEO orbit (D3M setting, mean RMS error of orbit determination ≈ 0.65 cm). They still offer potential for improvements.
- The D3M orbit modeling with the assumptions made in this test is clearly inferior to the DYNPAR parameterization defined in Sect. 6.1.1/**Test1**. Therefore and due to the large uncertainties of higher atmosphere density models (reported, e.g., by Bruinsma et al, 2004) the D3M setting is no longer considered in this work.
- In a reduced-dynamic orbit determination process with many pseudo-stochastic parameters the choice of the dynamic part of the orbit model is not crucial from the accuracy point of view, because the pseudo-stochastic parameters are able to absorb modeling deficiencies.

6.1.3 Accelerometer data

Non-gravitational accelerations acting on a LEO satellite may be measured by accelerometers. The accelerometer measurements may be used as empirically given accelerations in the orbit determination process. The CHAMP spacecraft is equipped with a three-dimensional accelerometer providing measurements in radial, along-track, and cross-track directions (see Sect. 2.2.5). In this subsection we study the properties of the CHAMP accelerometer data and check their impact on orbit and gravity field determination.

The CHAMP accelerometer measurements used subsequently are pre-processed and provided by the GFZ-Potsdam. The data are converted into an internal data format. The a priori offsets and scales, the Lorentz correction (for the influence of the Earth's magnetic field on the accelerometer test mass) and the correction of the radial accelerometer component (necessary because of an instrument failure) are applied according to Förste et al (2002) and Reigber (2002b). In GRAVDET the accelerometer data is smoothed (running average with a 100 s time window) prior to being used for orbit or gravity field determination in order to avoid problems in the numerical integration.

Figure 6.10 (a–c) shows CHAMP accelerometer measurements of the radial, along-track, and cross-track components for DOY 100–150/2002. In this time interval the data contains no outliers, but data gaps. The offset of the radial and the scale of the along-track component are not constant. Figure 6.10 (d) shows the radial accelerometer component for DOY 150–200/2002. Within this time interval we cannot only observe an offset drift and additional data gaps, but also other events: A detailed view of DOY 161–162 (Fig. 6.11 (a)) shows that the large amplitudes in the radial accelerometer component on these days are caused by a maneuver of the CHAMP satellite, consisting of a series of thruster firings (see Reigber, 2002a). The detailed view of DOY 182/2002 shows that an extreme offset drift of the radial accelerometer component occurred within this day (Fig. 6.11 (b)). Other excursions in Fig. 6.10 (d) are caused by outliers in the accelerometer data, e.g.,

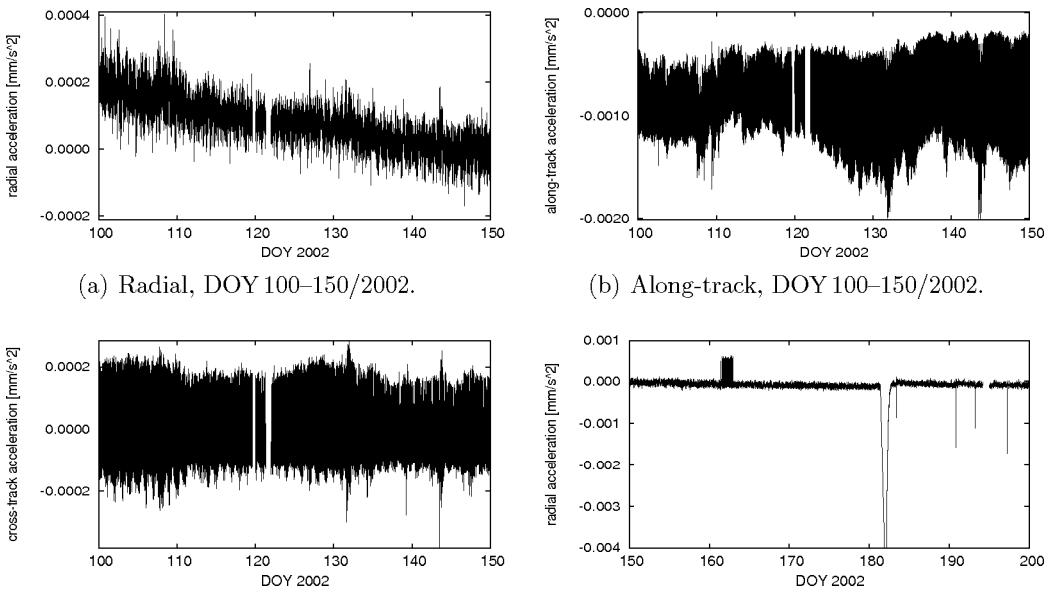

(a) Radial, DOY 100–150/2002.

(b) Along-track, DOY 100–150/2002.

(c) Cross-track, DOY 100–150/2002.

(d) Radial, DOY 150–200/2002.

Figure 6.10: CHAMP accelerometer measurements for DOY 100–150 and DOY 150–200/2002.

on DOY 197/2002 (see Fig. 6.11 (c)). These examples show that the accelerometer data need to be screened for data gaps, outliers, and other events such as offset drifts and maneuvers before usage. The scale and offset need to be estimated for each accelerometer component at least once per daily arc.

To assess the quality of the accelerometer data it is beneficial to know, whether excursions in the data can be assigned to real events. This is tried on the example of solar radiation pressure. Figure 6.12 (a) and (b) show the accelerometer measurements of the cross-track component on DOY 151 and 196/2002. The epochs, when the satellite entered and left the Earth's shadow, are marked with vertical lines. While the accelerations do not show a special behavior at shadow entries and exits on DOY 151 (Fig. 6.12 (a)), these events cause noticeable data "jumps" on DOY 196 (Fig. 6.12 (b)). The influence of radiation pressure on the cross-track component is zero if the Sun lies in the orbital plane of the satellite and reaches its maximum if the angle β between the satellite's orbital plane and the Sun is 90°. On DOY 151/2002 the β-angle was about 2.5°. The radiation pressure acting in cross-track direction was therefore close to zero. On DOY 196/2002 this angle was about 55°. The abrupt changes in the cross-track accelerometer measurements on DOY 196/2002 therefore are real. The non-gravitational accelerations in along-track direction are dominated by the air drag. Due to the eccentricity of the orbit the drag varies periodically, where the period is the satellite's revolution period. Drag is maximum at perigee (higher air density) and minimum at apogee (lower air density). The periodical drag signal in

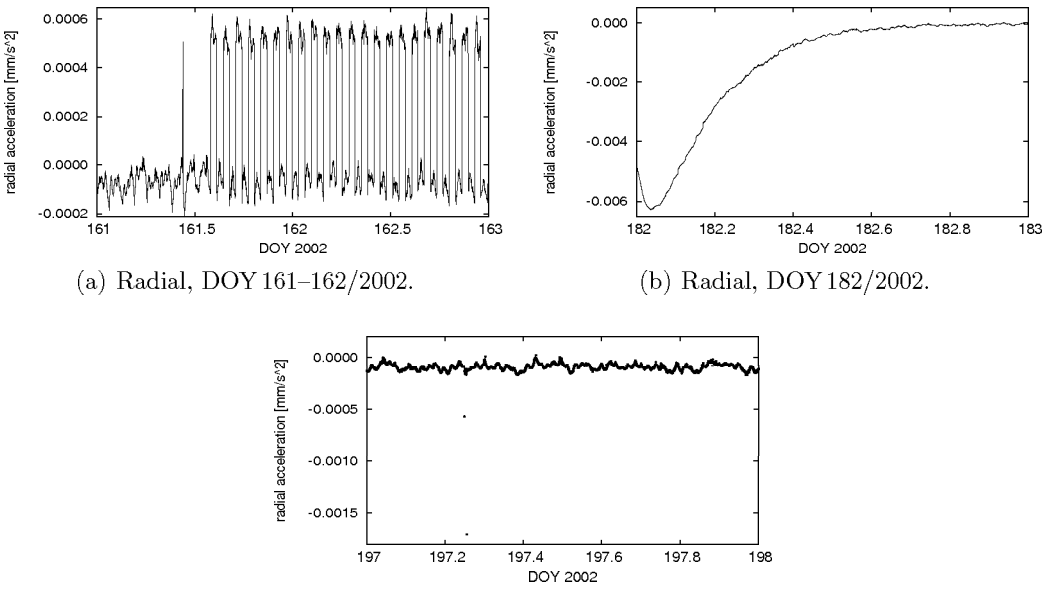

(a) Radial, DOY 161–162/2002.

(b) Radial, DOY 182/2002.

(c) Radial, DOY 197/2002.

Figure 6.11: Features of CHAMP accelerometer measurements.

along-track direction is clearly visible in the accelerometer data. Jäggi (2007) has shown that empirically estimated piecewise constant accelerations (PCAs) agree well with the accelerometer measurements — indicating the ability of pseudo-stochastic parameters to absorb non-gravitational perturbation signal.

Test1: Orbit determination using accelerometer data

Goals:

- Determination of an appropriate dynamic CHAMP orbit using accelerometer measurements for the non-gravitational perturbations.
- Determination of reduced-dynamic orbits based on this dynamic orbit.
- Comparison of these orbits with the dynamic and reduced-dynamic orbits based solely on arc-specific parameters (Sect. 6.1.1/**Test1**).

The impact of accelerometer measurements on orbit determination is checked by estimating dynamic orbits from 30 days of kinematic CHAMP positions (in analogy to Sect. 6.1.1/**Test1**). Instead of only orbit parameters (Sect. 6.1.1) or dynamical force models (Sect. 6.1.2) the non-gravitational perturbations are modeled by the accelerometer data. The radial accelerometer component is not used because of an instrument failure (Reigber, 2001) of the accelerometer on-board CHAMP. Table 6.5 informs about the applied orbit parameterizations, their abbreviations, the corresponding number of arc-specific parameters (n_{par}), and the mean RMS errors of orbit determination.

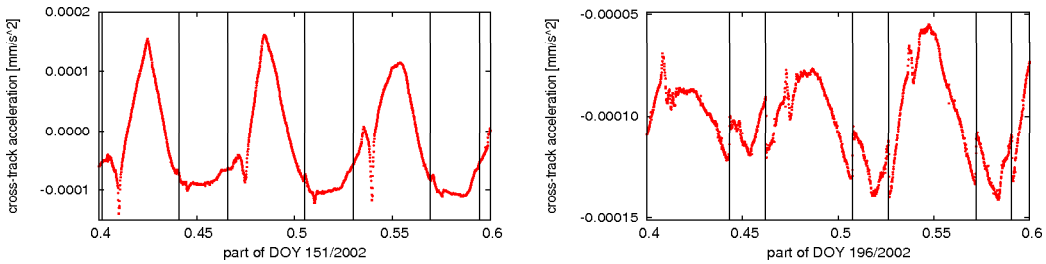

(a) Cross-track, DOY 151/2002. (b) Cross-track, DOY 196/2002.

Figure 6.12: Cross-track accelerometer component of CHAMP on DOY 151 ($\beta = 2.5°$) and 196/2002 ($\beta = 55°$). The vertical lines mark the epochs, when the satellite entered and left the Earth's shadow.

If only the six initial osculating elements are estimated, the mean RMS error is only slightly reduced when using accelerometer data (compare Table 6.5 (a) with Table 6.1 (a)), because the accelerometer measurements are affected by changing offsets and scales (see Fig. 6.10). When accelerometer offsets and scales are estimated once per daily arc in addition to the six initial osculating elements and the perturbations in the radial direction are partly absorbed by a constant acceleration and coefficients of 1/rev periodic acceleration functions, the mean RMS error of orbit estimation is reduced to about 13 cm with only 13 parameters (D7ACC setting, see Table 6.5 (b)). This is much better than the result achieved with the dynamical force models for non-gravitational perturbations (see Table 6.4 (b)) and better than the results achieved with the 18 parameters of the DYNPAR setting (see Table 6.1 (d)). Using accelerometer data is therefore the best way (tested in this work) of modeling the non-gravitational perturbations in a purely dynamic orbit determination. Neglecting the radial accelerometer component does not have a strong negative effect, because the most important non-gravitational perturbation in CHAMP's case is the air-drag, which affects mainly the along-track component. The dynamic orbit is, however, still affected by model insufficiencies and omission errors.

For higher accuracy requirements additional parameters must be set up, even if accelerometer data is used. When pseudo-stochastic pulses are set up in addition, the mean RMS errors (see Table 6.5 (c–e)) are very similar to those when using empirical parameters (see Table 6.1 (f–h)) or dynamical force models (see Table 6.4 (c–e)) for the dynamic part of the orbit modeling. The RMS error and the residuals are mainly determined by the spacing of the pseudo-stochastic parameters (see Fig. 6.13). If many pseudo-stochastic orbit parameters are set up, the advantage of using accelerometer data for dynamic orbit modeling vanishes.

Results:

- When using accelerometer data a dynamic CHAMP orbit may be determined with a mean RMS error of ≈ 13 cm within the test interval (D7ACC setting).

Table 6.5: Mean RMS errors (column 4) of 30 days CHAMP orbit determination in 2002 with different arc-specific parameterizations (column 1, abbreviations (ABB) in column 2, number of parameters (n_{par}) in column 3). Accelerometer data is used.

Parameterization	ABB	n_{par}	RMS error
a.) Osc. ele. + accelerometer data	ACC	6	126.250 m
b.) like a.) + offset in R,S,W + acc. scale in S,W + coeff. of 1/rev. period. funct. in R	D7ACC	13	0.130 m
c.) like b.) + pulses in R,S,W every 30 min.	DAP30	154	0.014 m
d.) like b.) + pulses in R,S,W every 15 min.	DAP15	298	0.010 m
e.) like b.) + pulses in R,S,W every 5 min.	DAP05	874	0.006 m

- This value is better than those of the dynamic orbit determinations solely based on dynamical orbit parameters (DYNPAR, $RMS \approx 20$ cm, Sect. 6.1.1/**Test1**) or using dynamic force models (D3M, $RMS \approx 65$ cm, Sect. 6.1.2).
- The advantages of using accelerometer data vanish when setting up many pseudo-stochastic pulses in a reduced-dynamic orbit determination, because the non-gravitational perturbation signal can as well be absorbed by the pseudo-stochastic parameters.

Test2: Impact of accelerometer data on the CHAMP-only gravity field determination using the CMA

Topics:

- Gravity field determination based on dynamic orbit parameterizations (with/without using accelerometer data).
- Gravity field determination based on reduced-dynamic orbit parameterizations (with/without using accelerometer data).

The "portability" of the results from orbit to gravity field determination is verified by comparing four annual gravity field solutions. One solution is AIUB-CHAMP01S (see Sect. 5.1), i.e., generated without accelerometer data. The second solution (AIUB-CHAMP01Sp-PA) is generated like AIUB-CHAMP01S, but using accelerometer measurements in addition. The third solution (AIUB-CHAMP01Sp-D) is generated like AIUB-CHAMP01S, but without any pulses. It uses the DYNPAR setting ($n_{par} = 18$, see Table 6.1 (d)). The fourth solution (AIUB-CHAMP01Sp-A) uses the D7ACC setting ($n_{par} = 13$, see Table 6.5 (b)), i.e., including the accelerometer measurements in along-track and cross-track direction, but no pulses.

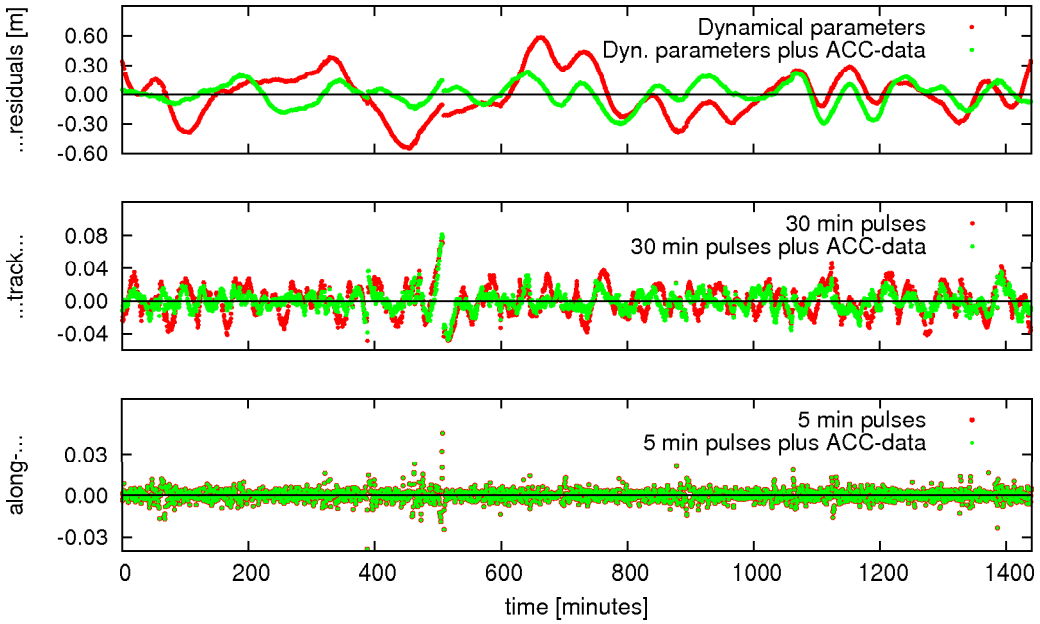

Figure 6.13: Residuals of the orbit fit in along-track direction on DOY 196/2002 with/without using accelerometer data. Parameterization: DYNPAR vs. D7ACC setting (top); DP30 vs. DAP30 setting (middle), DP05 vs. DAP05 setting (bottom). The abbreviations of the parameter settings are defined in Table 6.1 and Table 6.5.

Figure 6.14 shows that the solutions without pulses (AIUB-CHAMP01Sp-D and AIUB-CHAMP01Sp-A) are of poor quality, because they are affected by modeling deficiencies and omission errors. The solution using accelerometer data (AIUB-CHAMP01Sp-A) is slightly better than the solution based on empirical dynamic orbit parameters (AIUB-CHAMP01Sp-D). The solutions with pulses (AIUB-CHAMP01S and AIUB-CHAMP01Sp-PA) are much better and comparable to each other in quality. The pulses absorb much of the remaining modeling deficiencies. The accelerometer data has only a negligible effect on the gravity field solution, if many pulses are estimated. The findings of the orbit determination experiments are, therefore, also valid for the gravity field recovery.

We conclude:

- A gravity field based on a dynamic CHAMP orbit modeling (as used in this work) is absolutely insufficient — even if accelerometer data is used. Pseudo-stochastic parameters need to be set up to compensate for model deficiencies and absorb omission errors.
- If many pseudo-stochastic parameters are estimated, the advantages of using accelerometer data are negligible, because the pseudo-stochastic parameters are able

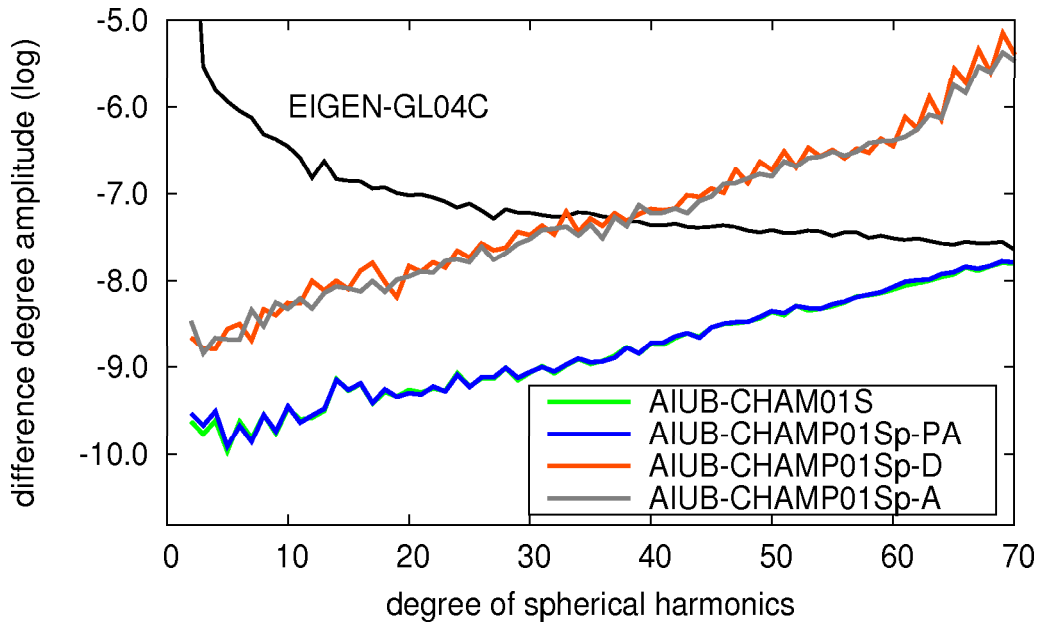

Figure 6.14: Difference degree amplitudes w.r.t. EIGEN-GL04C of annual gravity field solutions: AIUB-CHAMP01S (pulses, no acc. data), AIUB-CHAMP01Sp-PA (pulses, acc. data), AIUB-CHAMP01Sp-D (no pulses, no acc. data), AIUB-CHAMP01Sp-A (no pulses, acc. data).

to absorb the non-gravitational perturbation signal, as well (see also the simulation study in Sect. 6.1.4).

The CHAMP accelerometer data are affected by data gaps, may contain outliers (see Fig. 6.11 (c)), and therefore must be screened. The outlier screening, check for data gaps, and file handling of accelerometer data implies an increased complexity and error potential without a substantial gain in the accuracy of the estimated gravity fields. Accelerometer data was, therefore, not considered in the generation of AIUB-CHAMP01S, AIUB-CHAMP02S, and AIUB-CHAMP03S.

6.1.4 Simulation study

The experiments with real CHAMP data in Sect. 6.1.1 have shown that CHAMP orbits are affected by orbit perturbations and model deficiencies of different kinds that may be absorbed by a large number of pseudo-stochastic parameters. In Sect. 6.1.3 we have seen that accelerometer data have no impact on gravity field recovery (as performed in this work) when many pseudo-stochastic parameters are set up. In order to better understand these results a simulation study is performed with the following goals:

- Quantify and compare the impact of different isolated orbit perturbations in a controlled environment.
- Identify the most important error sources.
- Examine the impact of non-gravitational accelerations and omission errors on CHAMP orbit and gravity field determination separately and combined.

Different versions of fictitious CHAMP positions are generated from a simulated dynamic orbit with CHAMP orbit characteristics for a time interval of 20 days using GRAVDET (see Sect. 4.7). The true gravity field is EIGEN-GL04C, which is truncated at different SH degrees for different versions of LEO positions. Apart from this, the same background models are used as for the generation of AIUB-CHAMP01S (see Table 5.1). Some of the simulated orbit positions are disturbed by non-gravitational (n.g.) accelerations, which are taken from CHAMP accelerometer measurements. In one case the LEO coordinates are affected by white noise of 5 mm RMS errors. The properties of the simulated orbits are summarized in Table 6.6.

Table 6.6: Properties of simulated LEO positions (n.g. = non-gravitational).

Test	Noise	n_{max}	Other characteristics
Test1	no	120	—
Test2	no	120	n.g. accelerations taken from CHAMP accelerometer data
Test3	no	120	—
Test4	no	90	n.g. accelerations taken from CHAMP accelerometer data
Test5	no	120	n.g. accelerations taken from CHAMP accelerometer data
Test6	yes	120	n.g. accelerations taken from CHAMP accelerometer data

Table 6.7: Properties of orbit or gravity field determination experiments with simulated CHAMP-like positions.

Test	Determination of	n_{max}	Object of investigation
Test1	Orbit	70/120	Model errors, omission errors
Test2	Orbit	70/120	Omission errors and/or non-gravitational perturbations
Test3	Gravity field	50/70/90	Omission errors
Test4	Gravity field	90	Non-gravitational perturbations
Test5	Gravity field	70	Omission errors, non-gravitational perturbations
Test6	Gravity field	70	Omission errors, non-gravitational perturbations, noise

The simulated positions are used as pseudo-observations in orbit or gravity field determination experiments. The parameter settings and their abbreviations are provided in

Table 6.1. Omission errors are created by truncating the gravity field at a lower degree n_{max} than used in the simulation. If accelerometer data is used, it is smoothed like in the real-data experiments. This creates a small error. Apart from this, the accelerometer data is considered to be error-free in this study. The properties of the orbit or gravity field determination experiments are summarized in Table 6.7. The determined gravity fields are compared to EIGEN-GL04C, defining the truth in this simulation.

Test1: Orbit determination without non-gravitational accelerations

Questions:

- How large is the impact of several gravitational perturbations on a CHAMP-like orbit determination?
- How well can these errors be absorbed by the orbit parameterization?

In the 0-test the background models in the orbit determination are the same as those used for simulation and only the six initial osculating elements (OSCELE) are estimated. Table 6.8 shows that the mean RMS error is 0.0 mm in this case. Subsequently, the orbit determination is repeated with one background model being modified, respectively (first column in Table 6.8).

Table 6.8: Mean RMS errors (column 3) of orbit determination using 20 days of simulated CHAMP positions. Different error sources (column 1) are activated separately. Different orbit parameterizations (column 2, see Table 6.1) are used.

Error source	Parameter setting	Mean RMS error
—	OSCELE	0.0 mm
Solid Earth tides: IERS2000 instead of IERS1996	OSCELE	0.1 mm
Meanpole: IERS2003 instead of IERS1996	OSCELE	3.0 mm
	DYNPAR	2.0 mm
Ocean tides: CSRC instead of CSR3.0	OSCELE	45.0 mm
	DYNPAR	34.0 mm
	DP30	2.3 mm
	DP15	1.0 mm
Static gravity field: EIGEN-2 instead of EIGEN-GL04C	OSCELE	125.0 mm
	DYNPAR	51.0 mm
	DP30	3.5 mm
	DP15	2.1 mm
Omission error: $n_{max} = 70$ instead of 120	OSCELE	445.0 mm
	DYNPAR	309.0 mm
	DP30	15.0 mm
	DP15	5.0 mm

The mean RMS errors indicate that mis-modelings of the solid Earth tide model or of

the mean pole convention have only a minor influence on the orbit determination. Errors of the ocean tide model or the static gravity field model deteriorate the dynamic orbit determination much more. Omission errors are the largest errors in this experiment. The attempt is made to compensate for the errors by setting up more arc-specific parameters. The RMS errors show that parameterizations with many pulses (DP30, DP15) are able to absorb the largest part of the perturbations. Residual errors with sizes on the mm-level, however, remain.

Results:

- Omission errors are the largest gravitational orbit perturbations in this experiment.
- All tested gravitational perturbations may be absorbed by pulses to a large extent, but not completely.

Test2: Orbit determination with non-gravitational accelerations

Questions:

- How large is the impact of non-gravitational perturbations on a CHAMP-like orbit determination?
- How well can these errors be absorbed by the orbit parameterization?
- Which error dominates, when non-gravitational perturbations superimpose omission errors?

Dynamic and reduced-dynamic orbits with different parameterizations are estimated using simulated LEO positions that are influenced by non-gravitational accelerations. Table 6.9 provides information about the test scenario, the parameter settings, and the mean RMS errors.

Firstly the gravity field is not truncated, i.e., only non-gravitational perturbations occur. The upper part of Table 6.9 shows the RMS error for this scenario. Compared to the omission error (see Table 6.8) this error is much larger, if only the six initial osculating elements are determined. If dynamical orbit parameters and pulses are set up in addition, the error caused by non-gravitational perturbations is smaller than the omission error. Obviously non-gravitational perturbations are better absorbed than omission errors by the arc-specific parameters.

Secondly the LEO orbit is affected by both, non-gravitational perturbations and omission errors. The RMS errors in the lower part of Table 6.9 indicate that the orbit determination error is dominated by the non-gravitational perturbations if only the six initial osculating elements are estimated, and by the omission errors, if many arc-specific parameters are set up. This explains, why the use of accelerometer data in an orbit determination with many set up orbit parameters and in the presence of omission errors can only have a limited effect.

Results:

Table 6.9: Mean RMS errors (column 3) of orbit determination using 20 days of simulated CHAMP positions, affected by non-gravitational perturbations. Omission errors are activated or turned off (column 1). Different orbit parameterizations (column 2, see Table 6.1) are used.

Error source	Parameter setting	Mean RMS error
non-gravitational perturbations	OSCELE	149360.0 mm
	DYNPAR	207.0 mm
	DP30	5.5 mm
	DP15	2.0 mm
	DP05	1.6 mm
non-gravitational perturbations and omission error ($n_{max} = 70$ instead of 120)	OSCELE	149570.0 mm
	DYNPAR	374.0 mm
	DP30	17.0 mm
	DP15	5.0 mm
	DP05	1.8 mm

- Non-gravitational perturbations can be better absorbed by pseudo-stochastic parameters than omission errors.
- When only few arc-specific parameters are set up, the non-gravitational perturbations dominate the error budget.
- When many arc-specific parameters (including pulses) are set up, the omission errors dominate the remaining errors.

Test3: Gravity field determination with omission errors

Questions:

- What is the impact of omission errors on gravity field determination?
- How well can these errors be absorbed by the parameterization?

The simulated LEO positions from **Test1** ("true" gravity field up to SH degree and order 120) are used as pseudo-observations in a gravity field determination with the same background models as used in the simulation. The SH coefficients of the Earth's gravity field are set up up to degree and order 50, 70, 90, and 120, respectively, i.e., the solutions are affected by omission errors to a different extent.

The 0-test in Figure 6.15 (a) reveals an inconsistency in this simulation that affects SH coefficients of all degrees when the six initial conditions are the only estimated orbit parameters. When additional orbit parameters of the DP30 setting are set up, they absorb most of this error and only the SH coefficients of degrees 2 and 3 are affected. The comparison with AIUB-CHAMP01S in Figure 6.15 (a) and with simulated omission errors

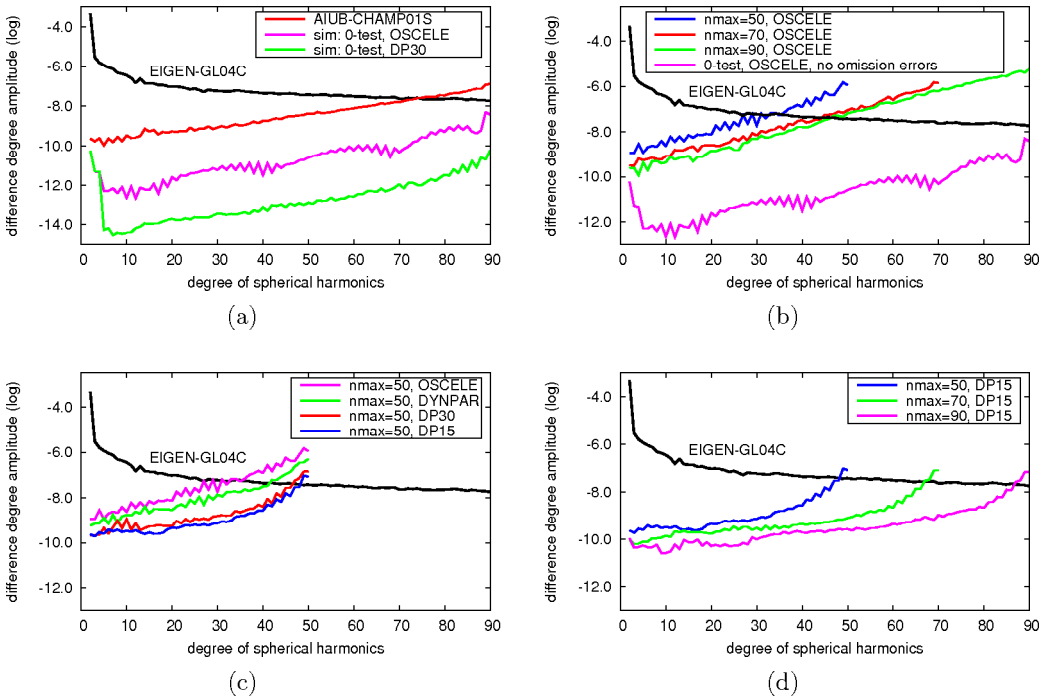

Figure 6.15: Difference degree amplitudes of gravity field solutions derived from simulated CHAMP positions. **Top left:** 0-test. **Top right:** Different cut-off degrees, OSCELE orbit parameterization (see Table 6.1). **Bottom left:** $n_{max} = 50$, different orbit parameterizations. **Bottom right:** Different cut-off degrees, DP15 orbit parameterization.

in Figure 6.15 (b) shows that the inconsistency is of small magnitude (in Table 6.8 it would correspond to a mean RMS error of orbit determination well below 0.1 mm). It is therefore assumed that the results of this simulation are not significantly degraded by the inconsistency.

Figure 6.15 (b) shows the errors of the gravity field solutions, when only the six initial osculating elements are estimated besides the gravity field parameters. The larger the cut-off degree n_{max} of the gravity field determination, the smaller the omission error. The solution with $n_{max} = 70$ corresponds to a mean RMS error of orbit determination of 445 mm in Table 6.8.

Figure 6.15 (c) shows that a large part of the omission errors is absorbed, if additional orbit parameters are set up (DYNPAR, DP30, DP15 settings). A significant part of the error, however, remains (which corresponds with the orbit determination experiment in **Test1**).

The remaining error can be further reduced by increasing the cut-off degree n_{max} in ad-

dition (see Fig. 6.15 (d)): The additionally estimated high degree SH coefficients absorb a significant part but not all of the remaining omission errors. The solution with $n_{max} = 70$ and the DP15 orbit parameterization corresponds to a mean RMS error of orbit determination of 5 mm in Table 6.8. Figures 6.15 (b) and (d) also show that significant omission errors do not only affect the SH coefficients of high degrees.

Results:

- Analog to the orbit determination (see **Test1**) a significant part of the omission errors is absorbed by setting up many orbit parameters.
- Remaining omission errors are partly but not completely absorbed by estimated SH coefficients of high degrees.
- Omission errors also affect SH coefficients of low and medium SH degrees.
- Omission errors may not be eliminated completely.

Test4: Gravity field determination with non-gravitational perturbations

Questions:

- What is the impact of non-gravitational perturbations on gravity field determination?
- How well can these errors be absorbed by the orbit parameterization?

Simulated CHAMP positions, affected by non-gravitational accelerations, are used as pseudo-observations in a gravity field determination with the same background models and cut-off degree as used in the simulation, i.e., the solutions are not affected by other perturbations.

The gravity field recovery is performed with different parameterizations (explained in Table 6.1) with or without using accelerometer data in addition. Figure 6.16 compares the resulting gravity field solutions. When using the same accelerometer data in simulation and gravity field recovery the error of the gravity field solution is supposed to be close to zero (as big as in the 0-test). This is not the case, because the accelerometer data is smoothed in the gravity field recovery process. The smoothing error is, however, small. Therefore the solutions using accelerometer data do not significantly change when setting up additional orbit parameters. Only if pulses are set up with the short spacing of 5 min (DP05) in addition to the accelerometer data, they compensate for a small share of the smoothing error (small gain in the high SH degrees), but also absorb much of the gravitational signal of the low SH degrees < 30 (over-parameterization effects). In the very low SH degrees we recognize the inconsistency already discussed in **Test3**.

If no accelerometer data is used and only few orbit parameters are estimated (DYNPAR setting), the error caused by the non-gravitational perturbations is rather large. Like in the orbit determination the error can be much reduced by additional orbit parameters, but

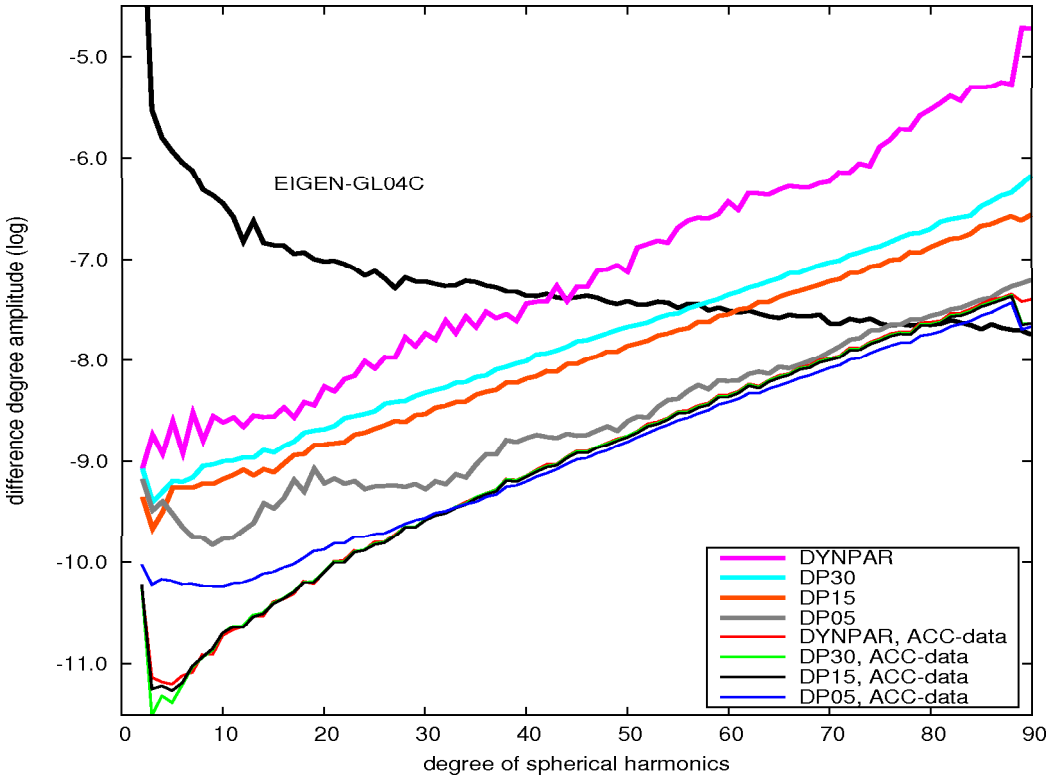

Figure 6.16: Difference degree amplitudes of gravity field solutions derived from simulated CHAMP positions affected by non-gravitational perturbations using different orbit parameterizations (see Table 6.1) with/without considering accelerometer data ("ACC-data").

all solutions without using accelerometer data are worse than those with accelerometer data. The solution with a short pulse spacing of 5 min (DP05 setting) recovers at least the SH coefficients of the higher degrees (> 60) almost as good as the solutions using the error-free, but smoothed accelerometer measurements. As also seen in Sect. 6.1.1 the solutions with short pulse spacings are over-parameterized, resulting in a poor determination of the low degree harmonics.

Results:

- Analog to the orbit determination (see **Test2**) a significant part of the non-gravitational signal is absorbed by a large number of orbit parameters.
- The compensation of the signal is, however, not complete, i.e., the solutions using accelerometer data are clearly superior.

Test5: Gravity field determination with non-gravitational perturbations and omission errors

Questions:

- How do non-gravitational perturbations and omission errors affect the gravity field solution, if they are superimposed?

The simulated LEO positions from **Test2** ("true" gravity field up to SH degree and order 120, non-gravitational accelerations taken from CHAMP accelerometer measurements) are used as pseudo-observations in a gravity field determination with the same background models as used in the simulation. The SH coefficients of the Earth's gravity field are set up up to degree and order 70, i.e., the solutions are affected by non-gravitational perturbations and omission errors. The gravity field recovery is carried out with different parameterizations (see Table 6.1) with or without using smoothed accelerometer data in addition.

Figure 6.17 illustrates the results. When using the DYNPAR parameterization the solution clearly benefits from using the error-free, but smoothed accelerometer data. Due to the presence of omission errors, however, the solutions with many pulses (e.g., DP05 setting) set up in addition are much better than the solutions based on the DYNPAR setting (compare with **Test3**). In the case of short pulse intervals the accelerometer measurements have no impact on the solution, because most of the the non-gravitational perturbations may be absorbed by the pulses as well and the remaining orbit errors are dominated by the omission errors (compare with **Test2** and **Test4**).

Results:

- Analog to the orbit determination (**Test2**) the solutions with many arc-specific parameters are generally superior.
- For such solutions the impact of accelerometer data is negligible, because the error budget is dominated by the remaining omission errors (see also **Test2**).

Test6: Gravity field determination with non-gravitational perturbations, omission errors, and noise

Goal:

- Illustrate the impact of the noise of the kinematic positions on the gravity field determination.

Simulated CHAMP positions affected by non-gravitational accelerations and noise are used as pseudo-observations in a gravity field determination with the same background models as used in the simulation. The SH coefficients of the Earth's gravity field is truncated at $n_{max} = 70$, i.e., the solutions are affected by non-gravitational perturbations,

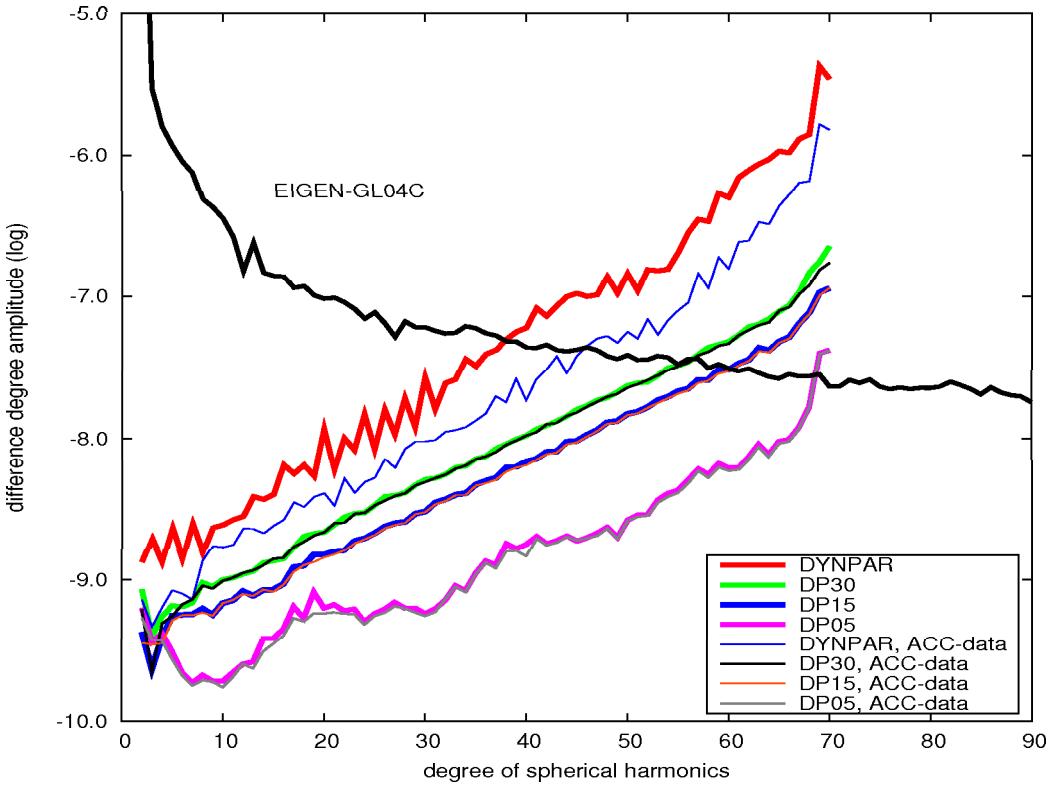

Figure 6.17: Difference degree amplitudes of gravity field solutions derived from simulated CHAMP orbits affected by non-gravitational perturbations and omission errors using different parameter settings (see Table 6.1) with/without considering accelerometer data ("ACC-data").

omission errors, and noise. The gravity field recovery is carried out with different parameterizations (explained in Table 6.1) with or without using smoothed accelerometer data in addition.

Figure 6.18 shows the results: Solutions, whose error in **Test5** is close to or even below the noise level (5 mm in this simulation), suffer most from the introduction of the noise in **Test6**. Therefore, the superiority of solutions with shorter pulse spacings (e.g., DP05) over solutions with longer pulse spacings (e.g., DP15) is reduced, compared to **Test5**. The results of **Test6** correspond well to the results obtained with experiments based on real CHAMP data (see, e.g., Fig. 6.6 and Fig. 6.14) indicating that the test scenario is relatively realistic. Only the difference between the DYNPAR solutions with and without accelerometer data is larger in the simulation than observed in the real data experiments (see Fig. 6.14). This is due to the accelerometer errors (in the simulation the accelerometers are considered to be nearly error free) and due to other model deficiencies that are excluded in the simulation. The simulation study is therefore in favor of the accelerometer

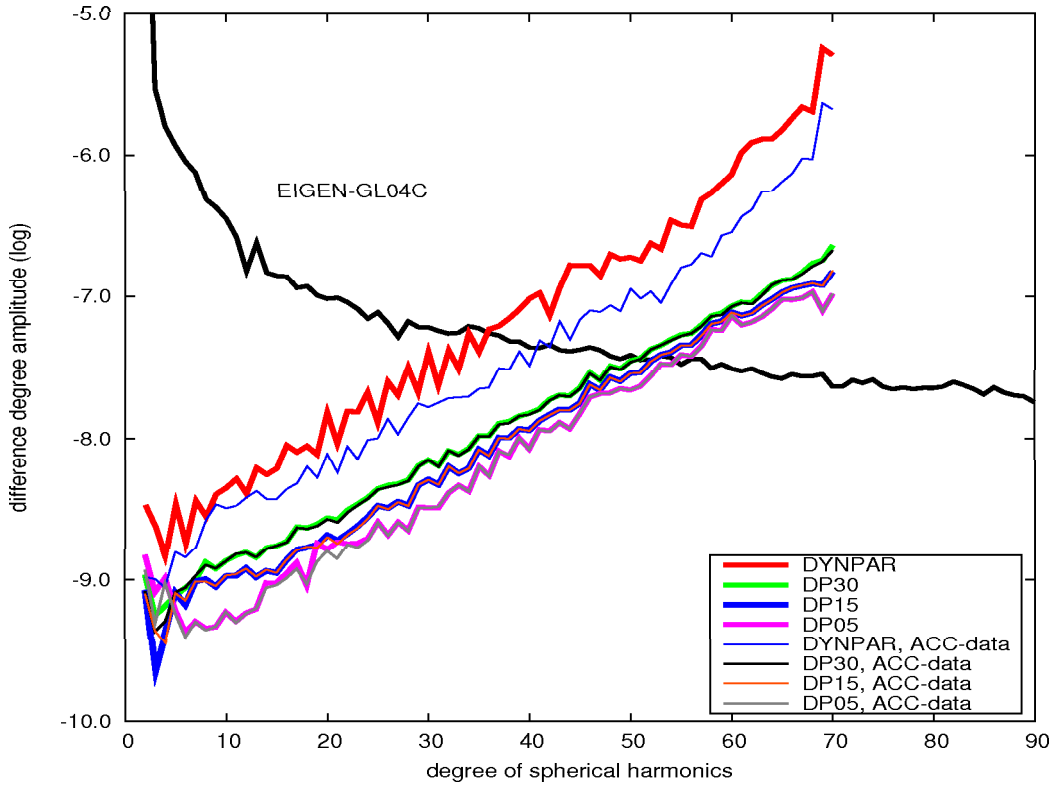

Figure 6.18: Difference degree amplitudes of gravity field solutions derived from simulated CHAMP orbits affected by non-gravitational perturbations, omission errors, and noise using different parameter settings (see Table 6.1) with/without considering accelerometer data ("ACC-data").

data.

The summary of this sub-section is:

- Non-gravitational forces and omission errors are the most important perturbations limiting the accuracy of orbit and gravity field determination with a CHAMP-like LEO satellite.
- These and other accelerations can be absorbed to a large extent by pseudo-stochastic parameters. Although the remaining errors are rather small in the case of a 5 min pulse spacing, they can still deteriorate an accurate gravity field solution.
- Omission errors are best avoided by estimating gravity field parameters up to the expected sensitivity limit of the LEO. As $n_{max} \rightarrow \infty$ for the real gravity field this would dramatically increase the number of parameters. Therefore, omission errors are absorbed by a combination of high degree SH coefficients and pseudo-

stochastic parameters in this work. Alternatively, information about the high degree SH coefficients could be introduced (e.g., by an a priori gravity field or K-band data).

- Non-gravitational perturbations are usually superimposed by remaining omission errors and other error sources (e.g., model deficiencies). If many pseudo-stochastic parameters must be set up in order to absorb these errors, they also absorb the non-gravitational perturbations. Therefore, the solution cannot benefit from the use of accelerometer measurements — even if they would be error-free (what nearly is the case in this simulation). Accelerometer measurements could only contribute to the solution, if the other errors would be reduced to a level allowing it to dramatically constrain or reduce the number of the pseudo-stochastic parameters.
- The accuracy of precise orbit and gravity field determination is finally limited by the noise of the kinematic LEO positions.

6.1.5 Observation weights

Questions:

- Is the epoch-specific weighting of the pseudo-observations important for gravity field recovery using the CMA?
- Is an approximated epoch-specific weight matrix sufficient or is the epoch-specific covariance information from the kinematic positioning required?

The LEO orbit determination provides the kinematic CHAMP positions $\boldsymbol{r}_i = \boldsymbol{r}(t_i)$ together with their associated epoch-specific covariance matrices $cov(\boldsymbol{r}_i)$. According to Eq. (3.4) the weight matrix for the pseudo-observations is defined by:

$$\boldsymbol{P}_i = \sigma_0^2 cov(\boldsymbol{r}_i)^{-1} \ , \tag{6.5}$$

where σ_0 is the error of unit weight (error of the L_1 phase observation at zenith). $\boldsymbol{P}_i$ may be used by GRAVDET. The error ellipsoid, which may be derived from $cov(\boldsymbol{r}_i)$, approximately is an ellipsoid of rotation, where the long axis is approximately oriented along the radial (UP) direction. The ratio of the mean errors can be approximated with (Dach et al, 2007):

$$\sigma(R) : \sigma(S) : \sigma(W) \approx 2 \ldots 3 : 1 : 1 \ . \tag{6.6}$$

One may therefore expect that a weight matrix

$$\boldsymbol{P1}_i = \begin{pmatrix} 0.25 & 0 & 0 \\ 0 & 1 & 0 \\ 0 & 0 & 1 \end{pmatrix} \tag{6.7}$$

in the (R, S, W)-coordinate system is a fair approximation of the more correct matrix $\boldsymbol{P}_i$. In addition to the weights defined by Eqs. (6.5) and (6.7) we include in this sub-section

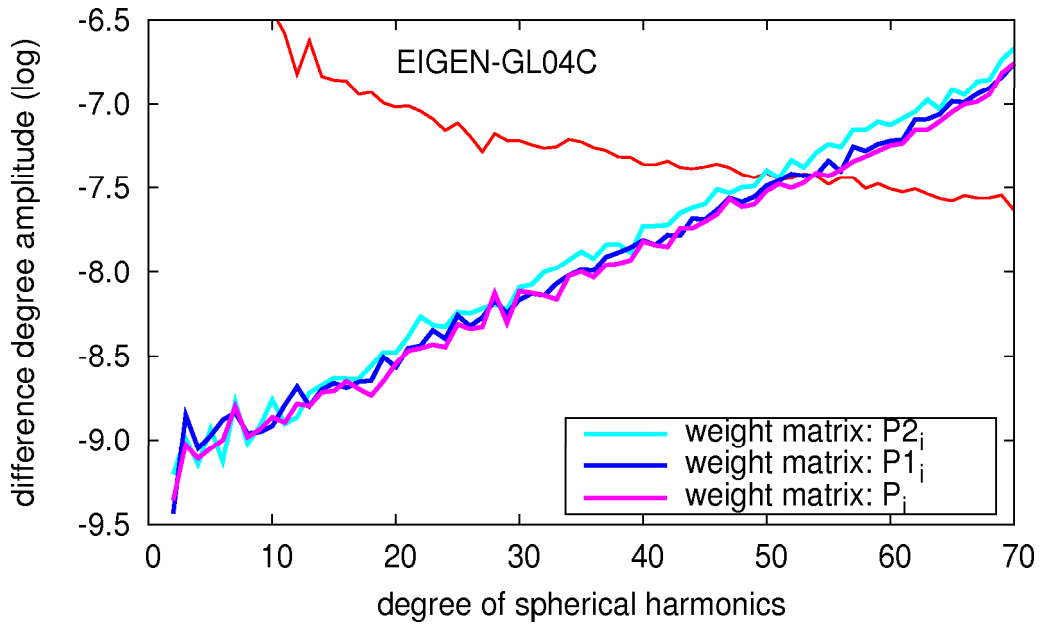

Figure 6.19: Comparison of monthly gravity field solutions based on differently weighted kinematic CHAMP positions and the DP15 orbit parameterization.

the weight matrix

$$\boldsymbol{P2}_i = \begin{pmatrix} 1 & 0 & 0 \\ 0 & 1 & 0 \\ 0 & 0 & 1 \end{pmatrix} , \tag{6.8}$$

assuming the same accuracy for all components of the kinematic position. We expect the best results when using $\boldsymbol{P}_i$, the second best when using $\boldsymbol{P1}_i$, and the worst when using $\boldsymbol{P2}_i$. These expectations are confirmed by Fig. 6.19. Therefore, AIUB-CHAMP01S and AIUB-CHAMP02S are generated using the $\boldsymbol{P}_i$-matrix for weighting the kinematic pseudo-observations. For the generation of AIUB-CHAMP03S the correlations between the kinematic positions belonging to different observation epochs are considered in addition. The corresponding experiments are discussed in Sect. 6.3.4.

We conclude:

- Weighting the pseudo-observations improves the gravity field solution.
- Down-weighting the radial (or UP-) component of the position vector is an acceptable approximation. Using the full epoch-specific covariance matrix (including the correlations between the components of the position vector) for weighting is, however, the best solution discussed here. This kind of weighting is therefore used for AIUB-CHAMP01S and AIUB-CHAMP02S.

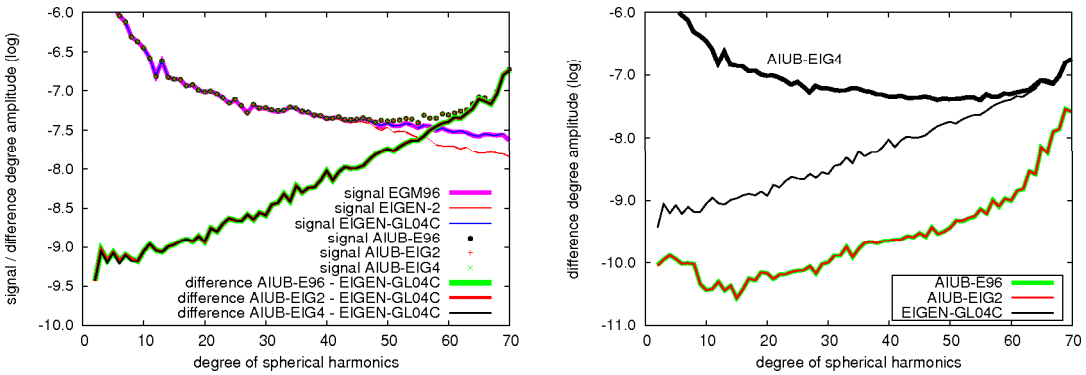

Figure 6.20: **Left:** Signal of different a priori gravity field models and of monthly AIUB-CHAMP solutions based on these a priori models. Comparison of EIGEN-GL04C with the monthly AIUB-CHAMP solutions. **Right:** Comparison of AIUB-EIG4 with the other AIUB-CHAMP solutions and with EIGEN-GL04C.

6.1.6 Influence of the a priori gravity field model

When using the CMA the estimated gravity field parameters are the sum of the a priori gravity field model parameters and the corresponding parameter improvements estimated in the LSA (see Eq. (3.1)). It is important to know, whether the improved parameters are independent from the a priori model parameters or whether the a priori model is partly reproduced. In the latter case the parameter estimation process needs to be iterated. The questions for this experiment are therefore:

- How large is the impact of the a priori gravity field model on the estimated gravity field model, when using the CMA?
- Are several iterations of the gravity field solution necessary?

Table 6.10: Properties of test solutions for a priori gravity field experiment.

Test solution	A priori gravity field model
AIUB-E96	EGM96 (Lemoine et al, 1998)
AIUB-EIG2	EIGEN-2 (Reigber et al, 2003)
AIUB-EIG4	EIGEN-GL04C (Förste et al, 2008)

Different gravity field solutions are derived from one month of kinematic CHAMP positions using different a priori gravity fields. Apart from this the background models are

the same as for AIUB-CHAMP01S. The DP15 parameterization (see Table 6.1) is used. The SH series is truncated at degree 70. The solutions are listed in Table 6.10.

Figure 6.20 (a) shows that the results are indistinguishable when compared to EIGEN-GL04C, although the three a priori models are very different. Figure 6.20 (b) shows that the differences are very small, when the two solutions using EGM96 or EIGEN-2 as a priori fields are compared to the solution using EIGEN-GL04C as a priori model. The comparison of the latter solution to its a priori model EIGEN-GL04C shows that it is much closer to the other AIUB-solutions than to the a priori model.

We conclude:

- The influence of the a priori gravity field on gravity field solutions based on the CMA as used in this work is very small.
- The gravity field recovery does not need to be re-iterated.

6.1.7 Screening the kinematic positions

In Sect. 5.1.1 the screening of the kinematic pseudo-observations as actually practiced in the AIUB-CHAMP processing is described. Experiments and considerations leading to the screening procedure as well as its impact on orbit and gravity field determination are described here.

Goals:

- Assessment of the necessity for screening kinematic CHAMP positions prior to using them as pseudo-observations in a gravity field recovery.
- Definition of an appropriate screening procedure.

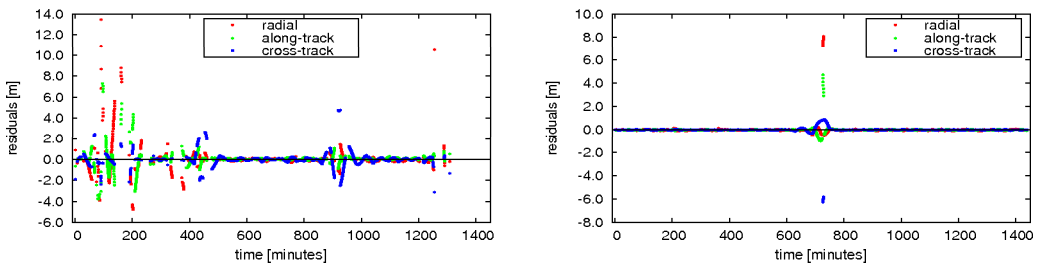

(a) DOY 107/2002. (b) DOY 129/2002.

Figure 6.21: Residuals of the CHAMP orbit determination on DOY 107 and 129/2002. The DP30 parameterization is used (159 arc-specific parameters).

A first screening step is performed when estimating the kinematic LEO positions, as only positions based on at least 5 GPS observations are accepted (4 would theoretically be sufficient, but without redundancy). The necessity of a further screening step is checked by

using the kinematic positions in an orbit determination process and analyzing the residuals in radial, along-track, and cross-track direction. Figure 6.21 shows the residuals of two days (DOY 107 and 129/2002) with data gaps, isolated outliers, and groups of outliers with sizes of several meters. Investigations by Montenbruck and Kroes (2003) suggest that the outliers (up to sizes $> 100\,\mathrm{m}$) and data gaps are mainly caused by CHAMP's GPS receiver. Groups of small outliers can be related to the set up of new GPS phase ambiguities due to changes of the GPS observation geometry in the LEO POD. The examples indicate the necessity of a refined outlier screening for CHAMP kinematic positions.

Outliers of meter-size (as shown in Fig. 6.21) may easily be detected in a "rough screening" by applying a residual-threshold. Setting up only few orbit parameters (e.g., the DYNPAR parameterization) in the orbit determination procedure is sufficient in this case. There are, however, also smaller outliers with sizes of few decimeters, which still may deteriorate a precise orbit determination or gravity field recovery (see Fig. 6.22 (a)). Such outliers are, e.g., caused by the set up of new GPS phase ambiguities due to changes of the GPS observation geometry. For the detection of these small outliers in a "fine screening" it is necessary to substantially reduce the general residual level, e.g., by setting up more orbit parameters (see Fig. 6.22 (b)). Too many orbit parameters (e.g., DP05 parameterization) may, however, also represent outliers (see Fig. 6.22 (c)). In this case some outliers may escape the detection. Therefore the DP30 parameterization is selected for the so-called "fine screening".

The appropriate selection of the threshold is delicate: One may define the threshold iteratively as a multiple of the day-specific RMS error of the previous orbit determination step. By doing that the threshold is automatically adapted to variations of the general residual level. Groups of large outliers may, however, significantly increase the daily RMS error and therefore also affect the screening threshold. In such cases large outliers remain undetected in the first screening iterations. In order to keep the number of screening iterations low, the thresholds are instead defined manually. The thresholds for the residuals in radial, along-tack, and cross-track direction are defined separately in order to take the different residual levels in the three coordinates into account. Typical threshold values in R-, S-, and W-direction are 15, 12.5, and 10 cm. These values are large enough to make sure that the screening is not biased by the a priori gravity field model used in the orbit determination (for the impact of the gravity field model on the CHAMP orbit determination using the DP30 parameterization see also Table 6.8 in Sect. 6.1.4). The effect of this "fine screening" on CHAMP orbit determination is demonstrated in Fig. 6.23: Figure 6.23 (a) shows the residuals and the marked outliers for the first 71 days of 2002 after the first screening iteration step. Figure 6.23 (b) shows the residuals and marked outliers for the same time interval after the fourth and — in this case — last iteration step. We recognize that the outliers with sizes on the meter- and decimeter-level disappeared.

The impact of data screening on gravity field recovery is illustrated in Fig. 6.24. Two months of kinematic positions are screened in different ways and are used to generate gravity field solutions. The DP15 parameterization and the same background models as

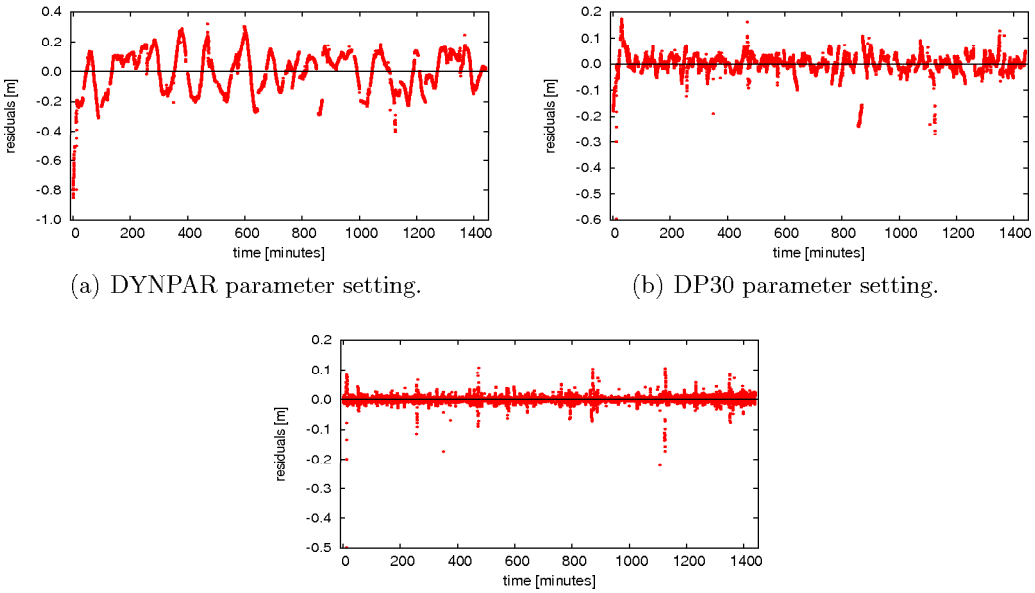

(a) DYNPAR parameter setting.

(b) DP30 parameter setting.

(c) DP05 parameter setting.

Figure 6.22: Residuals in radial direction of the CHAMP orbit determination on DOY 16/2009 containing outliers of decimeter-size. Different parameterizations are used in the orbit determination.

for AIUB-CHAMP01S are used for gravity field determination. If the kinematic positions are not screened at all, the corresponding gravity field is bad. If the positions undergo a "rough screening" with a residual threshold of one meter, the quality of the gravity field solution is dramatically improved. An additional "fine screening" of residuals that are generated using the DP30 parameterization, removing outliers on the decimeter level further improves the gravity field solution.

We conclude:

- The kinematic CHAMP positions are affected by outliers with sizes up to the meter-level.
- The outliers affect the precise orbit and gravity field determination using the CMA. An outlier screening is necessary.
- The screening with simple, user defined thresholds for the residuals of a reduced-dynamic orbit determination using the DP30 parameterization is sufficiently accurate and reliable for gravity field determination using kinematic CHAMP positions.

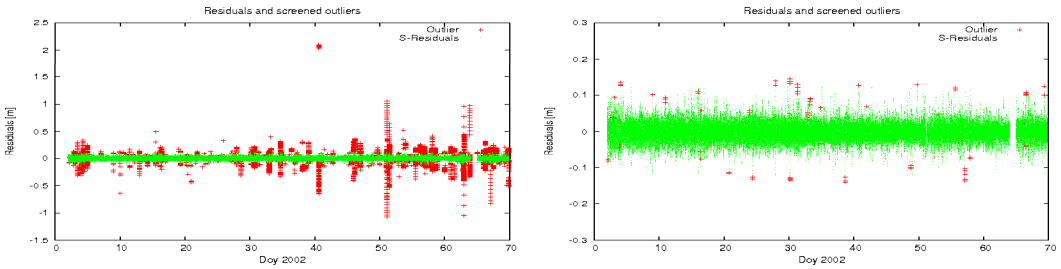

(a) First screening iteration.

(b) Fourth screening iteration.

Figure 6.23: Along-track residuals of the CHAMP orbit determination in the time interval DOY 1–70/2002. The crosses mark outliers that failed to pass one of the thresholds in the radial, along-track, cross-track direction. The DP30 parameter setting was used in the orbit determination.

6.1.8 Quality variations in monthly gravity field solutions

Question:

- Why are the CHAMP gravity field solutions derived from GPS observations of different time intervals not comparable in quality?

The quality of gravity field models based on GPS-derived LEO positions is influenced by different factors and is time-dependent. This is analyzed on the example of the monthly solutions contributing to AIUB-CHAMP01S. Figure 6.25 shows the daily RMS errors of the differences between the GPS-derived kinematic CHAMP positions and the reduced-dynamic positions in the time interval DOY 70/2002–70/2003. The quality of the kinematic positions depends on the GPS receiver and on the kinematic data processing. The receiver characteristics may change, e.g., due to firmware updates (e.g., influencing the number of tracking channels), aging, temporal cross-talk with other satellite components. This may influence the noise level of the kinematic positions and the number and size of data gaps and outliers. For a detailed discussion of the performance characteristics of CHAMP's BlackJack GPS receiver we refer to Montenbruck and Kroes (2003). Examples for a changing receiver behavior are given in Sect. 5.2.4 and Sect. 5.3.2. Observations from Block II and Block IIA GPS satellites during eclipses also affect the accuracy of the GPS positioning (see Sect. 4.3). Because the reduced-dynamic orbit determination is stabilized by dynamic laws and has a higher degree of freedom, most of the variations in Fig. 6.25 are assumed to be caused by the kinematic positions. The variations in the quality of the kinematic positions contribute to the large quality variations of the monthly gravity field solutions that are shown in Fig. 6.26.

In Fig. 6.26 three monthly solutions are highlighted. One of the worst monthly solutions corresponds to DOY 71–100/2002. The corresponding ground track (Fig. 6.27 (a)) shows systematic band-shaped data gaps near the equator. These gaps are already contained in the RINEX observation files. The reason for the data gaps is not known to us.

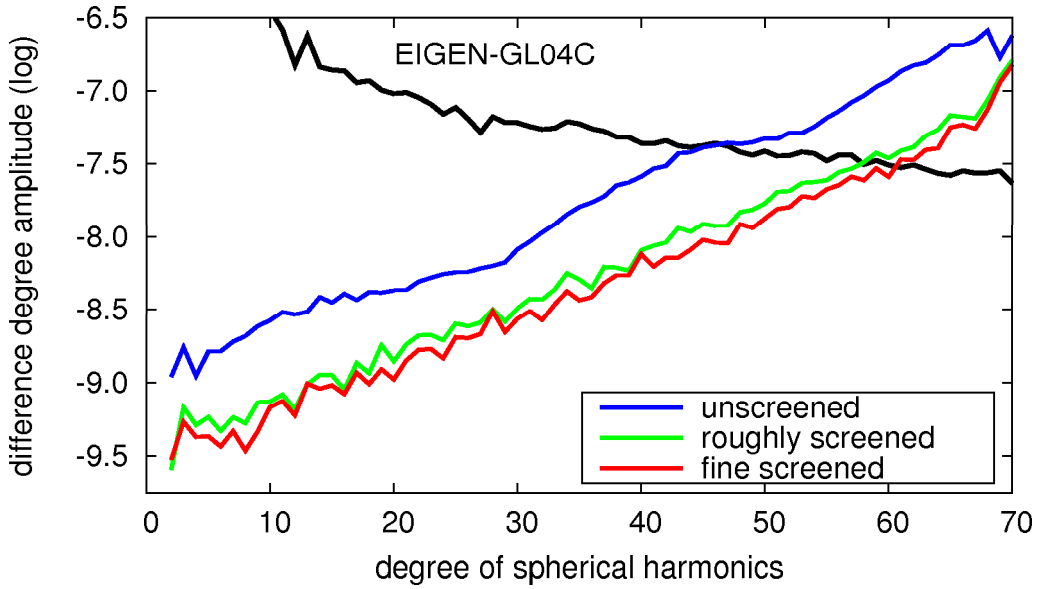

Figure 6.24: Comparison of gravity field solutions based on two months of kinematic CHAMP positions that are screened in different ways.

The quality of a gravity field solution also depends on the orbit characteristics of the satellite. Repeat orbits and orbital height are of special interest. Due to CHAMP's orbit decay the ground coverage pattern changes continuously (Sneeuw et al, 2005). In 2002 there are time periods with pronounced repeat orbits. In repeat mode the orbit is more sensitive to certain SH coefficients, but less sensitive to the majority of the SH coefficients, resulting in a reduction of the overall quality of the monthly gravity field solution (Sneeuw et al, 2005). During the time interval DOY 131–160/2002 CHAMP was in a repeat mode. The ground track shows that large areas of the Earth's surface were not covered by observations (see Fig. 6.27 (b)). The corresponding monthly solution is among the worst in Fig. 6.26. Between DOY 191–220/2002 the ground track led to a nearly perfect global coverage (see Fig. 6.27 (c)). The corresponding monthly gravity field solution is one of the best in Fig. 6.26.

The role of the orbital height is shown in a simulation experiment: 20 days of LEO positions affected by white noise of 1 cm RMS errors are generated from simulated orbits with CHAMP characteristics but different orbital heights of 450 and 500 km using the EIGEN-GL04C as gravity field. The positions are used for gravity field determination with identical parameterizations and background models. As expected from Eq. (3.26) the lower orbit is more sensitive for the short wavelengths of the gravity field, while both orbits are similarly sensitive for the long wavelengths (Fig. 6.28). The experiment thus illustrates the stronger attenuation of the gravity field signal of higher SH degrees with increasing orbital height. The change of the orbital height (see Fig. 2.7) due to orbit

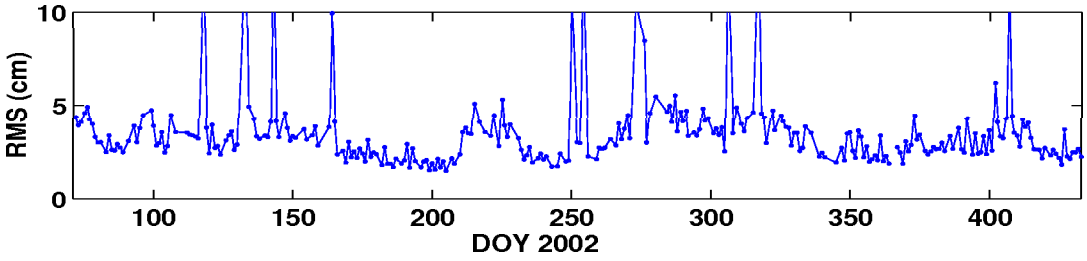

Figure 6.25: Daily RMS errors of the differences between GPS-derived kinematic positions and reduced-dynamic orbit positions of CHAMP between DOY 70/2002 and DOY 70/2003.

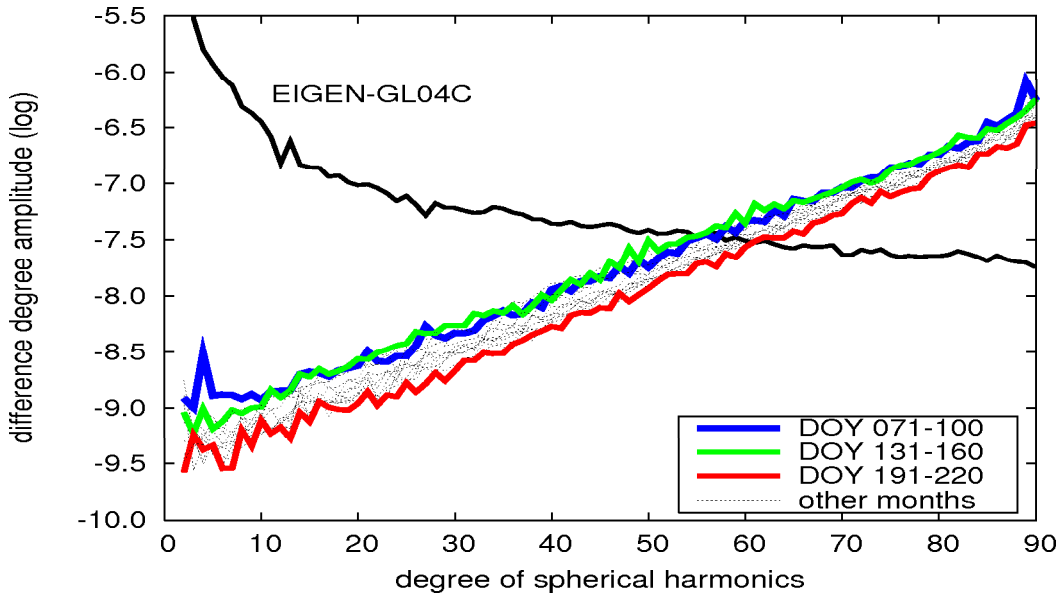

Figure 6.26: Monthly CHAMP gravity field solutions contributing to AIUB-CHAMP01S. The highlighted curves belong to the ground-tracks shown in Fig. 6.27.

decay and maneuvers therefore directly influences the quality of the monthly gravity field solutions. The impact of the orbital height is also seen in the better quality of the annual CHAMP gravity field solutions based on data of the later years of the mission (see Figs. 5.12 and 5.22).

We conclude:

- The quality of monthly and annual CHAMP gravity field solutions varies significantly.
- Reasons are the varying quality of the kinematic CHAMP positions used as pseudo-

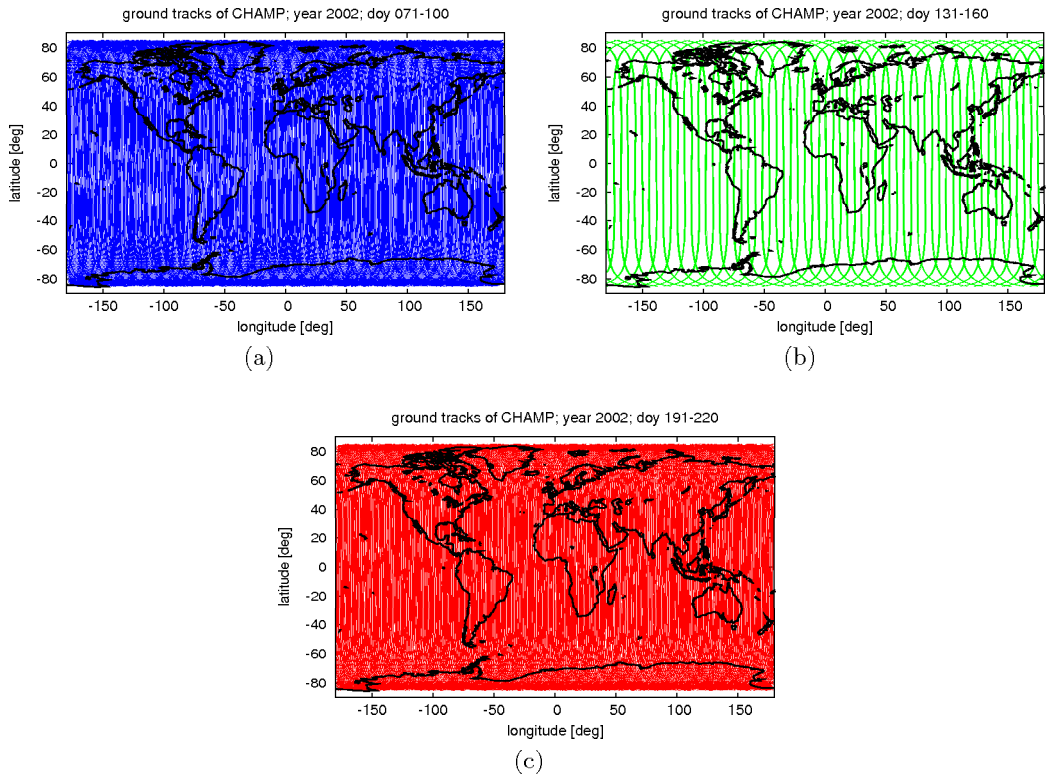

Figure 6.27: CHAMP ground-track coverage for different 30 day time-spans: Systematic, band-shaped data gaps near the equator (left), repeat mode with 31 revolutions in two days (right), good ground coverage (bottom).

observations and CHAMP's orbit decay (direct impact: varying signal attenuation; indirect impact: varying ground coverage).

6.1.9 Summary and discussion of the AIUB-CHAMP01S-related studies

With the experiments performed in Sect. 6.1.1–6.1.7 we have gained the experience and understanding necessary to create the CHAMP-only gravity field model AIUB-CHAMP01S using the CMA:
The experiments with real CHAMP positions in Sect. 6.1.1 illustrate that CHAMP's orbit is influenced by perturbations of different types. In the simulation study in Sect. 6.1.4 we have identified non-gravitational perturbations and omission errors as the largest error sources. We have defined dynamic orbits based on dynamical orbit parameters (DYNPAR setting, see Table 6.1), models for the non-gravitational perturbations (D3M-setting, see Table 6.4), or accelerometer measurements (D7ACC setting, see Table 6.5). The latter dynamic orbit is the best. We have, however, shown that in the given scenario (CHAMP-

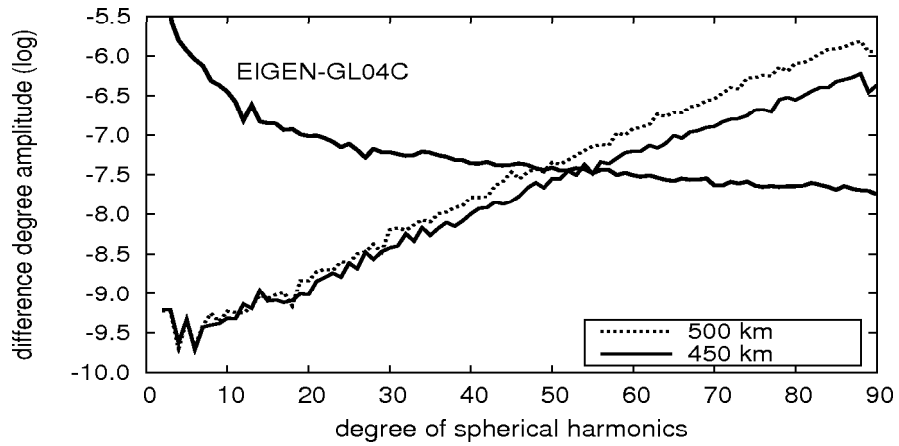

Figure 6.28: Gravity field solutions derived from simulated orbits with different orbital heights.

only gravity field solution, without information from a superior a priori gravity field model or K-band data) a dynamic orbit modeling is not sufficient (see, e.g., Fig. 6.14). Even if the non-gravitational perturbations could be completely compensated (e.g., by error-free accelerometer measurements) — what is not the case in reality — the orbit would still be affected by other perturbations, model deficiencies, and omission errors. The real data experiments (in Sect. 6.1.1) and the simulation study (in Sect. 6.1.4) have shown that errors of different types can be reduced by setting up many pseudo-stochastic parameters. We have shown that omission errors can be absorbed to a large extent, but not completely, by setting up a combination of pseudo-stochastic parameters with short intervals and SH coefficients of very high degrees (above the degree, where all SH coefficients can be determined reliably: "detectability limit", see Sect. 6.1.1/**Test3**). The DP05 orbit parameterization (5 min pulse spacing, Table 6.1) and a cut-off degree of $n_{max} = 90$ (the "detectability limit" of AIUB-CHAMP01S is at $n = 74$) are therefore assumed to be appropriate.

The simulation study (Sect. 6.1.4/**Test2** and **Test4**) and Jäggi (2007) have shown that the pseudo-stochastic parameters are also able to absorb the largest part of the non-gravitational perturbations. If many pseudo-stochastic parameters are set up in order to reduce the omission errors and other model deficiencies they also absorb the non-gravitational perturbations (see Sect. 6.1.4/**Test2** and **Test5**). Therefore, the use of accelerometer data has no impact on the CHAMP gravity field solution under the given circumstances (see Fig. 6.14). Accelerometer data is, therefore, not used for the determination of AIUB-CHAMP01S, AIUB-CHAMP02S, and AIUB-CHAMP03S. The role of accelerometer data could of course change, if no other error sources than non-gravitational perturbations would be present (or the other errors would be very small), because such a scenario would allow to set up less pseudo-stochastic parameters or to put heavier con-

straints on them.

The real data and simulation experiments have also shown the limitations of pseudo-stochastic parameters: (a) The spacing of the pseudo-stochastic parameters cannot be shorter than the spacing of the kinematic positions used as pseudo-observations. (b) The noise of the kinematic positions limits the accuracy of the gravity field solution. The presence of noise affects solutions, which would otherwise have errors below or close to the noise level (in our case solutions with many pseudo-stochastic parameters), relatively stronger than solutions with errors well above the noise level (see Sect. 6.1.4/**Test6**). (c) If the spacing of the pseudo-stochastic parameters becomes too short the gravity field solution is over-parameterized for the low SH degrees (see Sect. 6.1.1/**Test6**). Two options of avoiding over-parameterization effects have been discussed: (a) Combination of the DP05 solution (best performance in the medium and high SH degrees, but over-parameterization effects in the low SH degrees) with the DP15 solution (no over-parameterization effects) on the NEQ-level to the CDP0515 solution (good performance in the whole SH-spectrum, see Sect. 6.1.1/**Test6a**). (b) Constraining of the pseudo-stochastic parameters (see Sect. 6.1.1/**Test7**). As the constrained parameters are not "free" they are not able to absorb all of the perturbation signal (see Fig. 6.8). Therefore, the constrained solutions are not as good as unconstrained solutions in the high SH degrees. The CDP0515 setting is therefore the best choice for generating the AIUB-CHAMP gravity field solutions.

Sect. 6.1.5 has demonstrated that considering the different accuracy level of the components of GPS-derived kinematic positions is beneficial for the gravity field recovery. Therefore the epoch-specific covariance information from the kinematic positioning is used for weighting the pseudo-observations of AIUB-CHAMP01S and AIUB-CHAMP02S. Sect. 6.1.6 has shown that the impact of the a priori gravity field on CHAMP-only gravity field solutions created with the CMA in minimal. An iteration of the gravity field solution is therefore not necessary. Sect. 6.1.7 illustrates that the kinematic CHAMP positions may be affected by large outliers (up to many meters in the worst case) that deteriorate the gravity field solution. A simple, effective, and reliable screening procedure for removing outliers on the meter- and decimeter-level was designed. It detects outliers in the residuals of a reduced-dynamic orbit determination (using the kinematic positions as pseudo-observations) using thresholds. The screening procedure is used for screening the kinematic CHAMP positions used to generate AIUB-CHAMP01S, AIUB-CHAMP02S, AIUB-CHAMP03S, but also applied for screening GRACE positions, which are, e.g., used to generate AIUB-GRACE solutions (Jäggi, 2010).

The final study (see Sect.6.1.8) was performed after generating AIUB-CHAMP01S in order to better understand the reasons for the quality variations observed for the monthly (see Sect.5.1.3) and annual (see Sect.5.2.6 and Sect.5.3.4) AIUB-CHAMP gravity field solutions. On the example of the monthly contributions to AIUB-CHAMP01S it was shown that the quality variations are caused by accuracy variations of the kinematic positions and by the satellite's orbit decay (direct impact: signal attenuation; indirect impact: varying ground coverage). The variations must be considered when interpreting

or comparing gravity field models, and for detecting temporal gravity field variations, as tried in Sect. 6.3.7.

6.2 Experiments related to AIUB-CHAMP02S

The major changes of AIUB-CHAMP02S compared to AIUB-CHAMP01S are the amount of processed data and the use of more recent GNSS standards for the generation of the GPS satellite orbits and clock corrections, and for the computation of the CHAMP kinematic positions (see Sect. 5.2). The subsequent studies examine the influence of the GNSS model changes on gravity field recovery with CHAMP GPS measurements.

6.2.1 The impact of GNSS model changes

Question:

- Which impact do the GNSS model changes have on the gravity field determination using CHAMP GPS measurements?

The impact of the GNSS model changes (see Table 5.3) on the GPS satellite orbits is shown by the difference between the original GPS orbits stemming from the routine processing at CODE and the reprocessed GPS orbits (see Fig. 6.29). The numbers refer to the most important model changes listed in Table 5.3. Improvements in the ambiguity resolution and the consideration of the Earth gravity field model up to a higher SH degree introduced in March 2002 (1), the change of the radiation pressure (RPR) model and the nutation model in November 2005 (2), and the bundle of changes that took place in GPS week 1400 in November 2006 (3) contributed most significantly to the improvement of the GPS satellite orbits.

CODE and reprocessed GPS orbits become more similar in the recent years of the comparison and are very similar from GPS week 1400 onwards, when both are based on the same standards. They are, however, not completely identical after week 1400, because another version of the BSW is used and due to small differences in the modeling (e.g., treatment of satellite maneuvers, satellite problems, station problems). Furthermore the orbit reprocessing embraces not the whole final routine processing (as performed by Steigenberger, P., 2009) but only a part of it (see Sect. 5.2.2).

The reprocessed GPS satellite clock corrections are validated by a kinematic PPP of ground stations with known coordinates. For this purpose eight globally well distributed IGS stations are chosen. Within the whole reprocessing time interval 2002–2007 kinematic positions are computed with a spacing of 60 s in two versions: One version uses the CODE and the other the reprocessed orbit and clock products. The coordinates of both versions were compared with the known static station coordinates (based on the same standards as the compared kinematic positions, respectively). Figure 6.30 shows the results for the IGS station Zimmerwald. The accuracy of the PPP is about the same in the whole time interval when using the reprocessed GPS products. Since late 2005

the PPP with the CODE GPS products is almost as accurate as the PPP based on the reprocessed products. In the years 2002 to 2005, however, the PPP of static GPS stations considerably improves when using the reprocessed GPS orbits and clock corrections. A detailed view of the position differences (see Fig. 6.31 (a)) reveals that mainly the long wavelength signal could be reduced by adopting the new standards. The short wavelength part of the difference signal is generally at the same level and could only be improved for a limited number of epochs. This becomes evident by comparing the epoch to epoch differences of the kinematic positions, which are indicators for the noise level of the observations (Fig. 6.31 (b)).

The influence of the GNSS model changes on the generation of kinematic LEO positions is checked by an orbit determination experiment. The reprocessed kinematic orbit positions of the time interval DOY 70/2002 to 70/2003 are used as pseudo-observations in a reduced-dynamic orbit determination with the DP15 parameter setting (Table 6.1) and the same background models as used for the generation of AIUB-CHAMP02S (Table 5.7). The same is done for the old kinematic positions (based on the IGS standards of 2002/2003), which were used for the recovery of AIUB-CHAMP01S with the corresponding background models (Table 5.1). The daily RMS errors of both orbital fits are at the same level (Fig. 6.32). The CHAMP kinematic positions based on the original and the reprocessed GPS products are thus of the same quality with respect to their suitability for gravity field recovery. The PPP of CHAMP does not improve as much as the PPP of the static ground stations when changing the GNSS standards, because the noise of the kinematic positioning could only be reduced marginally (Fig. 6.31 (b)).

In order to study the influence of the GNSS model changes on gravity field recovery, the gravity field solution AIUB-CHAMP02Sp1y based on the same time interval as that underlying AIUB-CHAMP01S (DOY 70/2002 to 70/2003) is determined using the reprocessed kinematic positions as pseudo-observations and using the new processing standards and models. The parameterization is the same as that underlying AIUB-CHAMP01S. Figure 6.33 shows that AIUB-CHAMP01S and AIUB-CHAMP02Sp1y are of similar quality. There are marginal improvements in the high SH degrees and there is a degradation in the low degrees, in particular in the low even degrees.

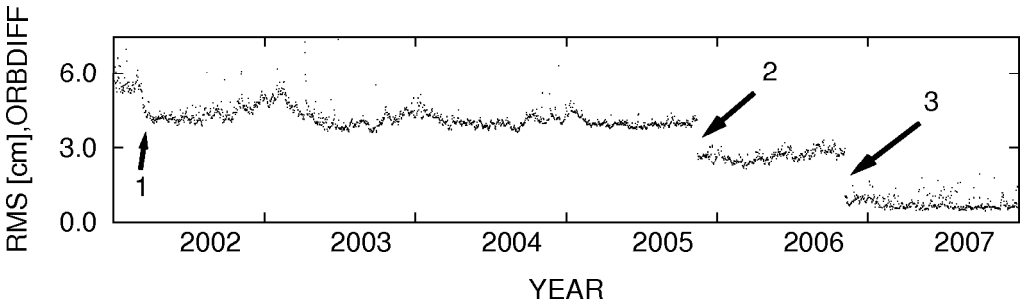

Figure 6.29: 3D-RMS of difference between CODE and reprocessed GPS orbits.

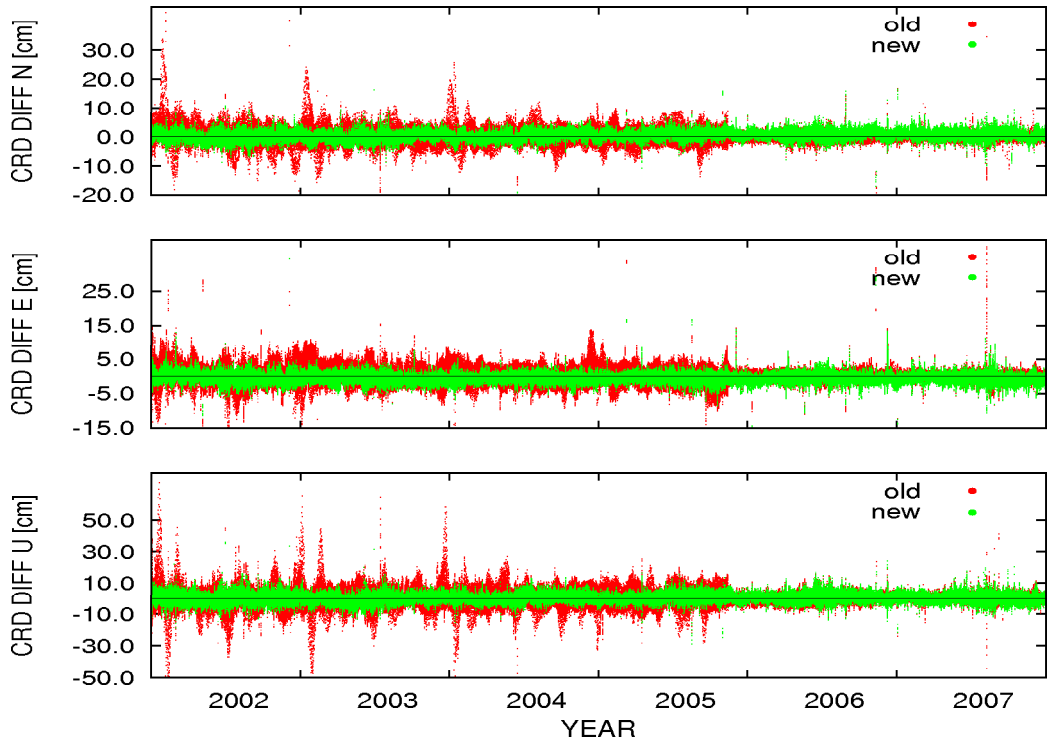

Figure 6.30: Differences in North (top), East (middle) and Up (bottom) between PPP-derived kinematic coordinates and static coordinates of the IGS station Zimmerwald in the years 2002 to 2007 when using CODE ("old") and reprocessed ("new") GPS orbit and clock products.

Results:

- The kinematic PPP of static ground stations improves when using the reprocessed GPS orbits and clock corrections. The improvement is mainly limited to long wavelength signal, while the high frequency part is only slightly improved.
- The gravity field estimation, mainly limited in quality by the high frequency noise of the kinematic positions, is only improved marginally in the high SH degrees.
- The gravity field solution is visibly deteriorated by an inconsistency in the low SH degrees.

6.2.2 Inconsistency in the low degree harmonics

Goals:

- Illustrate the effect of the inconsistency in the low SH degrees of the reprocessed gravity field solutions (Fig. 5.12 and 6.33).

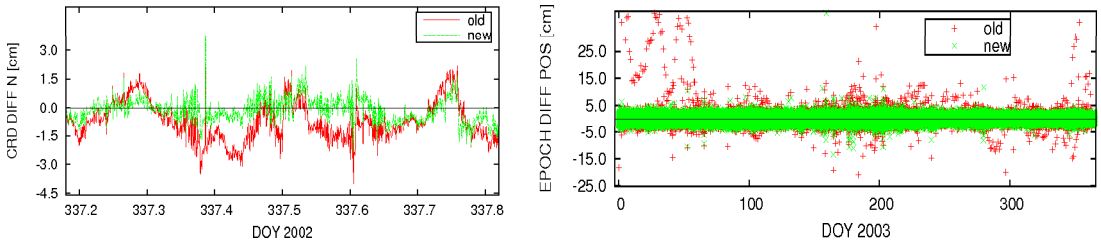

(a) Detailed view, DOY 337/2002 (b) Epoch to epoch differences

Figure 6.31: **Left:** Differences between kinematic and static coordinates of IGS station Zimmerwald when using CODE ("old") and reprocessed ("new") GPS clock corrections. Detailed view of North component on DOY 337/2002. **Right:** Epoch to epoch differences of the kinematic positions of IGS station Zimmerwald in 2003.

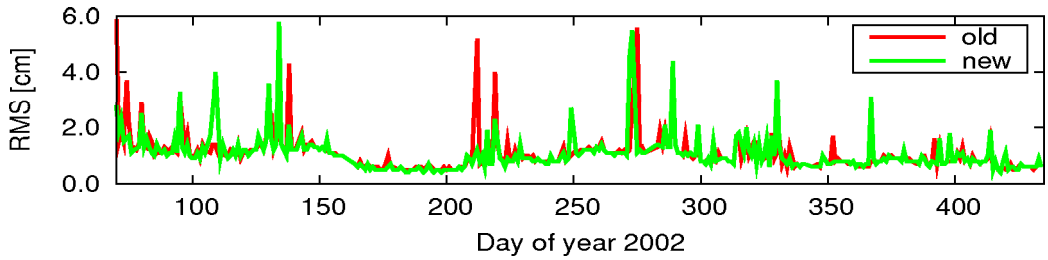

Figure 6.32: RMS error of orbit determination when using old or reprocessed kinematic CHAMP positions.

- Identify the reason for the inconsistency.

The reprocessed gravity field solutions AIUB-CHAMP02Sp1y, AIUB-CHAMP02S, and all annual solutions contributing to AIUB-CHAMP02S (see Fig. 5.12) show an inconsistency in the difference degree amplitudes w.r.t. EIGEN-GL04C — in particular in the low SH degrees. The inconsistencies are not visible in the AIUB-CHAMP01S nor do they disappear when other gravity fields are used as reference. As only gravity field models based on the reprocessed orbit and clock products are affected, the inconsistency must be related to the GNSS model changes.

In a first step the inconsistencies shall be described: If the difference degree amplitudes w.r.t. EIGEN-GL04C reference model are computed without taking the even zonal coefficients ($C_{2,0}$, $C_{4,0}$, $C_{6,0}$, ...) into account, the inconsistency is considerably reduced (Fig. 6.34 (a)). The odd zonal SH coefficients are only slightly affected by the inconsistency. The direct comparison of the SH coefficients of AIUB-CHAMP01S and AIUB-CHAMP02Sp1y underlines that mainly the even zonal coefficients are affected (Fig. 6.34 (b)). The zonal coefficients describe the rotational symmetric properties of the

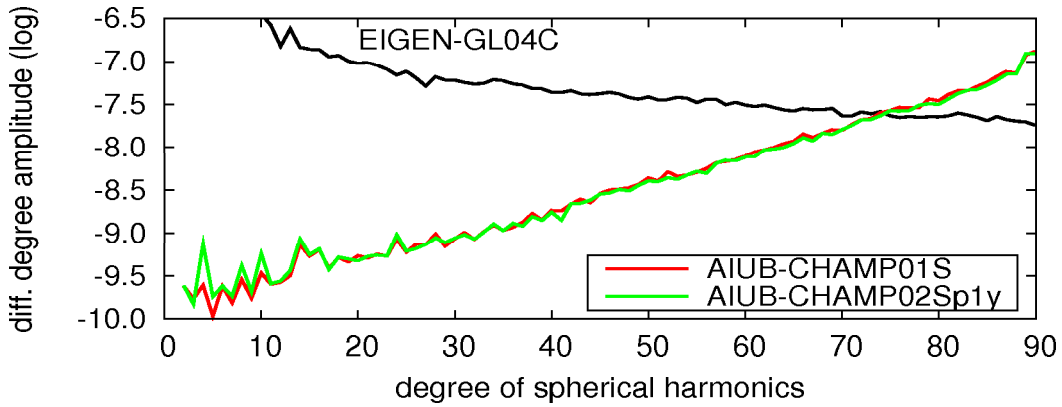

Figure 6.33: Comparison of AIUB-CHAMP01S and the reprocessed annual solution AIUB-CHAMP02Sp1y based on the same CHAMP GPS data.

gravity field and are, e.g., used for computing the normal potential of a rotational ellipsoid (see Sect. 3.5). The rotational symmetric nature of the inconsistencies is visualized by the gravity anomaly differences between AIUB-CHAMP01S and AIUB-CHAMP02Sp1y up to SH degree 10 (Fig. 6.34 (c)).

The effect could, e.g., be caused by a Z-scale in the Earth-fixed coordinate system. This is checked by the following experiment: Two months of kinematic CHAMP positions are separately affected by different kinds of simulated errors with a size of one meter, respectively. The errors correspond to the parameters of a Helmert transformation (translations, rotations, scales in X-, Y-, and Z-direction). The modified positions are introduced into a gravity field recovery using the DP15 parameterization. For each gravity field solution the difference degree amplitudes w.r.t. EIGEN-GL04C are computed (see Fig. 6.35) and compared to a gravity field solution generated in the same way but using the original kinematic positions.

We see that the rotations, a Z-translation, or a general scale of the kinematic LEO positions do not affect the gravity field solution. Translations in one of the horizontal directions are mapped into the estimated gravity field coefficients, in particular the coefficients of odd degrees. This error signature does, however, not explain the observed inconsistency. If a scale in Z-direction is applied, the simulated inconsistency is similar to the observed inconsistency in the sense that mainly the even zonal coefficients of the low SH degrees are affected. A Z-scale applied to the "true" positions generates in essence a wrong flattening parameter $C_{2,0}$. In the real data we do, however, observe the largest inconsistencies in $C_{4,0}$ and other even zonal coefficients. We conclude that the GNSS model changes have a systematic, latitude-dependent effect on the LEO orbits and on the derived gravity field model but that this effect is not a simple scale in the Z-direction. This finding is confirmed by a Helmert-transformation between the original and the reprocessed kinematic CHAMP positions (DOY 70/2002–70/2003) in the Earth-fixed coordinate system.

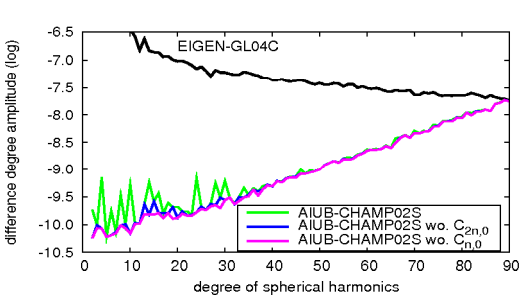

(a) Inconsistency in the diff. deg. ampl.

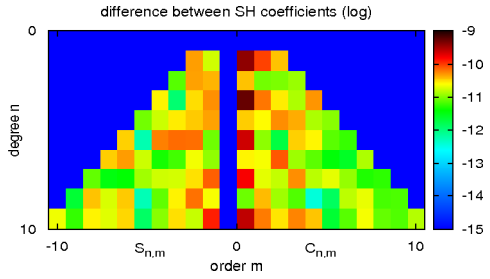

(b) Inconsistency in the SH coefficients

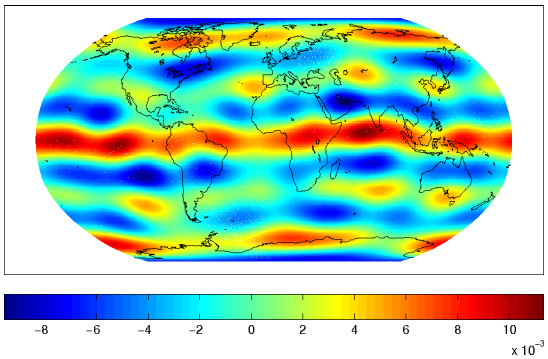

(c) Inconsistency in the gravity anomalies

Figure 6.34: Effect of the inconsistency. **Top left:** Difference degree amplitudes w.r.t. EIGEN-GL04C of AIUB-CHAMP02S, AIUB-CHAMP02S without considering the even zonal SH coefficients ("wo. $C_{2n,0}$"), and AIUB-CHAMP02S without considering any zonal SH coefficients ("wo. $C_{n,0}$"). **Top right:** Difference between the SH coefficients of AIUB-CHAMP01S and AIUB-CHAMP02Sp1y. **Bottom:** Difference of the gravity anomalies of AIUB-CHAMP01S and AIUB-CHAMP02Sp1y up to SH degree 10 [in mGal].

The transformation does not show a Z-scale but rather a general scale, as the X-, Y-, and Z-scale are of the same size. The general scale is caused by the change from the IGS00b to the IGS05 reference frame (Ferland, 2006), which is one of the GNSS model changes.

In order to find the reason for the inconsistency, the complete reprocessing (from GPS orbit processing to gravity field recovery, see Sect. 5.2) is performed several times for the year 2002. In each processing run, one model is changed back to the old standards, while the new standards are used for the other models. Additionally, the impact of different internal software versions and different treatments of GPS satellite problems are ruled out as reasons for the inconsistencies. The long time interval of one year is required, because the inconsistency is small and is not visible in gravity field solutions based on shorter

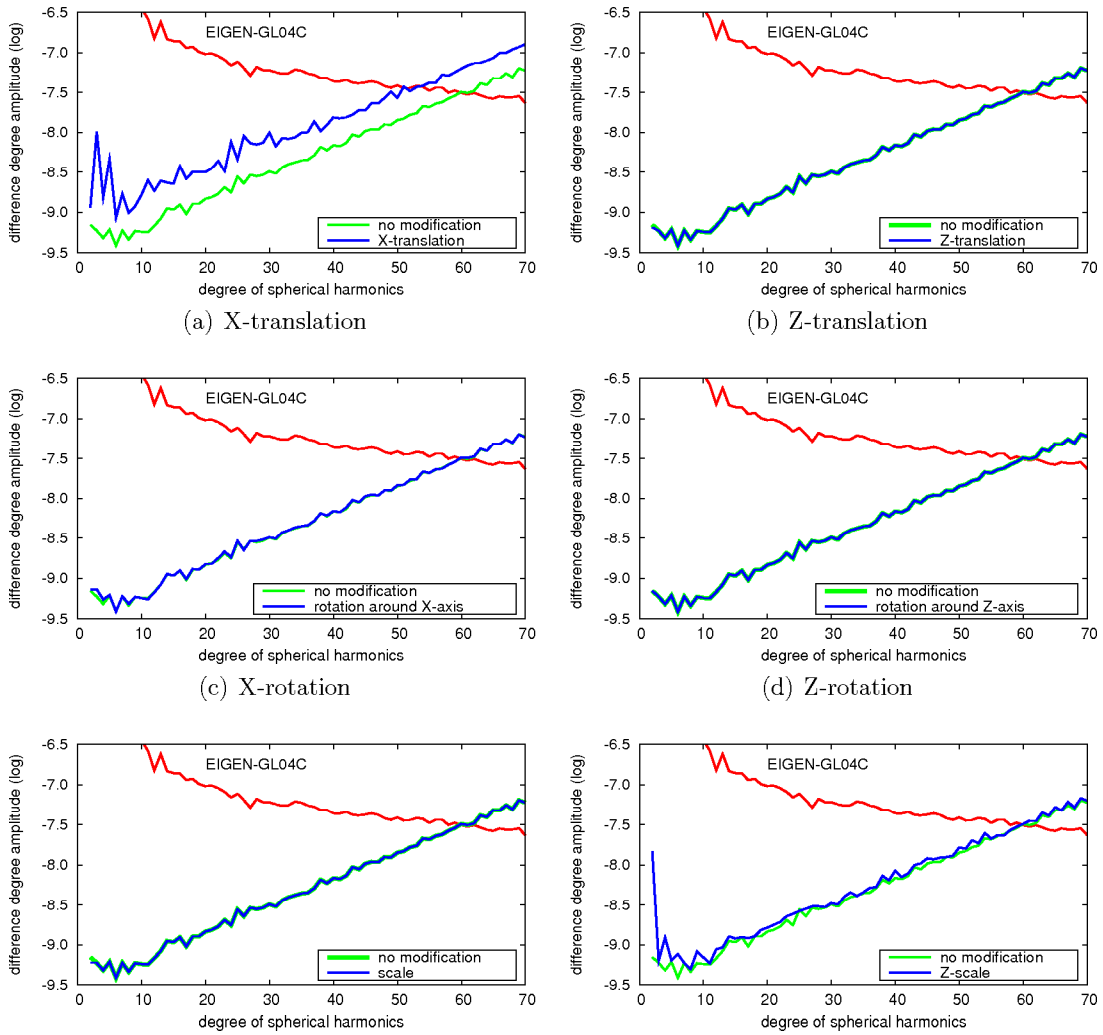

(a) X-translation (b) Z-translation

(c) X-rotation (d) Z-rotation

(e) Common scale (f) Z-scale

Figure 6.35: Difference degree amplitudes w.r.t. EIGEN-GL04C of gravity field solutions based on two months of CHAMP kinematic positions. The kinematic positions are modified by applying Helmert parameters.

data spans. The difference degree amplitudes w.r.t. EIGEN-GL04C of the annual test solutions with the most important model changes applied are shown in Figure 6.36 (a). The inconsistency in the gravity field solution does not disappear when **(a)** the center-of-mass (CMC)- or **(b)** the phase-windup-correction are switched off or **(c)** the a priori radiation pressure model for the GPS satellites or **(d)** the troposphere model are switched back to the old standards. The inconsistency disappears, however, when the PCV-model is switched from the absolute back to the relative standard and the reference frame from

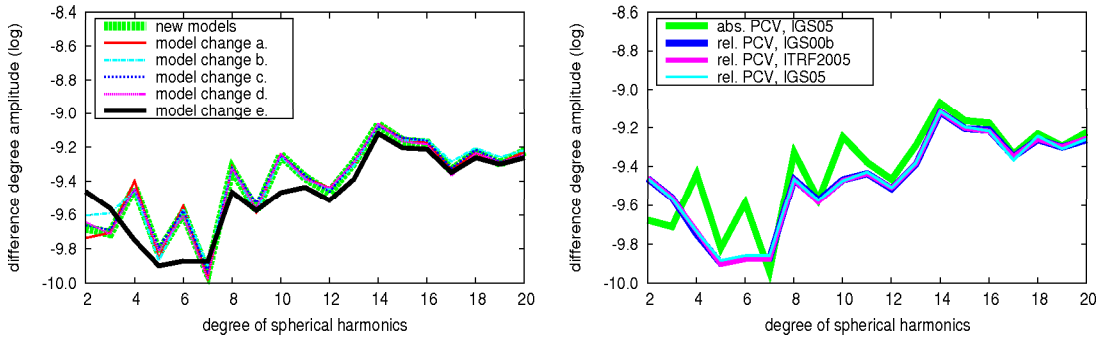

(a) Model changes (b) Reference frame and PCV

Figure 6.36: **Left:** Annual gravity field solutions with certain GPS models changed back to the old processing standards. **Right:** Annual gravity field solutions using the absolute PCV and the IGS05 reference frame vs. solutions using the relative PCV model and different reference frames.

IGS05 back to IGS00b (case **(e)** in Fig. 6.36 (a)). Furthermore, the relative PCV-model (old standard) is tested together with different reference frames (IGS00b, ITRF2005, IGS05). As only the solution using the absolute PCV model does show the inconsistency (Fig. 6.36 (b)), we conclude that the problem is caused by the change from the relative to the absolute PCV-model.

In order to illustrate the impact of a wrong LEO PCV-model, kinematic CHAMP positions are estimated using the IGS00b reference frame and the relative PCV-model (old standards). While the pattern of the CHAMP antenna is usually set to zero when using the relative PCV-model, the pattern of a randomly chosen ground antenna (type: TOP700779A) is applied to the CHAMP antenna, creating an artificial inconsistency. The annual gravity field model, computed from these CHAMP orbits, shows a strong inconsistency at degrees 2 and 4 (Fig. 6.37) due to the mis-modeled receiver antenna pattern. It is interesting that the LEO antenna PCV, which is set to zero when using the relative PCV standard, does not create a similar inconsistency pattern. The reason is possibly that the reference antenna (AOAD/M_T) of the relative PCV model (Dach et al, 2007) is — like CHAMP's POD antenna — a choke-ring antenna with a similar phase-pattern. Therefore the differences between both patterns are assumed to be relatively small.

Results:

- The GNSS model changes have a systematic, latitude-dependent effect on the estimated LEO orbits and on the derived gravity field models. This effect is not a simple scale in the Z-direction.
- The inconsistency is caused by the change from the relative to the absolute PCV-

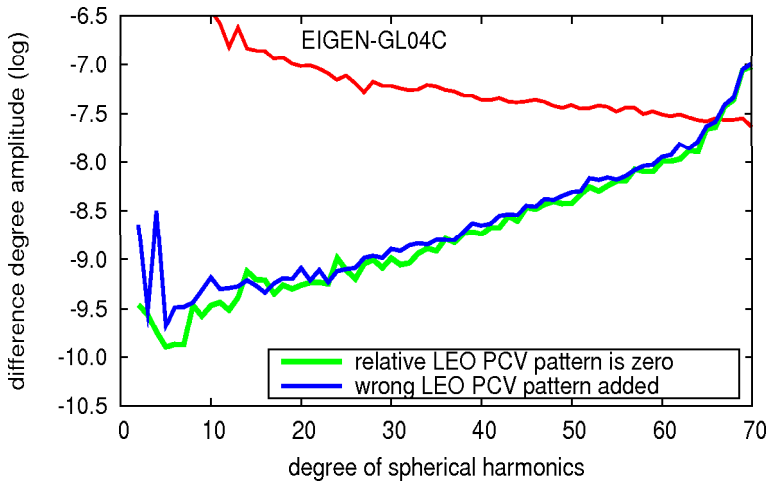

Figure 6.37: Impact of a wrong relative LEO antenna phase pattern on an annual gravity field solution.

model (part of the GNSS model changes).

6.2.3 Simulation study

Goal:

- Specify, which components of the PCV-model are able to cause inconsistencies of the observed kind.

Twenty days of CHAMP-like LEO orbits are simulated. AIUB-CHAMP01S up to SH degree 50 is the "true" gravity field. Using the simulated LEO orbits, the reprocessed GPS orbits and clock corrections, and the new processing standards (including absolute PCV), two sets of GPS observations for the fictitious LEO satellite are generated. One set of simulated observations is affected by white noise of 1 mm RMS error for the phase observations and 100 mm RMS error for the code observations. The other set is not affected by noise. In the simulation a nominal absolute PCV-model of the CHAMP GPS antenna (Montenbruck et al, 2009) is used.

The simulated GPS observations, the reprocessed GPS orbits, clock corrections, and ERPs are then used in a PPP. The estimated kinematic LEO positions are used as pseudo-observations for a LEO orbit (no noise) and for a gravity field determination (with noise). The SH series is truncated at degree and order 50, i.e., the solutions are not affected by omission errors. The estimated gravity field models are compared to the "true" AIUB-CHAMP01S.

Four aspects related to PCV-models are studied: (a) the phase center offset (PCO) of the GPS satellite's transmitting antennas, (b) the PCO of the LEO's receiving antenna,

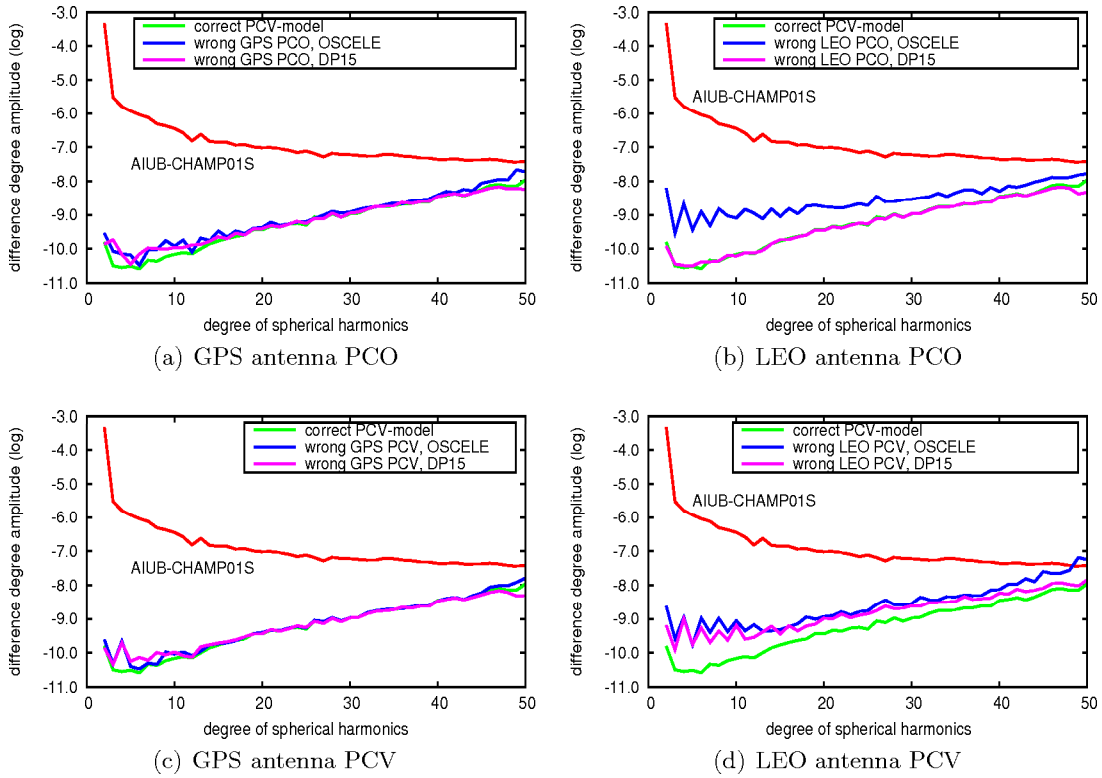

(a) GPS antenna PCO (b) LEO antenna PCO

(c) GPS antenna PCV (d) LEO antenna PCV

Figure 6.38: Gravity field solutions based on 20 days of simulated GPS observations affected by noise. The solutions are generated using the OSCELE or DP15 orbit parameterization and are affected by an inconsistency of one PCV model component, respectively.

(c) the phase center variations (PCV) of the GPS satellite's transmitting antennas, and (d) the PCV of the LEO antenna. Inconsistencies are introduced by modifying the PCOs or the PCVs in the PPP. Figures 6.38 and 6.39 illustrate the effects on gravity field and orbit determination, respectively, caused by changes in the mentioned four model constituents. Two different parameterizations (OSCELE and DP15, Table 6.1) are used in the estimation processes: The solutions based on the OSCELE parameterization are fully affected by the simulated inconsistencies. The DP15 parameterization is close to the parameterization used for generating the AIUB-CHAMP solutions. The corresponding solutions contain the residual inconsistency that cannot be absorbed by the parameters of the DP15 setting and therefore could affect an AIUB-CHAMP gravity field solution.

If the transmission antenna's offset of a single GPS satellite is increased by one meter the resulting gravity field is biased by effects barely visible in Fig. 6.38 (a). The systematic effects on the orbit determination residuals are small when determining a reduced dynamic

orbit (DP15 parameterization), see Fig. 6.39 (a). Results of a similar quality are obtained when the PCVs of the GPS transmitting antennas are ignored altogether (Fig. 6.38 (c)) — although a small inconsistency peak can be recognized at SH degree 4 in Fig. 6.39 (c). The effects on the gravity field are, in any case, much too small to explain the effects observed when analyzing real CHAMP data (see Fig. 6.33).

A change of the LEO antenna PCO causes a large inconsistency, if the OSCELE parameterization is used. The parameters of the DP15 setting, however, absorb most of the effect (Fig. 6.38 (b) and Fig. 6.39 (b)). Results of a different quality are obtained when ignoring the LEO antenna PCV pattern. Figure 6.39 (d) shows that fractions of the systematic effects in the residuals of the pure dynamic orbit determination (OSCELE) can be absorbed by the parameters of the DP15 reduced-dynamic orbit model. The remaining effect is, however, large enough to heavily bias the corresponding gravity field solution: Figure 6.38 (d) shows pronounced peaks in the even degree zonals of the order seen in the analysis of real data.

The residuals of the orbit determination (DP15 parameterization) based on the kinematic positions affected by inconsistencies of the GPS antenna PCV or LEO antenna PCV are used for visualization of the latitude-dependency of the PCV-induced errors. Figure 6.40 shows the corresponding residuals in the spacecraft-fixed RSW coordinate system as a function of the observer's latitude. Inconsistencies of the GPS antenna PCV generate a weak latitude-dependent effect in the residuals, while the inconsistency in the LEO antenna PCV is responsible for a very clear latitude-dependency.

Results:

- The prominent part of the inconsistency is due to the PCV pattern of the LEO POD antenna.
- Errors of the GPS transmission antenna PCV have a small influence, as well.
- Both antenna patterns have a latitude-dependent signature in the kinematic LEO positions.
- The effect of both antenna patterns can be compensated by the arc-specific parameters only to a very small extent.

6.2.4 Latitude dependency of the observation scenario

Goal:

- Illustration of the latitude dependency of PCV-induced errors.

In order to understand why the PCV-induced inconsistencies are indeed latitude-dependent, it is important to analyze the GPS observation scenario as seen from a LEO in a nearly polar orbit. Figures 6.41 and 6.42 are based on one year of CHAMP GPS observations. Figure 6.41 (a) shows that the number of observations at a given elevation e (in the antenna-fixed coordinate system) is indeed related to the latitude ϕ of the LEO GPS

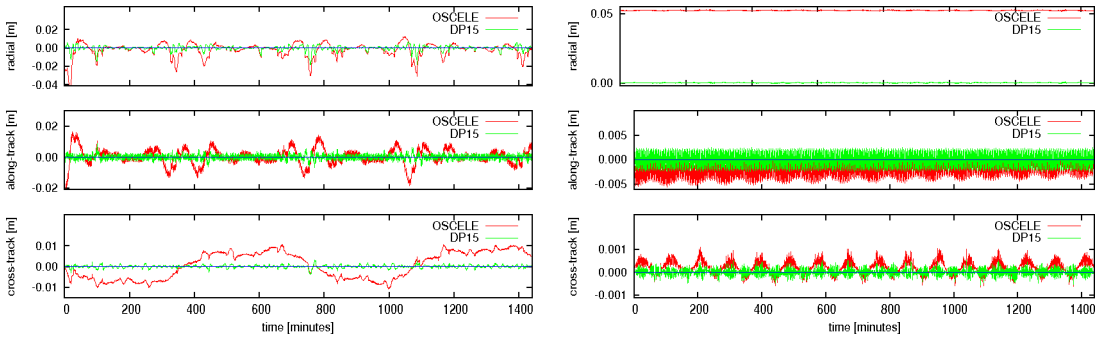

(a) GPS antenna offset

(b) LEO antenna offset

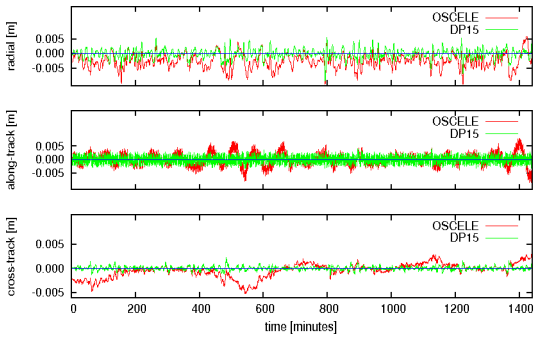

(c) GPS antenna pattern

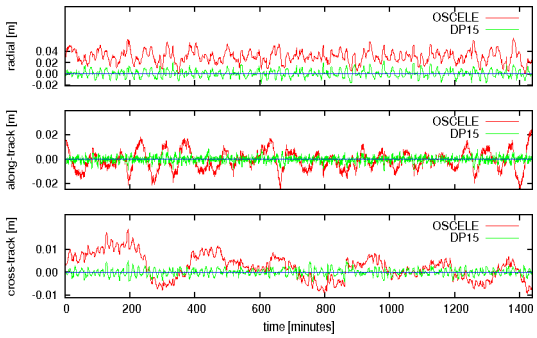

(d) LEO antenna pattern

Figure 6.39: Residuals of LEO orbit determination using one day of kinematic positions based on simulated GPS observations. The OSCELE or DP15 orbit parameterizations are used. The kinematic positions are affected by an inconsistency of one PCV model component, respectively.

antenna at observation time: It is, e.g., not possible to have observations at $e = 90°$ for $|\phi| > i \approx 55°$ (i is the inclination of the GPS orbits w.r.t. the equatorial plane). The inclination of $i \approx 55°$ of the GPS satellites also explains the large numbers of observations at medium elevations (about 30° to 45°) made from high (Northern and Southern) latitudes: At CHAMP's orbital height the maximum possible elevation angle at the poles is about 45°. The number of GPS satellites observed in the zenith ($e = 90°$) is largest for $|\phi| \approx 55°$. Figure 6.41 (b) illustrates that the azimuthal distribution of observations is latitude-dependent, as well.

The observation geometry can also be illustrated in the antenna-fixed azimuth/elevation coordinate system ("skyplot"-diagram). In the skyplots used in this work the azimuth is 0° on the top side (pointing into the satellite's flight direction) and is counted clock-wise (+90° on the right side and so on). The elevation angle is 0° at the edge and 90° in the center (representing the zenith) of the skyplot. Figure 6.42 (a) shows that the number of

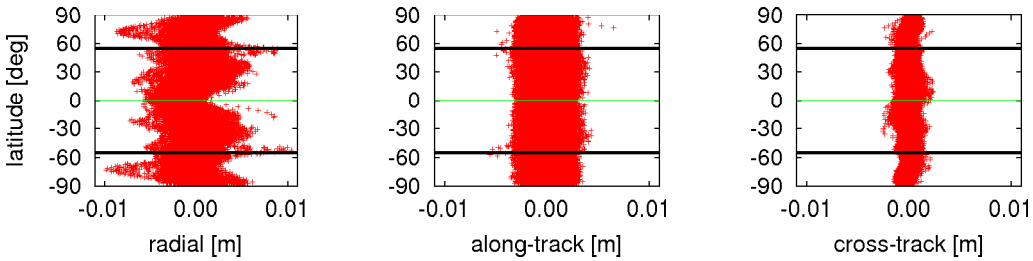

(a) GPS pattern inconsistent

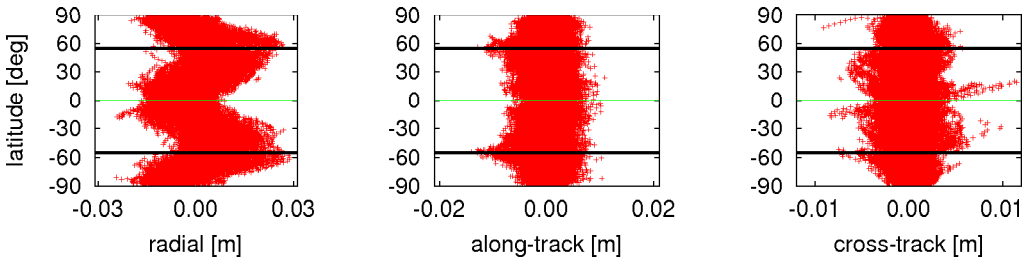

(b) LEO pattern inconsistent

Figure 6.40: Residuals from 20 days of orbit estimation using simulated kinematic LEO positions affected by an error of the GPS emitting (**top**)/LEO receiving (**bottom**) antenna pattern. The residuals are shown as a function of the satellite's latitude. The dark horizontal lines mark the maximum latitude, where GPS satellites can be observed in the zenith (corresponding to the inclination of the GPS satellites $i \approx 55°$).

observations is far from spherically symmetric. The reasons are the limited number of tracking channels (preventing the receiver from tracking all GPS satellites in view) and the channel allocation behavior of the GPS receiver: The accumulation of observations on the rear side of the spacecraft speaks for a channel allocation that favors GPS satellites with high elevation. This would make sense because the antenna gain and the signal to noise ratio (SNR) are better for higher elevation angles (Montenbruck and Kroes, 2003). Figure 6.42 (b) shows that the observations made at high latitudes (Northern and Southern) are predominantly mapped into an annulus with an elevation of about 30° to 45° in the skyplot. The concentration of observations in the higher third of possible elevation angles (0–45° over the poles) also speaks for a channel allocation in favor of high elevation angles. The observations made at lower (Northern and Southern) latitudes are, however, distributed more evenly in the skyplot. Corresponding to Fig. 6.41 (a) the figure shows that most observations close to the zenith are made from latitudes $|\phi| \approx 55°$.

Results:

- The GPS observation geometry generates a latitude-dependent distribution of the

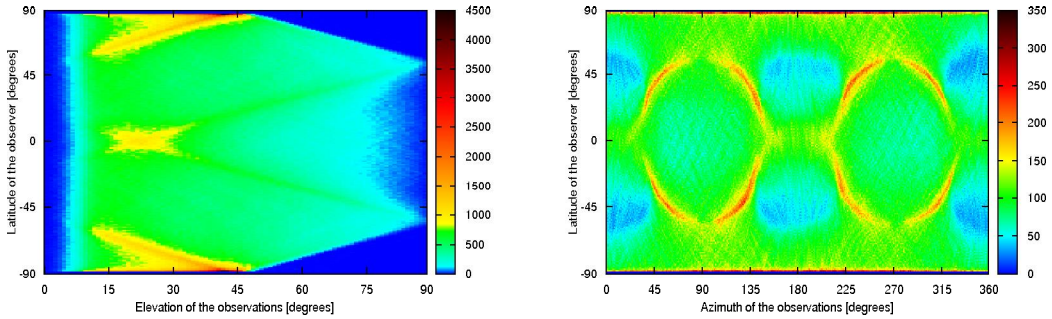

(a) Elevation (b) Azimuth

Figure 6.41: Number of GPS observations at a given elevation (**left**) or azimuth (**right**) in CHAMP's antenna-fixed reference system at different latitudes.

GPS observations in the antenna-fixed coordinate system of the LEO.

- As the PCVs are applied in the form of azimuth-elevation-specific corrections it is thus clear that PCVs can have a latitude-dependent influence on LEO orbit and gravity field determination.

6.2.5 Summary and conclusion of the AIUB-CHAMP02S-related studies

The studies performed in Sect. 6.2.1–6.2.4 illustrate the impact of the GNSS model changes (see Sect. 5.2.1/Table 5.3) on GPS-based gravity field determination using the CMA: The use of more recent processing standards and background models in the GPS orbit and clock reprocessing, and in the LEO PPP slightly reduced the noise level of the kinematic positions. This marginally improved the recovery of the SH coefficients of high degrees (Sect. 6.2.1). On the other side the even, zonal SH coefficients of low degrees are affected by an inconsistency, corresponding to a systematic, latitude-dependent effect on the kinematic LEO positions (Sect. 6.2.2). This effect is caused by the change from the relative to the absolute PCV-model or, more precisely, by the PCV-pattern of the LEO POD antenna (Sect. 6.2.3). The pattern of the GPS transmission antennas has a similar effect of smaller magnitude. The GPS observation geometry generates a latitude-dependent distribution of the GPS observations in the antenna-fixed coordinate system of the LEO (Sect. 6.2.4). As PCVs are applied in the form of azimuth-elevation-specific corrections they "inherit" the latitude-dependency. This PCV-induced effect cannot be completely compensated by the arc-specific parameterization.

The conclusion of this section is: For GPS-based LEO POD and gravity field recovery with high accuracy demands the PCV-pattern of the LEO POD antenna must be properly

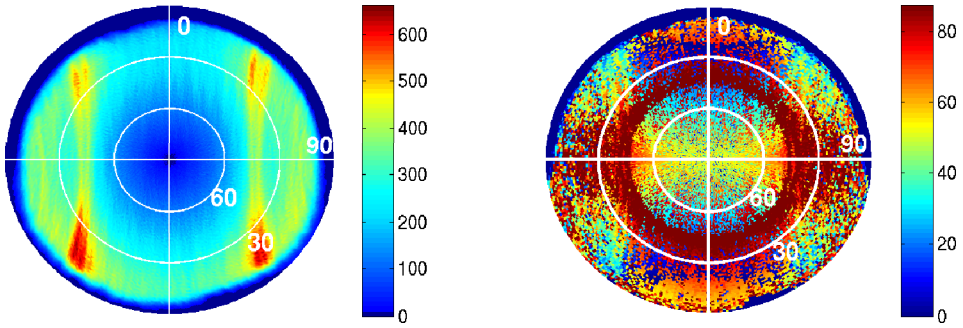

(a) Number of observations in bins of 1° (b) Dominating latitude $|\phi|$

Figure 6.42: **Left**: Number of observations in the antenna-fixed azimuth-elevation system. **Right**: Dominating observer's latitude ($|\phi|$ in [°]) in the antenna-fixed azimuth-elevation system.

taken into account — at least when using the absolute PCV model. The absolute pattern used in the reprocessing, stemming from a robot ground calibration is insufficient, because the phase pattern may change under operational conditions (e.g., due to cross-talk and multipath effects, Montenbruck et al, 2009). Therefore, the LEO POD antenna needs to be calibrated under operational conditions.

6.3 Experiments related to AIUB-CHAMP03S

The CHAMP-only gravity field solution AIUB-CHAMP03S is supposed to benefit from a larger amount of CHAMP GPS data and from processing improvements. Prior to generating AIUB-CHAMP03S the impact of those improvements has to be assessed and suitable processing strategies have to be defined in a series of experiments:

- The impact of empirical CHAMP POD antenna phase patterns on gravity field recovery is examined in Sect. 6.3.1 as a direct consequence of the results obtained in Sect. 6.2.
- While the empirical PCV-pattern is supposed to reduce systematic errors in the LEO POD, the elevation-dependent weighting studied in Sect. 6.3.2 shall take the stochastic properties of the GPS observations into account.
- The impact of the data sampling rate and GPS satellite clock interpolation in the LEO POD is examined in Sect. 6.3.3.
- In Sect. 6.3.4 we study the impact of the correlations between the kinematic positions of different epochs on gravity field determination aiming on an improved weighting of the pseudo-observations.

- In Sect. 6.3.5 we compare the suitability of kinematic positions and of position-differences as pseudo-observations for gravity field recovery. Special attention is paid to the problematic CHAMP data of the year 2009.
- Sect. 6.3.6 examines, whether the quality variations of monthly CHAMP gravity field solutions observed in Sect. 6.1.8 are partly related to observations of eclipsing GPS satellites in the LEO processing.

With these improvements applied the attempt is made to detect temporal changes of the Earth's gravity field using the monthly contributions to AIUB-CHAMP03S (Sect. 6.3.7). In a final study (Sect. 6.3.8) we discuss problems in the recovery of the low degree harmonics that showed up during the data analysis. We check, whether the recovery of these coefficients may be improved by introducing information about the higher degree harmonics. This question is important for the evaluation of CHAMP's possible contribution to a combined gravity field solution.

6.3.1 Influence of empirical PCV-models on gravity field recovery using CHAMP GPS data

Questions:

- How does an estimated CHAMP antenna PCV-pattern influence the gravity field determination?
- Which aspects must be considered when estimating the PCV-pattern?

Jäggi et al (2009b) have shown with GRACE data that the in-flight calibration of the LEO GPS antenna considerably improves the gravity field solution from GPS-derived kinematic LEO positions. The experiments performed in Sect. 6.2 underline that the estimation of the LEO antenna pattern is a necessity for precise LEO orbit and gravity field determination.

New absolute and relative PCV-patterns for the CHAMP GPS antenna are generated using the residuals of one year (DOY 70/2002 to DOY 70/2003) of reduced-dynamic orbit determination in the same way as described by Jäggi et al (2009b): The L_3 phase residuals from the reduced-dynamic orbit determination (with the LEO antenna PCV-pattern set to zero) are put into elevation/azimuth bins. For each bin with a size of 1° in azimuth and elevation, the mean residual value is computed. The empirical phase pattern is then used in a new iteration step of the LEO orbit determination and a new pattern is generated from the residuals of this run. In the case of the relative PCV model the CHAMP orbits are computed in the same way as described by Jäggi (2007) using the old GNSS standards and the original CODE GPS products. In the case of the absolute pattern the LEO orbits are computed according to Sect. 5.2.4 using the new standards and the reprocessed GPS products.

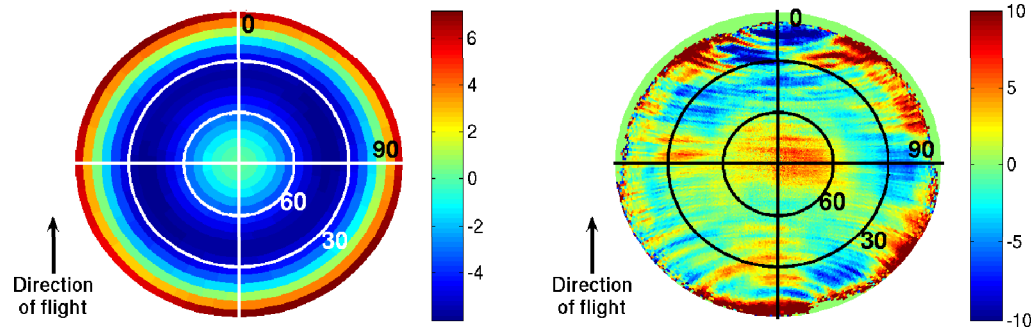

(a) Nominal pattern (b) Estimated pattern

Figure 6.43: Absolute pattern of the CHAMP GPS antenna [in mm]. **Left**: Nominal antenna pattern from a robot ground calibration of an antenna of equal type. **Right**: Pattern generated from the residuals of a reduced-dynamic orbit determination over one year in 2 iterations.

Fig. 6.43 (b) shows the resulting absolute PCV-pattern with a resolution of 1° in elevation and azimuth. It differs considerably from the nominal absolute pattern, generated in a robot ground calibration of the TerraSAR-X antenna (Montenbruck et al (2009), Fig. 6.43 (a)) and the estimated patterns of the GRACE A and B antennas (see Jäggi et al, 2009b) — despite the fact that the antennas of TerraSAR-X, GRACE A, GRACE B, and CHAMP are of the same type. The estimated CHAMP pattern (Fig. 6.43 (b)) shows complicated and small structures. The large correction values in the lowest part of the figure (rear side of the satellite) are most likely related to the cross-talk between CHAMP's POD and occultation antennas reported by Montenbruck and Kroes (2003). A similar relation is known from GRACE A (Jäggi et al, 2009b). Other differences between the nominal PCV-model (generated under laboratory conditions) and the estimated PCV-model may be due to the fact that the empirical PCV also absorbs a variety of other unmodeled error sources.

Figure 6.44 shows that the use of estimated CHAMP PCV-patterns improves annual gravity field solutions. The solution based on the estimated absolute phase pattern is better than the solutions based on the nominal pattern or without pattern (see Fig. 6.44 (a)). Most of the inconsistencies in the low even degrees disappear or can be significantly reduced. The gain is not limited to the low even SH degrees. The gravity field solution is also considerably better in the medium and higher SH degrees due to the fine structures in the estimated PCV. We also see a gain for the gravity field solution based on the old GNSS standards associated with the introduction of the estimated relative CHAMP PCV-model (see Fig. 6.44 (b)).

The quality of an empirical phase pattern of the LEO GPS antenna may be influenced

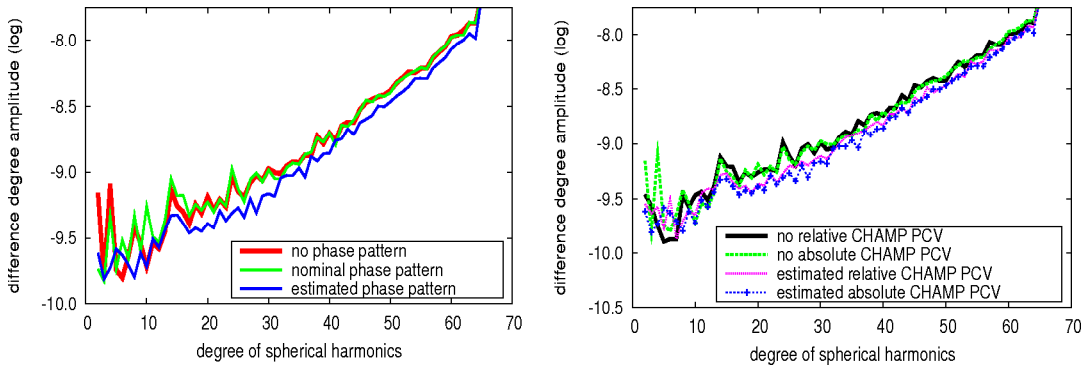

(a) Different absolute PCV-models (b) Rel. vs. abs. phase patterns

Figure 6.44: Impact of estimated PCV patterns on annual AIUB-CHAMP solutions. **Left**: Absolute PCV-model. **Right**: Absolute and relative PCV-models.

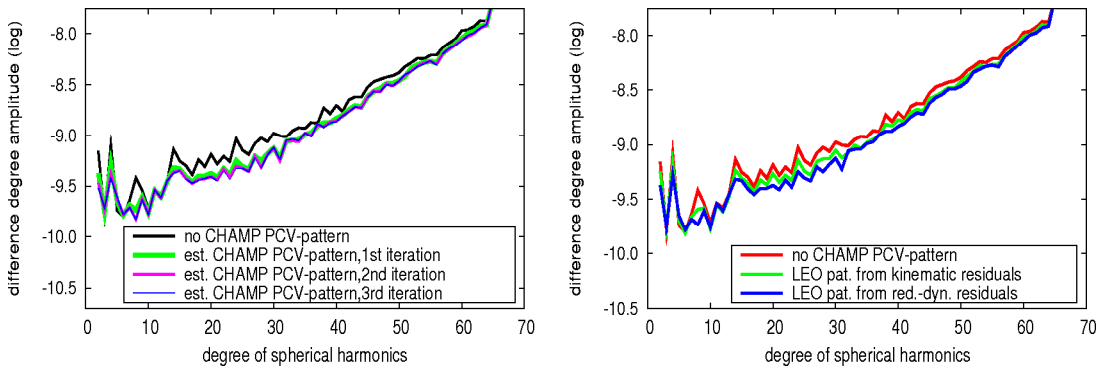

(a) Iterations (b) Kinematic and red.-dyn. residuals

Figure 6.45: Annual CHAMP gravity field solutions based on different estimated LEO PCVs. **Left**: PCVs generated from the residuals of a reduced-dynamic orbit determination in one, two, or three iterations. **Right**: PCVs generated from the residuals of a reduced-dynamic orbit determination/a kinematic PPP in one iteration.

by different aspects. Figure 6.45 (a) compares the impact of empirical absolute CHAMP PCV-patterns based on a different number of iteration steps. Large improvements are already possible with a pattern generated in only one iteration. A second iteration slightly improves the solution. The third iteration step does not significantly improve the solution.

Figure 6.45 (b) compares the impact of empirical CHAMP PCVs generated from the residuals of a reduced-dynamic orbit determination (like in the preceding examples) or of a kinematic PPP. In both cases only one iteration is used for pattern generation. Jäggi

et al (2009b) have shown on the example of GRACE that the quality of empirical LEO PCV-models generated from both residual types is similar, when using ten iterations for pattern generation. Figure 6.45 (b) shows that the pattern based on the residuals of the reduced-dynamic orbit determination is clearly better after the first iteration. The pattern generation from the residuals of a reduced-dynamic orbit determination thus converges more rapidly than the pattern generation from the residuals of a kinematic PPP.

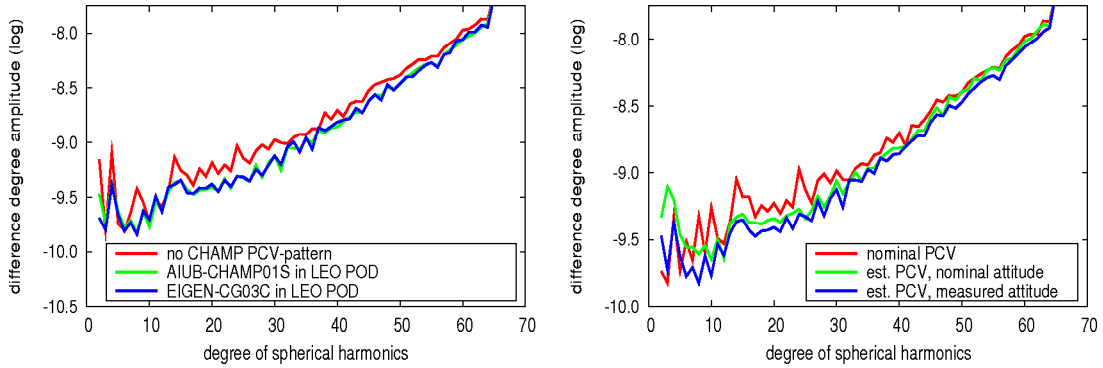

(a) A priori gravity field in LEO POD

(b) Attitude data in LEO POD

Figure 6.46: Annual CHAMP gravity field solutions based on different estimated LEO PCVs. **Left**: Different a priori gravity field models used in the LEO POD for residual generation. **Right**: Measured/nominal attitude used in the LEO POD for residual generation.

When using the residuals of a reduced-dynamic orbit determination there is, however, the possibility that the a priori gravity field might bias the pattern. In order to verify this aspect, two different versions of reduced-dynamic CHAMP orbits are determined. One version uses the AIUB-CHAMP01S gravity field model, the other uses EIGEN-CG03C (Förste et al, 2005). From the residuals of both versions PCV-models are generated in two iteration steps and used in a kinematic PPP. The kinematic positions are used as pseudo-observations in a gravity field determination. Figure 6.46 (a) shows that the two resulting gravity field solutions are very similar, suggesting that the impact of the a priori gravity field used for pattern generation is small.

From Sect. 5.2.4 we know already that there are time intervals when no attitude data is available for CHAMP, which apparently does not harm the gravity field determination. In order to check the influence of missing attitude information on LEO PCVs, two versions of reduced-dynamic CHAMP orbits are determined. One version uses the attitude measurements of CHAMP's star trackers. In the second case CHAMP's attitude is assumed to be nominal. The residuals are used for pattern generation as mentioned before. Figure 6.46 (b) compares the gravity field solutions based on the two patterns. The gravity field solution based on the pattern generated without using attitude measurements is clearly inferior — especially in the low SH degrees.

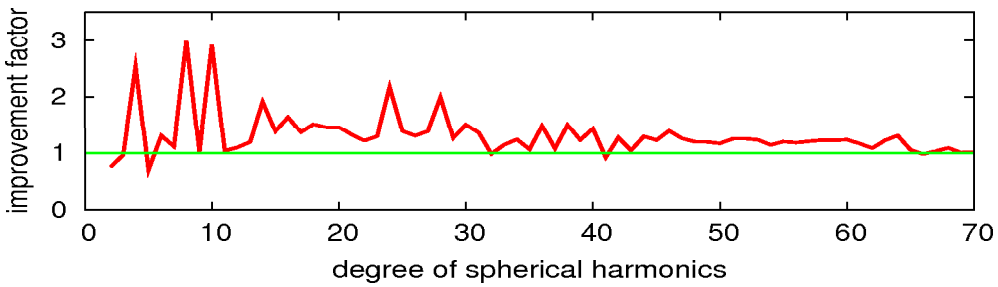

Figure 6.47: Improvement factor of the difference degree amplitude w.r.t. EIGEN-GL04C of an annual gravity field solution due to the use of an estimated instead of the nominal CHAMP GPS antenna phase pattern.

We conclude that the in-flight determination of the LEO antenna PCV-patterns is a necessity for high-quality LEO orbit and gravity field determination using GPS. The empirical patterns generated from residuals may not only describe the LEO antenna phase pattern itself, but also absorb other systematic effects like multipath or sensor cross-talk. In case of gravity field recovery this is seen as an advantage. Therefore, empirical CHAMP PCV-models are estimated and used for the generation of AIUB-CHAMP03S. The improvement factor of the difference degree amplitude w.r.t. EIGEN-GL04C of an annual gravity field solution (2002) due to using the estimated absolute CHAMP PCV model shown in Fig. 6.43 (b) is illustrated in Fig. 6.47.

Results:

- The in-flight calibration of the LEO POD antenna is a necessity for high-quality LEO orbit and gravity field determination using GPS. It significantly improves the gravity field solution in the whole SH spectrum.
- From the residuals of a reduced-dynamic orbit determination a suitable empirical pattern may be derived in only two iteration steps. When using the residuals of a kinematic PPP, more iterations are required to create a pattern of comparable quality.
- The resulting gravity field solutions are marginally influenced by the gravity field model used in the reduced-dynamic orbit determination. Therefore, AIUB-CHAMP02S is selected as a priori gravity field model in the LEO POD and PCV estimation for AIUB-CHAMP03S.
- The quality of an empirical LEO PCV-model may be degraded when the underlying residuals are generated without using attitude measurements. Therefore no residuals from time intervals without available attitude data are used for pattern generation in the AIUB-CHAMP03S processing.

6.3.2 Elevation-dependent weighting

Questions:

- Does the CHAMP-only gravity field solution benefit from elevation-dependent weighting of the GPS observations in the LEO PPP?
- How may an appropriate weighting function be defined?

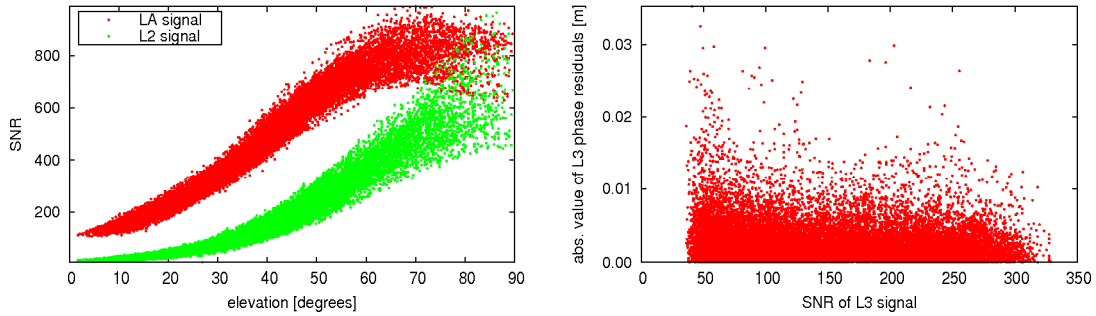

(a) SNR and elevation.

(b) SNR and residuals.

Figure 6.48: Signal to noise ratio (SNR) of CHAMP GPS observations on DOY 300/2002. **Left**: Relation between SNR and elevation angle. **Right**: Relation between SNR of L_3 observations and absolute value of the residuals of the kinematic PPP.

The empirical antenna PCV-pattern described in Sect. 6.3.1 absorbs the LEO antenna phase pattern itself, but also other systematic effects. In this section we will try to additionally consider the stochastic properties of the GPS observations. Some effects influencing the noise of the GPS observations (e.g., signal strength and multipath) are elevation-dependent (Montenbruck and Kroes, 2003). The relation between signal strength (represented by the signal to noise ratio, SNR) and elevation angle is shown for one day (DOY 300/2002) of CHAMP GPS observations in Fig. 6.48 (a). The SNR is larger for higher elevations. The relation between the signal strength of the L_3 phase observations and their residuals in the CHAMP PPP is shown on the example of the same day in Fig. 6.48 (b). Thereby the SNR of the L_3 observations is assumed to be approximately one third of the SNR of the LA observations (Montenbruck and Kroes, 2003; Dach et al, 2009). The residuals are generally larger for low SNRs. Due to the latter relation different authors, e.g., Kirchner and Becker (2005) and Luo et al (2009) suggest weighting models making use of the signal strength. In this work, however, we focus on an elevation-dependent treatment of the GPS observations.

GPS observations at low elevations, which usually suffer from a low SNR (see Fig. 6.48 (a))

may be removed from the GPS data processing by applying an elevation cut-off angle. A cut off angle of 10° is automatically applied for the front half of the CHAMP antenna's field of view since a receiver software update in 2001 (Montenbruck and Kroes, 2003). This cut off angle is also visible in the estimated PCV model in Fig. 6.43 (b). Low-elevation observations are therefore only available in the rear half of the CHAMP POD antenna's field of view and their number is low. Therefore the application of an elevation cut-off angle of 5° in the kinematic PPP has no significant impact on gravity field determination. With elevation cut-off angles well above 10° too many observations would be lost. Therefore we prefer an elevation-dependent weighting by defining a zenith distance-dependent observation weight

$$P(z) = P(z = 0) \cdot F(z) = F(z) \ , \tag{6.9}$$

where $F(z)$ is the mapping function relating the observation weight at $z = 0$ (assumed as 1 in the above formula) to that at zenith distance z (where $z = 0$ corresponds to the zenith of the antenna). The following weight function is routinely available in the BSW (Rothacher, 1992):

$$P(z) = cos^2(z) \ . \tag{6.10}$$

Weights of type (6.10) make sense if the observation noise is predominantly caused by tropospheric refraction. As the weighting of the observations using Eq. (6.10) has a remarkably positive impact on gravity field determination (although LEO GPS measurements are not affected by the troposphere), one may ask the question whether there are even better ways of weighting the observations. In analogy to the empirical antenna pattern an empirical weight function could be based on the residuals of the GPS observations. For that purpose all GPS residuals of a considered time interval (e.g., one year) can be assigned to 1° bins from bin 1 between $[0°, 1°]$ to bin 90 between $[89°, 90°]$ in zenith distance. For each bin the L1-norm of the residuals can be computed:

$$L1_i = \frac{\sum_{k=1}^{n_i} |v_{ik}|}{n_i} \ , \tag{6.11}$$

where v_{ik} are the individual residuals within bin i, n_i is the the number of residuals within bin i. Alternatively the root mean square (RMS) value can be used:

$$RMS_i = \sqrt{\frac{\sum_{k=1}^{n_i} (v_{ik})^2}{n_i}} \ . \tag{6.12}$$

The empirical weight function may then be defined as

$$P_{emp_i} = \left(\frac{L1_1}{L1_i} \right)^2 \ , \tag{6.13}$$

for an observation at zenith distances in the interval $[i - 1, i]°$. An empirical weighting function might be defined as a function of azimuth and zenith distance, as well.

For generating AIUB-CHAMP03S we follow a slightly different avenue by (a) deriving

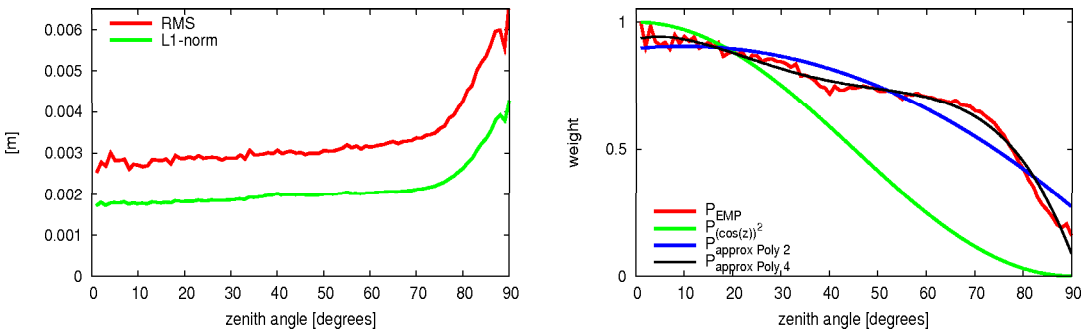

(a) (b)

Figure 6.49: **Left**: Bin-wise L1-norm and RMS of kinematic CHAMP residuals. **Right**: Elevation-dependent weight functions derived from the kinematic residuals.

the empirical weight function Eq. (6.13) from one year of CHAMP data (the year 2002 is used for that purpose) and (b) by fitting this function by polynomials of degrees 2 to 4. Let us call this approximating function $P_{approx}(z)$. The raw values (6.11) and (6.12) are provided in Fig. 6.49 (a), the resulting empirical and approximative weight functions (derived from the L1-norm), and the weight function Eq. (6.10) by Fig. 6.49 (b).

Although the weight functions in Fig. 6.49 (b) are different, the impact on gravity field recovery is similar when using polynomial approximations of different degrees or the weight function Eq. (6.10) (Fig. 6.50 (a)). For the generation of AIUB-CHAMP03S the polynomial approximation of degree 2 is used. Figure 6.50 (b) shows that the elevation-dependent weighting can improve an annual CHAMP gravity field solution to a similar extent as the use of an estimated PCV pattern. Moreover both effects are complementary. The improvement factor due to the use of elevation-dependent weighting is given in Fig. 6.50 (c). The largest improvements can be achieved for SH degrees above 15, indicating that the quality of the gravity field solutions is to a large extent limited by the stochastic properties of the GPS observations in this part of the SH spectrum. The small effect above degree 60 is explained by the low cut-off degree 70 of the test solutions, resulting in large omission errors dominating the error budget in the higher degrees. The smaller impact of elevation-dependent weighting in many SH degrees below 15 and the "bulge" between degrees 10 and 20 in Fig. 6.50 (a) indicate that the gravity field solution is limited by systematic errors in the lower part of the SH spectrum.

Results:

- Elevation-dependent weighting of CHAMP GPS observations in the kinematic PPP has a strong positive impact on gravity field recovery. It is therefore applied in the AIUB-CHAMP03S processing supplementary to the empirical PCV-model.
- An empirical weighting function based on the L_3 phase residuals of the LEO PPP

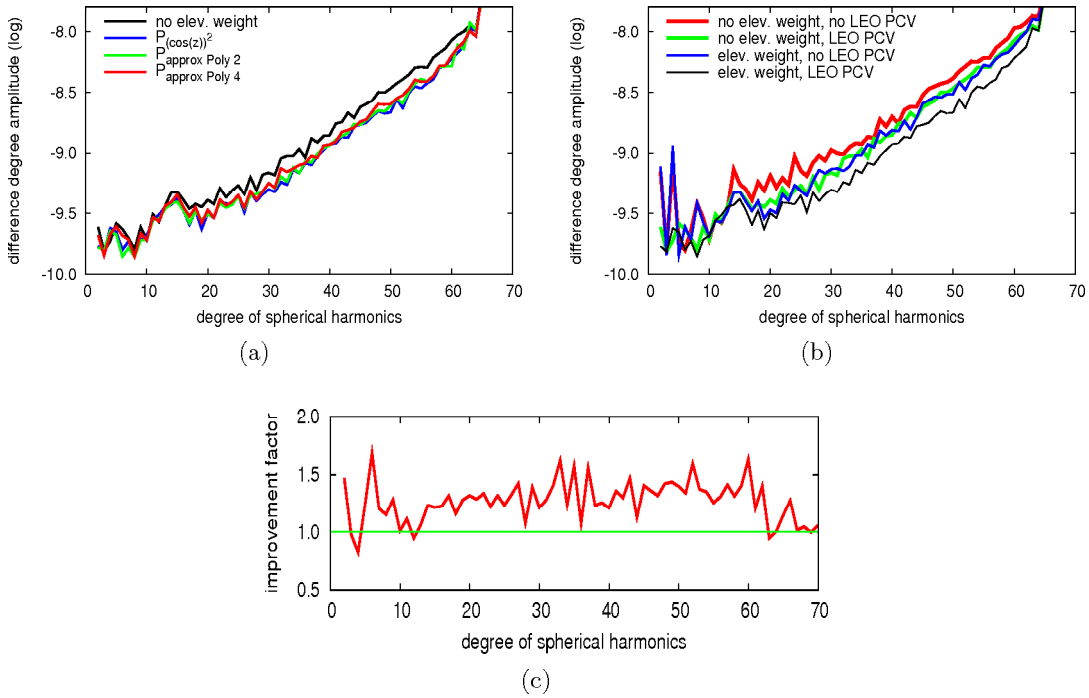

Figure 6.50: Impact of elevation-dependent weighting on annual CHAMP gravity field solutions. **Left**: Impact of different weighting functions. **Right**: Impact of empirical PCV-model or elevation-dependent weighting or both. **Bottom**: Improvement factor of the difference degree amplitudes due to the elevation-dependent weighting.

is defined.

6.3.3 Observation sampling

Questions:

- Does the CHAMP gravity field recovery profit from a higher observation sampling rate?
- Is the interpolation of the GPS satellite clock corrections from 30 s to 10 s sufficiently accurate?
- Is the quality of the available and newly generated (Sect. 5.3.1) high-rate GPS satellite clock corrections sufficient in the whole time interval 2002–2009?

The GPS receiver onboard CHAMP provides measurements every 10 s (see Sect. 2.2.5). So far, we only used kinematic positions with a sampling interval of 30 s. This raises the

question, whether gravity field determination could benefit from using the full sampling rate of CHAMP's GPS receiver. The interval of 30 s was dictated by the sampling interval of the GPS satellite clock corrections (computed from the 30 s observations of the IGS tracking network). If one would like to use CHAMP's 10 s data, the satellite clock corrections must either be available at the same spacing or lower-rate clock corrections must be interpolated to the epochs of the LEO positions. Since 2007 high-rate GPS satellite clock corrections with a spacing of 5 s are made available by CODE. Experiments with 10 s CHAMP data thus became possible.

37 days of CHAMP GPS observation from 2007 are used to compute kinematic CHAMP positions in three different ways: (a) Kinematic positions with a 30 s spacing are generated using 30 s GPS satellite clock corrections. (b) Kinematic positions with a 10 s spacing are generated using 30 s GPS satellite clock corrections interpolated to the 10 s epochs. (c) Kinematic positions with a 10 s spacing are generated using the high-rate (5 s spacing) GPS satellite clock corrections.

The kinematic CHAMP positions are then used as pseudo-observations in a gravity field determination. The resulting gravity fields in Fig. 6.51 (a) show that the solution (b) based on interpolated satellite clock corrections is even worse than the solution based on positions with a 30 s spacing. The solution using 10 s positions based on the high-rate clock corrections is the best. The test shows the potential of high observation sampling rates and that clock interpolation based on 30 s satellite clock corrections is not an option.

Kinematic positions with 10 s spacing based on the 5 s GPS clock corrections are then computed for the whole year 2007. Apart from that the processing is done in the same way as for AIUB-CHAMP02S. The resulting gravity field solution is compared to the annual solution of 2007 contributing to AIUB-CHAMP02S (Fig. 6.51 (b)). As expected from Fig. 6.51 (a) the solution based on the higher sampling rate is better — especially in the high SH degrees. Figure 6.51 (c) shows that — except for the high SH degrees — the actual improvement is below the value ($\sqrt{3}$) that would be expected for uncorrelated observations. The improvement is, however, significant and justifies the generation of AIUB-CHAMP03S with the full sampling rate of CHAMP's GPS observations. This requires a high-rate GPS satellite clock analysis for the years 2002 to 2006 (see Sect. 5.3.1).

From Sect. 5.3.1 we know that the number of high-rate IGS stations contributing to the high-rate GPS satellite clock corrections was quite low in the years 2002 and 2003. It is therefore not clear, whether the high-rate clock corrections of those years are good enough to be used for kinematic PPP. Gravity field test solutions (up to SH degree 70) based on short data time intervals (70 d) are therefore generated prior to the establishment of AIUB-CHAMP03S. These solutions are based on sampling intervals of 30 s and 10 s, respectively. The gravity fields are produced in versions with pulse spacings of 5 and 15 min, respectively. For each test the relative change of the difference degree amplitude when using the higher sampling rate is determined. This way the quality of the high-rate clock corrections is assessed indirectly. The results are shown in Fig. 6.52. Each picture

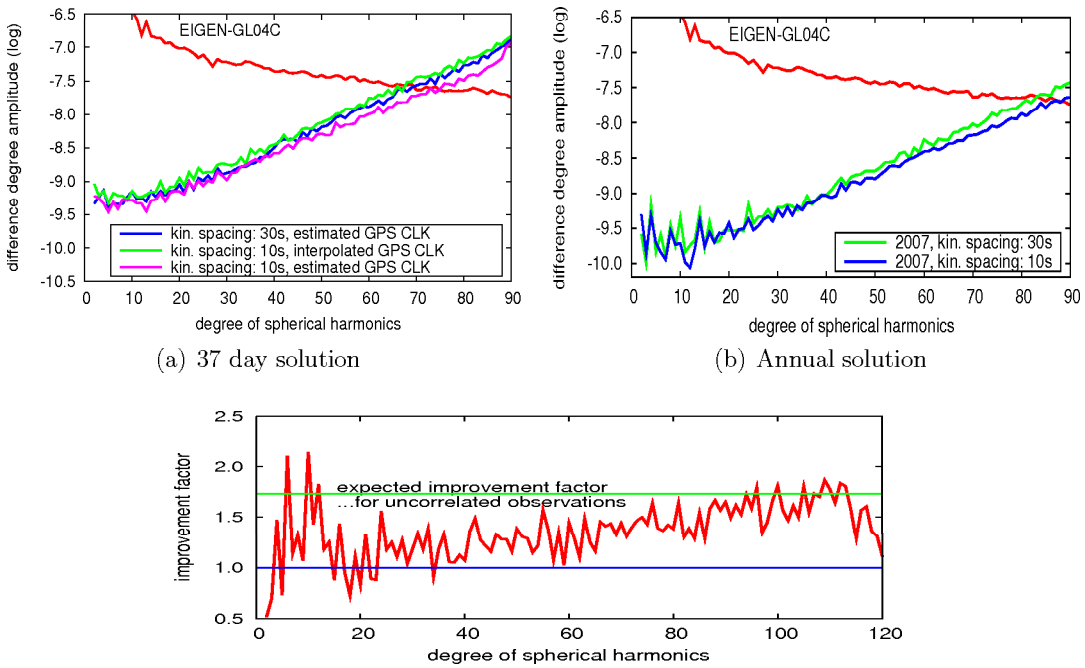

(a) 37 day solution

(b) Annual solution

(c) Improvement factor

Figure 6.51: Impact of the sampling rate of the kinematic CHAMP positions on gravity field recovery. **Top, left**: 37 d interval, estimated vs. interpolated GPS satellite clock corrections in PPP. **Top, right**: Annual solutions, based on different spacings of kinematic pseudo-observations. **Bottom**: Improvement factor of the difference degree amplitudes of the 2007 solution due to the 10 s instead of the 30 s sampling interval.

in Fig. 6.52 covers test intervals from two different years. An "improvement" factor of one stands for the same quality of the two gravity field solutions. Factors < 1 indicate degradations, values > 1 indicate that the 10 s solutions are better than the 30 s solutions.

Figure 6.52 (a) shows that the 10 s test solution performs poor in 2002. The high-rate clock corrections are obviously not as good as the 30 s clock corrections in 2002. The annual contribution of 2002 to AIUB-CHAMP03S is, therefore, based on kinematic positions with a 30 s spacing. In late 2003 the high- and low-rate solutions are of similar quality up to SH degree 40. The degrees above 40 are slightly better for the higher sampling rate. The quality of the high-rate clock corrections has improved during 2003 (corresponding to the increased number of contributing high-rate IGS stations). All annual contributions to AIUB-CHAMP03S from 2003 onwards are, therefore, based on 10 s kinematic positions.

Figure 6.52 (b) shows the improvement factors in late 2004 and late 2005. Above degree 30 the 10 s solutions are better. In 2006 and 2007 the 10 s solutions are significantly better than the 30 s solutions from degree 20 upwards (Fig. 6.52 (c)). In 2008 and 2009

(Fig. 6.52 (d)) the situation is similar for the solutions with 5 min pulses. Note that the solutions with fewer pulses do not improve in the same extent in those years. This could be related to the changed receiver behavior due to the change from the main to the redundant GPS receiver on DOY 280/2008 (see Sect. 5.3.2).

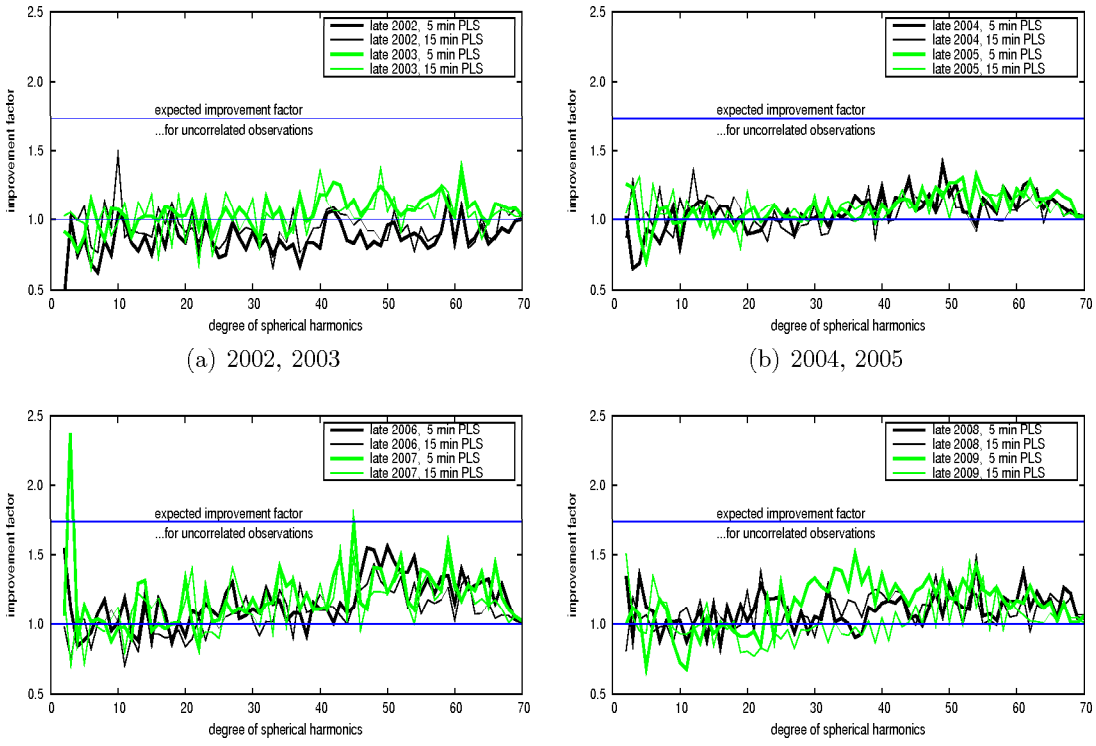

(a) 2002, 2003

(b) 2004, 2005

(c) 2006, 2007

(d) 2008, 2009

Figure 6.52: Improvement of 70 d CHAMP gravity field solutions based on 10 s instead of 30 s observation spacing. **Top, left**: Late 2002, and late 2003. **Top, right**: Late 2004, and late 2005. **Bottom, left**: Late 2006, and late 2007. **Bottom, right**: Late 2008, and late 2009.

Results:

- The gravity field recovery benefits from a shorter spacing (10 s instead of 30 s) of the kinematic CHAMP positions (also meaning an increased number of pseudo-observations) — in particular the coefficients of higher degrees.
- The generally poor improvement in the low SH degrees (< 20) indicates the presence of systematic errors affecting mainly the low degree harmonics. A similar observation is already made in Sect. 6.3.2.
- The interpolation of 30 s GPS satellite clock corrections to 10 s cannot be recom-

mended in general.

- The quality of the high-rate (5 s) GPS satellite clock corrections improves within the time interval 2002–2009 due to the increased number and better distribution of the tracking stations contributing to the high-rate IGS network (see Sect. 5.3.1).

6.3.4 Inter-epoch correlations of kinematic positions

Questions:

- Does the CHAMP-only gravity field solution benefit from the consideration of the correlations between the kinematic positions belonging to different epochs?

When generating AIUB-CHAMP01S and AIUB-CHAMP02S the kinematic positions were weighted using the inverse of the epoch-specific covariance matrix from kinematic PPP (see Sect. 6.1.5). The inter-epoch correlations between the GPS-derived kinematic positions, caused by the phase ambiguities, were so far neglected in this work.

The weight matrix P of the pseudo-observations is derived from the covariance information of the kinematic PPP according to Eq. (3.4). The covariance matrix applied in Eq. (3.4) is, however, only the sub-matrix of the full covariance matrix from the PPP referring to the kinematic positions. Due to the large number of kinematic positions this sub-matrix is still rather big. The amount of data is reduced by storing only the diagonal elements and a limited number of off-diagonal blocks. In the gravity field recovery the kinematic coordinates are processed batch-wise, including only the pseudo-observations of those epochs, which are covered by a covariance-block. The correlations between all pseudo-observations within each batch are taken into account correctly, but the correlations between pseudo-observations of different batches are neglected. This treatment is, however, statistically more correct than completely neglecting the inter-epoch correlations as done so far. In this work a maximum batch-size of 50 epochs (1500 s) is chosen for kinematic positions spaced by 30 s and 140 epochs (1400 s) for kinematic positions with 10 s spacing. These values are a trade-off between statistical correctness and manageable file size: The kinematic epochs are correlated by the phase ambiguities. The time intervals of uninterrupted visibility of particular GPS satellites (as viewed from the CHAMP receiver) have typical lengths of 20 (1200 s) to 35 min (2100 s). Therefore, the correlation interval of about 1500 s and 1400 s, respectively, seems appropriate.

In order to check the influence of the inter-epoch correlations, one year (DOY 70/2002 to 70/2003) of kinematic CHAMP positions with different spacings (10 s and 30 s) are used for gravity field recovery. The covariance information from the kinematic PPP is used for weighting the pseudo-observations in different ways: In the first case only the epoch-specific covariance information ("COV 1 EPO") is used. In the second case the correlations over a short time interval (20 epochs for 30 s data, 60 epochs for 10 s data, corresponding to 600 s) are considered, as well. In the third case correlations over a longer time interval (50 epochs for 30 s data, 140 epochs for 10 s data, corresponding to 1500 and 1400 s) are taken into account.

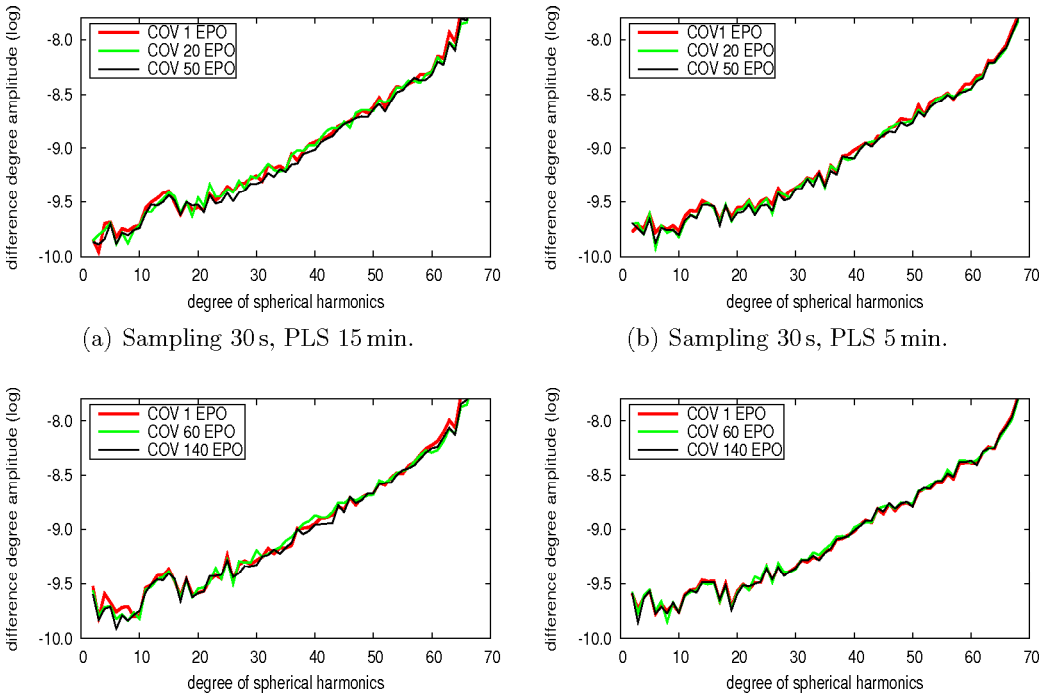

(a) Sampling 30 s, PLS 15 min.

(b) Sampling 30 s, PLS 5 min.

(c) Sampling 10 s, PLS 15 min.

(d) Sampling 10 s, PLS 5 min.

Figure 6.53: Impact of inter-epoch correlations on annual gravity field solutions based on different pseudo-observation samplings and different orbit parameterizations. **Top, left**: Sampling interval 30 s, pulse interval 15 min. **Top, right**: Sampling interval 30 s, pulse interval 5 min. **Bottom, left**: Sampling interval 10 s, pulse interval 15 min. **Bottom, right**: Sampling interval 10 s, pulse interval 5 min.

Figure 6.53 shows the difference degree amplitudes of the resulting gravity fields w.r.t. EIGEN-GL04C. The test suggests that the correlations between the kinematic epochs have a small effect on gravity field determination. The effect is, moreover, only measurable when taking into account the correlations over long time intervals. Solutions based on longer pseudo-observation spacings (30 s) and with fewer pulses (every 15 min) benefit more from considering the correlations than solutions based on short pseudo-observation spacings (10 s) and/or more pulses (every 5 min) (compare Fig. 6.53 (a) and Fig. 6.53 (d)).

Prior to the generation of the annual contributions to AIUB-CHAMP03S test solutions based on short data spans (70 d from the end of each year) and $n_{max} = 70$ are produced. The pseudo-observations are weighted in two different ways: The "old" (epoch-wise covariance) and the "new" (batch-size of 50 epochs for 30 s data spacing in 2002 and 140 epochs for 10 s data spacing in 2003–2009) way. The improvement factors between the

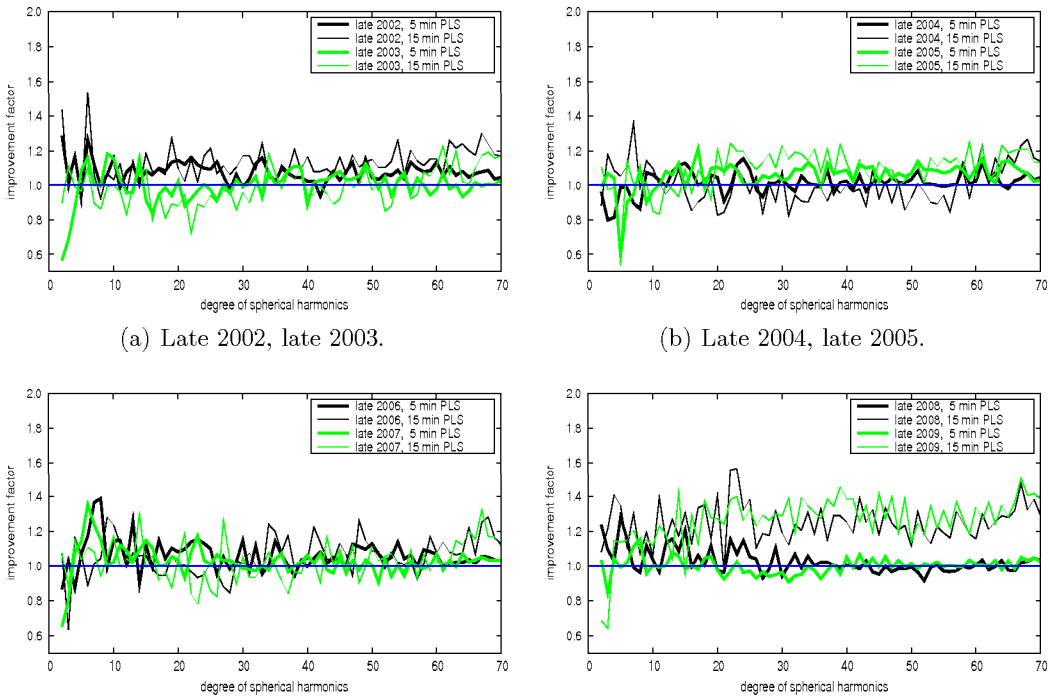

(a) Late 2002, late 2003.

(b) Late 2004, late 2005.

(c) Late 2006, late 2007.

(d) Late 2008, late 2009.

Figure 6.54: Quality improvement of gravity field solutions of different 70 d test periods when considering the inter-epoch correlations between the kinematic CHAMP positions. **Top, left**: Late 2002 (sampling interval here: 30 s) and late 2003. **Top, right**: Late 2004, and late 2005. **Bottom, left**: Late 2006, and late 2007. **Bottom, right**: Late 2008, and late 2009.

difference degree amplitudes of "old" and "new" solutions are computed.

The improvement factors in Fig. 6.54 (a–d) confirm that the impact of the inter-epoch correlations is generally small. Taking into account the correlations does not always have a positive effect in the entire SH spectrum: the gravity field solution from late 2003 is, e.g., partly degraded and partly improved (see Fig. 6.54 (a)). In late 2008 and late 2009 solutions with 5 min pulses do not benefit much from considering the inter-epoch correlations, whereas the improvement is exceptionally big for solutions with 15 min pulse interval (see Fig. 6.54 (d)). When looking at the corresponding difference degree amplitudes of the solutions from late 2008 (Fig. 6.55 (a)), we recognize that the solution with 15 min pulse interval is clearly inferior — although it benefits more from modeling the inter-epoch correlations than the solution with 5 min pulses. The different situation observed for the DP15 solution from late 2008 onwards indicates a stronger connection of the kinematic positions of different epochs. This may be related to switching from the main to the redundant board of the CHAMP GPS receiver on DOY 280/2008 and the

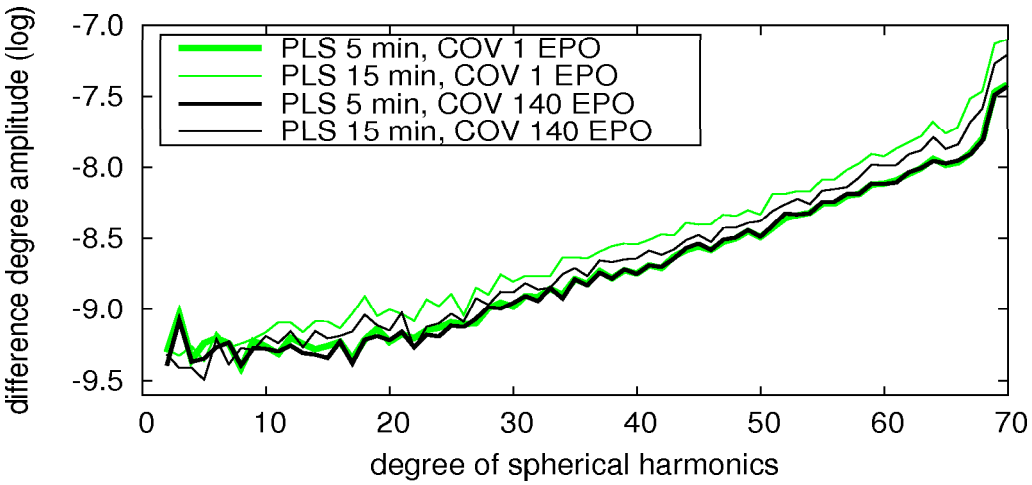

(a)

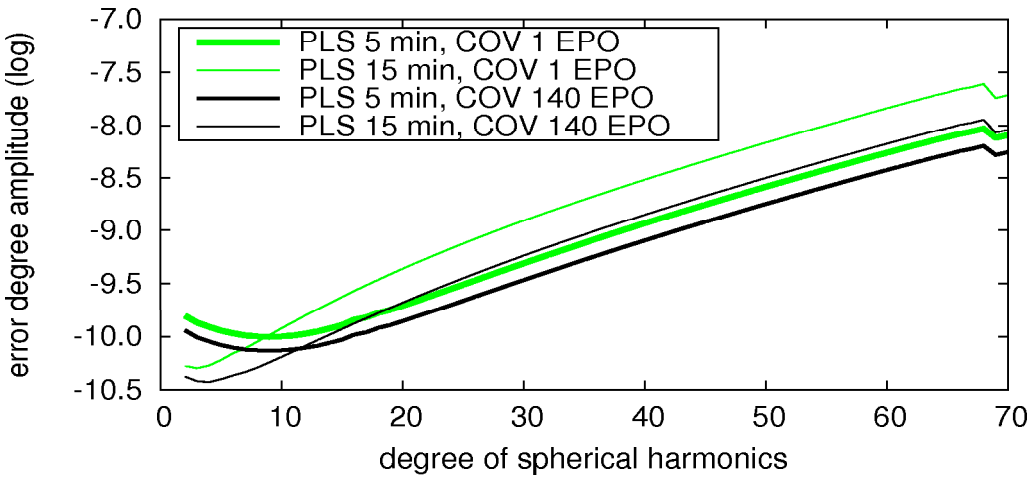

(b)

Figure 6.55: Impact of inter-epoch correlations on 70 d (late 2008) CHAMP gravity field solutions using different orbit parameterizations. **Top**: Difference degree amplitudes w.r.t. EIGEN-GL04C. **Bottom**: Error degree amplitudes.

related changes in the tracking behavior. The much better quality of the DP05 solutions (compared to the DP15 solutions) in 2008 and 2009 is related to the lower orbital height in the later years of the CHAMP mission increasing the air drag. Figure 6.55 (b) shows that the formal errors indicate a strong improvement when considering the correlations between the kinematic epochs. Especially in the case of the DP05 solution the improvement indicated by the formal errors is obviously too optimistic.

Results:

- The inter-epoch correlations (up to an interval of 1500 s) between the kinematic CHAMP positions have a small, mostly positive, impact on gravity field recovery.
- This finding agrees well with the results of corresponding experiments with GRACE conducted by Jäggi et al (2010b).

6.3.5 Position differences vs. positions

Questions:

- Are position differences suitable pseudo-observations in a CHAMP-only gravity field recovery?
- Can position differences raise the yield of the kinematic CHAMP positions from 2009 with their poor quality?

Table 6.11: Properties of test solutions for position difference experiments.

Solution	Pseudo-obs.	Screening	Parameterization	Standard
DP15-p-s-n	positions	yes	DP15	AIUB-CHAMP03S
DP15-p-us-n	positions	no	DP15	AIUB-CHAMP03S
DP15-pd-s-n	differences	yes	DP15	AIUB-CHAMP03S
DP15-pd-us-n	differences	no	DP15	AIUB-CHAMP03S
DP15-p-s-o	positions	yes	DP15	AIUB-CHAMP02S
DP15-pd-s-o	differences	yes	DP15	AIUB-CHAMP02S
D-pd-s-n	differences	yes	DYNPAR	AIUB-CHAMP03S

Our processing scheme allows it to use either positions or position differences for orbit and/or gravity field determination. As in the case of GPS observations (see Sect. 4.5.2) forming differences may significantly reduce systematic errors, which are constant or slowly varying. Such errors may, e.g., be caused by changes in the GPS observation scenario resulting in groups of large outliers in the kinematic positions.

The impact of using differences of subsequent positions instead of positions is checked by computing different annual gravity field solutions (DOY 70/2002 to 70/2003) up to SH degree 70. The test solutions are explained in Table 6.11. Depending on the test scenario the kinematic positions are taken from the AIUB-CHAMP02S or AIUB-CHAMP03S processing (last column in Table 6.11). The position differences are formed using these positions. The parameterizations are explained in Table 6.1.

Test1: Sensitivity to outliers
The importance of the outlier screening when using positions/position differences is checked by comparing the solutions DP15-p-s-n (based on screened positions), DP15-p-us-n (based on unscreened positions), DP15-pd-s-n (based on differences of screened positions), and DP15-pd-us-n (based on differences of unscreened positions). Figure 6.56 (a) shows that solutions based on position differences are not as sensitive to outliers as solutions based on positions. This could be explained by the presence of groups of large outliers (with a similar size for subsequent outliers) in the kinematic CHAMP positions (see, e.g., the residuals in Fig. 6.21). This kind of outliers has only a limited impact on position differences.

Test2: Parameterization
The DP15 parameterization (pulses every 15 min) is able to absorb errors of different types (e.g., omission errors, non-gravitational perturbations). In Sect. 6.1.1 and also in Fig. 6.14 we have seen that many pulses are required if kinematic positions are used for gravity field determination. Figure 6.56 (b) shows that this is different for gravity field solutions based on position differences. The solution D-pd-s-n (without pulses) is of similar quality like the DP15-pd-s-n solution (with pulses every 15 min) for most SH degrees. Only the lowest SH degrees are degraded. This indicates that not only the effect of outliers is reduced by forming position differences. Also the impact of other error sources (that must be absorbed by pseudo-stochastic parameters in the case of using positions) is much reduced.

Test3: Impact of systematic errors
Another question concerns the sensitivity of position differences to the systematic improvements of the kinematic PPP made since the generation of AIUB-CHAMP02S. The comparison of the solutions DP15-p-s-o (based on positions of the AIUB-CHAMP02S standard), DP15-pd-s-o (based on position differences of the AIUB-CHAMP02S standard), DP15-p-s-n (based on positions of the AIUB-CHAMP03S standard), and DP15-pd-s-n (based on position differences of the AIUB-CHAMP03S standard) in Fig. 6.56 (c) shows that both solution types benefit from the processing improvements. Systematic errors (e.g., inconsistency of the LEO PCV-pattern) affecting the kinematic positions contributing to AIUB-CHAMP02S, could thus not be reduced by forming position differences.

As mentioned in Sect. 5.3.2 the year 2009 is special — from the CHAMP GPS data processing point of view. As the number of tracking channels of CHAMP's GPS receiver is reduced from 10 to 7 since late 2008, many kinematic positions are determined very unreliably and more data gaps than usual occur. Therefore exceptionally many (about 19%) kinematic positions are lost in the conventional outlier screening (see Sect. 5.3.3). The poor quality of the kinematic positions and the large number of data gaps cause a poor quality of the resulting gravity field solutions in 2009. This is demonstrated by test solutions based on data from the last 70 days of 2009 (see Fig. 6.57).

We recognize that the solution based on kinematic positions is much improved, when more

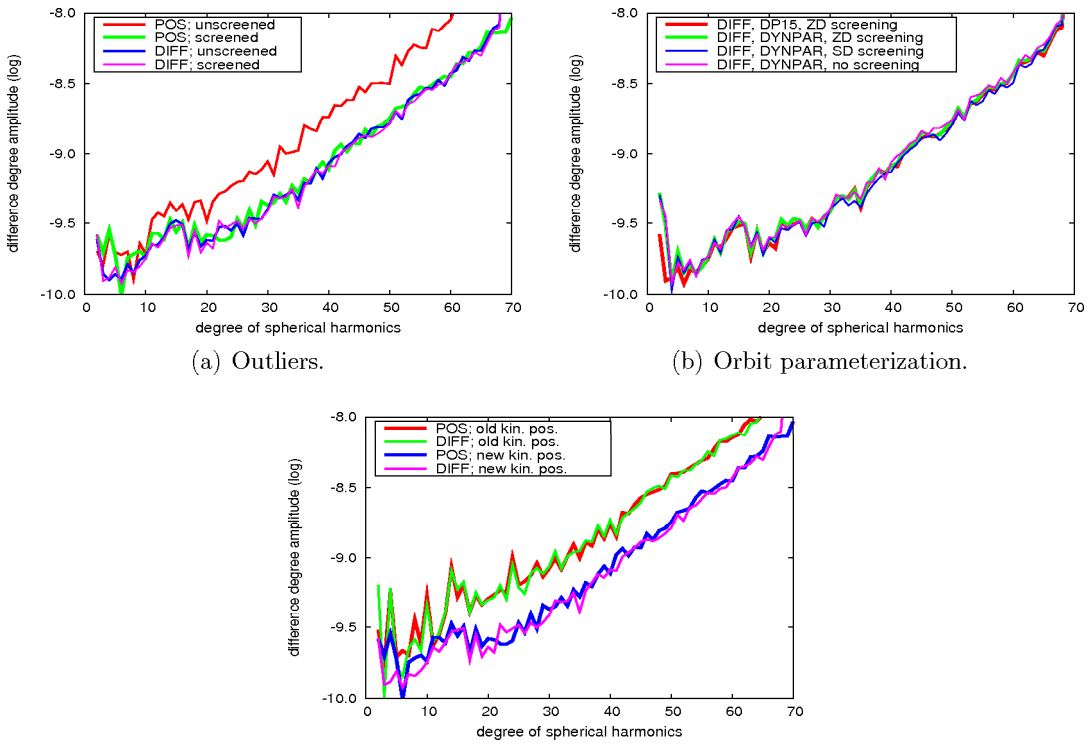

(a) Outliers.

(b) Orbit parameterization.

(c) Impact of systematic errors.

Figure 6.56: Quality of gravity field solutions based on positions and position differences. **Top, left**: Importance of outlier screening when using positions/position differences. **Top, right**: Influence of different orbit parameterizations when using position differences. **Bottom**: Usage of kinematic positions/position differences of AIUB-CHAMP02S ("old") and AIUB-CHAMP03S standards ("new").

pulses are set up (DP05 instead of DP15 setting, see Tab. 6.1). This is related to the poor quality of the kinematic positions and probably also to the lower orbital height in the later years of the CHAMP mission increasing the air drag. Both effects can be better compensated, if more pulses are set up. If the differences of the same kinematic positions are used as pseudo-observations, the solution using the DP15 setting is in general much better than the position-based solution with the DP15 setting and of similar quality as the position-based solution with the DP05 setting. Only the coefficients of the low SH degrees are degraded (as also seen in the example from 2002/2003 in Fig. 6.56 (b)).

Within the mentioned time interval the quality of the kinematic positions is so poor that even the solution based on position differences is significantly degraded, when the orbit parameterization is weakened (DYNPAR setting). In the test interval DOY 70/2002 to 70/2003 this is not the case (compare with Fig. 6.56 (b)).

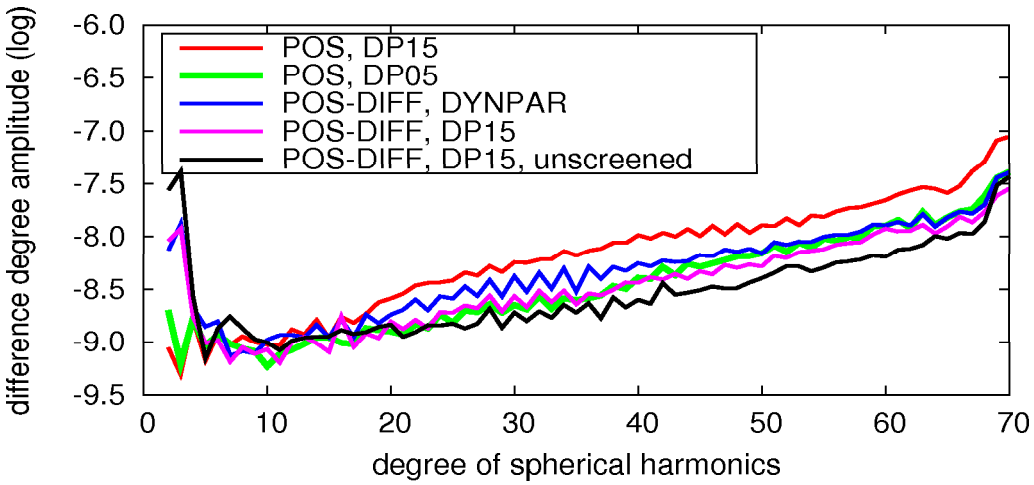

Figure 6.57: Gravity field solutions based on CHAMP kinematic positions and position differences of 70 d in late 2009.

If the position differences are formed from the unscreened kinematic positions (about 19% more pseudo-observations) and the DP15 orbit parameterization is used, the corresponding gravity field solution is significantly better in the higher SH degrees thanks to the larger number of pseudo-observations. The poor quality of the additional pseudo-observations affects mainly the coefficients of the low SH degrees (see Fig. 6.57).

As the gravity field solution using the screened kinematic positions and the DP05 orbit parameterization is good in the low SH degrees and the solution using the differences of the unscreened kinematic positions is superior in the medium and higher part of the SH spectrum, both solutions have their advantages. Therefore, the combination of both solution types on NEQ level, allowing it to retrieve as much information as possible from the kinematic CHAMP positions, is selected as 2009 contribution to AIUB-CHAMP03S. The difference degree amplitudes of the corresponding annual solutions are shown in Fig. 5.19. As the solutions based on (screened) positions and position differences are of comparable quality in "normal" years (see example 2002/2003 in Fig. 6.56 (a),(c)) the annual contributions of 2002–2008 to AIUB-CHAMP03S are generated in the conventional way using the undifferenced kinematic positions.

Results:

- Differences of kinematic LEO positions are suited for gravity field recovery.
- Compared to undifferenced positions the position differences are less sensitive to outliers.
- Problems of the kinematic positions show up mainly in the SH coefficients of low degrees when forming position differences as pseudo-observations.

- In 2009 the solution based on position differences complements the solution using directly the problematic CHAMP positions and increases the yield from the CHAMP data. In years with "normal" data quality the solutions based on (screened) positions and on position differences are of comparable quality (see Fig. 6.56 (a),(c)).

6.3.6 Impact of observations of eclipsing GPS satellites on CHAMP gravity field recovery

Questions:

- Which impact do observations of eclipsing GPS satellites have on gravity field recovery?

The transmission antennas of Block II and Block IIA GPS satellites are not mounted directly in the radial rotation axis (Bar-Sever, 1996). The deflection from the radial axis is about 28 cm. The attitude of these spacecrafts is measured by Sun and Earth sensors and is actively maintained. In the Earth's shadow, the attitude maintenance is hindered by the missing measurements of the Sun sensors. Therefore, the antenna offset may not

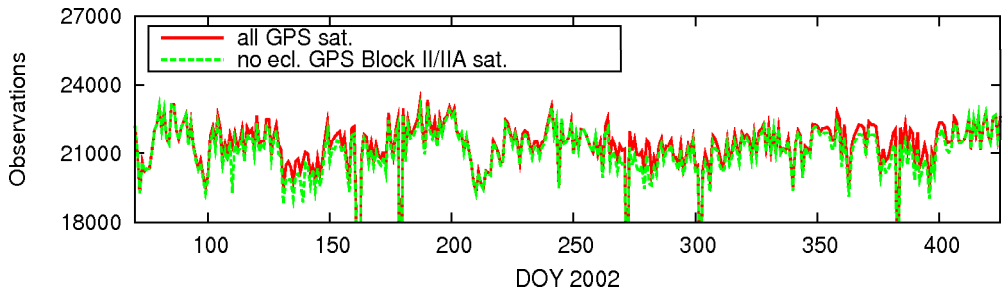

(a) Number of CHAMP GPS observations.

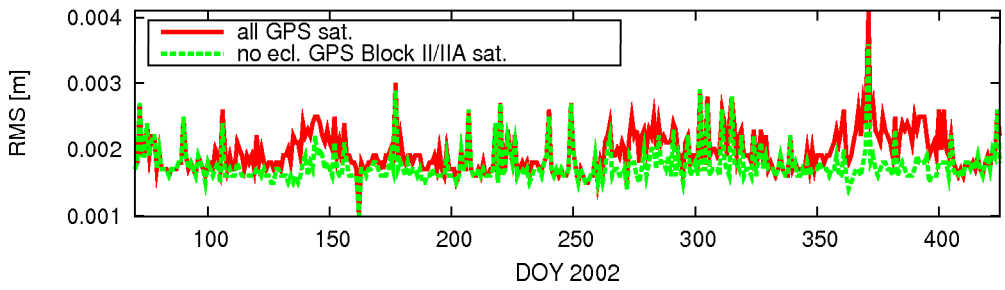

(b) RMS error of kinematic CHAMP positions.

Figure 6.58: Impact of eclipsing Block II and Block IIA GPS satellites on CHAMP kinematic PPP during (DOY 70/2002 to 70/2003). **Top**: Number of GPS observations per day. **Bottom**: RMS error.

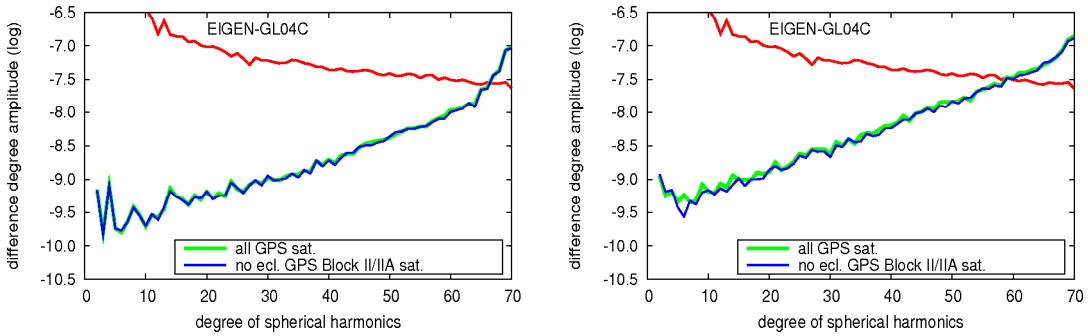

(a) Annual gravity field solution.

(b) Monthly gravity field solution.

Figure 6.59: Impact of eclipsing Block II and Block IIA GPS satellites on CHAMP gravity field recovery. **Left**: Annual gravity field solution (DOY 70/2002 to 70/2003). **Right**: Monthly gravity field solution (DOY 12–39/2003).

be transformed correctly from the spacecraft-fixed into the inertial or into the Earth-fixed reference frame during shadow passes and shortly after. In early 2002 this issue concerned 22 of 28 GPS satellites, in late 2009 still 13 of 32.

The impact of this effect on LEO POD and gravity field recovery is examined by computing one year (DOY 70/2002 to DOY 70/2003) of CHAMP kinematic positions in two ways. In one case the positions are generated in the same way as for AIUB-CHAMP02S. In the second case the GPS observations of Block II and Block IIA satellites during eclipses and up to half an hour afterwards are excluded in the kinematic PPP of CHAMP. Figure 6.58 (a) shows the number of observations, Fig. 6.58 (b) the RMS errors of the kinematic PPP for both versions. Without the observations from eclipsing satellites the number of observations and also the RMS errors are significantly reduced in some periods and remain unchanged in others. The effect therefore contributes to the varying accuracy of the kinematic CHAMP positions observed in Sect. 6.1.8/Fig. 6.25. About 1.2% of GPS observations are excluded during the processed year, resulting in a 0.5% lower number of kinematic positions. A comparison of DOY 90/2002 (not affected) and DOY 16/2003 (affected) shows that Block II/IIA satellites are eclipsing on 397 min and 437 min, respectively (i.e., about 1% of the daily "orbital time" of all GPS satellites on both days). The share of eclipsing Block II/IIA satellites in all CHAMP GPS observations is, however, 0.08% on DOY 90/2002 and 1.9% on DOY 16/2003. This imbalance is related to a combination of the GPS observation geometry as seen from the LEO satellite and the varying alignment of the GPS orbital planes w.r.t. the Sun.

The annual gravity field solution generated from the kinematic positions is not very sensitive to this effect, because the overall number of kinematic positions is not concerned (see Fig. 6.59 (a)). Gravity field solutions based on shorter data time intervals are, however, affected, if many observations stem from eclipsing Block II/IIA satellites within these

time intervals. Figure 6.59 (b) demonstrates this for a monthly solution from early 2003 (DOY 12–39) — a time interval when the PPP is influenced in an exceptionally strong way (see Fig. 6.58). The observations from eclipsing Block II and Block IIA satellites are, therefore, excluded in the AIUB-CHAMP03S processing.

Results:

- The observations of eclipsing Block II and Block IIA satellites have no significant effect on static gravity solutions generated from data of a long time interval (e.g., one year).
- Gravity field solutions based on short data intervals (e.g., one month) are, however, affected. The effect contributes to the varying quality of the monthly contributions to AIUB-CHAMP01S (see Sect. 6.1.8).

6.3.7 Temporal variations of the Earth's gravity field

Question:

- Is it possible to detect temporal variations of the Earths gravity with CHAMP data?

The gravity field of the Earth is variable in time due to loading effects, mass redistributions in the Earth's interior, surface mass redistributions on land, in the atmosphere, in the oceans, or between these constituents (Ilk et al, 2005). Mass redistributions in the Earth's interior (e.g., mantle convection) and loading effects (e.g., isostatic post-glacial rebound) usually generate long-term trends, while mass variations in the hydrological cycle and in the atmosphere are related to annual or seasonal phenomena (e.g., rain and dry seasons, Ilk et al, 2005). Today (in the year 2010), the resulting gravity field changes are routinely retrieved using GRACE data (see, e.g., Ramillien et al, 2004; Velicogna and Wahr, 2005; Steffen et al, 2009). The high precision of the GRACE K-band measurements (see Sect. 2.2.6) allows it to determine accurate monthly gravity field solutions (Tapley et al, 2004). By comparing different monthly solutions, by forming differences between monthly and static solutions, or by fitting the coefficients of the monthly solutions with mathematical models (e.g., Davis et al, 2008), gravity field variations can be monitored.

CHAMP was not designed to detect gravity field variations. Nevertheless, Cheng et al (2003), Reigber et al (2005), Han et al (2005), Sneeuw et al (2005), Moore et al (2006), and others addressed the topic of extracting information about temporal changes of the Earth's gravity field also from CHAMP data. Generally it was concluded that information about temporal variations can only be retrieved for few SH coefficients of very low SH degrees (2–6) without using constraints (Moore et al, 2006). The error level of CHAMP was found to be larger than most time variable gravity field signal (Sneeuw et al, 2005). In addition to the very limited overall accuracy of gravity field models derived from short time series of CHAMP GPS data (see Fig. 6.60), the inhomogeneous quality of the individual monthly CHAMP solutions (see Fig. 6.26) complicates the detection of temporal variations. Even the static eight-year CHAMP-only solution AIUB-CHAMP03S cannot

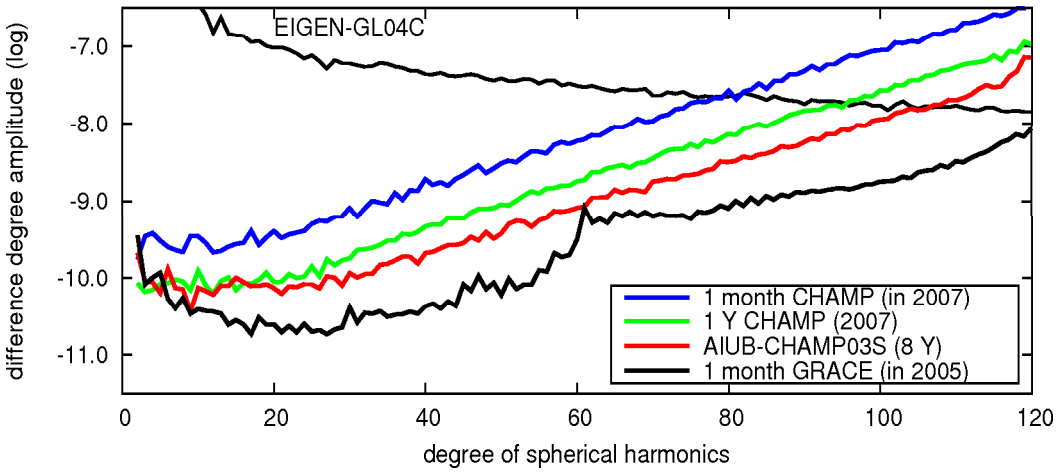

Figure 6.60: Comparison of gravity field solutions based on CHAMP and GRACE data: One of the best monthly CHAMP solutions (October 2007), one of the best annual CHAMP solutions (2007), AIUB-CHAMP03S (from 8 years of CHAMP data), a monthly AIUB-GRACE solution (February 2005).

compete with a monthly AIUB-GRACE K-band solution (Jäggi, 2010) in most SH degrees.

Thanks to the progress made in recent years in the fields of CHAMP data processing (described, e.g., in this work and in Flechtner et al, 2010) and detection of gravity field variations (e.g., Davis et al, 2008) it is worth to examine whether it is now possible to extract time variations using CHAMP solutions. For this purpose a new gravity field recovery is carried out using the kinematic CHAMP positions of the years 2002–2009 and the orbit parameterization from the AIUB-CHAMP03S processing. AIUB-CHAMP03S is introduced as a priori gravity field model. The SH coefficients of the Earth's gravity field are estimated up to SH degree and order 10. The information about the coefficients of degrees 11–120 is taken over from AIUB-CHAMP03S to avoid omission errors to the extent possible. The geoid height differences up to degree 10 between the monthly solutions of May/November 2007 and the annual solution of 2007 are shown in Fig. 6.61 (a–b). The over-estimation of the geoid height differences in the polar and equatorial regions is mainly caused by the coefficients of degree 2. Obviously the geoid height differences are dominated by noise (mean RMS of geoid height differences $\approx 3\,\mathrm{mm}$). Both, the varying accuracy and the — compared to monthly AIUB-GRACE solutions (mean RMS of geoid height differences $\approx 1\,\mathrm{mm}$) — high noise level of the monthly CHAMP solutions contribute to this.

The effect of the inhomogeneous accuracy of the monthly and annual CHAMP solutions (see Sect.6.1.8) can be reduced by combining the solutions belonging to the same month in different years on the NEQ level. This results in 12 stacked (or mean) monthly solutions,

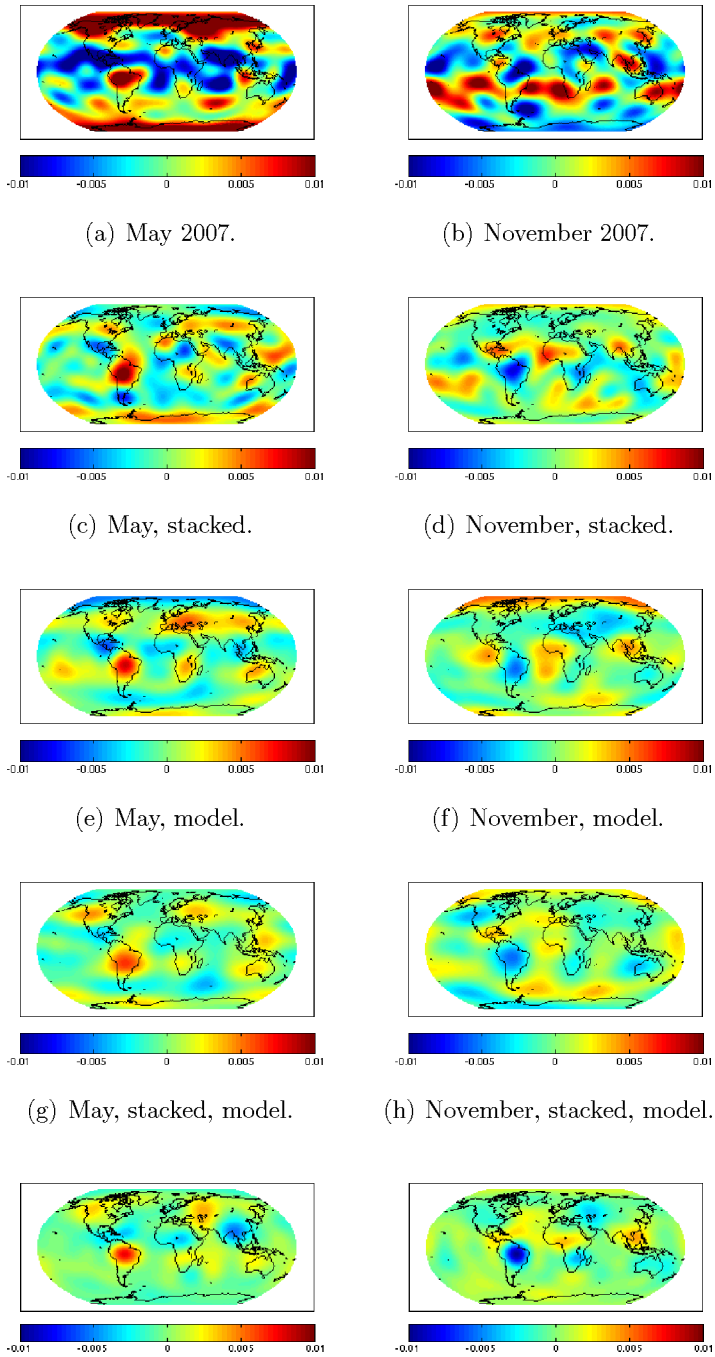

(a) May 2007. (b) November 2007.

(c) May, stacked. (d) November, stacked.

(e) May, model. (f) November, model.

(g) May, stacked, model. (h) November, stacked, model.

(i) May 2007, AIUB-GRACE. (j) Nov. 2007, AIUB-GRACE.

Figure 6.61: Geoid height differences between monthly and mean gravity field solutions ($n_{max} = 10$) in [m]. **a–b**: Monthly solutions from 2007, CHAMP. **c–d**: Stacked monthly solutions (over 8 Y), CHAMP. **e–f**: Model of monthly solutions, CHAMP. **g–h**: Model of stacked monthly solutions, CHAMP. **i–j**: Monthly solutions from 2007, GRACE.

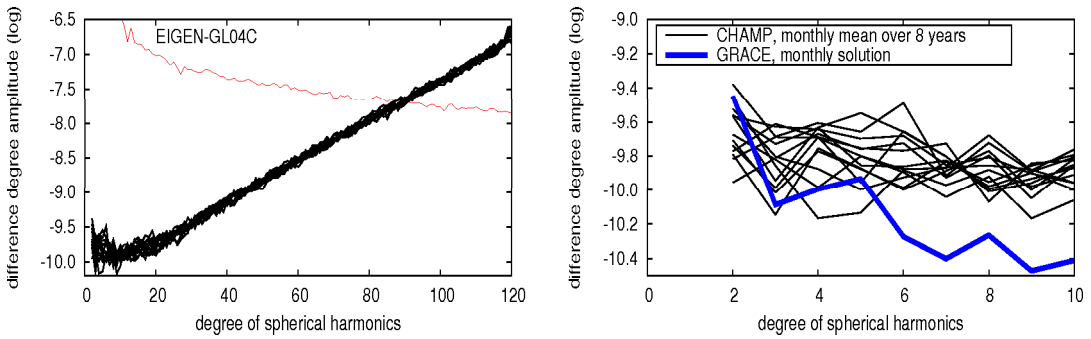

(a) Whole SH spectrum.

(b) Up to SH degree 10.

Figure 6.62: Stacked monthly CHAMP gravity field solutions (2002–2009). **Left**: Whole SH spectrum. **Right**: Up to SH degree 10. A monthly (February 2005) AIUB-GRACE solution is shown for comparison.

e.g., a stacked January solution, a mean February solution and so on. The errors of the mean monthly solutions (that are, in fact, eight-month solutions) are smaller and more homogeneous than those of the monthly solutions (see Fig. 6.62 (a)). The geoid height differences between the stacked monthly solutions and the 8-year solution are computed. The SH coefficients up to degree 10 are taken into account. The consideration of coefficients above SH degree 10 is not beneficial, because even the combined monthly CHAMP solutions are quite inferior to a monthly AIUB-GRACE solution from SH degree 3 on (see Fig. 6.62 (b)). Therefore, the geoid height differences of CHAMP would be dominated by the noise of the higher degree coefficients if they were included. Figure 6.61 (c–d) shows the geoid height differences for the months May and November. Compared to the monthly solutions (see Fig. 6.61 (a–b)) the noise of the geoid height differences is much reduced (mean RMS of geoid height differences ≈ 1.7 mm) and real signals are recognized (e.g., in the Amazon river basin). There is, however, still noise of the same size as the signal.

If the characteristics of the time varying signal are known, the time series may be represented by a mathematical model. In the case of the Earth's gravity field it is known that long-term changes (trend), superimposed by periodical annual and semi-annual variations occur (see, e.g., Ilk et al, 2005). Therefore, it makes sense to describe the time series of each estimated SH coefficient C_{nm} of degree n and order m with six parameters $(C_{nm,0}, \ldots, C_{nm,5})$ of a mathematical model as suggested by Davis et al (2008):

$$\begin{aligned} C_{nm}(t) \;=\; & C_{nm,0} + C_{nm,1} \cdot t + C_{nm,2} \cdot cos\left(\frac{2\pi t}{T_1}\right) + C_{nm,3} \cdot sin\left(\frac{2\pi t}{T_1}\right) \\ & + C_{nm,4} \cdot cos\left(\frac{2\pi t}{T_2}\right) + C_{nm,5} \cdot sin\left(\frac{2\pi t}{T_2}\right) \;, \end{aligned} \tag{6.14}$$

where t is the epoch time, T_1 is one year, and T_2 is half a year (analogous for the S_{nm} coefficients). Model parameter sets are estimated in a least squares adjustment from the

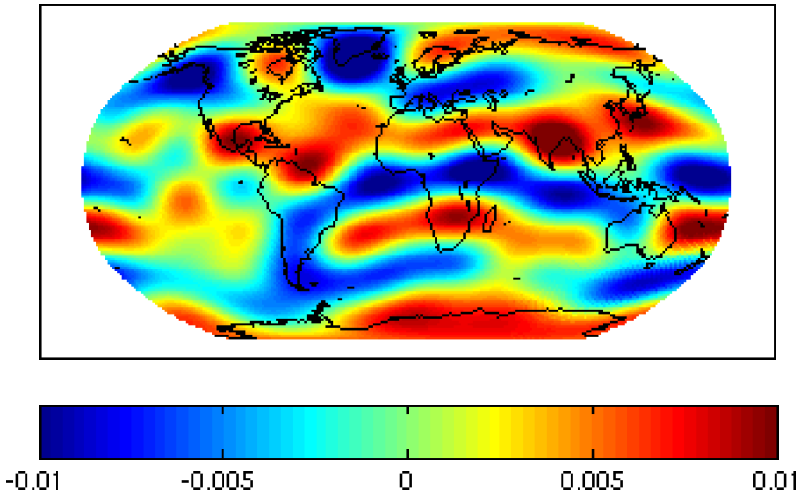

Figure 6.63: Geoid height differences over a 8-year time span according to the trend-parameters derived from monthly CHAMP gravity field solutions ($n_{max} = 10$) in [m].

time series of 96 monthly solutions and from the 12 stacked monthly solutions separately. The significance of each estimated model parameter is checked using a statistical test described by Davis et al (2008). Parameters not passing the test are set to zero. From the model parameters that are considered to be significant, fictitious SH coefficients may be computed for every epoch t using Eq. 6.14. Individual components (e.g., trend, periodical signal with an annual period) of the time variability signal may be separated by applying only the corresponding model parameters when computing the fictitious SH coefficients. The gravity field at a reference epoch t_0 is represented by the bias parameter $C_{nm,0}$. The difference to the gravity field at epoch t_0 is thus obtained by neglecting the bias term.

The long-term geoid change for a time interval of 2920 d (8 years) is computed using only the significant trend parameters $C_{nm,1}$ derived from the 96 monthly solutions. The bias and periodical terms in Eq. (6.14) are neglected. Figure 6.63 shows that the resulting geoid height differences are too noisy (mean RMS $\approx$ 3.6 mm) to recognize a real trend signal. We conclude that the trend signal cannot be detected with CHAMP in the described way.

The periodical geoid height variations are computed using the significant parameters $C_{nm,2}, \ldots, C_{nm,5}$ and neglecting the bias and trend terms in Eq. 6.14. Figure 6.61 (e–f) shows the geoid height differences for mid May/November computed using the parameters derived from the 96 month time series. Compared to Fig. 6.61 (a–b) the noise level is greatly reduced (RMS $\approx$ 1.6 mm) when using the model representation. The model fit,

the significance test, and the removal of the trend have a positive filtering effect. The geoid height differences for mid May/November computed using the periodical model functions derived from the stacked monthly solutions are shown in Fig. 6.61 (g–h). Compared to Fig. 6.61 (c–d) and Fig. 6.61 (e–f) the noise level is further reduced (mean RMS ≈ 1.2 mm). Although the signal amplitudes are reduced, as well, the most prominent signal known from the AIUB-GRACE solutions (Fig. 6.61 (i–j)) of the same months can be identified and distinguished from the noise. The separation of signal and noise is still much clearer in the unfiltered GRACE solutions than in the filtered CHAMP solutions.

Using the periodic model functions derived from the stacked monthly solutions the annual and semi-annual geoid height variations are computed for a full annual cycle (Fig. 6.64). Each picture in Fig. 6.64 represents the deviation from the mean geoid in the middle of the month. The oceans are masked in order to draw the attention to the land regions, relevant for continental water storage variations. The figure shows that CHAMP is to a limited extent sensitive to the largest seasonal geoid height variations that are known from the GRACE data analysis (occurring, e.g., in the Amazon river basin, in central and southern Africa, in Bangladesh) and that the corresponding signal can be retrieved by the applied model. The amount and location of gravity variations can, however, not be determined as precisely as it is possible with GRACE data (compare Fig. 6.64 with the GRACE-results presented, e.g., by Tapley et al, 2004). Weaker signals (e.g., in Europe, Western Asia, North America) are hardly distinguishable from noise and are partly under- or over-estimated in the CHAMP solutions. Moreover, the monthly GRACE solutions can be resolved up to higher SH degrees than 10 (corresponding to a higher spatial resolution), whereas the monthly CHAMP solutions are dominated by noise above degree 10.

In spite of stacking the monthly solutions, a model fit, and statistical significance tests of the model parameters, the noise level of the CHAMP solutions is generally higher than that of GRACE solutions and the detection of gravity field variations is difficult. We could not identify a trend signal in the CHAMP solutions. CHAMP is, however sensitive to the largest seasonal gravity field variations. Without the previous knowledge from GRACE the distinction between signal and noise would, however, be rather difficult. We conclude that a reliable monitoring of temporal variations of the Earth's gravity field with CHAMP alone is not possible. It is, however, remarkable that seasonal gravity field variations can be detected with CHAMP data at all.

Results:

- The detection of temporal gravity field variations from monthly CHAMP solutions is difficult, but not impossible: Seasonal gravity change signal may be retrieved by stacking monthly gravity field solutions (to compute a monthly mean over several years), by fitting the time series by a mathematical model, and filtering out the irrelevant SH coefficients with a statistical significance test according to Davis et al (2008).
- This way the most prominent seasonal signal (e.g., in the Amazon river basin) may be detected with CHAMP with a low resolution (up to SH degree 10).

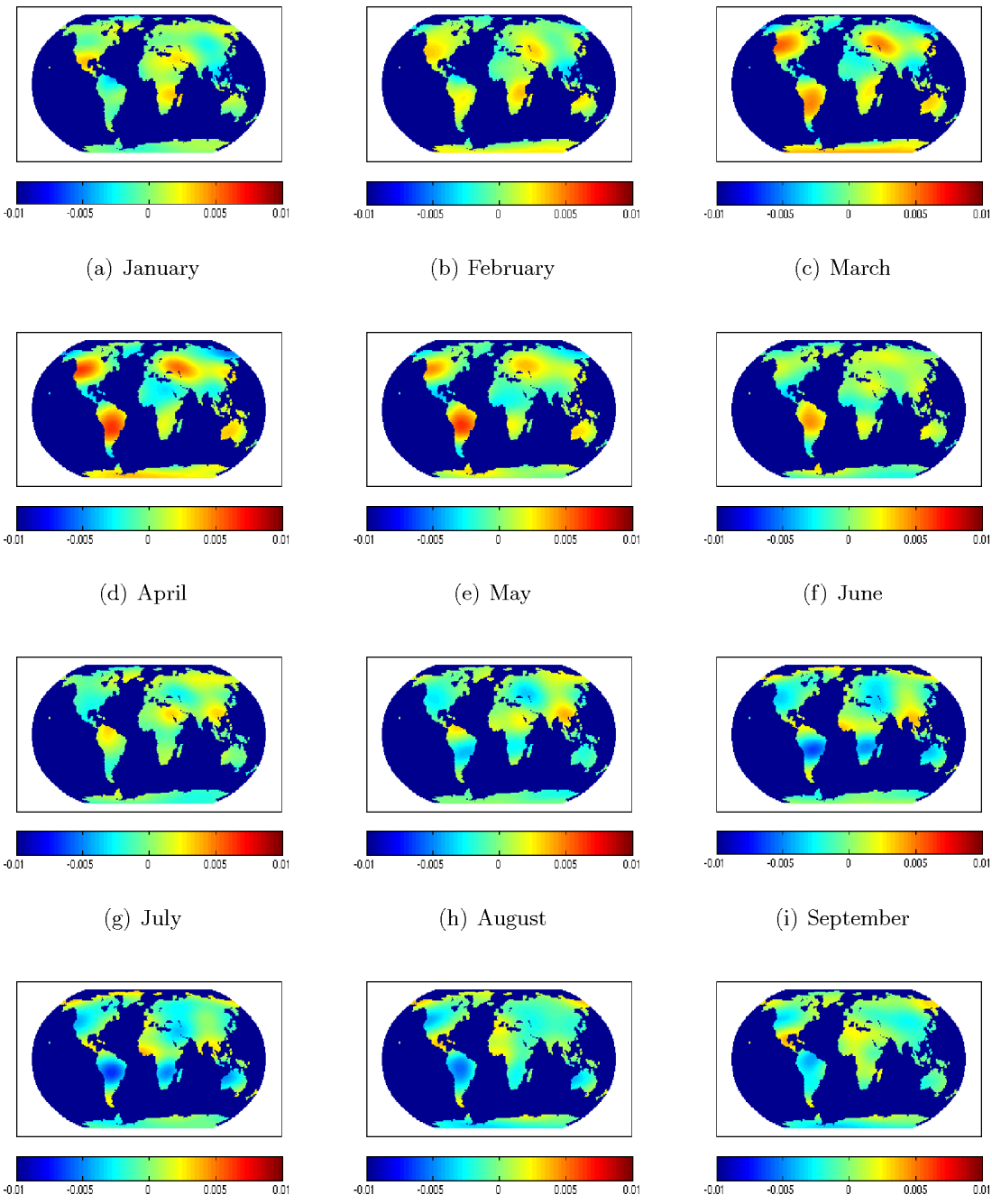

(a) January (b) February (c) March

(d) April (e) May (f) June

(g) July (h) August (i) September

(j) October (k) November (l) December

Figure 6.64: Seasonal geoid height variations in [m], derived from a model of stacked monthly CHAMP solutions up to SH degree 10.

- Seasonal signal of smaller amplitudes (or higher resolutions) and a trend signal could not be retrieved due to the noise still dominating the monthly CHAMP solutions.

6.3.8 Recovery of the low degree harmonics

Goals:

- Assessment of the impact of CHAMP accelerometer data on the recovery of the low degree harmonics in a scenario with reduced omission errors.
- Discussion of problems related to the recovery of the low degree harmonics with CHAMP data.

In Sect. 6.1.9 we summarize that the set up of many pseudo-stochastic orbit parameters is a necessity when generating high-quality CHAMP-only gravity field models with the CMA. We conclude that accelerometer data has no effect in the presence of many pseudo-stochastic parameters and that a too large number of such parameters (spacing shorter than 15 min) may deteriorate the solution in the low SH degrees (over-parameterization).

The CHAMP-only scenario is chosen for AIUB-CHAMP01S, AIUB-CHAMP02S, and AIUB-CHAMP03S in order to exploit the full potential of the CHAMP data for gravity field recovery without tampering the results with a priori information. In this section, however, we want to assess the possible contribution of CHAMP data to a combined gravity field solution. When comparing the formal errors (see Sect. 7.1.1) and the difference degree amplitudes of CHAMP-only and GRACE-only gravity field solutions in Sect. 7.4.1/ Fig. 7.8 it seems likely that CHAMP could only contribute to the lowest SH degrees in such a combined solution. In this case the information about the high degree coefficients is provided by terrestrial data, GRACE K-band data, and/or GOCE gradiometer data. Alternatively this information may be provided by a gravity field model based on these data sources. This way omission errors may be drastically reduced. It makes therefore sense to focus on the coefficients up to degree 20 when examining a possible CHAMP contribution to a combined model. In Sect. 6.3.1–6.3.5 several improvements are introduced as preparation for the AIUB-CHAMP03S processing. One could assume that these improvements and the nearly absence of omission errors reduce the need for setting up large numbers of pseudo-stochastic parameters — reducing possible over-parameterization effects. One could further assume that accelerometer data has a larger impact in such a scenario.

This is checked by the following experiment: The kinematic CHAMP positions, also used for the computation of the 2002 contribution to AIUB-CHAMP03S, are used to generate annual gravity field solutions. The different solutions are based on the DYNPAR, DP15, DP30 (without accelerometer data, see Table 6.1), and D7ACC (including accelerometer data, see Table 6.5) parameter settings. The a priori gravity field model is EGM2008 (Pavlis et al, 2008) up to degree and order 200. The gravity field coefficients up to degree and order 20 are estimated. The high cut-off degree of the a priori gravity field model

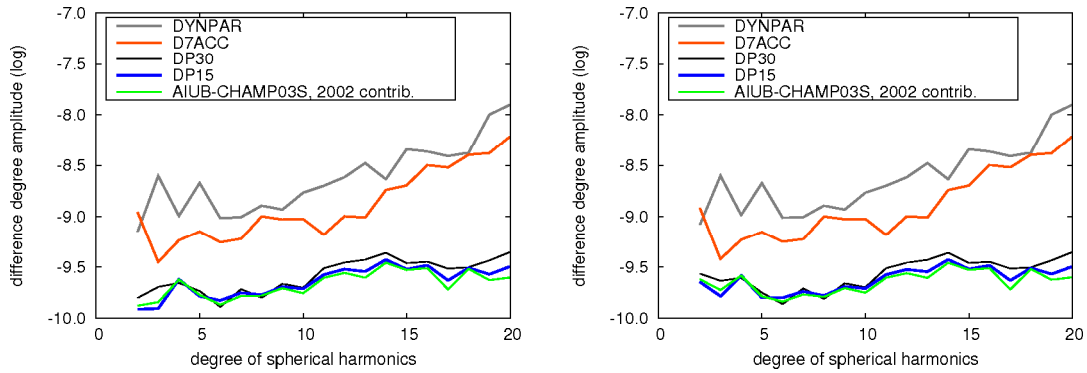

(a) Reference: EIGEN-GL04C. (b) Reference: EGM2008.

Figure 6.65: Difference degree amplitudes of annual (2002) CHAMP solutions with different parameterizations, estimated up to degree 20. **Left**: Reference model: EIGEN-GL04C. **Right**: Reference model: EGM2008.

shall prevent omission errors. Apart from this the same background models and processing standards as in the AIUB-CHAMP03S processing are applied.

Figure 6.65 (a) shows that the solution based on the DYNPAR setting is the worst. The D7ACC solution making use of accelerometer data performs better. The impact of the accelerometer data is therefore larger than in the CHAMP-only scenario (see Sect. 6.1.3/ Fig. 6.14). The best solutions are, however, still the solutions with pseudo-stochastic parameters. The solution with the DP15 parameterization performs as good as the annual contribution to AIUB-CHAMP03S that is included in the figure for reasons of comparison. The slightly poorer performance of the DP30 solution shows that the accuracy of the DP15 solution and the annual contribution to AIUB-CHAMP03S is not limited by over-parameterization effects.

The still poor quality of the D7ACC solution may either indicate the accuracy limit of the CHAMP accelerometer data or the presence of not yet modeled significant error sources other than non-gravitational accelerations and omission errors. The latter explanation is more likely: When applying processing improvements in Sect. 6.3.2 and 6.3.3 the low degree coefficients do not benefit to the same extent as the coefficients of higher degrees. The same can be observed when comparing AIUB-CHAMP03S with its annual contributions (see Sect. 5.3.4 /Fig. 5.22). Moreover a large discrepancy between formal errors and difference degree amplitudes in the low SH degrees of the AIUB-CHAMP solutions is observed in Sect. 6.1.1 /Fig. 6.7 and Sect. 5.3.4 /Fig. 5.20. Errors of the reference gravity field model EIGEN-GL04C can be ruled out as the reason for the discrepancy: The difference degree amplitudes are only slightly different, if EGM2008 is used as reference model (Figure 6.65 (b)). This speaks for the presence of systematic errors in the AIUB-CHAMP solutions that cannot be completely compensated by pseudo-stochastic parameters (similar to the inconsistencies induced by the phase pattern of the LEO POD

antenna discussed in Sect. 6.2). Such errors of small size show up in the low degree harmonics, because these coefficients have the lowest error level in the whole SH spectrum. As similar limitations in the low degree coefficients are also reported for GPS-only solutions based on GRACE (Jäggi et al, 2009a) and GOCE (Jäggi et al, 2010a) data, the errors are not CHAMP-specific. Possible candidates are the inconsistency at degree two observed in the simulation study in Sect. 6.1.4/**Test3** and the phase patterns of the GPS transmitting antennas checked in Sect. 6.2.3. The use of and the comparison with externally generated pseudo-observations might help to identify further error sources. A proper examination of the systematic effects limiting the accuracy of GPS-based gravity field solutions in the lower part of the SH spectrum is therefore required, but must be left to the future.

Results:

- Even in the absence of omission errors, the set up of pseudo-stochastic parameters is necessary for the recovery of the low degree harmonics when using CHAMP GPS data and the CMA.
- Therefore accelerometer data can still not contribute to the solution.
- The gravity field solutions based on LEO GPS measurements generated at the AIUB are degraded by small systematic effects (e.g., antenna phase patterns of the GPS transmitting antennas) in the low SH degrees.

6.3.9 Summary of the experiments related to AIUB-CHAMP03S

Compared to AIUB-CHAMP02S, AIUB-CHAMP03S takes advantage of substantial processing improvements — mainly related to the computation of the kinematic CHAMP positions. The significance of those is provided by Fig. 6.66 on the example of annual solutions based on CHAMP GPS measurements from the year 2002. We recognize that the empirical absolute PCV-pattern of CHAMP's POD antenna generated in Sect. 6.3.1 successfully removes the large inconsistencies in the low SH degrees and other systematic errors affecting the gravity field solutions of the AIUB-CHAMP02S-type. The empirical elevation-dependent weighting function defined in Sect. 6.3.2 additionally considers the stochastic properties of the GPS observations and further improves the gravity field solution — especially in the higher part of the SH spectrum. Both improvements complement each other very well. The use of the full observation sampling rate of CHAMP's GPS receiver improves the medium and higher degree coefficients of the annual contributions from 2003–2009 to AIUB-CHAMP03S (Sect. 6.3.3). In 2002 the used high-rate GPS satellite clock corrections turned out to be of insufficient quality, because the high-rate IGS tracking network, whose data was used to generate the clock corrections, was still in the build-up phase. Therefore, the kinematic positions of the 2002 contribution are sampled with 30 s. The poor quality of the kinematic CHAMP positions of 2009 could be partly compensated by combining the annual 2009 solution based on kinematic positions (acceptable quality in the low SH degrees) with a solution based on position-differences

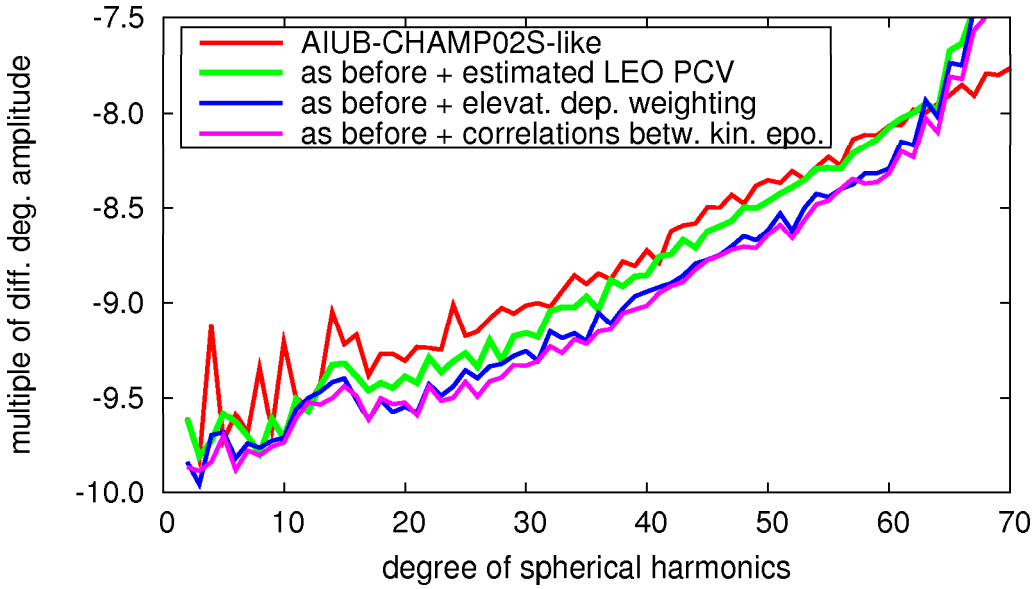

Figure 6.66: Quality improvements of AIUB-CHAMP gravity field determination based on annual solutions. (n_{max}=120 for AIUB-CHAMP02S-like and 70 for all other solutions)

(good quality in the high SH degrees) on the NEQ-level (Sect. 6.3.5). The consideration of inter-epoch correlations when weighting the pseudo-observations (Sect. 6.3.4) in the gravity field recovery and the neglect of observations of eclipsing GPS Block II/IIA satellites in the kinematic positioning (Sect. 6.3.6) improve the static gravity field solution only slightly.

The latter improvement, however, reduces the quality variations between monthly gravity field solutions and therefore contributes to the detection of the largest seasonal variations of the Earth's gravity field with CHAMP data (Sect. 6.3.7). Seasonal signal of small amplitudes and long-term trend signal can, however, not be detected with gravity field models of AIUB-CHAMP03S-quality. The analysis in Sect. 6.3.8 suggests that the gravity field solutions based on hl-SST and generated at the AIUB are limited in accuracy for the low degree harmonics due to systematic errors (caused, e.g., by the phase patterns of the GPS transmitting antennas) that are still not sufficiently modeled. As hl-SST data is supposed to contribute mainly to the SH coefficients of low degrees in a combined solution (including SLR, GRACE, GOCE, and terrestrial data), the examination of these small systematic effects has been identified as an important task for the future.

7 Gravity field validation

The quality of a model is assessed in a validation process. Different validation methods for gravity field models are introduced in the first section of this chapter. In the subsequent sections the results of the internal and external validation of the CHAMP-only gravity field models AIUB-CHAMP01S, AIUB-CHAMP02S, and AIUB-CHAMP03S are presented. The external validation was carried out by Thomas Gruber from the Institute for Astronomical and Physical Geodesy (IAPG) of the Technische Universität München following the procedures described in Gruber (2004).

7.1 Validation methods

With CHAMP and GRACE the accuracy of global gravity field models has improved to an extent that the validation of these models in an objective way has become rather difficult. The formal errors of the SH coefficients resulting from the least squares adjustment are often too optimistic for a reliable quality assessment. Because the truth is unknown, the models need to be directly or indirectly compared to other models or measurements. The reference data sets must at least have a comparable or better accuracy than the assessed model. Otherwise the errors of these data sets overlay the error of the gravity field to be validated.

7.1.1 Formal errors

The formal errors of the estimated gravity field parameters provide information about the internal accuracy achieved with a certain gravity field determination method using observations of a certain type. They indicate in a relative sense, which parameters are well determined and for which parameters a method is less sensitive. The external errors of the estimated parameters might be larger.

Formal errors may be displayed in different kinds. Triangular plots like those in Fig. 7.1 show the formal errors of all individual SH coefficients. This kind of representation is well suited to visualize, which part of the SH spectrum is best determined with a certain gravity field determination method. Figure 7.1 (a) shows the formal errors of GRIM5-S1 (Biancale et al, 2000). GRIM5-S1 is one of the last satellite-only gravity field models of the pre-CHAMP era, based on relatively sparsely distributed SLR and Doppler measurements of some tens of satellites and on the numerical integration of long orbit arcs. Figure 7.1 (a) illustrates that the classical gravity field recovery methods are most sensitive to the SH coefficients of the low degrees (due to the high orbits of most contributing

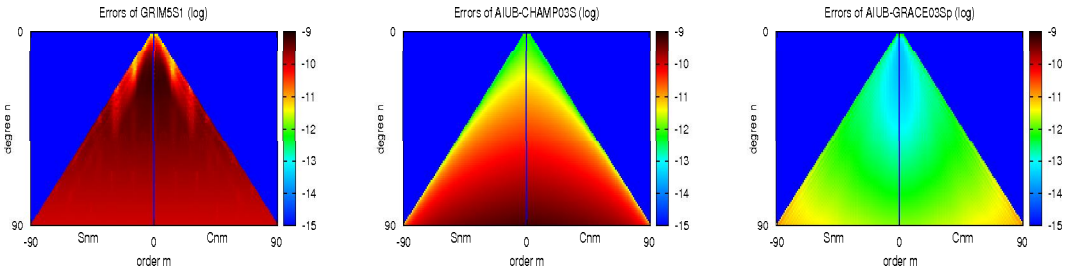

(a) GRIM5-S1. (b) AIUB-CHAMP03S. (c) AIUB-GRACE03Sp.

Figure 7.1: Formal errors of the coefficients of different types of gravity field models.

satellites). In higher degrees these methods are only sensitive to coefficients of certain orders due to orbit resonance effects. Coefficients of low order are not well determined (except in the lowest degrees) due to inclinations of $i << 90°$ for most contributing satellites. The error level does not much increase in the high SH degrees, because the SH coefficients are constrained according to Kaula's degree variance model (Kaula, 1966).

Figure 7.1 (b) shows the formal errors of AIUB-CHAMP03S. The high inclination of the CHAMP orbit and the dense global coverage with GPS measurements result in a more homogeneous error behavior. The error level steadily increases in the higher SH degrees, because the SH coefficients are not constrained. CHAMP-only models based on the CMA are more sensitive to the sectoral coefficients than to the coefficients of the lower orders.

Figure 7.1 (c) shows the formal errors of AIUB-GRACE03Sp (Jäggi, 2010). Like CHAMP, GRACE benefits from a near-polar orbit and a dense measurement coverage. The error behavior is in most degrees dominated by the highly accurate K-band measurements in along-track (i.e., North-South) direction. With the K-band observations the zonal coefficients are determined better than the sectoral coefficients and the general error level is much lower than for SLR- and GPS-based models.

Formal errors may also be visualized by error degree variances Eq. (3.33). They do not show the error of individual coefficients but represent the accumulated error of all coefficients of the same SH degree. This representation is well suited to compare the formal errors of different gravity field models. The error degree variances of GRIM5-S1, AIUB-CHAMP01S, AIUB-CHAMP02S, AIUB-CHAMP03S, and AIUB-GRACE03Sp are compared in Fig. 7.2. The figure shows that AIUB-CHAMP01S is theoretically more sensitive than GRIM5-S1 in most parts of the SH spectrum. In the lowest SH degrees both models are at a similar level. The error degree variance of GRIM5-S1 does not increase for degrees $n >> 20$ due to the applied constraints. The larger amount of data contributing to AIUB-CHAMP02S and AIUB-CHAMP03S and the processing improvements (e.g., the consideration of inter-epoch correlations) of AIUB-CHAMP03S further reduced the formal errors of these CHAMP-only solutions in the whole SH spectrum.

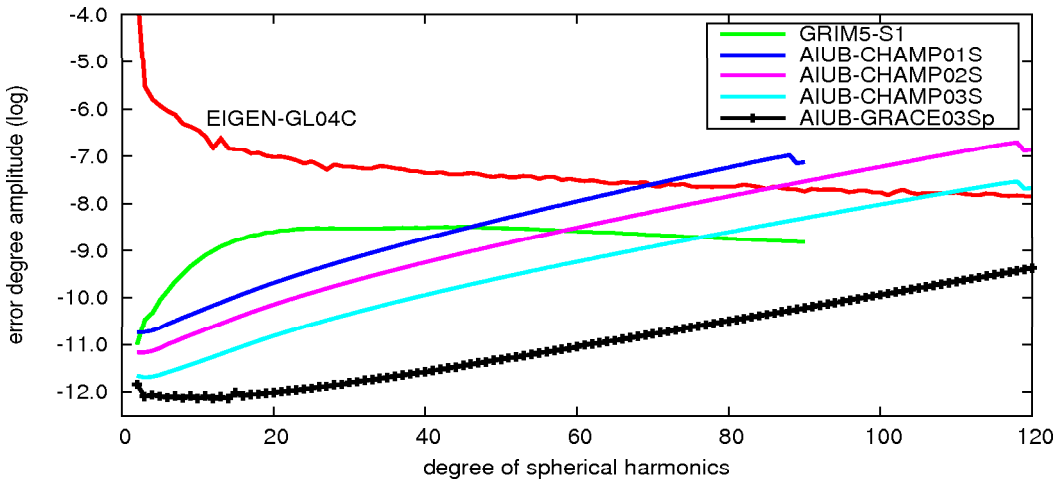

Figure 7.2: Error degree variances of different gravity field models.

The errors of the AIUB-CHAMP solutions are, however, much bigger than the formal errors of the GRACE solution AIUB-GRACE03Sp. This solution is mainly determined by the highly accurate K-band measurements as the GPS contribution is heavily down-weighted (see Jäggi (2010) for details). Only in the lowest part of the SH spectrum (below degree 4) the formal errors of AIUB-CHAMP03S and AIUB-GRACE03Sp are of comparable size. Note, that the inconsistency of AIUB-CHAMP02S caused by the PCV pattern (see Sect. 6.2.2) can not be noticed in the formal errors.

7.1.2 Comparison with other gravity field models

An objective, simple, and direct way of gravity field validation is the comparison with other gravity field models. The reliability of this validation method depends on the accuracy of the reference model, which may vary in different parts of the SH spectrum. In the ideal case more accurate models do exist and can be considered as "true". When the work on the AIUB-CHAMP gravity field models started this was the case, because very accurate models, based on GRACE data, were already available. One of these models, EIGEN-GL04C (Förste et al, 2008), is used as standard reference throughout this work. Models like EIGEN-GL04C are considered to be superior to CHAMP-only models, because the low degree harmonics (up to degrees ≈ 8) are well determined by SLR measurements, the medium degree harmonics (up to degrees ≈ 150) are determined by very precise GRACE K-band measurements, and the higher degree harmonics are determined by radar altimetry data and ground measurements, which are sensitive to the small-scale structures of the gravity field. Due to the contribution of satellite data, the comparison with such combined gravity field models cannot be considered to be fully independent.

Corresponding SH coefficients of different gravity field models may be directly compared.

This is, e.g., done in Fig. 6.34 (b) in order to identify individual SH coefficients that are especially affected by an inconsistency. The direct comparison is, however, not very practical for comparing more than two models.

Difference degree amplitudes Eq. (3.32) show the accumulated differences per degree between the coefficients of different gravity field models. This way the differences of several gravity field models to a common reference model may be compared in a simple and compact way. The contribution of individual coefficients may be examined indirectly, e.g., by neglecting these coefficients in the computation of the differences (see, e.g., Fig. 6.34 (a)). Difference degree amplitudes are used as the main validation method throughout this work.

SH coefficients of a gravity field model allow it to compute functionals, such as geoid heights or gravity anomalies using Eqs. (3.34) and (3.35) for each point on the Earth's surface. Geoid heights or gravity anomalies derived from different gravity field models may then be compared. Often the geoid heights or gravity anomalies of both models are computed for a grid of points. The differences may be visualized as it is done in Fig. 6.34 (c) and the RMS value of the differences might be computed. The contributions of individual coefficients may be examined indirectly by including or excluding them from the computation of the geoid heights or gravity anomalies. Geoid height and gravity anomaly differences are used for the internal validation of the AIUB-CHAMP models.

7.1.3 Comparison with ground data

Geoid heights derived from the SH coefficients of a gravity field model may be compared to geoid heights derived from GPS-leveling. Model-derived gravity anomalies may be compared to gravity anomalies measured by gravimeters. Satellite-only gravity field models may thus be validated using independent data sources. There are, however, also disadvantages (Gruber, 2004): Ground measurements may contain long wavelength errors due to the error propagation of the terrestrial measurement techniques and the connection to a national height datum. The ground data uncertainty is not always exactly known. Ground data represent the whole SH spectrum and must be low-pass filtered to the maximum SH degree of the gravity field model to be validated. The filter process is an additional error source.

Ground-measured and model-derived geoid heights may also be compared indirectly: Between all points of a ground data set the geoid height differences or geoid slopes can be computed and compared to the corresponding slopes derived from the gravity field model as a function of their distance (Gruber, 2004). This allows a wavelength-dependent validation of the gravity field model. Forming differences may also eliminate spatially correlated errors.

The AIUB-CHAMP gravity field models are compared to ground data in the external validation step.

7.1.4 Altimetry data

Gravity field models may be validated by comparing geometrically and oceanographically derived dynamic sea surface topographies. The dynamic sea surface topography may be computed geometrically by subtracting the geoid height computed from the SH coefficients of a gravity field model from the mean sea surface height measured by radar altimetry (see also Sect. 2.2.4). The oceanographically derived dynamic sea surface topography is given by oceanographic models. The accuracy of this validation method depends on different error sources (Gruber, 2004): The altimetry data is affected by systematic errors and corrections. It represents the whole SH spectrum and must be low-pass filtered to the maximum SH degree of the gravity field model. The oceanographic models have errors and are usually generated or improved using geoid information. Therefore, this validation method is not independent. The method is used for the external validation of AIUB-CHAMP01S.

7.1.5 Orbit determination

Satellite orbits depend on the Earth's gravity field. Therefore, the residuals of a dynamic or reduced-dynamic orbit determination could in principle be useful for gravity field validation.

The validation of high-precision gravity field models using LEO orbits is difficult, because non-gravitational forces, model errors, omission errors, and measurement errors overlay the error of the gravity field model to be validated. If many orbit parameters are set up in order to absorb unmodeled or insufficiently modeled perturbations, they also absorb gravity field errors (see Sect. 6.1.4/**Test1**). The use of gravity field models of different quality in the LEO POD therefore usually only results in slightly different observation residuals (Gruber, 2004). This is at least true for CHAMP and GRACE models. Therefore we abandon the presentation of corresponding results here.

The GOCE satellite is an exception, because it is able to operate in the so-called drag-free mode (see Sect. 2.2.7). This and the low orbital height increase the impact of the gravity field model in the orbit determination. Due to GOCE's sensitivity to the high SH degrees the gravity field models to be validated must have a high cut-off degree (e.g., GRACE models) in order to avoid omission errors. This excludes CHAMP-only models.

Satellites with high orbits are not affected by atmospheric drag. For geodetic SLR satellites such as LAGEOS or ETALON the radiation pressure might, in addition, be modeled realistically. Due to the signal attenuation their orbits are not very sensitive to the errors of higher degree SH coefficients. This is an advantage if exclusively the quality of the low degree SH coefficients of a gravity field model should be assessed. The validation by dynamic orbit determination of SLR and GNSS satellites was not accomplished within the scope of this work but is recommended for assessing the quality of the AIUB-CHAMP and other gravity field solutions in the low (< 20) SH degrees.

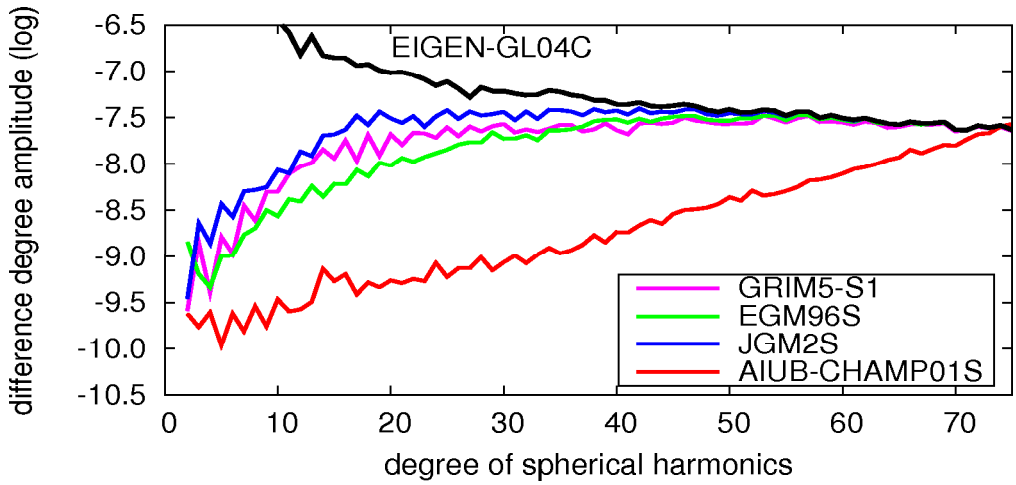

Figure 7.3: Difference degree variances w.r.t. EIGEN-GL04C of pre-CHAMP gravity field models and AIUB-CHAMP01S.

7.2 Validation of AIUB-CHAMP01S

AIUB-CHAMP01S is compared to the best satellite-only global gravity field models of the pre-CHAMP era and to external CHAMP-only solutions.

7.2.1 Internal validation

The comparison of the difference degree amplitudes w.r.t. EIGEN-GL04C of AIUB-CHAMP01S and some of the best pre-CHAMP satellite-only gravity field models (GRIM5-S1, EGM96S (Lemoine et al, 1998), JGM2S (Nerem et al, 1994)) is provided in Fig. 7.3. It confirms the results of the analysis of the formal errors (see Fig. 7.2). Except for the very low SH degrees, AIUB-CHAMP01S, based on only one year of CHAMP data, is much better than the pre-CHAMP models based on several years of measurements to tens of satellites. Like the error degree amplitudes, the difference degree amplitudes of these models do not increase much from about degree 20 on because the coefficients of the pre-CHAMP models were constrained according to Kaula's 'rule of thumb'. The difference between AIUB-CHAMP01S and EIGEN-GL04C increases steadily for higher degrees until it exceeds the signal at about degree 74 — indicating the "detectability" limit of AIUB-CHAMP01S.

AIUB-CHAMP01S was also compared to external CHAMP-only models based on alternative approaches. ITG-CHAMP01S (Mayer-Gürr et al, 2005) was the most interesting solution, because it was one of the best CHAMP-only models of the time (2007), it is based on a similar approach (short arc approach) as the CMA, it is not affected by regularizations, and it used the same CHAMP GPS data set. Figure 7.4 shows that AIUB-CHAMP01S and ITG-CHAMP01S are comparable in quality. ITG-CHAMP01S is slightly

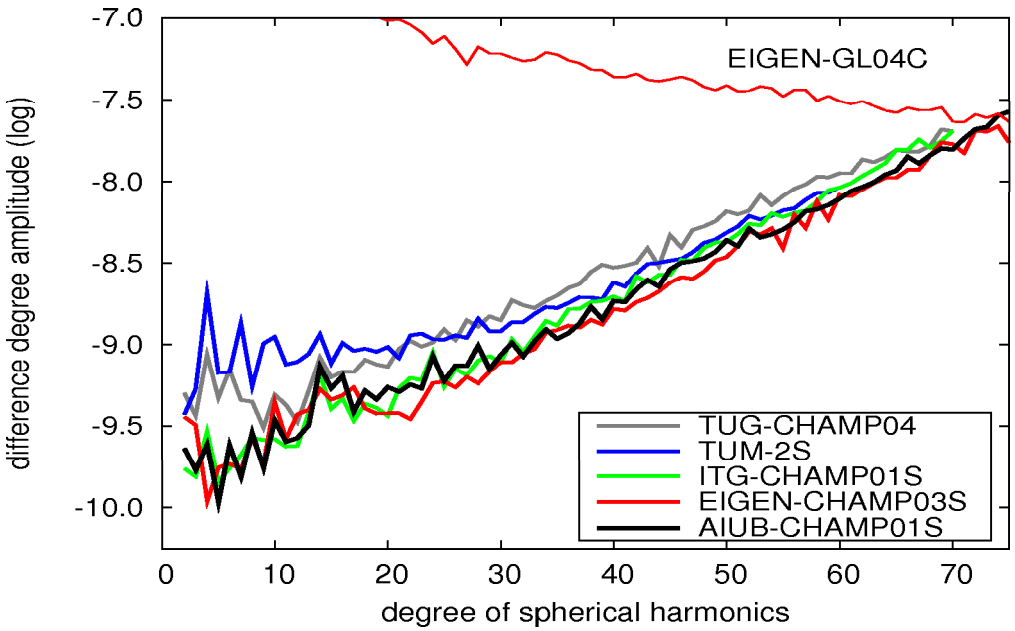

Figure 7.4: Difference degree variances w.r.t. EIGEN-GL04C of different CHAMP-only gravity field models.

better in the lower SH degrees, while AIUB-CHAMP01S is better in the higher SH degrees. EIGEN-CHAMP03S (Reigber et al, 2005) is based on a very similar approach and 2.5 years of CHAMP GPS data. It was considered as the best CHAMP-only gravity field model of that time (2007). Figure 7.4 shows that EIGEN-CHAMP03S is slightly superior to AIUB-CHAMP01S. TUM-2S (Wermuth et al, 2004), a two year CHAMP solution, was generated using the energy balance method. Despite the larger data set the model cannot compete with the other mentioned models — in particular in the low SH degrees. Another gravity field solution based on the energy integral approach is TUG-CHAMP04 (Badura et al, 2006). Although it uses the same one year data set as AIUB-CHAMP01S it is not comparable in quality. The generally poorer quality of the solutions based on the energy balance approach is explained by Ditmar and van Eck van der Sluijs (2004): The energy balance approach is only sensitive to the along-track force component, while the information about the radial and cross-track components does not contribute to the gravity field solution. DEOS_CHAMP-02S_70 (Liu, 2008) is based on the same data set as AIUB-CHAMP01S, but uses the acceleration approach. The external comparison of both models by Liu (2008) indicates that the models are coequal.

From the SH coefficients of different gravity field models (AIUB-CHAMP01S, GRIM5-S1, ITG-CHAMP01S, EIGEN-CHAMP03S) geoid heights and gravity anomalies were computed on a $1° \times 1°$ grid. Geoid height and gravity anomaly differences to the superior reference gravity field model EIGEN-GL04C were computed (including a latitude

dependent weighting) for different spectral ranges of the SH series. The maximum and minimum geoid height differences, the mean RMS of the geoid height differences, and the mean RMS of the gravity anomaly differences are provided in Tab. 7.1. If the coefficients of the SH degrees up to 30 are considered, ITG-CHAMP01S is slightly better than AIUB-CHAMP01S — indicating a slightly better agreement with the reference model in the long wavelength part of the SH spectrum. If the coefficients of higher SH degrees (up to 50 or 70) are considered, as well, AIUB-CHAMP01S is better. EIGEN-CHAMP03S is superior in the whole SH spectrum due to its larger data basis. The pre-CHAMP model GRIM5-S1 is clearly inferior to all CHAMP-only solutions.

Table 7.1: Comparison of AIUB-CHAMP01S and selected gravity field models with EIGEN-GL04C on a latitude-weighted $1° \times 1°$ grid.

Difference between EIGEN-GL04C and	Type of comparison		SH degree and order 0-30	0-50	0-70
GRIM5-S1	undulation [cm]:	RMS	59.8	98.3	130.6
		max.	266.0	573.1	1010.2
		min.	-258.0	-661.9	-838.5
	anomaly [mGal]:	RMS	2.09	5.30	9.44
ITG-CHAMP01S	undulation [cm]:	RMS	1.8	7.8	37.5
		max.	6.7	31.2	153.9
		min.	-6.2	-31.1	-161.2
	anomaly [mGal]:	RMS	0.06	0.53	3.65
AIUB-CHAMP01S	undulation [cm]:	RMS	2.0	7.4	31.5
		max.	7.7	30.5	137.6
		min.	-7.6	-32.9	-127.3
	anomaly [mGal]:	RMS	0.07	0.50	3.05
EIGEN-CHAMP03S	undulation [cm]:	RMS	1.6	5.4	25.3
		max.	6.4	23.1	141.0
		min.	-5.1	-19.5	-161.6
	anomaly [mGal]:	RMS	0.04	0.36	2.46

The internal validation once more confirms the early finding of (Reigber et al, 2002) that CHAMP GPS measurements greatly improved the determination of global gravity field models using satellite orbits (see Fig. 7.2 and Fig.7.3). The best pre-CHAMP satellite-only models can only compete with CHAMP-based models in the lowest SH degrees. Figure 7.4 and Tab. 7.1 indicate that AIUB-CHAMP01S is comparable in quality with the best other CHAMP-only gravity field models known in 2007. The CMA thus can compete with all alternative approaches for gravity field recovery based on CHAMP GPS measurements. It shows its strengths especially in the recovery of the higher degree coefficients — thanks to the strength and flexibility of the pseudo-stochastic orbit parameters.

7.2.2 External validation

AIUB-CHAMP01S was validated by Thomas Gruber using procedures described in detail in Gruber (2004).

Geoid heights derived from different gravity field models up to SH degree 60 were compared to different terrestrial geoid height data sets (based on GPS leveling). The mean RMS values of the geoid height differences are shown in Tab. 7.2. Apart from the CHAMP-only gravity field models AIUB-CHAMP01S, TUM-2S, and ITG-CHAMP01S the models GRIM5-C1 (Gruber et al, 2000) and ITG-GRACE02S (Mayer-Gürr et al, 2006) were included in the comparison. GRIM5-C1 is one of the last combined (satellite tracking data, altimetry data, terrestrial data) gravity field models of the pre-CHAMP era. ITG-GRACE02S — a solution based on GRACE GPS and K-band observations is superior in quality to all other models considered. As GRIM5-C1 and ITG-GRACE02S are included Tab. 7.2 does not only show the quality of the gravity field models, but also provides information about the quality of the ground data sets. An RMS value of comparable size for all gravity field models indicates a poor accuracy of the corresponding ground data set. This is, e.g., the case for the USA data set. Larger variations of the RMS values for different types of gravity field models indicate a high accuracy of the terrestrial data set. This is, e.g., the case for the German data sets.

Table 7.2: Mean RMS of geoid height differences in cm between terrestrial measurements and gravity field models (including AIUB-CHAMP01S) up to SH degree 60.

Height data set	No. of points	GRIM5-C1	TUM-2S	**AIUB-CHAMP01S**	ITG-CHAMP01S	ITG-GRACE02S
EUREF GPS	180	37.3	28.0	24.5	25.9	23.1
Germany EUVN	87	24.8	13.7	11.9	13.6	3.2
Germany GPS	675	27.9	13.6	12.1	13.5	3.5
Canada GPS 1998	1443	28.9	26.3	24.8	24.2	19.8
Canada GPS 2007	430	22.8	24.4	20.4	21.4	14.7
Australia GPS	197	29.6	30.7	28.4	31.0	24.1
Japan GPS	837	28.8	16.3	18.5	17.9	11.6
USA GPS	5168	37.5	37.9	35.1	37.5	33.3

As expected there are three accuracy levels: The pre-CHAMP model GRIM5-C1 shows

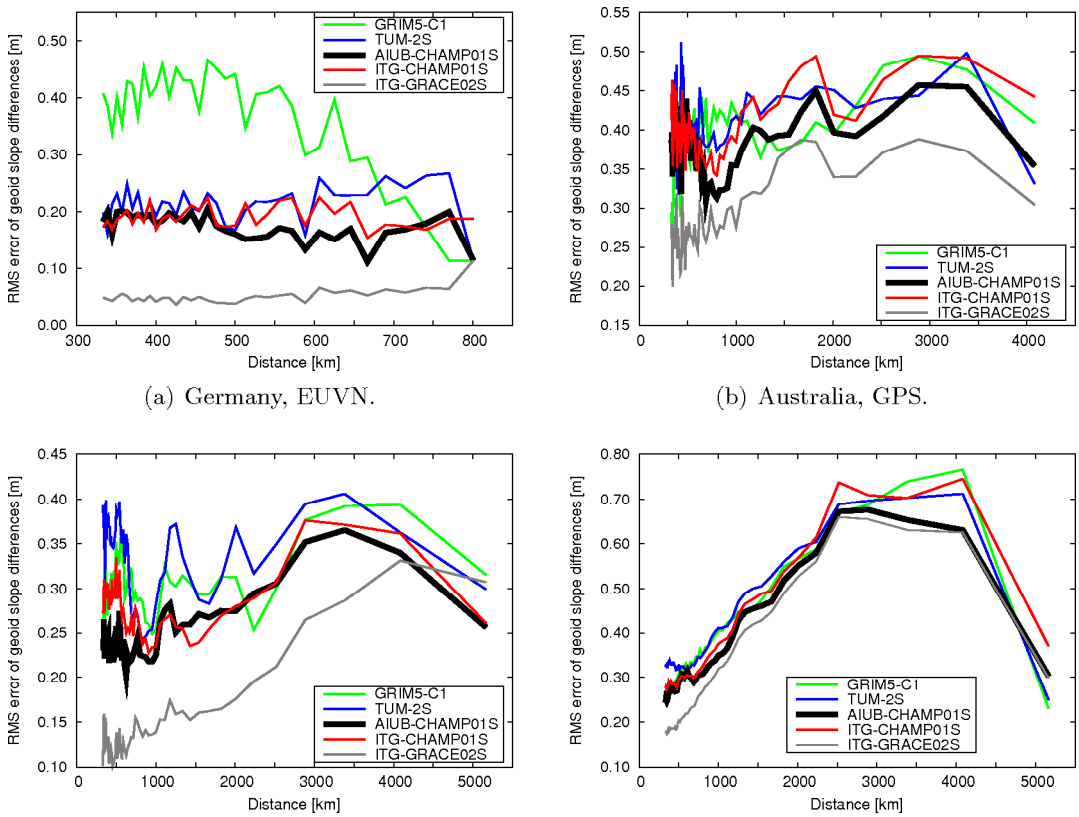

(a) Germany, EUVN.

(b) Australia, GPS.

(c) Canada 2007, GPS.

(d) USA, GPS.

Figure 7.5: Geoid slope differences between terrestrial height data sets and global gravity field models up to SH degree 60.

the largest RMS values, the CHAMP-only gravity field models are on a medium level, and the GRACE model is clearly the best. Among the three CHAMP-only models (AIUB-CHAMP01S, ITG-CHAMP01S, TUM-2S) AIUB-CHAMP01S usually performs very well.

In addition to the geoid heights, geoid slopes derived from the terrestrial data sets and the gravity field models were compared. Figure 7.5 shows the geoid slope differences for a subset of ground data sets. The poor accuracy of the USA data set is also visible in the geoid slope differences (Fig. 7.5 (d)). Other data sets allow a clear distinction between the superior GRACE model, the CHAMP models, and GRIM5-C1. AIUB-CHAMP01S and ITG-CHAMP01S are in general on a comparable level.

Using the procedures described in Gruber (2004) the sea surface topography of the Northern Atlantic Ocean was computed with AIUB-CHAMP01S. Like in the case of other CHAMP-only models the resulting sea surface topography map showed nearly no oceanographic features: According to Gruber (2004) the size of sea surface topography features

is beyond the sensitivity limit of CHAMP.

The external validation of AIUB-CHAMP01S confirms the findings of the internal validation. Independently derived geoid heights show that AIUB-CHAMP01S and comparable CHAMP-based gravity field models are standing in quality between the best gravity field models of the pre-CHAMP era and GRACE-based gravity field models. The limitations of CHAMP-based (or GPS based) gravity field models became obvious, when the attempt was made to derive sea surface topography information from it. The accuracy of AIUB-CHAMP01S is comparable to that of other CHAMP-only gravity field solutions — in particular those based on the short-arc method and the acceleration method. The CMA therefore proved to be suitable for gravity field recovery using LEO GPS measurements.

7.3 Validation of AIUB-CHAMP02S

The six year CHAMP-only gravity field solution AIUB-CHAMP02S was compared to its predecessor AIUB-CHAMP01S, to the best known CHAMP-only gravity field model of that time (2008) EIGEN-CHAMP03S, and to GRACE-only gravity field models. Apart from the overall quality of AIUB-CHAMP02S the influence of GNSS model changes (see Sect. 5.2.1) on gravity field recovery using CHAMP GPS data was of interest.

7.3.1 Internal validation

The difference degree amplitudes of the CHAMP-only gravity field models AIUB-CHAMP01S, AIUB-CHAMP02S, and EIGEN-CHAMP03S w.r.t. EIGEN-GL04C are shown in Fig. 7.6. AIUB-CHAMP02S is much better than AIUB-CHAMP01S and better than EIGEN-CHAMP03S. In the lower even degrees (up to 30) the peaks caused by the inconsistent CHAMP POD antenna PCV-pattern are visible for AIUB-CHAMP02S (see also Sect. 6.2.2 and Sect. 6.3.1). The PCV-model change is one of the GNSS model changes.

Geoid heights and gravity anomalies were computed for a $1° \times 1°$ grid from the SH coefficients of the above mentioned CHAMP models and the reference model. The annual solution AIUB-CHAMP02Sp1y (see Sect. 6.2.1) based on the reprocessed GPS orbit and clock products and on CHAMP GPS measurements of the period DOY 70/2002 to 70/2003 (the same as used for AIUB-CHAMP01S) was included to study the effect of the GNSS model changes on gravity field recovery.

Table 7.3 contains the mean RMS values of geoid height and gravity anomaly differences between the CHAMP-only models and the reference model for different spectral ranges. The comparison of the reprocessed annual solution AIUB-CHAMP02Sp1y with AIUB-CHAMP01S shows minor improvements in the higher SH degrees and a slight degradation in the lower degrees due to the GNSS model changes. This observation agrees with the comparison of the difference degree amplitudes of both annual solutions (see Fig. 6.33).

Figure 7.6 and Tab. 7.3 indicate that the multi-annual solution AIUB-CHAMP02S is the

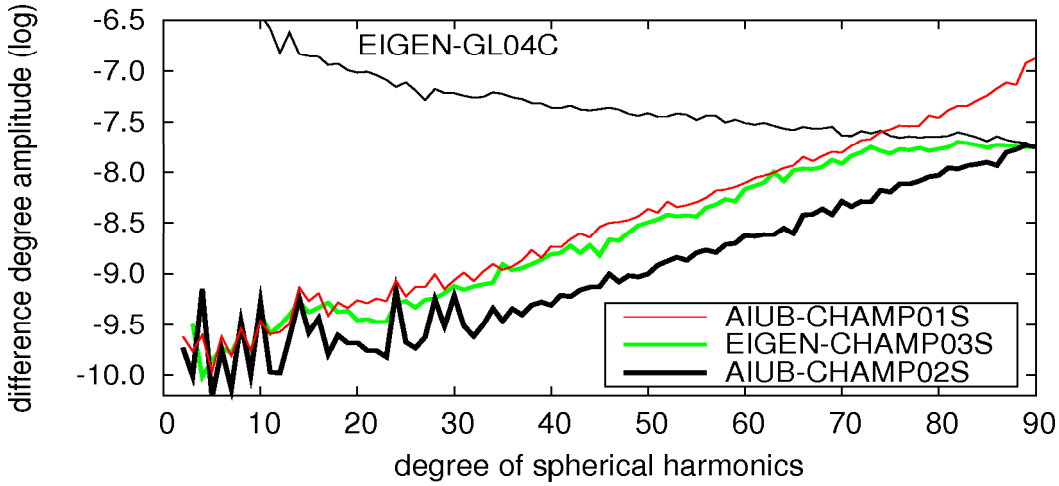

Figure 7.6: Comparison of CHAMP-only gravity field models.

best CHAMP-only gravity field model in this comparison — despite the inconsistency. With the results of the comparison between AIUB-CHAMP01S and the reprocessed annual solution in mind it becomes clear that the improvement of AIUB-CHAMP02S over AIUB-CHAMP01S is mainly due to the larger amount of processed CHAMP data (six years instead of one year). The GNSS model changes have only a small impact on the overall quality of the gravity field solution.

The AIUB-CHAMP02S validation reveals a disadvantage of geoid height comparisons: The geoid height error contains the accumulated errors of all included SH coefficients. These errors are dominated by the generally larger errors of the higher degree coefficients. Weaknesses of a few low degree coefficients with their generally lower error level do not carry much weight. They can be better recognized in the difference degree amplitudes.

7.3.2 External validation

AIUB-CHAMP02S was externally validated by Thomas Gruber using methods described in Gruber (2004).

The differences between geoid heights derived from the CHAMP-only gravity field models AIUB-CHAMP01S, AIUB-CHAMP02S, and EIGEN-CHAMP03S up to SH degree 60 and geoid heights derived from terrestrial measurements were computed. The terrestrial height data sets were the same as those used for the external validation of AIUB-CHAMP01S (see Sect. 7.2.2). The mean RMS values of the geoid height differences are contained in Tab. 7.4. The superior GRACE-only model ITG-GRACE03 (Mayer-Gürr, 2007) was included for indicating the different accuracies of the terrestrial data sets. Data sets showing RMS values of similar size when compared to AIUB-CHAMP01S and ITG-GRACE03S are probably not accurate enough (within the SH range 0–60) for this validation. The

Table 7.3: Comparison of AIUB-CHAMP02S and selected gravity field models with EIGEN-GL04C on a latitude-weighted $1° \times 1°$ grid.

Difference between EIGEN-GL04C and	Type of comparison	SH degree and order 0-30	0-50	0-70
AIUB-CHAMP01S	undulation [cm]: RMS	2.0	7.4	31.5
	max.	7.7	30.5	137.6
	min.	-7.6	-32.9	-127.3
	anomaly [mGal]: RMS	0.07	0.50	3.05
AIUB-CHAMP02Sp1y	undulation [cm]: RMS	2.1	7.1	29.8
	max.	6.9	31.9	128.7
	min.	-8.5	-25.5	-115.7
	anomaly [mGal]: RMS	0.07	0.47	2.88
AIUB-CHAMP02S	undulation [cm]: RMS	1.1	2.3	8.5
	max.	3.6	8.6	94.5
	min.	-3.8	-8.5	-50.1
	anomaly [mGal]: RMS	0.03	0.14	0.82
EIGEN-CHAMP03S	undulation [cm]: RMS	1.6	5.4	25.3
	max.	6.4	23.1	141.0
	min.	-5.1	-19.5	-161.6
	anomaly [mGal]: RMS	0.04	0.36	2.46

data sets from Germany, Canada, and Australia are assumed to be the most reliable ones.

The comparison shows a strong improvement of AIUB-CHAMP02S over AIUB-CHAMP01S. AIUB-CHAMP02S is also superior to EIGEN-CHAMP03S and is surprisingly close in quality to ITG-GRACE03. This does not only show the quality of AIUB-CHAMP02S, but also indicates the sensitivity limits of even the best terrestrial data sets for the long and medium wavelengths (SH degrees 0–60) of the gravity field signal.

Geoid slopes were computed from the above mentioned gravity field models (considering the degrees up to 60) and from the points of the terrestrial data sets. The geoid slope differences between selected terrestrial data sets and the gravity field models are shown in Fig. 7.7. In most comparisons the AIUB-CHAMP02S-curve is closer to the curve of the GRACE-model than to the curves of the other CHAMP-only models. In the comparison with the Japanese data set, EIGEN-CHAMP03S appears even better than the GRACE-model, indicating that this terrestrial data set is probably at its sensitivity limit in the considered spectral range.

The internal and external validations show that AIUB-CHAMP02S is a significant improvement over AIUB-CHAMP01S. It was probably the best CHAMP-only gravity field model at the time of its completion (fall 2008). The improvement is mainly due to the large amount of processed CHAMP GPS data (six years instead of one). The GNSS model changes have only a small positive impact on the recovery of the higher degree

Table 7.4: Mean RMS of geoid height differences in cm between terrestrial measurements and gravity field models (including AIUB-CHAMP02S) up to SH degree 60.

Height data set	No. of points	AIUB-CHAMP01S	**AIUB-CHAMP02S**	EIGEN-CHAMP03S	ITG-GRACE03
EUREF GPS	180	23.9	22.8	22.8	22.1
Germany EUVN	87	10.7	3.9	7.8	3.0
Germany GPS	675	11.0	4.3	7.9	3.9
Canada GPS 1998	1443	24.3	19.6	22.2	19.4
Canada GPS 2007	430	19.9	14.5	17.4	14.3
Australia GPS	197	28.4	23.7	27.8	24.1
Japan GPS	837	18.1	10.1	10.6	10.2
USA GPS	5168	35.1	33.6	35.3	33.4

coefficients. The good overall accuracy of the model is overshadowed by the low even zonal SH coefficients, which are affected by an inconsistency caused by an insufficiently modeled absolute CHAMP POD antenna PCV-pattern. The results of the external validation indicate that many terrestrial geoid height data sets are not sensitive enough in the low to medium SH spectrum (degrees 0–60) to clearly recognize the accuracy differences between AIUB-CHAMP02S and GRACE solutions.

7.4 Validation of AIUB-CHAMP03S

The validation of AIUB-CHAMP03S has the focus on the comparison with its predecessor AIUB-CHAMP02S and with GRACE solutions.

7.4.1 Internal validation

The difference degree amplitudes of the CHAMP-only solutions AIUB-CHAMP02S, AIUB-CHAMP03S, EIGEN-CHAMP05S (Flechtner et al, 2010), the GRACE-only solution AIUB-GRACE03Sp, and the combined solution EIGEN-GL04C w.r.t. the new combined model EGM2008 (Pavlis et al, 2008) are provided in Fig. 7.8. EGM2008 is assumed to be superior, because it is based on GRACE-data (for the determination of the low to medium SH degrees), and a very large number of globally well distributed terrestrial

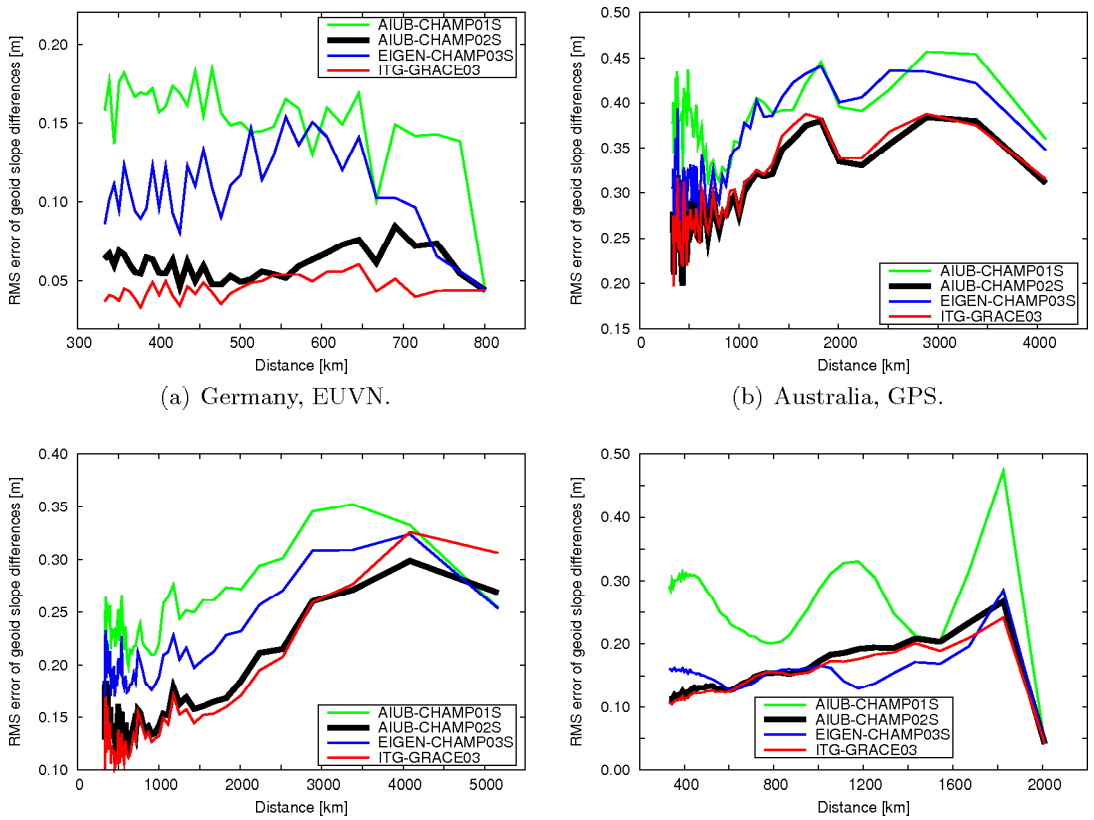

(a) Germany, EUVN.

(b) Australia, GPS.

(c) Canada 2007, GPS.

(d) Japan, GPS.

Figure 7.7: Geoid slope differences between terrestrial height data sets and global gravity field models up to SH degree 60.

gravity anomaly data sets (for the determination of the high SH degrees). It is therefore selected as reference model.

Figure 7.8 shows that the new CHAMP-only gravity field model EIGEN-CHAMP05S, based on 6 years of CHAMP data is slightly better than AIUB-CHAMP02S. Its significantly lower error in the high SH degrees is due to the regularization to Kaula from degree 70 on. AIUB-CHAMP03S is a significant improvement over AIUB-CHAMP02S and is the best CHAMP-only solution in this comparison. Most of the improvement was achieved by processing improvements (see Sect. 6.3). The figure shows, however, that the difference to the reference model is still about one order of magnitude larger for the best CHAMP solution than for the GRACE solutions. Only in the lowest SH degrees (in particular degree 2) the CHAMP and GRACE solutions are of comparable quality.

The mean RMS values of the geoid height differences and gravity anomaly differences between the aforementioned gravity field models and EGM2008 are presented in Tab. 7.5.

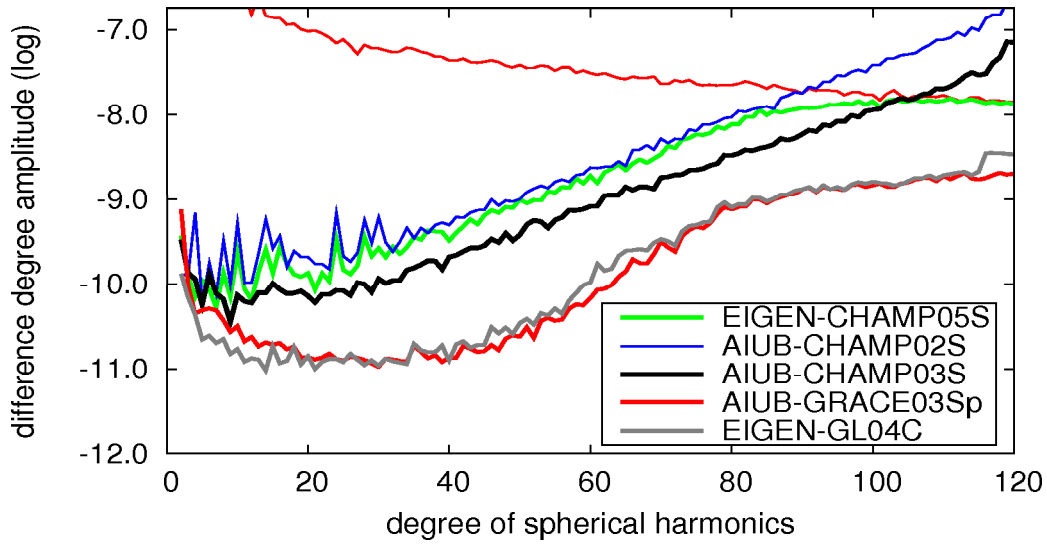

Figure 7.8: Comparison of AIUB-CHAMP03S and GRACE gravity field models.

Table 7.5 confirms the large improvement of AIUB-CHAMP03S over AIUB-CHAMP02S. The values of EIGEN-CHAMP05S are between those of the AIUB-CHAMP solutions. If only the coefficients of the lower SH spectrum (degrees 0–30) are considered, the difference between AIUB-CHAMP03S and the solutions based on GRACE-data is small. When extending the spectral range the much better agreement of the GRACE solutions with the reference model in the higher SH degrees becomes obvious.

7.4.2 External validation

AIUB-CHAMP03S was externally validated by Thomas Gruber using methods described in Gruber (2004).

The differences between terrestrial geoid heights and geoid heights derived from different gravity field models were computed. Apart from AIUB-CHAMP03S, the GRACE-only solutions AIUB-GRACE03Sp and ITG-GRACE03 (Mayer-Gürr, 2007) and the combined solutions EIGEN-GL04C and EGM2008 were included in the validation. The terrestrial geoid height data sets were nearly the same as used for the validation of AIUB-CHAMP01S and AIUB-CHAMP02S. Only one new data set (EUREF EUVN 2007) was added to the list. The mean RMS values of the geoid height differences are provided in Tab. 7.6. The validation of AIUB-CHAMP02S has shown the accuracy limits of many terrestrial geoid height data sets in the lower part (degrees 0–60) of the SH spectrum. Therefore, the validation of AIUB-CHAMP03S was additionally carried out with extended spectral ranges (0–90 and 0–120). When the higher degree coefficients are included in the geoid height comparison the better accuracy of the GRACE solutions becomes more obvious.

Table 7.5: Comparison of AIUB-CHAMP03S and selected gravity field models with EGM2008 on a latitude-weighted $1° \times 1°$ grid.

Difference between EGM2008 and	Type of comparison	SH degree and order 0–30	0–50	0–70	0–90
EIGEN-CHAMP05S	undulation [cm]: RMS	0.6	1.7	6.1	25.6
	max.	2.5	7.6	27.6	186.4
	min.	-2.4	-7.9	-33.9	-178.4
	anomaly [mGal]: RMS	0.018	0.107	0.588	3.205
AIUB-CHAMP02S	undulation [cm]: RMS	1.1	2.3	8.1	33.7
	max.	3.7	8.1	76.5	329.5
	min.	-3.7	-8.3	-40.6	-153.8
	anomaly [mGal]: RMS	0.034	0.132	0.777	4.263
AIUB-CHAMP03S	undulation [cm]: RMS	0.4	0.9	3.1	11.2
	max.	1.3	3.4	13.7	45.7
	min.	-1.3	-3.8	-13.3	-48.5
	anomaly [mGal]: RMS	0.009	0.048	0.297	1.406
AIUB-GRACE03Sp	undulation [cm]: RMS	0.4	0.4	0.6	2.6
	max.	1.2	1.2	3.6	38.8
	min.	-0.7	-0.8	-3.8	-38.4
	anomaly [mGal]: RMS	0.001	0.004	0.041	0.329
EIGEN-GL04C	undulation [cm]: RMS	0.1	0.1	0.6	2.7
	max.	0.4	0.6	4.5	39.3
	min.	-0.3	-0.4	-3.8	-38.1
	anomaly [mGal]: RMS	0.001	0.004	0.055	0.346

The CHAMP-only solution suffers from its steadily increasing error level in the high SH degrees.

Table 7.6: Mean RMS values of geoid height differences in cm between gravity field models and terrestrial measurements up to degree 60, 90, and 120.

Height data set	No. of points	Spectral range	**AIUB-CHAMP03S**	AIUB-GRACE03Sp	EIGEN-GL04C	ITG-GRACE03	EGM 2008
EUREF	180	0–60	22.2	22.2	22.1	22.1	22.1
GPS		0–90	24.4	22.4	22.4	22.3	22.1
		0–120	131.5	22.1	23.8	21.9	22.1
EUREF	1233	0–60	21.6	21.6	21.5	21.5	21.5
EUVN		0–90	23.5	21.6	21.6	21.6	21.5
2007		0–120	136.6	21.9	23.1	21.9	21.5
Germany	87	0–60	3.5	3.1	3.1	3.0	3.0
EUVN		0–90	7.3	3.2	3.2	3.1	3.0
		0–120	91.5	4.1	7.7	3.7	3.0
Germany	675	0–60	4.0	3.9	3.9	3.9	3.9
GPS		0–90	7.2	4.1	4.0	4.0	3.9
		0–120	95.4	4.7	8.2	4.4	3.9
Canada	1443	0–60	19.4	19.4	19.4	19.4	19.4
GPS		0–90	22.4	19.5	19.4	19.4	19.4
1998		0–120	88.0	19.7	19.7	19.6	19.4
Canada	430	0–60	14.4	14.3	14.3	14.3	14.3
GPS		0–90	17.6	14.4	14.3	14.4	14.3
2007		0–120	80.7	14.4	15.1	15.0	14.3
Australia	197	0–60	23.9	24.2	24.1	24.1	24.1
GPS		0–90	27.3	24.3	24.2	24.2	24.1
		0–120	91.3	24.4	24.5	24.3	24.1
Japan	837	0–60	10.2	10.3	10.2	10.2	10.2
GPS		0–90	15.4	10.1	10.2	10.0	10.2
		0–120	67.2	10.3	11.9	10.3	10.2
USA	5168	0–60	33.5	33.5	33.4	33.4	33.4
GPS		0–90	34.5	33.6	33.3	33.4	33.4
		0–120	85.6	33.4	33.4	33.4	33.4

The geoid slope differences shown in Fig. 7.9 are well suited to visualize these results: In the spectral range 0–60 the terrestrial data sets (apart from the German data sets) are not accurate enough to clearly distinguish between AIUB-CHAMP03S and the GRACE solutions (see Fig. 7.9, left side). When extending the spectral range to SH degrees 0–90 (see Fig. 7.9, right side) the CHAMP solution differs much more from the terrestrial data

than the GRACE solutions. Different GRACE solutions, however, can hardly be distinguished, indicating that their error is still below the sensitivity limit of most terrestrial data sets in the spectral range (0–90).

The internal and external validations show that AIUB-CHAMP03S is much better in quality than AIUB-CHAMP02S. It is the best currently available CHAMP-only gravity field model known to the author. On the other hand the validation shows that AIUB-CHAMP03S is clearly inferior to GRACE-only gravity field solutions in most parts of the SH spectrum. Only in the lowest SH degrees (up to SH degree 4) AIUB-CHAMP03S, SLR-based, and GRACE solutions are on a similar level (see also Fig. 7.2). With the validation methods used here it is difficult to decide which kind of model is really superior in the lowest part of the SH spectrum. A validation by dynamic orbit determination (see Sect. 7.1.5) or orbit prediction of high-altitude satellites could possibly help to make a decision, but must be left to the future.

The quality differences between AIUB-CHAMP03S and the GRACE solutions in the low and medium SH spectral domain (degrees 0–60) are hardly recognizable by comparison with terrestrial geoid height data sets due to the limited sensitivity of terrestrial measurements to the long wavelengths of the gravity field. Only the best data sets (Germany EUVN and Germany GPS in Tab. 7.6) are accurate enough in this part of the SH spectrum. For coefficients above SH degree and order 60 the superior accuracy of GRACE K-band solutions over the CHAMP solution can clearly be recognized in the comparison with ground data.

The comparison of internal and external errors of the AIUB-CHAMP solutions (see Fig. 5.20) shows that both agree well in the medium and upper part of the SH spectrum. In the lower part (below SH degree 30 for AIUB-CHAMP01S and AIUB-CHAMP02S, below degree 40 for AIUB-CHAMP03S), however, the difference degree amplitudes are much larger than the formal errors. This could either indicate that the formal errors are too optimistic or that there is still potential for improvements regarding the recovery of the low degree harmonics using spaceborne GPS measurements (see also Sect. 6.3.8).

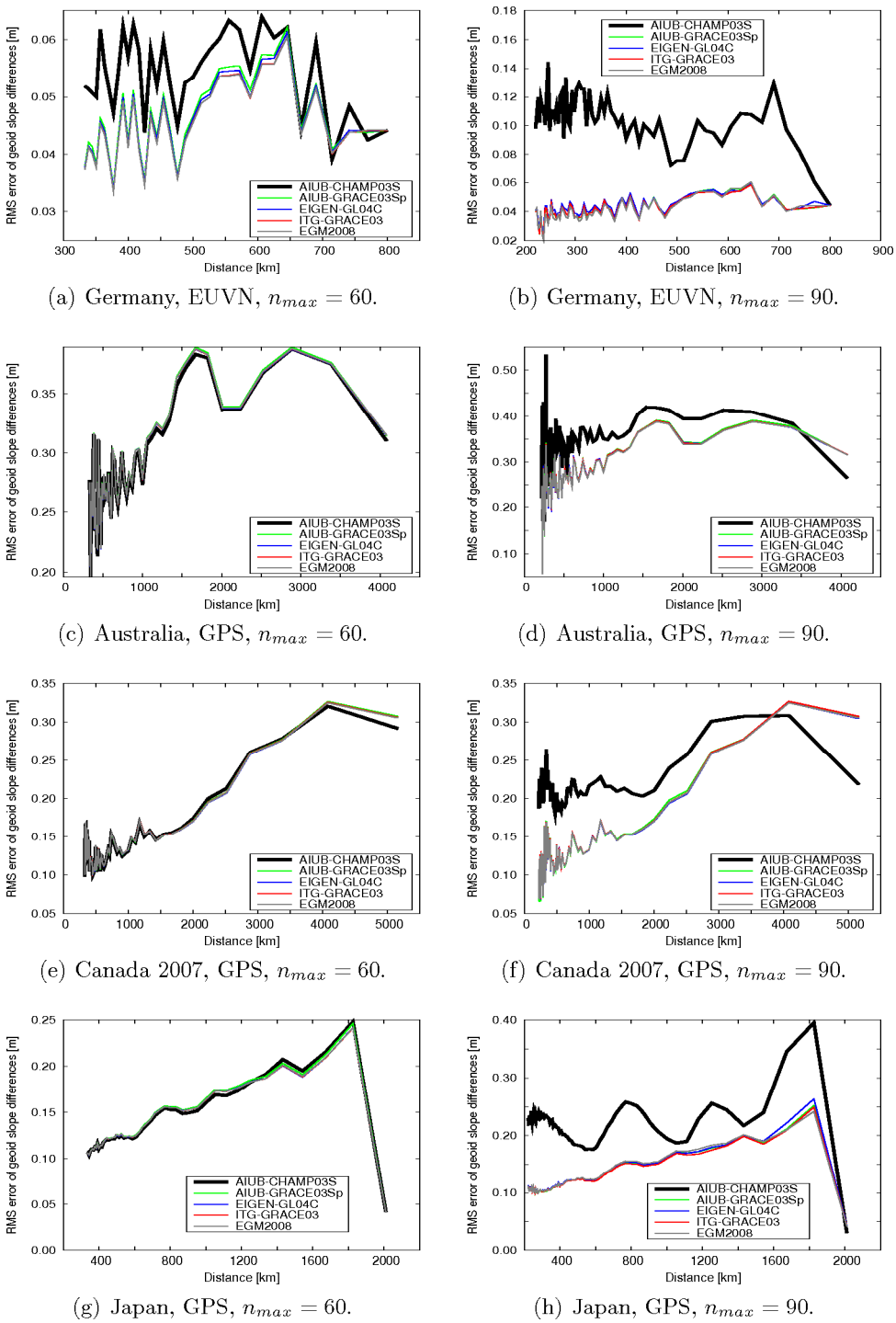

(a) Germany, EUVN, $n_{max} = 60$.

(b) Germany, EUVN, $n_{max} = 90$.

(c) Australia, GPS, $n_{max} = 60$.

(d) Australia, GPS, $n_{max} = 90$.

(e) Canada 2007, GPS, $n_{max} = 60$.

(f) Canada 2007, GPS, $n_{max} = 90$.

(g) Japan, GPS, $n_{max} = 60$.

(h) Japan, GPS, $n_{max} = 90$.

Figure 7.9: Geoid slope differences between terrestrial height data sets and global gravity field models up to SH degree 60 (left) and 90 (right).

8 Summary and conclusions

The major goal of this work was to to generate "the best possible" static CHAMP-only gravity field model using most of the openly available CHAMP data. Firstly we wanted to assess the full potential but also the limitations of CHAMP data and a CHAMP-like satellite mission for gravity field determination. Secondly we wanted to gain as much insight as possible in determining gravity fields (static and time variable) from space-based GNSS data in general, because several current and future satellite missions (dedicated to gravity field research, but also non-dedicated) equipped with GNSS receivers could benefit from improvements made here. We believe to have come close to achieving these goals by generating, validating, and publishing the static Earth gravity field models AIUB-CHAMP01S, AIUB-CHAMP02S, and AIUB-CHAMP03S. Furthermore, the largest constituents of the seasonal gravity field variations could be retrieved from CHAMP data, as well. The Celestial Mechanics Approach (CMA) was successfully applied for gravity field determination.

We use the CMA as a two-step approach: In the first step kinematic positions are estimated with the PPP approach using observations of a GPS receiver on-board a LEO satellite. The GPS orbits and GPS satellite clock corrections are introduced as known. In the second step the kinematic positions are used as pseudo-observations in a reduced-dynamic orbit determination. Apart from the orbit parameters the SH coefficients describing the Earth's gravity field are set up. A NEQ system is established for each day. The orbit parameters are pre-eliminated on the NEQ-level in order to reduce the number of parameters to be estimated. The arc-specific NEQs are stacked. Eventually the gravity field parameters are determined by solving the stacked NEQs.

AIUB-CHAMP01S is based on one year (DOY 70/2002–70/2003) of kinematic CHAMP positions provided by Adrian Jäggi and based on the GPS orbit and clock products of the CODE analysis center of the IGS. In order to generate gravity field models from long time series of kinematic LEO positions, a suitable processing infrastructure was developed as part of this work, making use of the automation capabilities of the Bernese GPS Software. An effective outlier screening procedure for the kinematic positions was established.

Extensive orbit determination and gravity field recovery experiments, and a simulation study were carried out in order to find the optimal orbit modeling. It was shown that a modeling of the non-gravitational perturbations, solely based on dynamical force models, accelerometer measurements, or dynamical orbit parameters is insufficient in a CHAMP-only scenario due to the superposition of different kinds of orbit perturbations. Therefore, the set up of pseudo-stochastic orbit parameters is a necessity. Pseudo-stochastic orbit parameters proved to be a powerful tool for absorbing the effects of insufficiently modeled or unmodeled orbit perturbations of different types. This was demonstrated for non-

gravitational perturbations, insufficiently modeled ocean tides, and omission errors. In the presence of strong orbit perturbations a large number of orbit parameters with a spacing of only 5 min is required for CHAMP — especially for the recovery of the high degree harmonics. Pulses were found to be slightly better suited for gravity field determination than piecewise constant accelerations, because they do not affect the satellite orbit in-between the pulse epochs and may be set up without constraints. Over-parameterization effects in the low degree harmonics of the computed gravity fields are avoided by combining solutions with unconstrained pulses set up every 5 min and 15 min on the NEQ-level. The formal errors of the combined solution were found to be not more optimistic than the formal errors of the individual solutions. Accelerometer data or non-gravitational force models were not used in the final analysis, because studies with real and simulated CHAMP data demonstrated that the non-gravitational signal is absorbed by the large number of pseudo-stochastic parameters that have to be set up anyway.

Omission errors are a major error source as CHAMP's orbit turned out to be sensitive to SH coefficients of degrees above 100, although their reliable determination by CHAMP data is close to impossible. Omission errors are absorbed by a combination of pseudo-stochastic orbit parameters and high degree SH coefficients. AIUB-CHAMP01S is thus cut off at degree 90, AIUB-CHAMP02S and AIUB-CHAMP03S at degree 120.

AIUB-CHAMP01S was compared with other gravity field models and externally validated with ground data by Thomas Gruber from the IAPG of the Technische Universität München. The internal and external validations confirmed that AIUB-CHAMP01S is comparable in quality to the best CHAMP-only gravity field solutions based on the same set of CHAMP GPS data and thus demonstrated the suitability of the CMA and the processing routines for gravity field recovery using GPS observations from LEO satellites.

AIUB-CHAMP02S is a solution based on six years (2002–2007) of CHAMP GPS data. Within this time interval many GNSS model changes took place in the IGS processing performed at CODE. Therefore, a partial reprocessing of the CODE GPS orbit and clock products was conducted in the framework of this work. The IGS standards introduced in GPS week 1400 (November 2006) were applied to the entire time interval 2002–2007. Using the reprocessed GPS orbit and clock products kinematic CHAMP positions were generated and used for gravity field recovery.

The validation of the reprocessed GPS orbits and clock corrections with a PPP of ground stations showed that mainly long periodic variations of the kinematic positions could be reduced by using the reprocessed GPS products. The high frequency variations of the kinematic positions were only slightly reduced. The GNSS model changes thus have a small positive effect on the recovery of the medium and higher degree harmonics (whose accuracy is to a large extent limited by the noise of the kinematic positions), but cause a prominent inconsistency of the even zonal SH coefficients of low degrees. Real data and simulation experiments showed that the inconsistency was caused by the change from the relative to the absolute PCV model, in particular by an insufficiently modeled absolute phase center variation (PCV) pattern of CHAMP's GPS antenna. The GPS observation geometry generates a latitude-dependent distribution of the observations in

the antenna-fixed coordinate system of the LEO. As the PCVs are applied in the form of azimuth-elevation-specific corrections, a mismodeled PCV pattern can cause latitude-dependent systematic errors in the LEO orbit and gravity field determination. A similar effect of smaller size was observed for the transmitting antennas of the GPS satellites. The internal and external validations of AIUB-CHAMP02S showed that AIUB-CHAMP02S is, despite the PCV-induced inconsistency, clearly better than AIUB-CHAMP01S — mainly thanks to the larger data amount.

AIUB-CHAMP03S is the final product of this work. It is based on CHAMP GPS measurements of the years 2002–2009 and qualitatively much improved w.r.t. its predecessors. The sampling interval of the kinematic CHAMP positions was reduced from 30 s to 10 s, using the full tracking capability of CHAMP's GPS receiver. The required high-rate GPS clock corrections for the years 2002–2006 were computed using the measurements of the high-rate IGS tracking network. For 2007–2009 the already available corresponding CODE products were used. From 2004 onwards the annual gravity field solutions contributing to AIUB-CHAMP03S profit significantly from the higher sampling rate. The solutions from earlier years did not benefit, because the quality of the high-rate clock corrections suffered from a not yet optimal number and distribution of the high-rate IGS network stations in those years. CHAMP's POD antenna phase pattern was estimated empirically from the residuals of a reduced-dynamic orbit determination. As expected from the analysis of the GNSS model changes, the empirical phase pattern significantly improved the quality of the gravity field solution. The elevation-dependent weighting of the GPS observations with an empirical weighting function complementary improves the solution in a significant way. Taking into account the correlations between kinematic epochs has a small positive effect on gravity field recovery, as well. Using position differences instead of kinematic positions as pseudo-observations reduces the effect of outliers on gravity field recovery. This circumstance was used for the computation of the 2009 annual contribution to AIUB-CHAMP03S, because the data quality suffered from the reduced number of only seven tracking channels of CHAMP's GPS receiver since late 2008. The neglect of eclipsing Block II/IIA satellites reduces the quality variations of the kinematic positions and the monthly gravity field solutions.

All internal and external validations of AIUB-CHAMP03S indicate a great improvement w.r.t. AIUB-CHAMP02S. AIUB-CHAMP03S is the best currently (2010) known CHAMP-only gravity field model published by the International Centre for Global Earth Models (see http://icgem.gfz-potsdam.de/ICGEM/ICGEM.html). The Earth gravity field could be resolved up to SH degree 106. This is much better than expected for CHAMP, but far away from the resolutions and accuracies achievable with GRACE K-band data. It was shown that — thanks to the improvements made — it is in principle possible to detect the largest seasonal variations of the Earth's gravity field with CHAMP data. This is remarkable, because CHAMP was not designed to perform this task. A reliable monitoring and quantification of seasonal gravity field changes with spaceborne GPS data alone is, however, not possible without further improvements, because the error of GPS-only gravity field solutions is still too high.

The experiences made in the context of this work may be used for other LEOs equipped with GNSS receivers. This is being done currently at the AIUB by setting up the GPS-specific NEQs for the GRACE and the GOCE missions, which both require accurate orbits established by GPS. GRACE-only gravity field solutions will probably not improve significantly due to the progress made here, because the quality of GRACE solutions is mainly determined by the K-band measurements. GOCE-only solutions will, however, benefit, because the low and medium degree harmonics are mainly determined by the GPS measurements. It is no question that the best possible gravity field solutions will be based on the combination of different data sources (including GNSS, K-band, gradiometer, terrestrial, and SLR data) sensitive to different parts of the SH spectrum. Also non-dedicated LEO satellites equipped with geodetic GNSS receivers (e.g., SWARM) may contribute to such solutions: Similar to the combined gravity field models of the pre-CHAMP era the combination of tracking data from satellites with different inclinations could possibly help to decorrelate the determined gravity field parameters.

The gravity field recovery performed in this work did not focus on a certain part of the SH spectrum. It aimed on the general improvement of the global gravity field determination using spaceborne GPS and on the assessment of the capabilities of the CMA using CHAMP as an example. The validation methods were chosen accordingly. The analysis results suggest that the largest potential of spaceborne GNSS to contribute to combined gravity field solutions lies (similar to SLR) in the lowest part ($<$ degree 20) of the SH spectrum. For the future research we, therefore, recommend to focus on improvements here for the following reasons: (a) In the remaining part of the SH spectrum other measurements (K-band, gradiometer, terrestrial data) are clearly superior. (b) The formal errors of the gravity field solutions based on spaceborne GNSS are too optimistic for the low degree harmonics. This and the limited effect of several processing improvements in this part of the SH spectrum indicate the presence of not yet covered systematic errors and therefore potential for further improvements. The PCV patterns of the GPS transmission antennas were identified as possible error sources. (c) The detectability of temporal gravity field variations would benefit particularly from improvements in these degrees. Accordingly we recommend to also apply validation methods that are particularly suited for validating the low degree harmonics (e.g., orbit predictions of high altitude satellites such as GNSS and geodetic SLR satellites).

Gravity field recovery using the CMA is treated as generalized orbit determination problem. Therefore the results of this work may also contribute to the improvement of LEO orbit determination using GNSS. The studies regarding orbit modeling, impact of the POD/GPS antenna PCV pattern, elevation-dependent weighting, inter-epoch correlations of the kinematic positions, and the neglect of observations from eclipsing GPS satellites are examples. Further potential for improvements is seen in a weighting based on the signal-to-noise ratio of the GPS observations, in the in-flight calibration of the GPS transmission antennas similar to the calibration of the LEO POD antenna, and for the dynamic force models.

Bibliography

Badura T, Sakulin C, Gruber C, Klostius R (2006) DERIVATION OF THE CHAMP-ONLY GLOBAL GRAVITY FIELD MODEL TUG-CHAMP04 APPLYING THE ENERGY INTEGRAL APPROACH. Studia Geophysica et Geodaetica 50:59–74

Bar-Sever YE (1994) Improvement to the GPS Attitude Control Subsystem Enables Predictable Attitude During Eclipse Seasons. IGS Mail No. 591, IGS Central Bureau Information System

Bar-Sever YE (1996) A new model for GPS yaw attitude. Journal of Geodesy 70:714–723

Beutler G (2005) Methods of Celestial Mechanics. Springer-Verlag, Berlin, Heidelberg, New York

Beutler G, Brockmann E, Gurtner W, Hugentobler U, Mervart L, Rothacher M (1994) Extended Orbit Modeling Techniques at the CODE Processing Center of the International GPS Service for Geodynamics (IGS): Theory and Initial Results. Manuscripta Geodaetica 19:367–386

Beutler G, Brockmann E, Hugentobler U, Mervart L, Rothacher M, Weber R (1996) Combining Consecutive Short Arcs into Long Arcs for Precise and Efficient GPS Orbit Determination. Journal of Geodesy 70:287–299

Beutler G, Jäggi A, Mervart L, Meyer U (2010a) The Celestial Mechanics Approach—application to data of the GRACE mission. Journal of Geodesy 84:661–681, DOI 10.1007/s00190-010-0402-6

Beutler G, Jäggi A, Mervart L, Meyer U (2010b) The Celestial Mechanics Approach—theoretical foundations. Journal of Geodesy 84:605–624, DOI 10.1007/s00190-010-0401-7

Biancale R, Balmino G, Lemoine J, Marty J, Moynot B, Barlier F, Exertier P, Laurain O, Gegout P, Schwintzer P, Reigber C, Bode A, König R, Massmann F, Raimondo J, Schmidt R, Zhu S (2000) A new global Earth's gravity field model from satellite orbit perturbations: GRIM5-S1. Geophysical Research Letters 27(22):3611–3614

Bock H (2004) Efficient Methods for Determining Precise Orbits of Low Earth Orbiters Using the Global Positioning System. Geodätisch-geophysikalische Arbeiten in der Schweiz, Band 65, Schweizerische Geodätische Kommission, Institut für Geodäsie und Photogrammetrie, Eidg. Technische Hochschule Zürich, Zürich

Bock H, Dach R, Jäggi A, Beutler G (2009) High-rate GPS clock corrections from CODE: support of 1 Hz applications. Journal of Geodesy 83(11):1083–1094, DOI 10.1007/s00190-009-0326-1

Boehm J, Niell A, Tregoning P, Schuh H (2006) Global Mapping Function (GMF): A new empirical mapping function based on numerical weather model data. Geophysical Research Letters 33

Brockmann E (1997) Combination of Solutions for Geodetic and Geodynamic Applications of the Global Positioning System (GPS). Geodätisch-geophysikalische Arbeiten in der Schweiz, Band 55, Schweizerische Geodätische Kommission, Institut für Geodäsie und Photogrammetrie, Eidg. Technische Hochschule Zürich, Zürich

Bruinsma S, Tamagnan D, Biancale R (2004) Atmospheric densities derived from CHAMP/STAR accelerometer observations. Planetary and Space Science 52:297–312, DOI 10.1016/j.pss.2003.11.004

Cheng M, Gunter B, Ries J, Chambers D, Tapley B (2003) Temporal Variation in the Earth's Gravity Field from SLR and CHAMP GPS Data. In: Tziavos I (ed) Gravity and Geoid, pp 424–431

CODE (2010) http://igscb.igs.org/igscb/center/analysis/code.acn

Dach R, Beutler G, Bock H, Fridez P, Gäde A, Hugentobler U, Jäggi A, Meindl M, Mervart L, Prange L, Schaer S, Springer T, Urschl C, Walser P (2007) Bernese GPS Software Version 5.0. Astronomical Institute, University of Bern, Bern, Switzerland, URL `http://www.bernese.unibe.ch/docs/DOCU50.pdf`, user manual

Dach R, Brockmann E, Schaer S, Beutler G, Meindl M, Prange L, Bock H, Jäggi A, Ostini L (2009) GNSS Processing at CODE: Status Report. Journal of Geodesy 83(3–4):353–365, DOI 10.1007/s00190-008-0281-2

Davis J, Tamisiea M, Elósegui P, Mitrovica J, Hill E (2008) A statistical filtering approach for Gravity Recovery and Climate Experiment (GRACE) gravity data. Journal of Geophysical Research 113(B04410), doi:10.1029/2007JB005043

Dilssner F, Seeber G, Schmitz M, Wübbena G, Toso G, Maeusli D (2006) Characterization of GOCE SSTI Antennas. Zeitschrift für Geodäsie, Geoinformation und Landmanagement 2/2006:61–71

Ditmar P, van Eck van der Sluijs AA (2004) A technique for modeling the Earth's gravity field on the basis of satellite accelerations. Journal of Geodesy 78(1–2):12–33, DOI 10.1007/s00190-003-0362-1

Dow JM, Neilan RE, Rizos C (2009) The International GNSS Service in a changing landscape of Global Navigation Satellite Systems. Journal of Geodesy 83(3–4):191–198, DOI 10.1007/s00190-008-0300-3

Drinkwater M, Haagmans R, Muzi D, Popescu A, Floberghagen R, Kern M, Fehringer M (2006) The GOCE gravity mission: ESA's first core explorer. In: Proceedings 3rd GOCE User Workshop, 6-8 November 2006, Frascati, Italy, ESA SP-627, pp 1–7

Dunn C, Bertiger W, Bar-Sever Y, Desai S, Haines B, Kuang D, Franklin G, Harris I, Kruizinga G, Meehan T, Nandi S, Nguyen D, Rogstad T, Thomas J, Tien J, Romans L, Watkins M, Wu S, Bettadpur S, Kim J (2003) Instrument of GRACE: GPS Auguments Gravity Measurements. GPS World 14(2):16–28

Eanes R, Bettadpur S (1996) The CSR3.0 global ocean tide model: Diurnal and Semi-diurnal ocean tides from TOPEX/POSEIDON altimetry. Tech. rep., University of Texas, Centre for Space Research, Austin, In: CSR-TM-96-05

Ferland R (2003) IGS00(V2) final. IGS Mail No. 4666, IGS Central Bureau Information System

Ferland R (2006) Proposed IGS05 realization. IGS Mail No. 5447, IGS Central Bureau Information System

Flechtner F (2007) AOD1B Product Description Document for Product Releases 01 to 04. Tech. Rep. GR-GFZ-AOD-0001, GeoForschungszentrum Potsdam

Flechtner F, Dahle C, Neumayer KH, König R, Förste C (2010) The Release 04 CHAMP and GRACE EIGEN Gravity Field Models. In: Flechtner F, Gruber T, Güntner A, Mandea M, Rothacher M, Schöne T, Wickert J (eds) System Earth via Geodetic-Geophysical Space Techniques, Springer, pp 41–58, DOI 978-3-642-10228-8, ISBN 978-3-642-10227-1

Fliegel HF, Gallini TE, Swift ER (1992) Global Positioning System Radiation Force Model for Geodetic Applications. Geophysical Research Letters 97(B1):559–568

Flohrer C (2008) Mutual Validation of Satellite-Geodetic Techniques and its Impact on GNSS Orbit Modeling. Geodätisch-geophysikalische Arbeiten in der Schweiz, Band 75, Schweizerische Geodätische Kommission, Institut für Geodäsie und Photogrammetrie, Eidg. Technische Hochschule Zürich, Zürich

Förste C, Schwintzer P, Reigber C (2002) The champ data format. http://op.gfz-potsdam.de/champ/index_CHAMP.html, CH-GFZ-FD-001

Förste C, Flechtner F, Schmidt R, Meyer U, Stubenvoll R, Barthelmes F, Knig R, Neumayer K, Rothacher M, Reigber C, Biancale R, Bruinsma S, Lemoine J, Raimondo J (2005) A New High Resolution Global Gravity Field Model Derived From Combination of GRACE and CHAMP Mission and Altimetry/Gravimetry Surface Gravity Data. Poster presented at EGU General Assembly 2005, Vienna, Austria

Förste C, Schmidt R, Stubenvoll R, Flechtner F, Meyer U, König R, Neumayer H, Biancale R, Lemoine J, Bruinsma S, Loyer S, Barthelmes F, Esselborn S (2008) The GeoForschungsZentrum Potsdam/Groupe de Recherche de Geodesie Spatiale satellite-only and combined gravity field models: EIGEN-GL04S1 and EIGEN-GL04C. Journal of Geodesy 82, 6:331–346, doi:10.1007/s00190-007-0183-8

Fu L, Chelton D (2001) Large-Scale Ocean Circulation. In: Fu L, Cazenave A (eds) Satellite Altimetry and Earth Sciences, Academic Press, pp 133–169

Gerlach C, Sneeuw N, Visser P, Švehla D (2003) CHAMP gravity field recovery using the energy balance approach. Advances in Geosciences 1:73–80

Gruber T (2004) Validation concepts for gravity field models from satellite missions. In: Proceedings of Second International GOCE User Workshop "GOCE, The Geoid and Oceanography", ESA-ESRIN, Frascati, Italy

Gruber T, Bode A, Reigber C, Schwintzer P, Biancale R, Balmino G, Lemoine J (2000) GRIM5-C1: Combination solution of the global gravity field to degree and order 120. Geopyhsical Research Letters 27(24):4005–4008

Grunwaldt L, Meehan T (2003) CHAMP Orbit and Gravity Instrument Status. In: Reigber C, Lühr H, Schwintzer P (eds) First CHAMP Mission Results for Gravity, Magnetic and Atmospheric Studies, Springer, pp 3–10

Gurtner W (1994) RINEX: The Receiver-Independent Exchange Format. GPS World 5(7):48–52, URL `ftp://igscb.jpl.nasa.gov/igscb/data/format/rinex2.txt`

Han S, Shum C, Jekeli C, Braun A, Chen Y, Kuo C (2005) CHAMP Gravity Field Solutions and Geophysical Constraint Studies. In: Reigber C, Lühr H, Schwintzer P, Wickert J (eds) Earth Observation with CHAMP—Results from Three Years in Orbit, Springer, Berlin, pp 108–114

Hedin AE (1991) Extension of the MSIS Thermosphere Model into the Middle and Lower Atmosphere. Journal of Geophysical Research 96(A2):1159–1172

Heiskanen W, Moritz H (1967) Physical Geodesy. Freeman

Helmert FR (1872) Die Ausgleichsrechnung nach der Methode der kleinsten Quadrate. Teubner, Leipzig

Hirt C, Flury J (2007) Astronomical-topographic levelling using high-precision astrogeodetic vertical deflections and digital terrain model data. Journal of Geodesy 82(4–5):231–248

Hoffmann-Wellenhof B, Moritz H (2006) Physical Geodesy, 2nd edn. Springer

Hoffmann-Wellenhof B, Lichtenegger H, Wasle E (2008) GNSS – Global Navigation Satellite Systems GPS, GLONASS, Galileo, and more. Springer

Hugentobler U (2004) CODE high rate clocks. IGS Mail No. 4913, IGS Central Bureau Information System

Hugentobler U, Meindl M, Beutler G, Bock H, Dach R, Jäggi A, Urschl C, Mervart L, Rothacher M, Schaer S, Brockmann E, Ineichen D, Wiget A, Wild U, Weber G, Habrich H, Boucher C (2006) CODE IGS Analysis Center Technical Report 2003/2004. In: Gowey K, Neilan R, Moore A (eds) IGS 2004 Technical Reports, IGS Central Bureau, Jet Propulsion Laboratory, Pasadena, California, USA

IAG (2010) www.iag-aig.org

IAU (2000) Resolutions of the 24th General Assembly, Manchester, UK. www.iau.org/administration/resolutions/general_assemblies

IGS (2010) www.igs.org or http://igscb.jpl.nasa.gov/

Ilk K, Flury J, Rummel R, Schwintzer P, Bosch W, Haas C, Schröter J, Stammer D, Zahel W, Miller H, Dietrich R, Huybrechts P, Schmeling H, Wolf D, Götze H, Riegger J, Bardossy A, Güntner A, Gruber T (2005) Mass Transport and Mass Distribution in the Earth System – Contribution of the New Generation of Satellite Gravity and Altimetry Missions to Geosciences. GOCE-Projektbüro Deutschland, Technische Universität München, GeoForschungsZentrum Potsdam

ILRS (2010) http://ilrs.gsfc.nasa.gov/satellite_missions/list_of_satellites/index.html

Jäggi A (2007) Pseudo-Stochastic Orbit Modeling of Low Earth Satellites Using the Global Positioning System. Geodätisch-geophysikalische Arbeiten in der Schweiz, Band 73, Schweizerische Geodätische Kommission, Institut für Geodäsie und Photogrammetrie, Eidg. Technische Hochschule Zürich, Zürich

Jäggi A (2010) Gravity Field Determination at AIUB: From annual to multi-annual solutions. Presentation at the EGU General Assembly, Vienna, Austria

Jäggi A, Beutler G, Bock H, Hugentobler U (2006) Kinematic and highly reduced-dynamic LEO orbit determination for gravity field estimation. In: Rizos C, Tregoning P (eds) Dynamic Planet—Monitoring and Understanding a Dynamic Planet with Geodetic and Oceanographic Tools, Springer, pp 354–361

Jäggi A, Beutler G, Prange L, Dach R, Mervart L (2009a) Assessment of GPS-only observables for gravity field recovery from GRACE. In: Sideris M (ed) Observing our Changing Earth, Springer, Berlin, Heidelberg, New York, vol 133, pp 113–123, DOI 10.1007/978-3-540-85426-5_14

Jäggi A, Dach R, Montenbruck O, Hugentobler U, Bock H, Beutler G (2009b) Phase center modeling for LEO GPS receiver antennas and its impact on precise orbit determination. Journal of Geodesy 83(12):1145–1162, DOI 10.1007/s00190-009-0333-2

Jäggi A, Bock H, Prange L, Meyer U, Beutler G (2010a) GPS-only gravity field recovery using GOCE, CHAMP, and GRACE. submitted to Advances in Space Research

Jäggi A, Prange L, Hugentobler U (2010b) Impact of covariance information of kinematic positions on orbit reconstruction and gravity field recovery. Advances in Space Research DOI 10.1016/j.asr.2010.12.009

Jorgensen J (1999) In Orbit Performance of a fully Autonomous Star Tracker. In: Proceedings of the 4th ESA International Conference on Spacecraft Guidance, Navigation and Control Systems, pp 103–110

Kaula W (1966) Theory of Satellite Geodesy—Applications of Satellites to Geodesy. Blaisdell Publ. Comp., Waltham, Toronto, London

Kirchner M, Becker M (2005) The Use of Signal Strength Measurements for Quality Assessments of GPS Observations. Reports on Geodesy 2(73)

Koch K (1988) Parameter estimation and hypothesis testing in linear models. Springer, Berlin, Heidelberg, New York

Köhler W (2001) RINEX format observable extensions for CHAMP SST Data. http://op.gfz-potsdam.de/champ/docs_CHAMP/CH-RINEX-EXT.html

Koop R, Gruber T, Rummel R (2006) The status of the GOCE high-level processing facility. In: Proceedings 3rd GOCE User Workshop, 6-8 November 2006, Frascati, Italy, ESA SP-627, pp 199–205

Kouba J, Ray J, Watkins MM (1998) IGS Reference Frame Realization. In: Dow J, Kouba J, Springer TA (eds) Proceedings of the 1998 IGS Analysis Center Workshop, ESA/ESOC, Darmstadt, Germany

Kuang D, Bar-Sever Y, Bertiger W, Desai S, Haines B, Iijima B, Kruizinga G, Meehan T, Romans L (2001) Precise Orbit Determination for CHAMP Using GPS Data from BlackJack Receiver. presented at the ION National Technical Meeting, Long Beach, California, USA

Leick A (1995) GPS Satellite Surveying. Wiley, iSBN 0-471-30626-6

Lemoine F, Kenyon F, Factor J, Trimmer R, Pavlis N, Chinn D, Cox C, Klosko S, Luthke S, Torrence M, Wang Y, Williamson R, Pavlis E, Rapp R, Olsen T (1998) The development of the joint NASA GSFC and the National Imagery and Mapping Agency (NIMA) geopotential model EGM96. NASA/TP 1998-206861, Goddard Space Flight Center, Greenbelt, USA

Liu X (2008) Global gravity field recovery from satellite-to-satellite tracking data with the acceleration approach, Publications on Geodesy, vol 68. Nederlandse Commissie voor Geodesie, Delft

Lundquist C, Veis G (1966) Geodetic parameters for a 1966 Smithsonian Institution Standard Earth. Special Report 200, Smithsonian Institution

Luo X, Mayer M, Heck B (2009) Improving the Stochastic Model of GNSS Observations by Means of SNR-based Weighting. In: Sideris M (ed) Observing our Changing Earth, Springer Verlag, vol 133, pp 725–734

Mayer-Gürr T (2007) ITG-Grace03s: The latest GRACE gravity field solution computed in Bonn. Presentation at GSTM+SPP, Potsdam

Mayer-Gürr T, Ilk K, Eicker A, Feuchtinger M (2005) ITG-CHAMP01: a CHAMP gravity field model from short kinematic arcs over a one-year observation period. Journal of Geodesy 78(7-8):462–480

Mayer-Gürr T, Eicker A, Ilk K (2006) ITG-GRACE02s: a GRACE gravity field derived from short arcs of the satellite's orbit. In: Proceedings of the First Symposium of the International Gravity Field Service, Istanbul

McCarthy D (1996) IERS Conventions (1996). IERS Technical Note 21, Observatoire de Paris, Paris

McCarthy D, Petit G (2000) Draft of IERS Conventions (2000). IERS technical note, Observatoire de Paris, Paris, draft

McCarthy D, Petit G (2004) IERS Conventions (2003). IERS Technical Note 32, Bundesamt für Kartographie und Geodäsie, Frankfurt am Main, URL `http://www.iers.org/iers/publications/tn/tn32/`

Mervart L (1995) Ambiguity Resolution Techniques in Geodetic and Geodynamic Applications of the Global Positioning System. Geodätisch-geophysikalische Arbeiten in der Schweiz, Band 53, Schweizerische Geodätische Kommission, Institut für Geodäsie und Photogrammetrie, Eidg. Technische Hochschule Zürich, Zürich

Montenbruck O, Gill E (2000) Satellite orbits – models, methods, and applications. Springer, Berlin

Montenbruck O, Kroes R (2003) In-flight performance analysis of the CHAMP BlackJack GPS receiver. GPS Solutions 7(2):74–86

Montenbruck O, Garcia-Fernandez M, Yoon Y, Schön S, Jäggi A (2009) Antenna Phase Center Calibration for Precise Positioning of LEO Satellites. GPS Solutions 13(1):23–34

Moore P, Zhang Q, Alothman A (2006) Recent results on modelling the spatial and temporal structure of the Earth's gravity field. PHILOSOPHICAL TRANSACTIONS OF THE ROYAL SOCIETY A—MATHEMATICAL PHYSICAL AND ENGINEERING SCIENCES 364 (1841):1009–1026

NASA (2010) http://www.jpl.nasa.gov/news/news.cfm?release=2010-195

Nerem R, Lerch F, Marshall J, Pavlis E, Putney B, Tapley B, Eanses R, Ries J, Schutz B, Shum C, Watkins M, Klosko S, Chan J, Luthcke S, Patel G, Pavlis N, Williamson R, Rapp R, Biancale R, Nouel F (1994) Gravity Model Developments for Topex/Poseidon: Joint Gravity Models 1 and 2. Journal of Geophysical Research 99(C12):24,421–24,447

Niell AE (1996) Global Mapping Functions for the Atmosphere Delay at Radio Wavelengths. Journal of Geophysical Research 101(B2):3227–3246

Niemeier W (2008) Ausgleichungsrechnung — Statistische Auswertemethoden, 2nd edn. de Gruyter, Berlin, New York, iSBN: 978-3-11-019055-7

Noll C, Pearlman M (eds) (2009) INTERNATIONAL LASER RANGING SERVICE 2007–2008 REPORT. Goddard Space Flight Center, NASA/TP-2009-215848

Pavlis N, Holmes S, Kenyon S, Factor J (2008) An Earth Gravitational Model to Degree 2160: EGM2008. presented at the 2008 General Assembly of the European Geosciences Union, Vienna, Austria

Prange L, Jäggi A, Beutler G, Dach R, Mervart L (2009) Gravity Field Determination at the AIUB – the Celestial Mechanics Approach. In: Sideris M (ed) Observing our Changing Earth, vol 133, pp 353–62

Prange L, Jäggi A, Dach R, Bock H, Beutler G, Mervart L (2010) AIUB-CHAMP02S: The influence of GNSS model changes on gravity field recovery using spaceborne GPS. Advances in Space Research 45:215–224, DOI 10.1016/j.asr.2009.09.020

Ramillien G, Cazenave A, Brunau O (2004) Global time variations of hydrological signals from GRACE satellite gravimetry. Geophysical Journal International 158(3):813–826, doi: 10.1111/j.1365-246X.2004.02328.x

Reigber C (2000) The champ satellite. http://op.gfz-potsdam.de /champ/systems/index_SYSTEMS.html

Reigber C (2001) Champ newsletter no. 4. www-app2.gfz-potsdam.de/pb1/op/champ/more/newsletter_CHAMP_004.html

Reigber C (2002a) CHAMP newsletter no. 10. www-app2.gfz-potsdam.de/pb1/op/champ/more/newsletter_CHAMP_010.html

Reigber C (2002b) CHAMP newsletter no. 9. www-app2.gfz-potsdam.de/pb1/op/champ/more/newsletter_CHAMP_009.html

Reigber C, Lühr H, Schwintzer P (1998) Status of the CHAMP Mission. In: Rummel R, Drewes H, Bosch W (eds) Towards an Integrated Global Geodetic Observing System (IGGOS), Springer, pp 63–65, ISBN 3-540-67079-3

Reigber C, Balmino G, Schwintzer P, Biancale R, Bode A, Lemoine J, König R, Loyer S, Neumayer H, Marty J, Barthelmes F, Perosanz F, Zhu S (2002) A high quality global gravity field model from CHAMP GPS tracking data and accelerometry (EIGEN-1S). Geophysical Research Letters 29(14), DOI 10.1029/2002GL015064

Reigber C, Schwintzer P, Neumayer K, Barthelmes F, König R, Förste C, Balmino G, Biancale R, Lemoine J, Loyer S, Bruinsma S, Perosanz F, Fayard T (2003) The CHAMP-only Earth Gravity Field Model EIGEN-2. Advances in Space Research 31(8):1883–1888

Reigber C, Jochmann H, Wünsch J, Petrovic S, Schwintzer P, Barthelmes F, Neumayer K, König R, Förste C, Balmino G, Biancale R, Lemoine J, Loyer S, Perosanz F (2005) Earth Gravity Field and Seasonal Variability from CHAMP. In: Reigber C, Lühr H, Schwintzer P, Wickert J (eds) Earth Observation with CHAMP—Results from Three Years in Orbit, Springer, Berlin, pp 25–30

Reissmann G (1980) Die Ausgleichungsrechnung: Grundlagen und Anwendungen in der Geodäsie, 5th edn. Verlag für Bauwesen, Berlin

Rothacher M (1992) Orbits of Satellite Systems in Space Geodesy. Geodätisch-geophysikalische Arbeiten in der Schweiz, Band 46, Schweizerische Geodätische Kommission, Institut für Geodäsie und Photogrammetrie, Eidg. Technische Hochschule Zürich, Zürich

Savcenko R, Bosch W (2008) EOT08a—Empirical ocean tide model from multi-mission satellite altimetry. Report 81, DGFI

Schaer S (1999) Mapping and Predicting the Earth's Ionosphere Using the Global Positioning System. Geodätisch-geophysikalische Arbeiten in der Schweiz, Band 59, Schweizerische Geodätische Kommission, Institut für Geodäsie und Photogrammetrie, Eidg. Technische Hochschule Zürich, Zürich, Switzerland

Schaer S (2002) Refined ambiguity resolution scheme at CODE. IGS Mail No. 3823, IGS Central Bureau Information System

Schaer S (2003) CODE GNSS final orbits. IGS Mail No. 4474, IGS Central Bureau Information System

Schaer S (2006) GPS week 1400 model changes made at CODE. IGS Mail No. 5518, IGS Central Bureau Information System

Schaer S, Dach R (2008) Model changes made at CODE. IGS Mail No. 5771, IGS Central Bureau Information System

Schwintzer P, Lühr H, Reigber C, Grunwaldt L, Förste C (2002) CHAMP Reference Systems, Transformations and Standards. GFZ Potsdam, CH-GFZ-RS-002

Sedwick J (1956) Interpretation of Observed Perturbations on a Minimal Earth Satellite. In: Allen JV (ed) Scientific Uses of Earth Satellites, Upper Atmosphere Rocket Panel, University of Michigan, vol 43, pp 44–48

Seeber G (2003) Satellite Geodesy, 2nd edn. de Gruyter

Seidelmann PK (1982) 1980 IAU Nutation: The Final Report of the IAU Working Group on Nutation. Celestial Mechanics 27:79–106

Seidelmann PK (1992) Explanatory Supplement to the Astronomical Almanac. University Science Books, ISBN 0-935702-68-7

Sneeuw N, Gerlach C, Földváry L, Gruber T, Peters T, Rummel R, Švehla D (2005) One year of time-variable CHAMP-only gravity field models using kinematic orbits. In: Sansò F (ed) A Window on the Future of Geodesy, IAG, Springer-Verlag, vol 128, pp 288–293, DOI 10.1007/3-540-27432-4_49

Springer T (1998) CODE RPR Model. IGS Mail No. 1842, IGS Central Bureau Information System

Springer T (2000) Modeling and Validating Orbits and Clocks Using the Global Positioning System. Geodätisch-geophysikalische Arbeiten in der Schweiz, Band 60, Schweizerische Geodätische Kommission, Institut für Geodäsie und Photogrammetrie, Eidg. Technische Hochschule Zürich, Zürich

Springer T, Beutler G, Rothacher M (1998) A new Solar Radiation Pressure Model for the GPS Satellites. In: Dow J, Kouba J, Springer T (eds) Proceedings of the 1998 IGS Analysis Center Workshop, ESA/ESOC, Darmstadt, Germany, pp 98–106

Standish E (1990) The Observational Basis for JPL's DE200, the Planetary Ephemerides of the Astronomical Almanac. Astronomy and Astrophysics 233:252–271

Steffen H, Gitlein O, Denker H, Müller J, Timmen L (2009) Present rate of uplift in Fennoscandia from GRACE and absolute gravimetry. Tectonophysics 474:69–77, DOI 10.1016/j.tecto.2009.01.012

Steigenberger, P (2009) Reprocessing of a global GPS network. DGK, Reihe C, Heft 640, Verlag der Bayerischen Akademie der Wissenschaften, ISBN: 978-3-7696-5052-5

Tapley B, Reigber C (2001) The GRACE Mission: Status and future plans. EOS Transactions 82(47)

Tapley B, Watkins M, Ries J, Davis G, Eanes R, Poole S, Rim H, Schutz B, Shum C, Nerem R, Lerch F, Marshall J, Klosko S, Pavlis N, Williamson R (1996) The Joint Gravity Model 3. Journal of Geophysical Research 101(B12):28,029–28,049

Tapley B, Bettadpur S, Ries J, Watkins M (2004) Grace measurements of mass variability in the earth system. Science 305(5683):503–505

Teunissen PJG, Kleusberg A (eds) (1998) GPS for Geodesy. Springer

Touboul P, Foulon B, Clerc GL (1998) STAR, the accelerometer of the geodesic mission CHAMP. In: Proceedings of the 49th IAF Congress, IAF-98-B.3.07

Touboul P, Willemenot E, Foulon B, Josselin V (1999) Accelerometers for CHAMP, GRACE, and GOCE space missions: synergy and evolution. Bollettino di Geofisica Teorica ed Applicata 40(3-4):321–327

Velicogna I, Wahr J (2005) Greenland mass balance from GRACE. GEOPHYSICAL RESEARCH LETTERS 32(L18505), doi: 10.1029/2005GL023955

Verdun J, Klingele E, Bayer R, Cocard M, Geiger A (2003) The Alpine Swiss French airborne gravity survey. Geophysical Journal International 152:8–19

Švehla D, Rothacher M (2002) Kinematic orbit determination of LEOs based on zero or double-difference algorithms using simulated and real SST data. In: Adam J, Schwarz K (eds) Vistas for Geodesy in the New Millennium, Springer, vol 125, pp 322–328, iSBN: 978-3-540-43454-2

Wermuth M, Švehla D, Földváry L, Gerlach C, Gruber T, Frommknecht B, Peters T, Rothacher M, Rummel R, Steigenberger P (2004) A gravity field model from two years of CHAMP kinematic orbits using the energy balance approach. In: Geophysical Research Abstracts, European Geosciences Union, vol 6

Wolf H (1997) Ausgleichungsrechnung — Formeln zur praktischen Anwendung, vol 1, 3rd edn. Dümmler, Bonn, iSBN: 3-427-78353-7

Wolf P, Ghilani C (1997) Adjustment Computations: Statistics and Least Squares in Surveying and GIS, 3rd edn. John Wiley & Sons, Canada, iSBN: 978-0471168331

Yun HS (1999) Precision geoid determination by spherical FFT in and around the Korean peninsula. Earth Planets Space 51:13–18

Zin A, Landenna S, Conti A, Marradi L, Raimondo MD (2006) ENEIDE: an Experiment of a Space-borne, L1/L2 Integrated GPS/WAAS/EGNOS Receiver. In: Proceedings of the European Navigation Conference, Manchester, United Kingdom

Zumberge JF, Heflin MB, Jefferson DC, Watkins MM, Webb FH (1997) Precise point positioning for the efficient and robust analysis of GPS data from large networks. Journal of Geophysical Research 102(B3):5005–5017